Stress-Strain Behaviour of Rubber

by

Julia Gough

A Thesis submitted for the degree of

Doctor of Philosophy

Queen Mary and Westfield College
University of London

2000

ABSTRACT

Several aspects of the stress-strain behaviour of rubber, important for evaluating its properties for finite element analysis and engineering applications, are investigated.

Measurements of the deformation behaviour of an elastomer containing a compressible filler are used to assess theoretical equations for the compression modulus of rubber pads bonded to rigid endplates. The volume fraction of filler is estimated from a simple model.

The first cycle stress-strain behaviour of filled and unfilled rubbers is characterised from uniaxial tests and by measuring both non-zero principal stresses with a novel pure shear technique. Various theoretical forms for the strain energy density function are assessed. The results support the assumption that the strain energy of filled natural rubber is a function only of the first strain invariant.

Finite element modelling of the behaviour of a hyperelastic material in simple shear reveals that the proximity of the free edges in conventional simple shear testpieces strongly influences the stresses and deflections in the thickness direction. These finding are qualitatively supported by experiment. The effect of free edges on the shear modulus is also assessed.

Deviations from hyperelastic behaviour are investigated through experimental studies of stress relaxation, cyclic stress softening and the superposition of a torsion on a uniaxial extension. Anisotropic deformations can result in corresponding differences in the amounts of stress relaxation or stress softening in different directions. Isotropic models cannot model these features but may be adequate for most practical applications.

The relationship between the modulus and crystallinity of partially crystalline rubber is determined experimentally. The reinforcing effect of the crystals is found to be approximately independent of their morphology and of the modulus of the amorphous rubber. Studies of yielding of partially crystalline rubber show that the yield stress increases with increasing amounts of crystallization whereas the yield strain remains roughly constant.

ACKNOWLEDGEMENTS

"Begin at the beginning and carry on till you come to the end: then stop."*

This is roughly what I had in mind when I embarked on this project. Of course, things are never that simple and there were many dead ends, wrong turnings and rough tracks along my route.

I would like to thank everyone who has guided me, helped me or encouraged me along the way. In particular, Professor Alan Thomas took a keen interest in the work and was a valuable source of ideas. Dr. Alan Muhr supervised most of the work. His technical knowledge and willingness to answer questions were indispensable, and his constructive advice never failed to encourage and inspire me. I also wish to thank Professor Craig Davies and Dr. Keith Fuller for supervising this work.

The work was carried out as part of the research programme of T.A.R.R.C. (formerly the Malaysian Rubber Producers' Research Association). I would like to thank the Board of T.A.R.R.C. for funding and my colleagues at T.A.R.R.C. for their assistance, particularly Richard Ward, Ian Stephens, Ian Goodchild, Ian Gregory and Colin Hull for help with various aspects of the experimental work, the staff of the millroom and workshop for preparing some of the testpieces and metalwork, and Sue Luck for typing a large part of this thesis. Finally, I wish to thank Carol Muhr for her hospitality, the use of a computer and help with word processing, and Hamid Ahmadi for his unfailing encouragement.

Julia Gough

November 1999

* "Alice's Adventures in Wonderland." Lewis Carroll.

They that sow in tears shall reap in joy.

Psalm 126, verse 5.

CONTENTS

LIST OF SYMBOLS

A	Helmholtz free energy (Section 1.2)
A	cross-sectional area of testpiece
A	constant in equation (1.26), (1.27) and their derivatives, equations (4.16) to (4.20)
A_0	cross-sectional area of undeformed block
A_2	cross-sectional area of crystallized block
a	radius of cylinder
B	constant in equation (1.26), (1.27) and their derivatives, equations (4.16) to (4.20)
B	material constant in equation (1.34)
b	arc length displacement of pointer
C	constant
C_1	Mooney constant
C_2	Mooney constant
C_4	constant
C_{ij}	constants in series expansion of strain energy function
c	constant
d	distance from centre of cylinders to chart (Chapter 7)
E	Young's modulus
E_∞	confined compression modulus
E_a	apparent compression modulus of incompressible bonded block
E_c	apparent compression modulus of compressible bonded block
e_i	strain in ith direction (i=1,2,3)
F	peak force in cyclic stress relaxation (Chapter 8)
F	applied force on block (Chapter 9)
F_N	normalised peak force
F_{10}	peak force of 10^{th} cycle
f	force
f_1	main force in split pure shear
f_2	transverse force in split pure shear
f_{300}	force after 300 seconds

f_A, f_B forces recorded by separate transverse load cells

f_N normalised force

f_{NA}, f_{NB} normalised forces recorded by separate transverse load cells

f_m component of main force in transverse force

f_t force at time t

G shear modulus

G Gibbs free energy (section 1.5.1)

G_a Gibbs free energy of amorphous rubber

G_{app} apparent shear modulus of a bonded block

G_c Gibbs free energy of crystalline rubber

G_{eff} apparent shear modulus of rubber containing voids or compressible filler

G_f shear modulus of filled rubber

G_g shear modulus of gum rubber

G′ in phase shear modulus

G′′ out of phase shear modulus

G* complex modulus

H enthalpy of melting

h height of testpiece between bonded surfaces

I_1 first strain invariant

I_{1P} first strain invariant in pure shear

I_{1T} first strain invariant in tension or compression

I_2 second strain invariant

I_3 third strain invariant

I_E first invariant of n-measure strain

I_m maximum value of I_1

J volumetric extension ratio

K bulk modulus

K_{eff} apparent bulk modulus of rubber containing voids or compressible filler

k stiffness

k Boltzmann constant (Section 1.2.1)

k rate constant (Section 1.5)

ℓ length of link in molecular chain

ℓ_0 initial length of cylinder (Chapter 7)

ℓ_0 height of undeformed block

ℓ_1 height of compressed block

ℓ_2 height of crystallized block

M torsional couple

m constant in equation (1.26) and its derivatives, equations (4.16) to (4.20)

m constant in equation (1.34)

N number of molecular chains per unit volume (Chapter 1)

N normal force in axial direction on cylinder (Chapter 7)

n number of links in a molecular chain (Section 1.2.1)

n number of voids per unit volume (Section 1.3.3)

n constant in equation (1.26) and its derivatives, equations (4.16) to (4.20)

n material constant in equation (1.34)

n number of tenfold increments of time (Chapter 8)

P pressure of void in thick spherical shell

p arbitrary hydrostatic pressure

Q weight applied to one arm of torsion beam

r end to end chain length (Section 1.2.1)

r radius of void (Section 1.3)

r radius of cylindrical block in shear (Chapter 6)

r radial distance from centre of cylinder (Chapter 7)

S entropy of network (Section 1.2.1)

S shape factor

s entropy per chain (Section 1.2.1)

s_i nominal stress in ith direction (i=1,2,3,)

s_N nominal stress in axial direction of cylinder

s_p s_1 in pure shear

s_T s_1 in tension

T absolute temperature

T_m thermodynamic melting temperature

t time (Chapters 1 and 8)

t thickness of bonded pure shear testpiece

U internal energy

V_0 volume of bonded block

V_c volume fraction of crystalline phase

v volume fraction of voids or filler

W strain energy (density) function

W_t time dependent strain energy function

$\bar{W}$ strain energy function for compressible material

$\tilde{W}$ strain energy function for hyperelastic material

w width of pure shear testpiece

x deflection

y linear contraction of bonded block perpendicular to the bonded faces

z half length of torsion bar

α constant in Ogden strain energy function (Section 1.2)

α aspect ratio of filler particles

β empirical factor

γ shear strain

δ phase angle

ζ rate of decay of force

η damage parameter in Ogden and Roxburghs' model of Mullins' effect

θ angle of rotation of cylinder

Λ first Lamé constant

λ_i principal extension ratio in ith direction (i=1,2,3)

μ constant in Ogden strain energy function

ν Poisson's ratio

ϕ see equation (1.30)

σ_i true (Cauchy) stress in ith direction (i=1,2,3)

σ_P σ_i in pure shear

σ_T σ_i in tension

σ_{xy} shear stress in x direction of xy plane

σ_{xx} true (Cauchy) normal stress in x direction

σ_{yy} true (Cauchy) normal stress in y direction

σ_{zz} true (Cauchy) normal stress in z direction

τ shear stress

ψ angle of rotation per unit length of cylinder

ω angular frequency

CHAPTER 1

A review of the literature and scope of this thesis

1.1 Introduction: Rubber as an engineering material and the need to characterise its stress-strain behaviour.

Natural rubber, and polymers known as synthetic elastomers, form a distinctive class of engineering materials which may be deformed elastically under quite small stresses to very large extensions. This is known as hyperelasticity. Many engineering applications of rubber exploit its unique stress-strain behaviour of low elastic modulus, high extensibility and a high ratio of bulk to shear modulus. There is a need to be able to predict this behaviour and to establish how it can be modified to suit particular engineering purposes. This chapter reviews existing knowledge, and subsequent chapters of this thesis seek to clarify a range of issues and develop and apply appropriate techniques for characterising the stress-strain behaviour of rubber.

The unique hyperelastic behaviour of rubber is attributed to a structure made up of a large number of long chain molecules, in random conformations, and chemically bonded to one another by crosslinks in a few places to form a continuous network (Figure 1.1). Under deformation, the molecules adopt a slightly straighter conformation with a consequent reduction in configurational entropy. The restoring force required for elastic recovery arises from the tendency for the molecules to resort to their state of maximum configurational entropy and increases with increasing temperature, a phenomenon first observed by Gough (1805).

The long chain molecules in natural rubber are cis-polyisoprene (Figure 1.2). The rubbery behaviour arises from the fact that the single bonds are free to rotate and are thereby able to adopt random conformations which change under the application of an applied force. The presence of the double bond is important since it reacts readily with sulphur to form crosslinks during the process of vulcanization. Rubber is not useful as an engineering material unless chemically crosslinked and all the work in this thesis is concerned with vulcanized rubber. Vulcanization is usually carried out at an elevated temperature (typically 140°C) in a mould at a sufficiently high pressure to achieve good

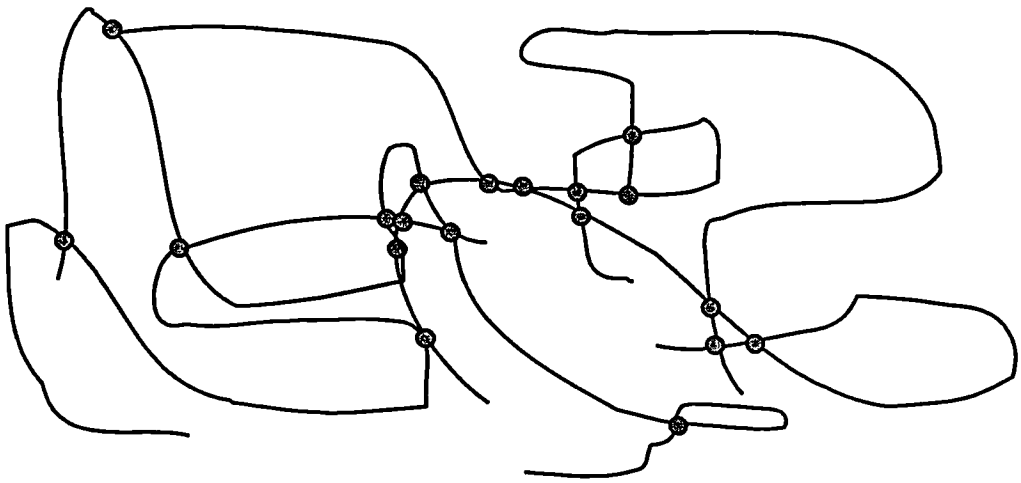

Figure 1.1 Schematic diagram of the molecular structure of a rubber

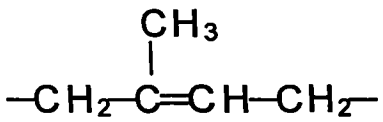

Figure 1.2a Chemical structure of polyisoprene

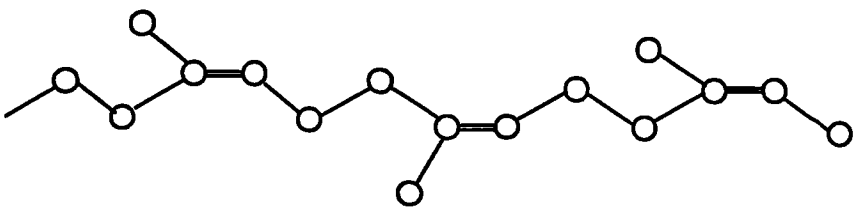

Figure 1.2b Arrangement of carbon atoms in cis-polyisoprene

conformation to the mould shape. Bonding to other materials such as metals can be carried out at the same time. An alternative to sulphur vulcanization is peroxide vulcanization. In this case the rubber is heated with an organic peroxide such as dicumyl peroxide and the crosslinks formed are direct carbon-carbon bonds between adjacent chains. In the case of sulphur vulcanization more complicated crosslinks are likely to be formed, comprising one or more sulphur atoms bridging the neighbouring molecules. Additional chemicals, usually zinc oxide, stearic acid and an accelerator are required. The ratio of sulphur to accelerator is the principal factor in determining the type of sulphur crosslinks formed. High ratios of sulphur to accelerator give mainly polysulphidic crosslinks (conventional vulcanizates), lower ratios give more monosulphidic crosslinks. Increasing the number of crosslinks (crosslink density) affects the physical behaviour of rubber principally by causing an increase in elastic modulus. A variety of chemicals may be used to crosslink synthetic rubbers depending on the active groups available, though many contain unsaturated carbon-carbon bonds and may be crosslinked using similar systems to those for natural rubber.

In addition to vulcanizing ingredients, engineering elastomer compounds usually contain antidegradants, such as antioxidants, and fillers. Ingredients in rubber formulations are expressed in parts per hundred of rubber by mass. By far the most commonly used filler is carbon black which is available in various grades, depending on its particle size and extent of aggregation. The filler affects the physical properties of rubber in a number of ways. The effects are most pronounced for carbon black or silica particles of small size; such fillers are said to "reinforce" the rubber. Primarily, reinforcing fillers increase the stiffness of the material, but also change the relationship between the elastic modulus and the strain causing a much higher modulus at low strains and a reduction of the strain at which stiffening at large strain occurs (Figure 1.3). Greater departures from perfect elastic behaviour are seen with filled rubber, such as increased hysteresis, stress relaxation and softening under repeated loadings. Further discussion of these effects is given in Section 1.4. Strength properties of rubber, such as tear strength and abrasion resistance can be improved by the incorporation of carbon black fillers and many synthetic elastomers are too weak to be useful for engineering purposes unless they are appropriately reinforced with filler.

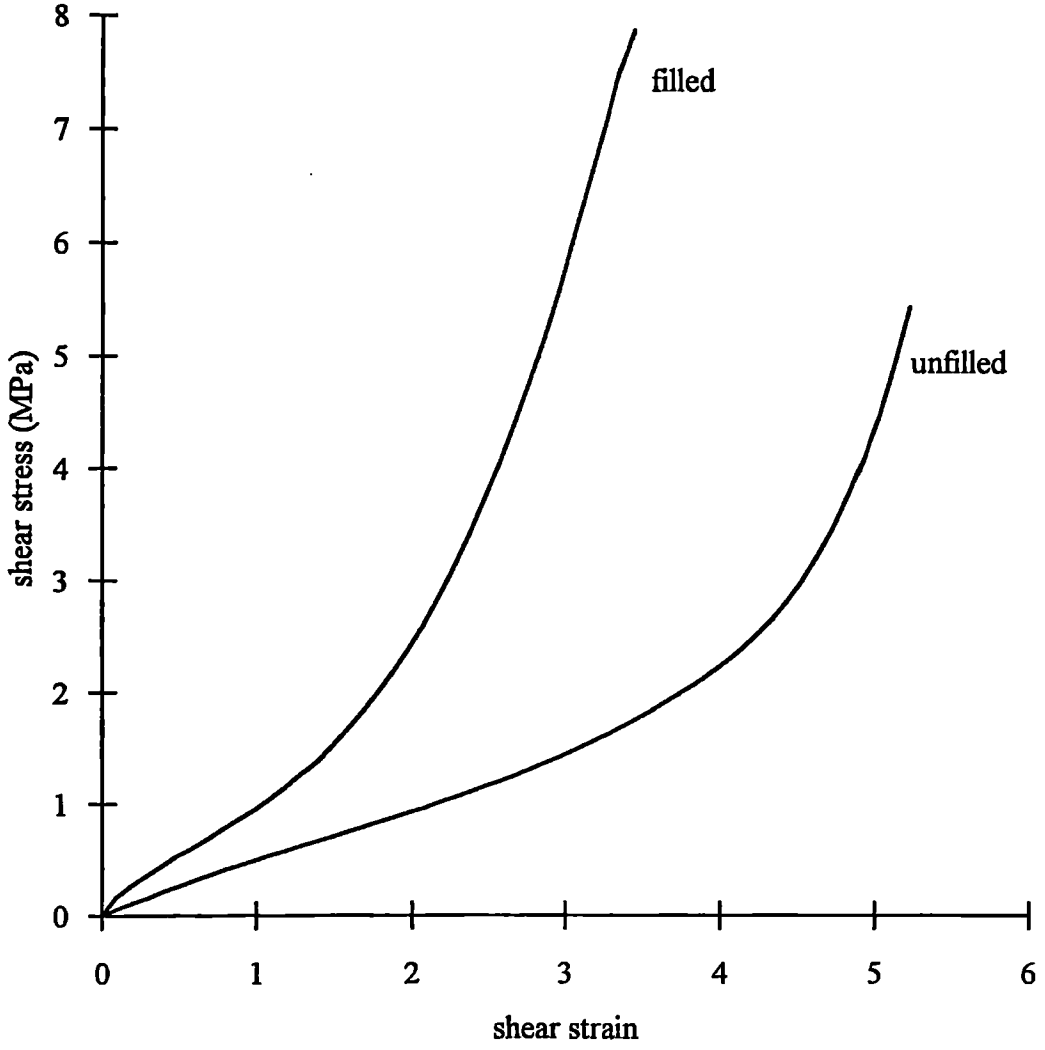

Figure 1.3 Typical stress-strain curves of filled and unfilled natural rubber in simple shear

Exposure of rubber to low temperatures is liable to cause a phase transition. At very low temperatures the rubber instantaneously becomes hard and brittle as it passes through its glass transition temperature. For unvulcanized natural rubber this occurs at about -70°C and for vulcanized natural rubber 1 to 2°C higher. Below this temperature the freedom of rotation of the bonds does not take place since there is insufficient thermal energy to enable the molecules to overcome the energy barrier which exists between two stable configurations. Thus a particular structure is "frozen in" and the material is hard and rigid like a glass. As the temperature is raised slightly above the glass transition temperature molecular motions return but the material has very high damping. Elastic behaviour is manifested as the temperature is raised well above the glass transition temperature.

At low temperature rubbers with a sufficiently regular chemical repeat structure, such as natural rubber and polychloroprene, are liable to crystallize. The process tends to be very slow, taking from a few days to many months. The maximum rate for natural rubber occurs at about -25°C and for polychloroprene at about -10°C. Crosslinking inhibits crystallization. Partially crystalline rubber is a stiff, tough material and low temperature crystallization is a problem for some engineering components which are exposed to low temperatures for long periods. For example, the expansion of a bridge deck caused by temperature fluctuations may be accommodated by incorporating a rubber bearing which is soft in shear. If, however, the bearing stiffens due to crystallization, damaging stresses may be transferred to the bridge piers if the bridge deck undergoes a further change in temperature (Figure 1.4). Malfunctioning of earthquake bearings is also probable; the high damping natural rubber compounds developed for seismic isolation of buildings are often vulnerable to low temperature crystallization due to their low crosslink density.

Crystallization also takes place almost instantaneously and at higher temperatures under an applied strain and accounts, in part, for the stiffening of rubber at high strains (Figure 1.3). Strain crystallization improves the tensile and tear strength of rubber and thus strain crystallizing rubbers, such as natural rubber, are favoured over certain non-crystallizing synthetics for applications where good strength properties are required.

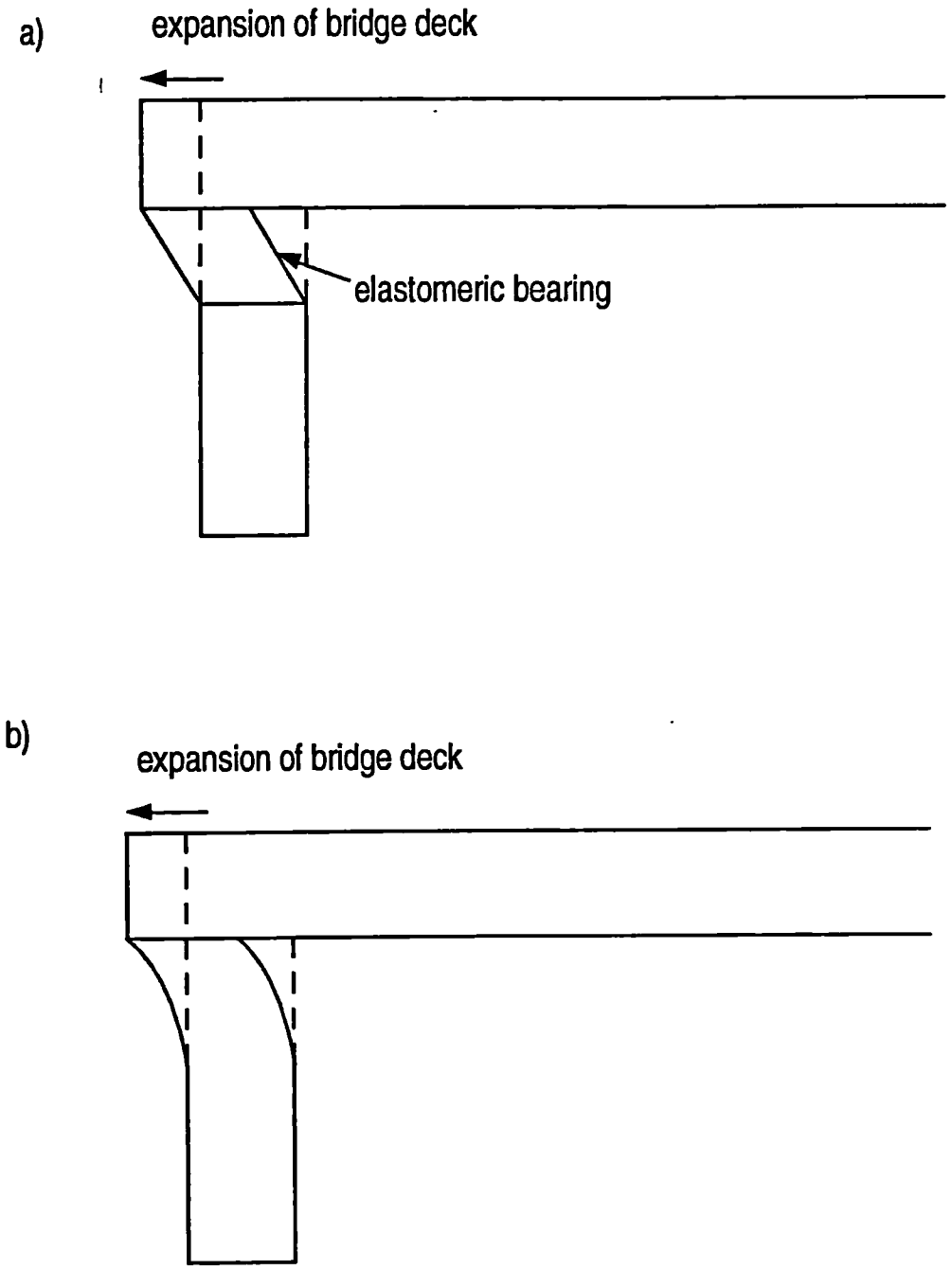

Figure 1.4 Expansion of a bridge deck (a) with and (b) without a compliant elastomeric bearing.

The design of rubber engineering components is facilitated by the use of finite element analysis (FEA). These computerised codes require a three dimensional description of the force-deformation behaviour of rubber. The usual procedure involves describing the rubber by a strain energy density function, expressed as a mathematical function in terms of the extensions in three dimensions. The user may specify one or more material constants, such as the shear modulus. It is also possible to use sets of stress-strain data to describe the material but these are limited to the modes of deformation which are convenient experimentally and some assumption about the form of the strain energy density function is required to enable the experimental data to be applied to a general deformation. The need for an accurate and useable mathematical model for filled rubbers for use in finite element analysis is addressed in this thesis.

1.2 Rubber elasticity of incompressible materials

Throughout this section the assumption is made that no volume change of the rubber occurs on deformation. This assumption simplifies the mathematics somewhat and is borne out by experiment (Holt & McPherson, 1936). However, there exists considerable literature on the effect of compressibility and the behaviour of compressible elastomers is considered in Section 1.3. Also, consideration of effects associated with imperfect elasticity are deferred to Section 1.4.

1.2.1 *Statistical theory*

The description given in the previous section, of a continuous network of freely jointed long-chain molecules, has been developed into a quantitative model to describe the elastic behaviour of rubber called the statistical theory. The theory was originally developed by Kuhn (1936) and additional contributions have been made by James & Guth (1943), Wall (1942), Flory & Rehner (1943) and Treloar (1943a & b). An account of it is provided by Treloar (1975).

The assumptions of the theory are:-

(i) The network contains N chains per unit volume each containing n identical, freely jointed links of length ℓ. A chain is defined as a segment of molecule between

successive crosslinks.

(ii) The rubber deforms in a manner which causes the configurational entropy of the chains to alter, but with no change in the internal energy.

(iii) The distribution of end-end chain length, r, follows a Gaussian distribution in the unstrained state described by a probability density function:-

$$P(r)dr = \frac{6}{n\ell^3}\sqrt{\frac{3}{2\pi n}}\, r^2\, e^{-\left(\frac{3r^2}{2n\ell^2}\right)} dr \qquad (1.1)$$

It follows that the root-mean-square length is given by $\sqrt{\bar{r}^2} = \ell\sqrt{n}$ and it is implicit in assuming a Gaussian distribution that $r \ll n\ell$; in other words the end-end length of the chains is much less than their fully extended length.

(iv) The volume remains unchanged on deformation (ie. the material is incompressible).

(v) The crosslinks move on deformation as if embedded in an elastic continuum so that the components of length in each chain change in the same ratio as in the bulk rubber. This is known as the assumption of affine deformation.

(iv) The entropy of the individual chains is given by:-

$$S = C - \frac{3kr^2}{2n\ell^2} \qquad (1.2)$$

where C is an arbitrary constant and k is the Boltzmann constant. The entropy of the network is the sum of the entropies of the individual chains.

Using equation (1.2) to calculate the entropy change associated with deforming a chain and summing over all chains yields:-

$$\Delta S = -\tfrac{1}{2}Nk\left(\lambda_1^2 + \lambda_2^2 + \lambda_3^3 - 3\right) \qquad (1.3)$$

where ΔS is the change in entropy of the network per unit volume under a deformation in which λ_1, λ_2 and λ_3 are the three principal extension ratios (the ratios of stretched to unstretched length) along three mutually perpendicular axes. Thus a unit cube would be deformed into a cuboid of edge lengths λ_1, λ_2 and λ_3.

For a reversible deformation, the work of deformation is equal to the change in the Helmholtz free energy (Treloar 1975). The Helmholtz free energy, A, is defined as

$$A = U - TS \qquad (1.4a)$$

where U is the internal energy. Hence, for an isothermal deformation, the work of deformation for a unit volume, W, is given by

$$W = \Delta A = \Delta U - T\Delta S \qquad (1.4b)$$

and, assuming no change in internal energy (Treloar, 1975),

$$W = -T\Delta S \qquad (1.4c)$$

where T is the absolute temperature. Hence, from equation (1.3):-

$$W = \tfrac{1}{2}NkT\left(\lambda_1^2 + \lambda_2^2 + \lambda_3^2 - 3\right) \qquad (1.5)$$

W represents the elastically stored energy per unit volume and is also called the strain energy function.

It is convenient to write:-

$$G = NkT \qquad (1.6)$$

$$\text{so} \qquad W = \tfrac{1}{2}G\left(\lambda_1^2 + \lambda_2^2 + \lambda_3^2 - 3\right) \qquad (1.7)$$

thus the strain energy function represented by equation (1.5) involves only one physical constant, G, which may be determined from the degree of crosslinking in the rubber.

It follows from the assumption of constant volume that:-

$$\lambda_1 \lambda_2 \lambda_3 = 1 \tag{1.8}$$

so equation (1.7) may be written:-

$$W = \tfrac{1}{2}G\left(\lambda_1^2 + \lambda_2^2 + (\lambda_1\lambda_2)^{-2} - 3\right) \tag{1.9}$$

Thus, for an incompressible material, W is a function of two independent variables, in this case chosen to be λ_1 and λ_2.

For an incompressible material the state of deformation is unaffected by the imposition of a hydrostatic stress. It follows that the stresses are indeterminate to the extent of an arbitrary hydrostatic pressure, p:-

$$\sigma_i = \lambda_i \frac{\partial W}{\partial \lambda_i} + p \tag{1.10}$$

where σ_i is the true (or Cauchy) stress, defined as the force per unit area in the deformed state (Treloar, 1975) (i takes the values 1, 2 or 3 and there is no summation over i). However, the differences between any two principal stresses may be determined absolutely. These are given by:-

$$\begin{aligned} \sigma_1 - \sigma_2 &= G\left(\lambda_1^2 - \lambda_2^2\right) \\ \sigma_2 - \sigma_3 &= G\left(\lambda_2^2 - \lambda_3^3\right) \\ \sigma_3 - \sigma_1 &= G\left(\lambda_3^2 - \lambda_1^2\right) \end{aligned} \tag{1.11}$$

The stress-strain behaviour for particular modes of deformation may be determined from equation (1.11) by substitution of appropriate relationships for the stresses and extension ratios. It is interesting to note that, in simple shear, the shear stress is given by

$$\tau = G\gamma \tag{1.12}$$

where γ is the shear strain (Treloar, 1975). Thus the material constant, G, is equivalent to the shear modulus. We see also that Hooke's law is obeyed in simple shear (though not in other deformations) and Rivlin (1948a) has shown that the statistical theory is the natural extension of Hooke's law to large deformations, thus a material obeying it is called neo-Hookean.

An evaluation of how well the statistical theory describes the behaviour of unfilled vulcanized rubber was carried out by Treloar (1944). He compared the stress-strain behaviour predicted by the theory with experiments in uniaxial extension, equibiaxial extension and pure shear. Deviations from theory were apparent, especially in uniaxial extension, where, at low strains (below about 50%), the modulus was too high relative to its value at moderate strains (up to 400%). At even higher strains a rapidly rising modulus was seen which was not predicted by the theory presumably because the statistical theory, based on Gaussian chain statistics, does not take into account the finite extensibility of the chains. Various workers (Kuhn & Grun, 1942; James & Guth, 1943; Isihara et al ,1951; Wang & Guth, 1952; Flory, 1953; Treloar & Riding, 1979; Arruda & Boyce, 1993) have developed models for rubber elasticity based on networks of non-Gaussian chains. The use of inverse Langevin functions to describe the finite extensibility of the chains complicates the mathematics somewhat and Gent (1996) has proposed a simple empirical equation to describe this behaviour.

$$W = -\tfrac{1}{2}G\left(I_m - 3\right)\ln\left(1 - \frac{I_1 - 3}{I_m - 3}\right) \tag{1.13}$$

where $I_1=\lambda_1^2+\lambda_2^2+\lambda_3^2$ and I_m is the value of I_1 when the chains are fully extended. No widely accepted explanation for the differences between theory and experiment at low strain has been proposed although Thomas (1955) has suggested an empirical modification of the stored energy of a single chain, representing an attractive force, which agrees quite well with the observed behaviour. Nevertheless, the statistical theory provides a valuable model of the main features of rubber elasticity and explanation of them in terms of the molecular structure. It contains only one constant and is based on

features of the molecular structure which enhances its usefulness and credibility.

1.2.2 *Phenomenological theory*

An alternative approach to modelling the hyperelastic behaviour of rubber is to dispense with any attempt to utilize features of the molecular structure to predict the behaviour and consider the problem from a purely mathematical standpoint. The most complete analysis of this type was developed by Rivlin (1948a, b)

The two fundamental assumptions of Rivlin's large strain elasticity theory for incompressible materials are:

(i) the material is isotropic in the unstrained state and

(ii) no volume change occurs on deformation.

Based on arguments of symmetry Rivlin deduced that the strain energy function was expressible in terms of the strain invariants, I_1, I_2 and I_3 , defined as:-

$$\begin{aligned} I_1 &= \lambda_1^2 + \lambda_2^2 + \lambda_3^2 \\ I_2 &= \lambda_1^2\lambda_2^2 + \lambda_2^2\lambda_3^2 + \lambda_3^2\lambda_1^2 \\ I_3 &= \lambda_1^2\lambda_2^2\lambda_3^2 \end{aligned} \qquad (1.14)$$

It may be noted that I_1, I_2 and I_3 arise naturally as coefficients in the characteristic equation for solving for the eigenvalues (λ_1^2, λ_2^2, λ_3^2) of both the left and the right Cauchy-Green stretch tensors.

Since for constant volume, $\lambda_1 \lambda_2 \lambda_3 = 1 = I_3$:-

$$W = W(I_1, I_2) \qquad (1.15)$$

where I_1 and I_2 are independent variables.

Use of equation (1.10), combined with differentiation of equation (1.14), provides expressions for the principal stresses which (for an incompressible material) are indeterminate to the extent of an arbitrary hydrostatic pressure:

$$\sigma_i = 2\left(\lambda_i^2 \frac{\partial W}{\partial I_1} - \frac{1}{\lambda_i^2}\frac{\partial W}{\partial I_2}\right) + p \qquad (1.16)$$

The differences in principal stresses become:-

$$\begin{aligned}
\sigma_1 - \sigma_2 &= 2\left(\lambda_1^2 - \lambda_2^2\right)\left(\frac{\partial W}{\partial I_1} + \lambda_3^2 \frac{\partial W}{\partial I_2}\right) \\
\sigma_2 - \sigma_3 &= 2\left(\lambda_2^2 - \lambda_3^2\right)\left(\frac{\partial W}{\partial I_1} + \lambda_1^2 \frac{\partial W}{\partial I_2}\right) \qquad (1.17) \\
\sigma_3 - \sigma_1 &= 2\left(\lambda_3^2 - \lambda_1^2\right)\left(\frac{\partial W}{\partial I_1} + \lambda_2^2 \frac{\partial W}{\partial I_2}\right)
\end{aligned}$$

It is equally acceptable to take λ_1 and λ_2 as the independent variables in equation (1.15), having used the constant volume assumption to substitute for λ_3, and write:-

$$W = W\left(\lambda_1, \lambda_2\right) \qquad (1.18)$$

This is the approach favoured by Ogden (1982).

1.2.3 *Experimental evaluation of the strain energy function*

In order to use equation (1.16) to calculate the stresses for any given deformation $\partial W/\partial I_1$ and $\partial W/\partial I_2$ need to be found. In other words W must be evaluated over the full range of values of I_1 and I_2 relevant for the application. Such an evaluation is not straightforward; permissible regions for I_1 and I_2 are shown in Figure 1.5, together with a set of lines representing the experiments of Rivlin and Saunders (1951). It can be seen that, to cover the whole region, an experiment is required which enables I_1 and I_2 to be varied independently. This can be achieved by allowing λ_1 and λ_2 to vary independently as in the biaxial straining of a thin sheet. Even so, a large number of experimental points is required if the evaluation of W is to be comprehensive.

The earliest biaxial experiments were carried out by Treloar (1948) who devised a method of straining a sheet of natural rubber in two perpendicular directions by means of strings, loaded with suitable weights, attached to projecting lugs around the edges of

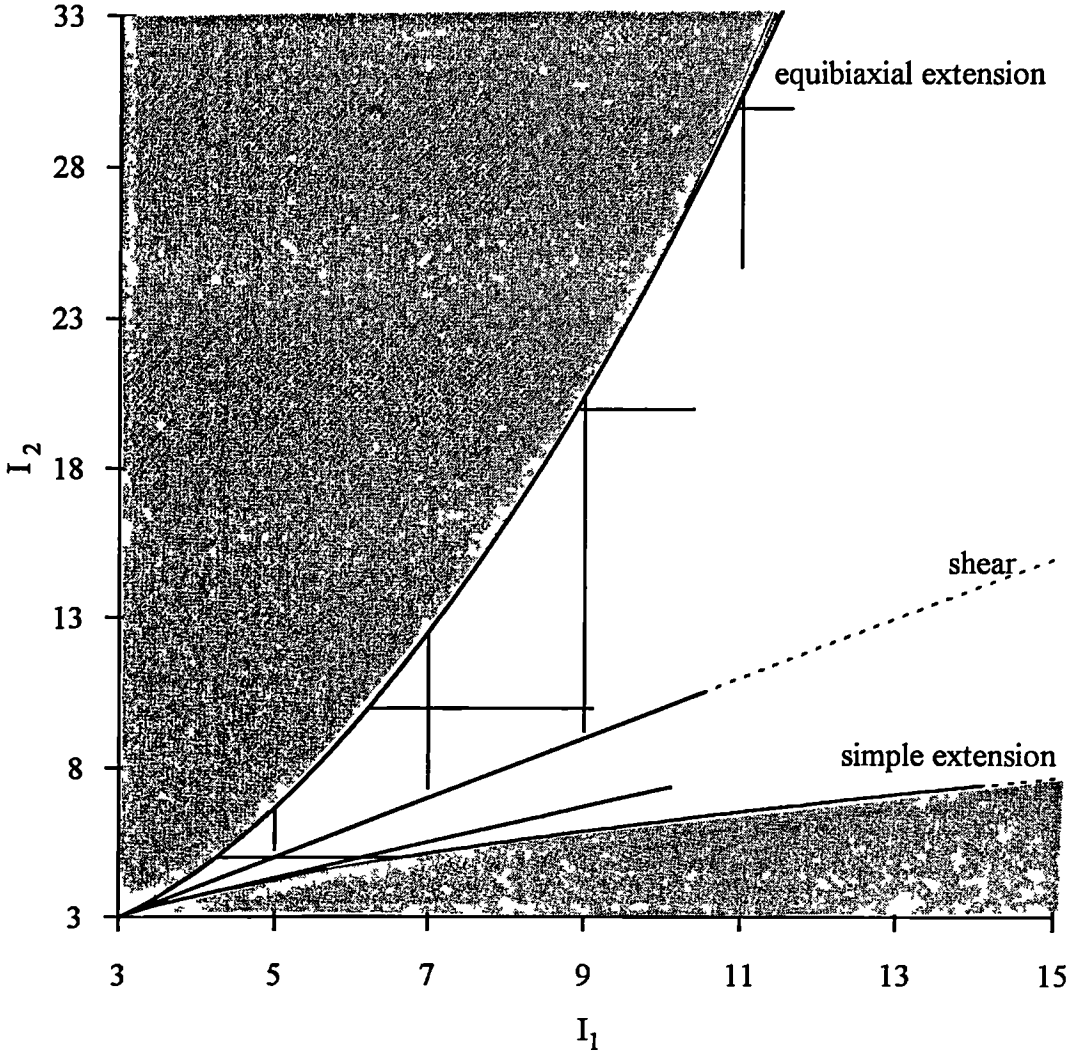

Figure 1.5 Permissible values of I_1 and I_2. Shaded area represents physically impossible region. Solid lines represent the experiments of Rivlin and Saunders (1951).

the sheet. Rivlin and Saunders (1951) extended Treloar's work by arranging their experiments such that one of I_1 and I_2 was varied while the other was held constant (see Figure 1.5). The experimentation is complicated by the fact that rubber is not perfectly elastic, but exhibits hysteresis, strain softening and permanent set (see Section 1.4) and is liable to strain crystallize at high extensions. In order to minimise these effects an unfilled rubber with low hysteresis and set was chosen for the experiments. All measurements were taken from the loading curve and confined to deformations below those at which crystallization was expected to occur. $\partial W/\partial I_1$ and $\partial W/\partial I_2$ were plotted, each as functions of I_1 and I_2, using equation (1.17) for the case where $\sigma_3 = 0$:-

$$\frac{\partial W}{\partial I_1} = \frac{\dfrac{\lambda_1^2\sigma_1}{\lambda_1^2 - 1/\lambda_1^2\lambda_2^2} - \dfrac{\lambda_2^2\sigma_2}{\lambda_2^2 - 1/\lambda_1^2\lambda_2^2}}{2\left(\lambda_1^2 - \lambda_2^2\right)}$$

$$\frac{\partial W}{\partial I_2} = \frac{\dfrac{\sigma_1}{\lambda_1^2 - 1/\lambda_1^2\lambda_2^2} - \dfrac{\sigma_2}{\lambda_2^2 - 1/\lambda_1^2\lambda_2^2}}{2\left(\lambda_2^2 - \lambda_1^2\right)} \qquad (1.19)$$

However, Rivlin & Saunders (1951) pointed out that equation (1.19) is of such a form as to magnify greatly the experimental errors, especially at small strains, and renders the experimental results too inaccurate to be of use for values of I_1 and I_2 less than about 5.

For I_1 and I_2 greater than 5 they concluded from their results that:-

$$W = C\left(I_1 - 3\right) + w(I_2) \qquad (1.20)$$

where C is a constant and $w(I_2)$ is a function of I_2 such that $\partial W/\partial I_2$ decreases with increasing I_2. They found that $\partial W/\partial I_2$ ranged from 1/8 $\partial W/\partial I_1$ at $I_2 = 5$ to 1/24 $\partial W/\partial I_1$ at $I_2 = 30$. For characterising the behaviour at lower values of I_1 and I_2, they obtained load deformation relations in pure shear, pure shear superimposed on a constant simple extension, and simple extension. In accord with equation (1.20) they assumed that $\partial W/\partial I_1$ was independent of I_1 and I_2, $\partial W/\partial I_2$ was independent of I_1, and $(\partial W/\partial I_2)/(\partial W/\partial I_1)$ took the same value at $I_2 = 5$ as it did in the biaxial experiment. They concluded that the ratio $(\partial W/\partial I_2)/(\partial W/\partial I_1) = ¼$ at $I_2 = 3$ and fell steadily but with

decreasing rate with increasing I_2.

Obata et al (1970) performed biaxial experiments at various temperatures on natural rubber vulcanizates with a range of crosslink densities. In order to minimise the Mullins effect (see Section 1.4) every testpiece was conditioned by subjecting it to at least 10 cyclic deformations to the maximum extension ratios used in subsequent experiments. However, the benefits of any such conditioning procedure are doubtful, as further changes, such as recovery of the specimen, are likely to cause confusion of the same magnitude as the effect one is trying to eliminate. Also, the applicability of the results to rubber that has not been subjected to such treatment is questionable. They concluded that, for I_1 or I_2 less than about 5, $\partial W/\partial I_1$ and $\partial W/\partial I_2$ changed rapidly as a function of both I_1 and I_2 ($\partial W/\partial I_1$ decreased, and $\partial W/\partial I_2$ increased with increasing I_1 or I_2). At larger deformations $\partial W/\partial I_1$ and $\partial W/\partial I_2$ were fairly constant. In spite of acknowledging Rivlin & Saunders (1951) caution concerning the accuracy of the experiments for small deformations they offer no comment on the accuracy of their own data for I_1 or I_2 less than 5; it should be noted that the tendency for $\partial W/\partial I_1$ and $\partial W/\partial I_2$ to diverge towards plus and minus infinity as the strains decrease to zero is an inevitable consequence of the form of equations (1.19). Kawabata (1973) reports a similar functional form for $\partial W/\partial I_1$ and $\partial W/\partial I_2$ for polystyrene-butadiene and polyacrylonitrile-butadiene though no data for the latter are presented. In a later paper, Kawabata et al (1981) suggest that their previous experiments were affected by friction in the biaxial test machine and present data obtained on improved apparatus without adopting the cyclic deformation conditioning treatment. Their conclusions about the behaviour of $\partial W/\partial I_1$ and $\partial W/\partial I_2$ remain much the same. Other workers report broadly similar behaviour (Becker, 1967; James et al, 1975) but differences in detail, especially for small deformations: Jones & Treloar (1975) found both $\partial W/\partial I_1$ and $\partial W/\partial I_2$ fell with increasing I_1 and I_2. Biaxial straining may also be obtained by simultaneous axial extension and inflation of a thin walled tube. This method has been employed by Boonstra (1950), Vangerko & Treloar (1978) and Chow & Cundiff (1987).

Characterization of filled natural rubber by full biaxial testing has been less widely reported and the difficulties caused by imperfect elasticity such as stress softening, set and stress relaxation are much more severe. James & Green (1975) and Chow &

Cundiff (1987) attempted to minimise these by pre-straining all testpieces and allowing sufficient time between measurements for stress recovery to take place. They found broadly similar behaviour to unfilled rubber, with $\partial W/\partial I_1$ and $\partial W/\partial I_2$ only slightly dependent on strain and $\partial W/\partial I_1 >> \partial W/\partial I_2$. A more restricted evaluation of $\partial W/\partial I_1$ and $\partial W/\partial I_2$ for I_1 and I_2 was carried out by Fukahori & Seki (1992) for a range of filled and unfilled natural rubbers, polybutadiene, polystyrene-butadiene and polyacrylonitrile-butadiene although only data for filled and unfilled natural rubber are given in their paper. Their conclusions were broadly similar but again the validity of the small strain data is open to question. Kawabata et al (1995) adopted a similar technique for natural rubber and polystyrene-butadiene with a range of filler loadings and found that $\partial W/\partial I_1$ increased and rose more sharply at lower strains as the filler content increased whilst $\partial W/\partial I_2$ remained constant.

The overall picture is that $\partial W/\partial I_1 >> \partial W/\partial I_2$ and is not strongly dependent on strain at large strains in unfilled rubber, but rises with strain in filled rubbers. At small strains much confusion exists about the exact behaviour due to difficulties in interpreting imperfect data using equations (1.19).

1.2.4 *Particular forms of the strain energy function*

The need for a full biaxial test can be avoided if a suitable simplifying assumption about the form of the strain energy function can be made. An adequate check of the validity of any particular proposal is that it is able to predict accurately the stress-strain behaviour in a range of widely varying deformations or that the behaviour in one deformation can be used to provide an accurate prediction of the behaviour in other modes of deformation. The original data of Treloar (1944) (see Section 1.2.1) has been widely used as a basis for evaluating the quality of the fit.

The statistical theory is an example of such a simplification and its ability to describe the behaviour of unfilled rubber was reported in section (1.2.1). Equation (1.15) may be rewritten as a Taylor expansion about the stress free state (Rivlin & Saunders, 1951):-

$$W = \sum_{i,j=0}^{\infty} C_{ij} (I_1 - 3)^i (I_2 - 3)^j \qquad (1.21)$$

The first non-zero term of this series (ie. the simplest function of I_1 alone) is:-

$$W = C_{10}(I_1 - 3) \qquad (1.22)$$

which is seen to be identical to the form of the strain energy function for the statistical theory, equation (1.7), with $C_{10} = G/2$.

Another widely used equation was proposed by Mooney (1940) who deduced by arguments of symmetry, a general form of strain energy function which was consistent with a material which obeyed Hooke's law in simple shear:-

$$W = C_1(I_1 - 3) + C_2(I_2 - 3) \qquad (1.23)$$

which is the truncation of equation (1.21) at i+j = 1. The Mooney equation is better able to fit experimental data in uniaxial extension than the statistical theory, but the values thereby obtained for the Mooney constants, C_1 and C_2 do not necessarily result in good fits for other deformations such as uniaxial compression. Differentiation of equation (1.23) yields:-

$$\frac{\partial W}{\partial I_1} = C_1 \qquad \text{and} \qquad \frac{\partial W}{\partial I_2} = C_2 \qquad (1.24)$$

and some workers (Mullins & Tobin, 1954; Finney and Kumar, 1988) have been tempted to equate the values obtained for the Mooney constants in simple extension with $\partial W/\partial I_1$ and $\partial W/\partial I_2$. However, as Rivlin and Saunders (1951) pointed out, this approach is invalid if $\partial W/\partial I_1$ and $\partial W/\partial I_2$ are functions of I_1 and I_2 even if the appropriate Mooney plots give a straight line. The ratio C_2/C_1 obtained, for example, by Gumbrell et al (1953) ranged from about 1 to ⅓, depending on crosslink density - far higher than the ratio of $(\partial W/\partial I_2)/(\partial W/\partial I_1)$ of 1/8 to 1/24, obtained from the biaxial experiments of Rivlin & Saunders (1951) reported in Section (1.2.3). Mooney developed his mathematics to cover the more general case where the condition of linearity in simple shear was replaced with the condition that the material obeyed an analytic function in

shear. Little use has been made of this more general form although Carmichael & Holdaway (1961) suggested an explicit 3-parameter function and reported a good fit to the data of Treloar (1944).

Attempts to fit data to more terms of equation (1.21) are widespread (Tschoegl, 1971; James & Green, 1975; Chow & Cundiff, 1987; Yeoh, 1990), especially since many FEA packages offer up to five terms as standard. The fit for both the statistical and the Mooney-Rivlin equation is poor for highly filled rubbers whose behaviour is much more non-linear than unfilled rubbers, thus invalidating the assumption of linearity in simple shear. For normal engineering vulcanizates these functions provide a reasonable description of the stress-strain behaviour although care must be taken to ensure that the fitting procedure is done over a large enough range of strain, and that the fitting constants are obtained from more than one mode of deformation; otherwise completely unrealistic behaviour is likely to be predicted (Peeters & Küssner, 1999; Yeoh and Fleming, 1997). The difficulty of obtaining a good fit becomes more severe if an attempt is made to model highly non-linear rubbers, developed for special applications such as seismic isolation (Fuller et al, 1996)

Rather cumbersome functions of I_1 and I_2, containing three or more fitting constants have been proposed by Hart-Smith (1966) and Alexander (1968) and shown to fit certain data well. Such expressions tend to be little used due either to mathematical complexity or the need to obtain a large amount of experimental data in order to evaluate the fitting constants.

Gregory (1979), from measurements on filled natural rubber in uniaxial tension, compression and simple shear, showed that setting $\partial W/\partial I_2 = 0$ in equations (1.17) and plotting the apparent values of $\partial W/\partial I_1$ as a function of $I_1 - 3$ yielded a single mastercurve for all modes of deformation. Thus he concluded that $\partial W/\partial I_2$ is small compared to $\partial W/\partial I_1$ and $\partial W/\partial I_1$ is independent of I_2; in other words for filled rubbers W is a function of I_1 only. It has already been shown that the statistical theory gives a function of I_1 only and later workers have made use of Gregory's conclusion in suggesting particular functional forms for $W(I_1)$ designed to model the non-linear features of the stress-strain curve for filled rubbers. Yeoh (1990) used a cubic form of equation (1.21):-

$$W = C_{10}(I_1 - 3) + C_{20}(I_1 - 3)^2 + C_{30}(I_1 - 3)^3 \qquad (1.25)$$

which is convenient for use with FEA programs and suggested adding an exponential term to model the sharp downturn in stiffness with increasing strain at small strains. This idea was modified by Othman & Gregory (1990), Davies et al (1994) then by Gregory et al (1997) whose proposed function took the form:-

$$W = \frac{A}{(2-n)}(I_1 - 3)^{\left(\frac{2-n}{2}\right)} + \frac{B}{(2+m)}(I_1 - 3)^{\left(\frac{2+m}{2}\right)} + \text{constant} \qquad (1.26)$$

where A, B, m and n are constants. Finally Yeoh & Fleming (1997) combined these ideas with Gent's (1996) form for the strain energy function, equation (1.13), and suggested:-

$$W = A\left(1 - e^{-B(I_1 - 3)}\right) - C(I_m - 3)\ell n\left(1 - \frac{(I_1 - 3)}{(I_m - 3)}\right) \qquad (1.27)$$

Experimental work to check the applicability of equations such as (1.25), (1.26) and (1.27) has added further support to the conclusion of Gregory that it is often adequate to regard W as a function of I_1 only (Yeoh, 1990; Davies et al 1994; Yeoh & Fleming, 1997). Moreover, the elimination of I_2 terms improves the quality of fits to general strains from data obtained from a single uniaxial test. (Peeters & Küssner, 1999)

Another approach to evaluating W was provided by Valanis & Landel (1967) who expressed W as a function of the extension ratios, rather than the strain invariants, and proposed:-

$$W(\lambda_1, \lambda_2, \lambda_3) = w(\lambda_1) + w(\lambda_2) + w(\lambda_3) \qquad (1.28)$$

subject to the incompressibility condition $\lambda_1 \lambda_2 \lambda_3 = 1$. This separable form of the strain energy function is a natural generalization from the statistical theory in which the total configurational entropy is the sum of the configurational entropies in each of the three principal directions. Use of equation (1.10) provides expressions for the differences in

the principal stresses:-

$$\begin{aligned}\sigma_1 - \sigma_2 &= \lambda_1 w'(\lambda_1) - \lambda_2 w'(\lambda_2)\\ \sigma_2 - \sigma_3 &= \lambda_2 w'(\lambda_2) - \lambda_3 w'(\lambda_3)\\ \sigma_3 - \sigma_1 &= \lambda_3 w'(\lambda_3) - \lambda_1 w'(\lambda_1)\end{aligned} \tag{1.29}$$

where $w'(\lambda_i)$ is $\partial w/\partial\lambda_i$. The material can be characterized from a single experiment in pure shear where both σ_1 and σ_2 are measured ($\sigma_3 = 0$ and $\lambda_2 = 1$) since it follows that:-

$$\begin{aligned}\sigma_1 - \sigma_2 &= \phi(\lambda_1)\\ -\sigma_2 &= \phi(1/\lambda)\end{aligned} \tag{1.30}$$

where

$$\phi(\lambda) = \lambda w'(\lambda) - w'(1) \tag{1.31}$$

Valanis & Landel (1967) and Peng & Landel (1972) developed empirical formulae for $w(\lambda_i)$ and obtained a good fit to experimental data for unfilled rubber over a limited range of strain, but a very poor fit at low strains. The formulae contained only one material constant and enabled the rubber to be characterized from a single uniaxial test. Shariff (1997) suggested another single-constant function which improved the fit at low strains for unfilled rubbers and gave reasonable agreement with experiment for a black filled rubber.

Many of the simpler functions already discussed satisfy equation (1.28) including the function for a neo-Hookean material (equation (1.7)) and the Mooney function (equation (1.23)). In addition, Varga (1966) suggested:-

$$W = G(\lambda_1 + \lambda_2 + \lambda_3 - 3) \tag{1.32}$$

as a simple first approximation of the behaviour of rubber.

A further development was made by Ogden (1972) who proposed a strain energy function:-

$$W = \Sigma_n \frac{\mu_n}{\alpha_n}\left(\lambda_1^{\alpha_n} + \lambda_2^{\alpha_n} + \lambda_3^{\alpha_n} - 3\right) \qquad (1.33)$$

where μ_n and α_n are not restricted to integral values. He reported a good fit to the data of Treloar (1944) with a three term function. Jones & Treloar (1975) tested the validity of the Valanis-Landel hypothesis (equation (1.28)) against their biaxial strain data for unfilled rubber and found good agreement. Furthermore they were able to express equation (1.28) in terms of an explicit function based on Ogden's formula (equation (1.33). Ogden's function has been incorporated into FEA programs and an appropriate algorithm for optimising the values of the parameters, α_n and μ_n, has been published (Twizell & Ogden, 1983). However, a quite sophisticated curve-fitting program is required and one FEA user has found inaccuracies in the software supplied (Gregory, private communication). Also Yeoh (1997) suggested that the parameters obtained are liable to be unrealistic and Fuller et al (1997) reported difficulties in obtaining a good fit for very non-linear materials.

Blatz et al (1974) chose to use invariants based on a different measure of strain. They defined

$$I_E = \Sigma_i \frac{1}{n}\left(\lambda_i^n - 1\right) \qquad (1.34a)$$

and proposed a strain energy function

$$W = \left(\frac{2G}{n}\right) I_E + B I_E^m \qquad (1.34b)$$

where G, n, m and B are material dependent constants. They report a good fit to the stress-strain data of Treloar (1944). If n=2 Equation (1.34b) is consistent with Gregory's (1979) hypothesis that W is a function of I_1 only.

In summary, there exist a large number of explicit forms for the strain energy function, W. Some are purely empirical or phenomenological, others are derived on the basis of molecular descriptions of rubber. Their mathematical complexity varies considerably; in general those containing a large number of material constants or fitting parameters are

more versatile and able to provide an accurate description of the behaviour of a particular rubber, provided sufficient experiments to characterize the material are carried out. However, a need remains for functions which are simple enough to enable straightforward experimental characterization of the material, preferably from a single uniaxial test, and which may conveniently be implemented in finite element analysis and used correctly by practitioners without specialist knowledge of rubber elasticity. Also, much of the earlier effort was directed at unfilled rubbers; applicability to filled materials and synthetic elastomers needs further examination. More importantly, methods of addressing the imperfections in elasticity in modelling the behaviour of components by FEA are needed; this matter is addressed in Section 1.4.

1.3 Compressibility

1.3.1 *Modification of the strain energy function*

Usually the compressibility of rubber may be safely ignored (as in Section 1.2) as the hydrostatic component of the stress system will be negligible compared to the deviatoric component. In a few instances compressibility should be taken into account. These are:-

(i) when the imposed stress is largely hydrostatic

(ii) when the rubber is more compressible than usual due to high porosity or a compressible filler

(iii) when there is a need to know the volume change on deformation, for example for measurement of crystallinity by dilatometry.

For a compressible isotropic elastic material it can be shown that for a strain energy function $W = W(\lambda_1, \lambda_2, \lambda_3)$, (Treloar, 1975):-

$$s_i = \frac{\partial W}{\partial \lambda_i} \qquad (i = 1, 2, 3) \tag{1.35}$$

where s is the force per unit of undeformed cross-sectional area (the nominal stress) and λ_i are the principal extension ratios. Hence the true stresses, σ_i are given by:-

$$\sigma_i = \frac{\lambda_i s_i}{J} = \frac{\lambda_i}{J} \frac{\partial W}{\partial \lambda_i} \tag{1.36}$$

where

$$J = \lambda_1 \lambda_2 \lambda_3 = \frac{V + \Delta V}{V} \tag{1.37}$$

where V is the unstrained volume. The strain energy function may also be expressed as a function of J and the "volumetrically neutralized" extension ratios, $\hat{\lambda}_i$:

$$\hat{\lambda}_i = \lambda_i J^{-1/3} \qquad (i = 1, 2, 3) \tag{1.38}$$

Thus

$$\hat{\lambda}_1 \hat{\lambda}_2 \hat{\lambda}_3 = 1 \tag{1.39}$$

parallelling the result $\lambda_1 \lambda_2 \lambda_3 = 1$ for an incompressible material.

Then if, for example, $W = \bar{W}(\hat{\lambda}_1, \hat{\lambda}_2, \hat{\lambda}_3, J)$ it can be shown that the difference in two principal stresses of the form given by equation (1.36) is:-

$$\sigma_1 - \sigma_2 = \frac{1}{J}\left(\hat{\lambda}_1 \frac{\partial \bar{W}}{\partial \hat{\lambda}_1} - \hat{\lambda}_2 \frac{\partial \bar{W}}{\partial \hat{\lambda}_2}\right) \tag{1.40}$$

and the hydrostatic pressure, p is given by:-

$$p = \frac{1}{3}(\sigma_1 + \sigma_2 + \sigma_3) = \frac{\partial \bar{W}}{\partial J} \tag{1.41}$$

A possible form for $\partial \bar{W}/\partial J$ is (Murnaghan, 1951):

$$\frac{\partial \bar{W}}{\partial J} = \frac{K}{c}(J^{-c} - 1) \tag{1.42}$$

where K is the bulk modulus and c is a positive constant. Equation (1.42) satisfies the requirements that $p = K\Delta V/V$ for small ΔV in accordance with classical elasticity theory and that p rises towards infinity as the volume approaches zero.

It is convenient to assume that the strain energy function may be separated into two terms; the first governs the deviatoric component and the second the hydrostatic component of strain. Thus:-

$$W = \hat{W}\left(\hat{\lambda}_1, \hat{\lambda}_2\right) + W_c(J) \tag{1.43}$$

It is equally legitimate to express $\hat{W} = \hat{w}(I_1, I_2)$ where $\hat{I}_1$ and $\hat{I}_2$ are volumetrically neutralized strain invariants.

Integration of equation (1.42) yields:-

$$\begin{aligned} \bar{W}(J) &= K(\ell n J - J) \qquad (c = 1) \\ \bar{W}(J) &= \frac{K}{c}\left(\frac{J^{1-c}}{1-c} - J\right) \qquad (c \neq 1) \end{aligned} \tag{1.44}$$

as the second term of equation (1.43). The first term of equation (1.43) is analogous to the strain energy function for an incompressible isotropic material (equation (1.18)) and thus any of the specific forms discussed in Section 1.2 may be substituted. Workers such as Blatz and Ko (1962) and Treloar (1969) have adopted different methods of taking the compressibility into account, although in both cases they modify well-known forms of the strain energy function for incompressible elastic materials. Blatz and Ko (1962) used a modified Mooney-Rivlin type function (see equation (1.23)) whereas Treloar (1969) modified the statistical theory.

However, the basic form of equation (1.43) has been rejected (Ogden, 1976; Peng and Landel, 1975) on the basis of the experiments of Penn (1970) who found that the volume change in simple tension at strains greater than 50% was not strictly proportional to the true tensile stress, as it would be if equation (1.43) held and the bulk modulus was constant, as reported by Wood and Martin (1964). Penn(1970) therefore concluded that the hydrostatic component of the strain energy depended on the state of strain rather than solely on the volume change. However, since the discrepancy was modest, about 15% at a strain of 100%, equation (1.43) can still be expected to be an adequate approximation for most purposes.

1.3.2 *Behaviour of foamed rubbers*

A significant amount of compressibility is found in rubbers containing voids or compressible fillers. Blatz and Ko (1962) studied the behaviour of solid and foamed polyurethanes. They treated the foamed material as a homogeneous continuum and only investigated deformations which caused an increase in the total volume. They concluded that the experimentally observed stress-strain behaviour could be described by a strain energy function of the form:-

$$W = \frac{G}{2}\left(I_2 + 2J - 5\right) \qquad (1.45)$$

and that Poisson's ratio was ¼ for the foamed rubbers investigated.

Gent and Thomas (1959) presented a model for foamed rubber consisting of a network of fibres connected at their ends by particles of undeformed material. They assumed that, for small deformations, the threads were in uniaxial tension or compression and derived an expression for the strain energy which gave a value for Poisson's ratio of ¼ in agreement with Blatz and Ko's (1962) experiment on foamed polyurethane. However, Gent and Thomas's (1959) own experiments on natural rubber foams of various densities yielded a mean value for Poisson's ratio of 0.33. Their model gave good predictions of Young's modulus for foams of various densities without the need for any fitting constants. For larger deformations in compression the model took into account buckling of the fibres and gave a good prediction of the effect of foam density on stiffness although the model required the relationship of stiffness with strain to be determined experimentally for one of the foam rubbers.

1.3.3 *Behaviour of rubber containing voids*

The presence of voids, in an otherwise incompressible material, results in a compressible "composite"; the compressibility is determined by the volume fraction of voids and the shear modulus of the matrix..

Green and Zerna (1954) have derived an expression for the deformation of a thick shell of incompressible material containing a central spherical void at a pressure P. For the case where the material is neo-Hookean and the shell is infinitely thick:-

$$P = \frac{G}{2}\left(5 - \frac{4}{\lambda} - \frac{1}{\lambda^4}\right) \tag{1.46}$$

where λ is the radial extension ratio, and G is the shear modulus of the incompressible material.

Thomas (private communication) has considered the case of an incompressible rubber matrix containing a volume fraction, v, of spherical empty voids subjected to a hydrostatic pressure. For a small strain $e = 1-\lambda$, equation (1.46) becomes:-

$$P = 4eG \tag{1.47}$$

The change in volume of a spherical void of radius, r, due to the strain, e, is $4\pi r^3 e$. Thus, for n voids per unit volume, the macroscopic change in volume is given by:-

$$\frac{\Delta V}{V} = 4\pi r^3 en \tag{1.48}$$

The volume fraction of voids is:-

$$v = \frac{4\pi r^3 n}{3} \tag{1.49}$$

substituting from equations (1.47) and (1.49) into equation (1.48) gives:-

$$K_{eff} = \frac{P}{(\Delta V/V)} = \frac{4G}{3v} \tag{1.50}$$

where K_{eff} is the effective bulk modulus of the material containing voids. It is assumed in equation (1.50) that a macroscopic hydrostatic tension is the equivalent to a negative hydrostatic pressure inside the voids, since the matrix is incompressible. For voids which are not spherical or contain material a larger value for K_{eff} would be expected. Mackenzie (1950) considered a more general case where the matrix was not assumed to be incompressible and the voids were of variable volume. For the specific case of an incompressible matrix and identical spherical voids, his equation reduces to equation (1.50). The analysis of Kerner (1956), however, for the same conditions yields:-

$$K_{eff} = \frac{4G(1-\nu)}{3\nu} \tag{1.51}$$

which approximates to equation (1.50) for small volume fractions of voids.

The behaviour of a material containing a compressible filler will be examined in Chapter 2.

1.3.4 *Poisson's Ratio*

The most widely used measure of compressibility is Poisson's ratio, υ, defined for a measurement in uniaxial tension as:-

$$\nu = \frac{-e_2}{e_1} \tag{1.52}$$

where e_1 and e_2 are the small strains in the direction of the force and in the perpendicular direction respectively. Since, for no change in volume, $e_1+e_2+e_3 = 0$, then $\upsilon = ½$ for an incompressible material.

The above definition is based on classical elasticity theory where the strains are assumed to be infinitesimal. For materials such as rubber where large elastic deformations are possible, υ is a function of strain; for example for an incompressible material $\upsilon = ½ + 3e/8 - 5e^2/16 + ...$. Classical elasticity theory may be used to derive relationships between υ and moduli for various types of deformation as outlined below.

For a pure homogeneous deformation, the strain energy W is given as a function of the principal strains, e_i, as (Timoshenko, 1934):-

$$W = \frac{\Lambda}{2}\left(e_1 + e_2 + e_3\right)^2 + G\left(e_1^2 + e_2^2 + e_3^3\right) \tag{1.53}$$

Λ and G are the first and second Lamé constants (G is equal to the shear modulus).

The principal stresses, σ_i, are given by:-

$$\sigma_i = \frac{\partial W}{\partial e_i} \tag{1.54}$$

By considering uniaxial homogeneous compression, $\sigma_2 = \sigma_3 = 0$ expressions for Poisson's ratio, υ, and Young's modulus, E, may easily be derived:

$$\nu = \frac{-e_2}{e_1} = \frac{\Lambda}{2(\Lambda + G)} \tag{1.55}$$

$$E = G\left(\frac{3\Lambda + 2G}{\Lambda + G}\right) \tag{1.56}$$

Similarly, by considering hydrostatic compression, the bulk modulus, K, is found to be:-

$$K = \Lambda + \frac{2}{3}G \tag{1.57}$$

For a deformation where $e_2 = e_3 = 0$, the constrained compression modulus, E_∞, is:-

$$E_\infty = \Lambda + 2G \tag{1.58}$$

For nearly incompressible material $\Lambda >> G$, thus the distinction between K and E_∞ is insignificant.

One further useful relationship may be derived by substituting from equation (1.57) into equation (1.55) to give:-

$$\nu = \frac{3K - 2G}{6K + 2G} \tag{1.59}$$

Hence, if two of the above material constants are determined experimentally, the others may be calculated from the above equations. For instance, it is often easier to measure G and K and calculate υ from equation (1.59) than to measure υ directly. Experimental techniques for determining these parameters are discussed in the next section.

1.3.5 *Experimental methods of measuring compressibility*

Direct measurements of the bulk modulus of rubbers have been made by, among others, Bridgeman (1945), Wood and Martin (1964), Holownia (1975) and Peng et al (1994). Wood and Martin's measurements were made by pressurising a mercury filled dilatometer. The other workers confined their samples in a rigid metallic container and compressed them with a piston. Good agreement is seen between the results of Wood and Martin (1964) and Holownia (1975) who both report a value of around 2000MPa for the bulk modulus of unfilled natural rubber. Bridgeman's (1945) value is rather higher, perhaps due to the very high pressures used. Holownia (1975) reported a linear increase in bulk modulus with increasing content of carbon black; natural rubber containing 100 parts of black had a bulk modulus of 2300MPa. The behaviour of other rubbers was similar; polybutadiene and a synthetic cis-polyisoprene had slightly lower bulk moduli, about 1800MPa for the unfilled material, and polychloroprene had a similar bulk modulus to natural rubber when unfilled but it rose slightly more with the addition of carbon black. The difference between the natural rubber and synthetic polyisoprene was not commented upon and could suggest some unaccounted for variation between nominally similar materials. Indeed, Penn (1970) has reported variations in compressibility of 20% for nominally identical rubbers.

Direct measurement of Poisson's ratio has proved more difficult, especially for rubbers where Poisson's ratio is very close to 0.5. Often the experimental precision is insufficient to yield meaningful results and Poisson's ratio is better obtained by calculation from experimentally determined values of the bulk and shear moduli. Kugler et al (1990), however, obtained precise measurements using a light scattering technique to provide very accurate measurements of strains. Even so, they report various experimental difficulties.

1.3.6 *Effect of compressibility on the compression stiffness of bonded rubber pads*

If a rubber block is compressed uniaxially so that the surfaces normal to the direction of the compression are constrained from expanding, such as by bonding to rigid plates, the apparent stiffness in compression will be greater than for unconstrained compression. The stiffness will be strongly dependent on the geometry of the block; pads with a large ratio of area to thickness will be stiffest, and a small degree of compressibility of the

material will reduce their stiffness significantly. In the limit of an infinite ratio of area to thickness, the apparent Young's modulus will be E_∞, while in the opposite limit it will be just the Young's modulus E. As is apparent from the discussion above (see equations (1.56) and (1.58)) the ratio of E_∞ to E is large if $\Lambda >> G$. In most engineering applications of rubber blocks in compression the ratio lies in between these limits and it is of interest to have a method for calculating their stiffness.

Various equations have been proposed to relate the apparent compression modulus of such blocks to their geometry and compressibility. Gent and Lindley (1959) derived an expression for the apparent Young's modulus, E_a, of bonded blocks of circular cross-section of an incompressible material. Their derivation is based on the assumptions that the planes parallel to the bonded surfaces remain plane and the planes perpendicular to the bonded surfaces adopt a parabolic profile. The relationships between the applied force and the strains are obtained from classical (small strain) elasticity theory (Timoshenko, 1934) since E_a is a small strain modulus. Their expression for E_a is:-

$$E_a = E(1 + 2S^2) \tag{1.60}$$

where E is the Young's modulus and S is the shape factor defined by:-

$$S = \frac{\text{area of one loaded face}}{\text{force free area}} = \frac{r}{2h} \tag{1.61}$$

for a block of height h and radius r. Gent and Meinecke (1970) extended the analysis to blocks of any cross-section and obtained:-

$$E_a = E(1 + 2.256S^2) \tag{1.62}$$

for a square cross-section. The dissimilarity of equations (1.60) and (1.62) is an indication that use of shape factor as the geometrical parameter is only approximately correct. They suggested that equation (1.60) could be modified to take account of compressibility by the addition of a term for the bulk compliance:

$$E_c = \left(\frac{1}{E_a} + \frac{1}{E_\infty} \right)^{-1} \tag{1.63}$$

where E_c is the apparent Young's modulus of the compressible material when bonded, and E_∞ is the uniaxial compression modulus for the case where lateral expansion is prevented (see equation (1.58)). Equation (1.63) satisfies the requirements that $E_c = E_\infty$ as $S \to \infty$ and $E_c = E$ for $S = 0$. Equation (1.63) was found to work well for square and circular blocks of unfilled natural rubber under small compressions. For larger compressions reasonable agreement with experiment was obtained if the homogeneous compression expression derived from the statistical theory was modified by replacing 3G with E_c. For filled rubbers a modification to equation (1.60) was found to be necessary:-

$$E_a = E(1 + \beta S^2) \tag{1.64}$$

where β was an empirical factor decreasing from 2 towards 1 as the filler loading was increased. Gent and Lindley (1959) suggested that the need for β had its origins in the non-linear "thixotropic" character of filled rubber, and this has been supported by Muhr et al (1988) although they tackled the non-linearity issue more directly by regarding E and E_a as strain-dependent.

Lindley (1979), adapted the analysis of Gent and Lindley (1959) to take account of compressibility. By use of classical (small strain) elasticity theory and making some assumptions about the strain distribution in a bonded rubber block under compression he derived a small strain compression modulus for a cylindrical block:-

$$E_c = 2G + \frac{\Lambda G}{\Lambda + G}\left\{1 + \frac{6\Lambda S^2}{(\Lambda + G)}\left(1 - \frac{32GS^2}{4(\Lambda + G) + 33GS^2}\right)\right\} \qquad S < S_a \tag{1.65a}$$

$$E_c = \Lambda + 2G - \frac{\Lambda^2}{15(\Lambda + G)}\left(\frac{S_a}{S}\right)\left(8 - \frac{S_a}{S}\right) \qquad S_a \le S \tag{1.65b}$$

$$S_a^2 = \frac{4(\Lambda + G)}{15G} \tag{1.65c}$$

Λ is the second Lamé constant (see section 1.3.4) and G is the shear modulus.

Equations (1.65) were found to agree to within 6% with finite element analysis (Lindley and Teo, 1978) for blocks of various shape factors.

A more exact solution to the same problem was derived by Moghe and Neff (1971) and found to agree well with experimental results in the literature (eg. Gent and Lindley, 1959). Since the solution involves series of Bessel functions, some computation is required to provide numerical values of E_c and for many applications the approximate equations (1.63) or (1.65) are adequate. Chalhoub and Kelly (1986) provide other approximations to the exact solution for small shape factors:-

$$E_c = 6GS^2(1 - 8GS^2/K) \qquad S \leq (K/12G)^{1/2} \tag{1.66}$$

and

$$E_c = \left(\frac{1}{6GS^2} + \frac{4}{3K}\right)^{-1} \qquad S \leq 25 \tag{1.67}$$

The case where the cross-section of the block is rectangular, rather than circular, has been considered by Conversey (1967) who derived:-

$$E_c = \frac{96GS^2}{C_4} \tag{1.68}$$

C_4 is a parameter dependent on the width to length ratio of the cross-section of the pad and the compressibility of the rubber. Since its numerical evaluation from the appropriate analytical expression is somewhat labourious, Conversey (1967) provided values for C_4 in tables.

As equations (1.66) to (1.68) are based on classical elasticity theory they are valid only for small compressions. However, as they relate the bulk modulus to the compression stiffness, they enable the bulk modulus to be estimated from a straightforward test in uniaxial compression.

In Chapter 2, a comparison is made of the predictions of the equations discussed in this Section.

1.4 Departures from perfect elasticity

The theory developed in Section 1.2 has assumed that rubber behaves as a perfectly elastic material. Thus it was assumed that the stored energy, and therefore the stress, depends only on the magnitude and geometry of the strain, not on the method (or path) adopted in obtaining it. It is clear that although this view provides a sensible first approximation to the behaviour of rubbery materials it is never strictly true and for some materials the departures from perfect elasticity are quite significant.

In this section the various departures are described and methods of modelling them discussed.

1.4.1 *Hysteresis*

On stretching and relaxing rubber energy is dissipated. As a consequence the rubber appears softer on unloading than on loading. The energy loss or hysteresis is given by the area between the loading and unloading curves on a force-deformation plot (Figure 1.6). Harwood et al., (1967) found that the hysteresis was approximately proportional to the energy input for filled and unfilled natural rubber, polyacrylonitrile-butadiene and polystyrene-butadiene. The hysteresis, as a proportion of the energy input, is greater in a filled than an unfilled rubber. This has been attributed to breakdown of the network of carbon black particles dissipating energy (see Sections 1.4.4 and 1.4.5) (Payne, 1962). In unfilled natural rubber the hysteresis becomes large at high strains. This has been attributed to energy losses associated with strain crystallization. A definition of hysteresis, in terms of linear viscoelasticity theory, is given in Section 1.4.9.

The hysteresis is usually especially large for the first cycle. This semi-permanent stress-softening, as contrasted with the rapidly recoverable softening responsible for hysteresis in subsequent cycles, is discussed in the next section.

1.4.2 *Softening due to repeated stressing - Mullins' effect*

If a series of repeated strains is applied to a sample of rubber, the rubber becomes progressively softer on each loading cycle. This effect was investigated for natural rubber in uniaxial tension by Mullins (1947); thus it became known as the Mullins'

(a)

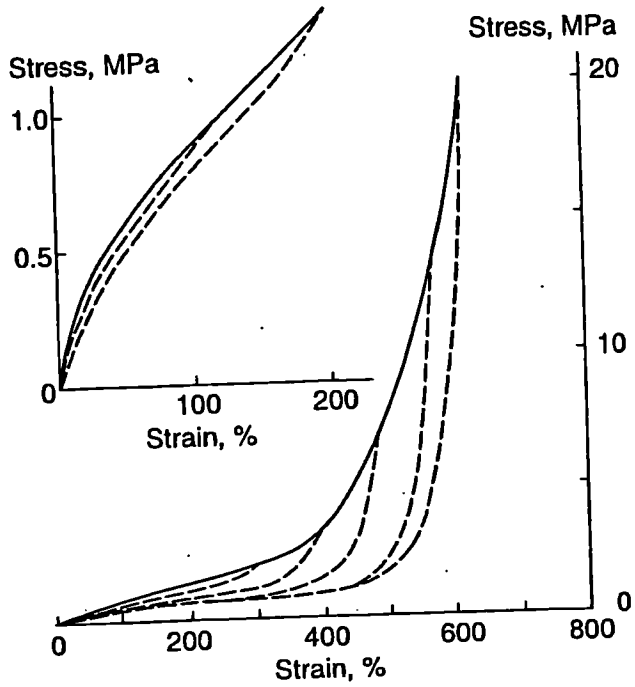

(b)

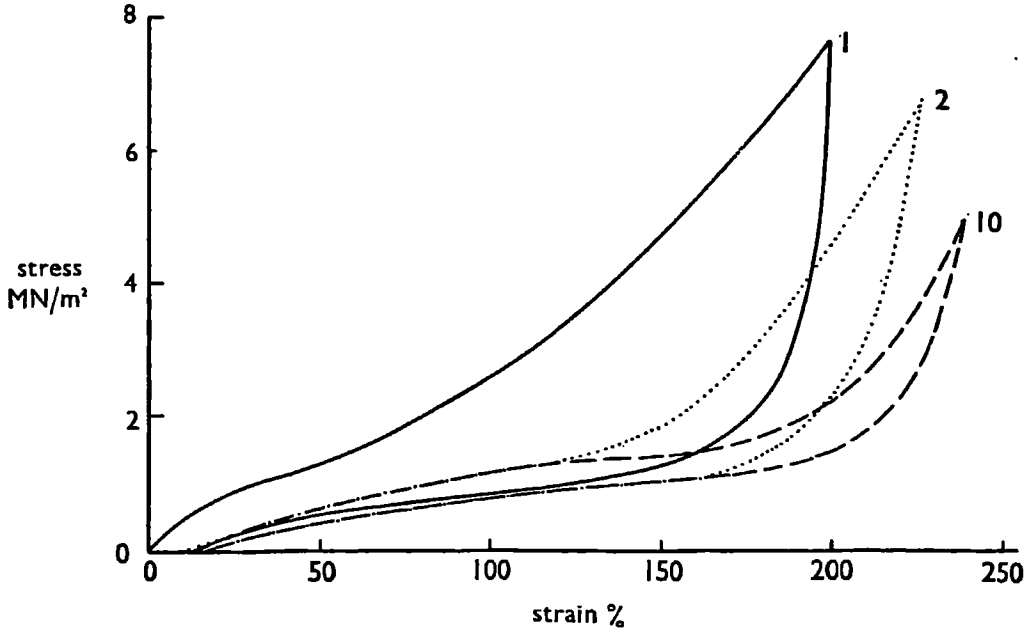

Figure 1.6 Hysteresis loops for natural rubber.
(a) First cycle loops for unfilled natural rubber extended to various strains.
(b) First, second and tenth cycle loops for a rubber containing 50 parts of carbon black.
(From Lindley, 1974).

effect. Typical curves are shown in Figure 1.7 in which the permanent set (see Section 1.4.7) has been subtracted from the length measurements so that all curves pass through the origin. The main features of the behaviour are:-

(i) The softening occurs for all strains smaller than the maximum strain previously applied to the rubber.

(ii) The largest reduction in stiffness occurs after the first cycle. After several cycles a steady-state is approached when the softening effect of further cycling becomes minimal.

(iii) If rubbers are compared at equal strains, the amount of softening is much greater in rubbers containing a reinforcing filler. However, if comparisons are made at equal stress similar behaviour is seen in filled and unfilled rubber (Harwood et al., 1965).

(iv) The softening recovers slowly at room temperature but is accelerated at elevated temperatures.

Similar softening behaviour has been reported for polyurethane (Trick, 1960) and for partially crystalline polymers (Puett et al., 1965), with the softening mechanism for the partially crystalline polymers being attributed to structural breakdown of crystalline regions.

Discussion of softening due to large numbers of repeated cycles (cyclic stress relaxation and creep) will be deferred to section 1.4.8 where comparisons with the equivalent static effects can more conveniently be made.

1.4.3 *Effect of strain amplitude on stiffness*

The Mullins' effect primarily describes softening at moderate or large strains. Another interesting feature in filled rubber is the high modulus at small strains in previously unstrained rubber (Figure 1.8). Investigation of small strain deformation was carried out by Fletcher and Gent (1953) and Payne (1962) on a range of filled natural rubber compounds. They measured the dynamic modulus, that is the ratio of stress and strain amplitudes in a deformation which varied sinusoidally with time (see section 1.4.10).

The main features of the "Payne effect" are:-

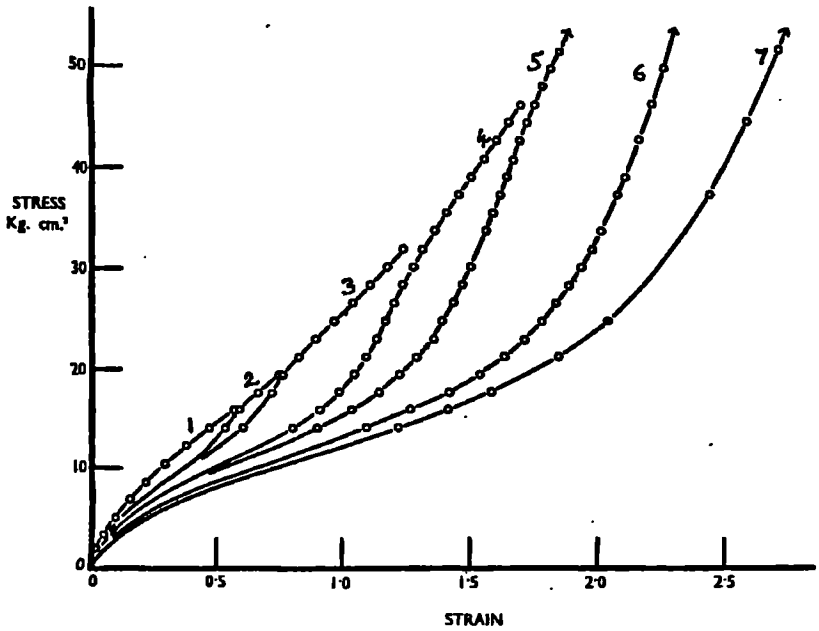

Figure 1.7 Effect of repeated straining on a natural rubber compound containing 50 parts of carbon black. The strains were applied in the order 1 to 7 indicated.
(From Mullins and Tobin, 1954)

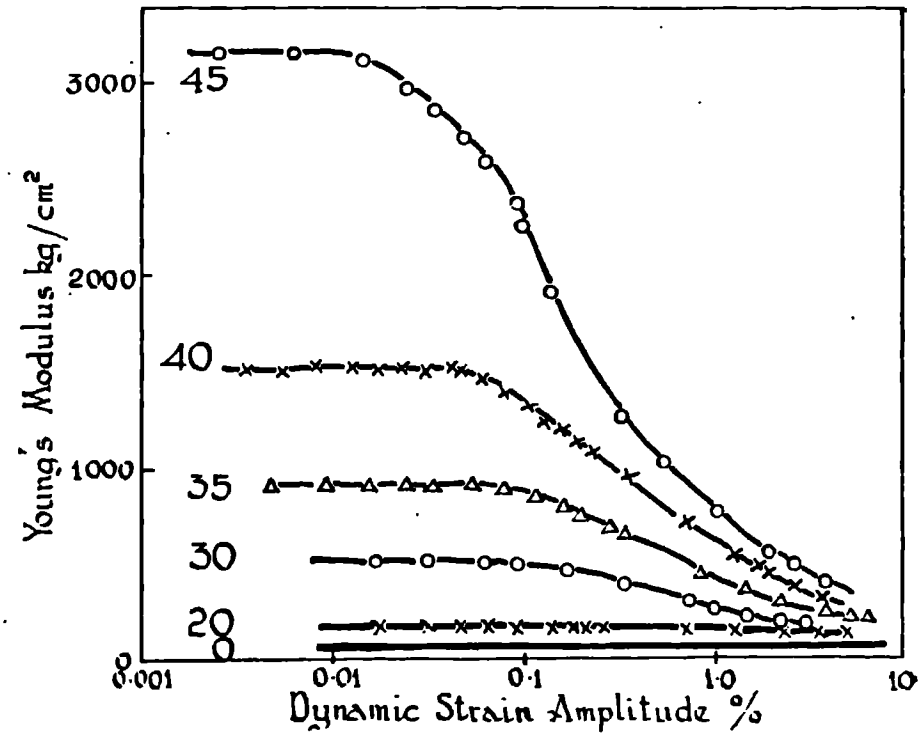

Figure 1.8 Variation of Young's modulus with strain amplitude for natural rubber vulcanizates containing various loadings of carbon black.
(From Payne, 1962)

(i) At very low strain amplitudes (less than 0.01%), the modulus is independent of strain amplitude and strongly dependent on filler loading; for example the modulus of a rubber containing 45 parts of carbon black was about 60 times the modulus of the equivalent unfilled rubber.

(ii) If the strain amplitude was raised above 0.1% the modulus decreased with increasing strain amplitude. The decrease was largest for highly filled rubber and zero in unfilled rubber. The rate of decrease of the modulus was fastest below 10% strain. Thus the stiffening effect of the filler was much reduced for large strains.

(iii) The dynamic modulus of filled rubber decreases with increasing temperature. This contrasts with the behaviour of unfilled rubber which stiffens if the temperature is raised in accordance with the statistical theory (equation 1.5). Filler also increases the tendency for the modulus to increase with increasing strain rate.

(iv) On subsequent deformations the dynamic modulus was much lower than on the first deformation but, if the rubber was left unstrained for a while, the modulus would "recover" towards its original high value.

Another related feature of the non-linearity of the force-deformation behaviour in filled rubber is the effect of superimposing a small cyclic deformation on a large strain as, for example, in an antivibration mount operating under a static load. It was reported by Dillon et al (1944) that the ratio of dynamic to static modulus in filled rubber was much greater than 1. More exact definitions of these terms were provided by Mullins (1950) and Gregory (1984) (Figure 1.9), who explained that the modulus of the small cyclic strain (the dynamic modulus) was determined from the stiffness of the deformed rubber in retraction rather than in extension (the static modulus). Further care is needed in establishing whether the relevant static modulus is determined from the tangent to the stress-strain curve at an appropriate amplitude (the tangent modulus) or from the ratio of stress to strain at that amplitude (the chord or secant modulus). Gregory also evaluated, for a highly filled natural rubber vulcanizate, the variation of dynamic shear modulus with dynamic strain amplitude and with static shear strain. He found a large decrease with increasing dynamic amplitude up to 10%, especially in the region of 1-2% and a slight reduction (5-10%) with increasing static strain up to about 40% static strain followed by a gradual increase with higher strains. The small strain modulus was not

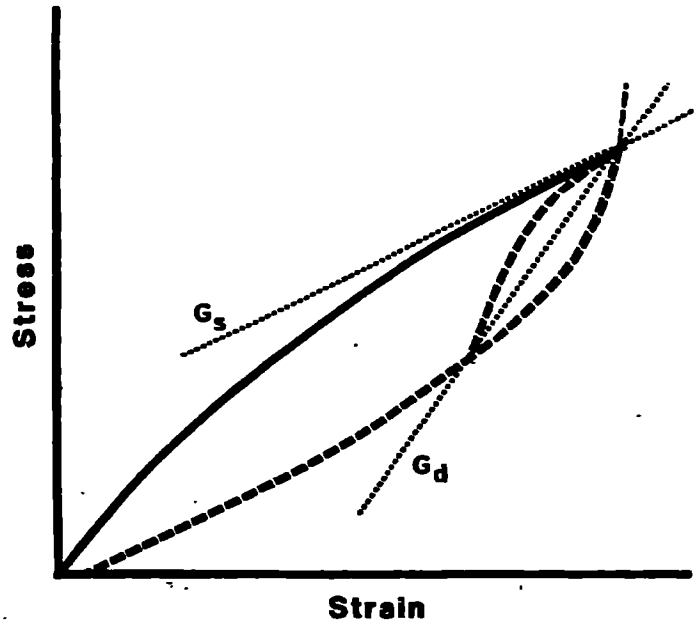

Figure 1.9 Relationships between static, G_s, and dynamic, G_d, moduli for a rubber subjected to vibration about a mean strain.
(From Gregory, 1984)

grossly affected by the addition of a static strain.

1.4.4 *Effect of carbon black on the stiffness of rubber*

The stiffness of filled rubber is related to the type of carbon black. Both the surface area and structure of the black are important. Structure refers to the extent to which individual (approximately spherical) particles adhere to one another to form aggregates. Medalia (1978) reported that the small strain modulus was principally determined by the surface area of the black with a higher modulus resulting from blacks with a large surface area, equivalent to a small particle size. The large strain modulus depended mainly on the structure of the black. A greater reduction in the dynamic modulus with increasing strain amplitude was seen for blacks with less aggregation.

The small strain modulus was reduced if the dispersion of the carbon black aggregates was improved, for example, by extensive milling (Boonstra and Medalia, 1963) though the modulus at high strains remained largely unaffected. The effect of an increase in crosslink density was to raise the modulus at all strains; thus changes in crosslink density are not believed to alter significantly the behaviour of the carbon black (Payne et al, 1972).

Payne et al (1972) attributed much of the stiffening effect of carbon black to a hydrodynamic effect, parallelling Einstein's (1906, 1911) theory of suspension of spheres in a liquid. The Guth equation (1945):

$$G_f = G_g (1 + 0.67\alpha v + 1.62\alpha^2 v^2) \qquad (1.69)$$

where G_f and G_g are the moduli of the filled and gum rubber respectively, α is the aspect ratio of the carbon black and v is the volume fraction of filler, is applicable for small volume fractions of filler. It has been widely applied to obtain a quantitative estimate of the stiffening. The aspect ratio in equation (1.69) was defined as the length to breadth ratio of a rodlet. Cohen (1947) reported satisfactory agreement between equation (1.69) and experiment for $\alpha = 6$ up to carbon black loadings of about 30 parts. For higher loadings the stiffening was greater than predicted by equation (1.69). Payne et al (1972) found that somewhat higher values of α were needed to fit experimental data than

electron microscopy studies (Medalia, 1974) suggested were appropriate but, in view of the difference in shape between idealized rodlets and actual carbon black aggregates, the inconsistencies are not unreasonable. Also, other mechanisms of reinforcement are likely. For example, an additional stiffening effect, caused by a shell of immobilized rubber within and around the carbon black aggregates was identified by Harwood et al (1969). This was developed by Medalia (1974) into a theory based on a concept of "occluded" rubber which behaved like filler.

1.4.5 *Mechanisms of stress softening*

A model for describing the Mullins' effect was proposed by Mullins and Tobin (1954) who drew attention to the fact that the stress-strain curve for the filled rubber was similar to that for the unfilled, except that the increase in stiffness with strain occurred at lower strains and was more rapid. They adopted a model comprising regions of hard and soft material which deformed in series under an applied stress. If the stress was raised above the maximum previously applied some material from the hard region became soft. Using a simple equation in which deformation of the hard region was assumed to be negligible they were able to fit a set of stress-strain curves by choosing an appropriate value for the volume fraction of rubber in the soft regions. However, the predictive power of their model was limited by the lack of any theoretical basis for the value of this parameter.

Many workers have suggested that the softening of filled rubbers is caused either by changes in the carbon black structure or by changes in the interactions between the carbon black and the rubber molecules. Bueche (1960, 1961) proposed a molecular model in which the softening was caused by the polymer chains breaking free from the filler particles, or by highly extended chains breaking. He derived an equation which was able to account for Mullins' effect in terms of material parameters related to the size and distribution of filler particles and the strength of the bonds in the polymer chains. However, as an independent measure of these parameters was difficult to obtain, the proposed molecular mechanisms remained speculative. Bueche (1961) used his model to account for the absence of a softening effect in unfilled rubber in contradiction to the results of later experiments where softening in unfilled rubber was seen (Harwood et al, 1965). Thus, although his model goes some way towards explaining the behaviour using

a molecular approach, some modifications are needed.

Payne (1965) attributed the large reduction in dynamic modulus to the existence at low strains of an elastic component of the modulus due to a carbon black network which is destroyed at higher strains. He (Payne, 1962) proposed that the carbon black structure reformed, either when the rubber was left undeformed, or during a short retraction cycle as in the case of measurement of a dynamic stiffness, thus accounting for hysteresis, recovery and set. Later workers have attempted to incorporate these mechanisms into quantitative models (Klüppel and Heinrich, 1995) in which the existence and breakdown of primary and secondary carbon black networks are defined by parameters, such as the carbon black loading, and forces required to break the network. Although such workers report success in modelling the behaviour of real materials and some electron microscopy evidence exists in support of the existence of carbon black structures (Medalia, 1974) uncertainty about the exact mechanisms of carbon black reinforcement remains.

Other recent workers have adopted a more phenomenological approach to modelling the stress-softening behaviour in rubber, often attempting to incorporate Mullins' effect, hysteresis and the dependence of the modulus on the strain amplitude in a single model. These workers are motivated by the need for suitable equations for use in Finite Element packages. Some have used the methods of continuum mechanics to derive somewhat elaborate equations which are intended to be amenable to three dimensional finite element modelling. For example, Simo (1987) and Miehe (1995) used the concept of a damage parameter to reduce the stress in the second cycle in a way which depended on the maximum strain seen in a previous cycle. Simo (1987) claimed in this way to take account of the strain amplitude dependence of the storage modulus but, since the damage parameter operates irreversibly, anomalous behaviour is predicted for cycles of decreasing strain amplitude as no increase in modulus at small strains can occur. A similar difficulty is apparent in Miehe's (1995) model in predicting the combined effects of strain softening and hysteresis as his concept of continuous damage results in loading curves always being softer than the previous unloading curve. Besdo and Ihlemann (1996) developed an eight parameter model which takes into account hysteresis, set and Mullin's effect. The authors were careful to point out the limitations of their model in

that it is unable to take account of softening occurring in a direction-dependent manner, nor does it address rate-dependent effects. The mathematical complexity of these models restricts their practical applicability.

Johnson and Beatty (1993) formalized the hard and soft region model of Mullins and Tobin (1954) to produce a much simpler model. Ogden and Roxburgh (1999) further developed these ideas to produce an isotropic model based on a hyperelastic strain energy function modified by a term containing a damage parameter to model the softening behaviour which only operated when the strain energy was decreasing. Subsequent loading curves followed the previous unloading path until the strain energy exceeded the previous maximum at which point the behaviour was described solely by the unmodified strain energy function until unloading commenced again (Figure 1.10). A possible damage function was suggested which required two constants. For a general strain, the model predicted that the stresses would decrease pro-rata (see Section 8.3.4).

All of the above authors (Simo, 1987; Miehe, 1995; Besdo and Ihlemann 1996; Ogden and Roxburgh, 1999) presented comparisons between their model and appropriate uniaxial experiments and showed good agreement with the chosen data though the effects of different modes of deformation and strain history were not thoroughly evaluated.

1.4.6 *Viscoelastic behaviour*

Sections 1.4.1 to 1.4.5 have focussed on departures from perfect elasticity resulting from effects of previous deformations on the rubber. Additional changes occur as a function of time, reflecting the viscoelastic nature of rubbery materials which is, in some respects, analogous to the behaviour of viscoelastic liquids. In the following sections the most important experimental manifestations of viscoelastic behaviour will be described, followed by a brief interpretation of the behaviour in terms of the linear theory of viscoelasticity.

1.4.7 *Stress relaxation, creep and set*

If a vulcanized rubber is deformed to a constant strain, the magnitude of the stress gradually diminishes. This is stress relaxation. If the rubber is deformed to a constant

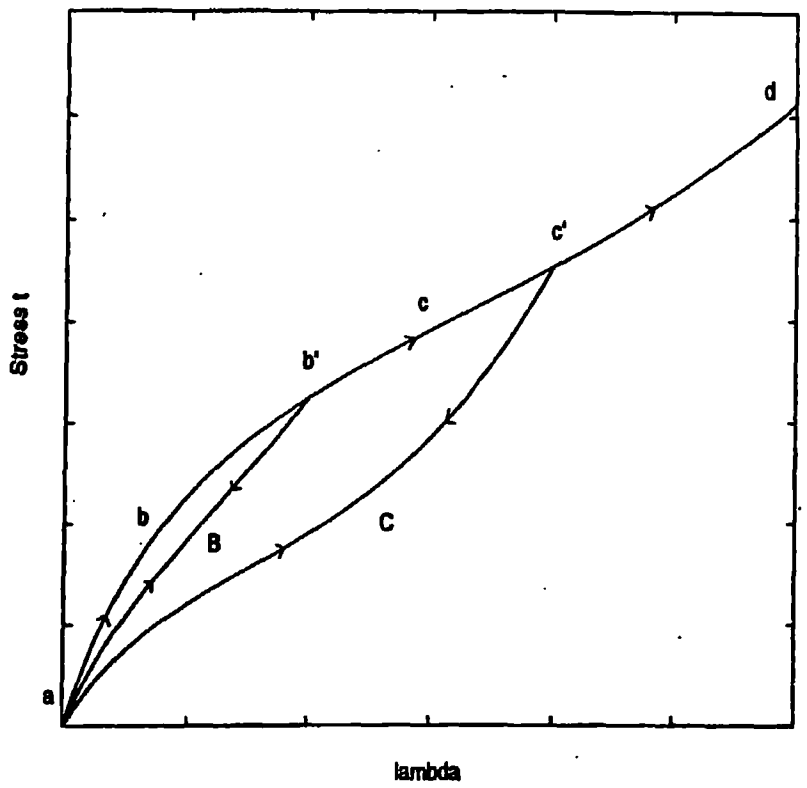

Figure 1.10 Idealized Mullins' effect, assumed in the model of Ogden and Roxburgh (1999). a to d represents loading of virgin testpiece. First loading path is along b. First unloading path is along B. Second cycle loading along B where damage parameter is operative until b' where the behaviour reverts to the virgin curve. Second cycle unloading along C. Third cycle loading along C(with damage parameter) until c' where behaviour reverts to virgin cycle to d.

stress its length gradually increases. This is creep. If the stress is removed the rubber does not return to its original length, but retains some deformation known as set. Gent (1962a) has derived expressions relating these processes and found that, for unfilled natural rubber and polystyrene butadiene, the rates of stress relaxation and creep are comparable once geometric non-linearity (due to the change in shape of a testpiece during uniaxial extension) has been taken into account; thus it is reasonable to assume that they are separate manifestations of a single relaxation process. The amount of stress relaxation was found to be approximately proportional to the logarithm of time, typically 2% per tenfold increase in time, except at very long times when chemical, rather than physical, processes become significant. The relaxation rate was largely independent of the magnitude of the deformation up to strains of about 200%. At higher strains, a sharp increase in rate was seen (Gent, 1962b) which correlates with the amount of strain crystallization (see section 1.5). In non-strain-crystallizing rubbers, such as butyl rubber and polystyrene-butadiene, a decrease in stress relaxation rate was seen with increasing strain.

For filled natural rubber, even at moderate strains, a different picture emerges (Gent, 1962b). The rates of stress relaxation and creep are much higher than for unfilled vulcanizates, typically in the region of 5-10 per cent per tenfold increase in time for a natural rubber containing 54 parts of carbon black. This may be attributed to "strain amplification" (Mullins and Tobin, 1965); the local strains in the rubber molecules being greater than the macroscopic strain due to the inextensibility of the filler. Thus the rate of stress relaxation would be expected to be similar to that in unfilled rubber at much greater extensions as was found experimentally.

1.4.8 *Stress relaxation and creep under cyclic loading*

Similarities have been drawn between so-called "static" stress relaxation and creep as described above and "cyclic" stress relaxation and creep, in which the testpiece is subjected to a large number of loading and unloading cycles to a constant deflection or load. Derham and Thomas (1977) found a linear relationship between the amount of creep and the logarithm of the number of cycles, analogous to the linear relationship between static creep and the logarithm of time. However, the amount of creep in the cyclic tests was much greater than in the static tests - 17.4% per tenfold increase in time

for a natural rubber vulcanizate containing 40 parts of carbon black, as opposed to 2% per tenfold increase in time for unfilled natural rubber, under a load which caused an initial extension of 100%. The high cyclic creep rates were not seen, however, at extensions below about 200% in unfilled rubbers, and indeed Hillmer and Scheele (1970) report considerable data for unfilled rubbers under various loading and unloading cycles to low strains which show cyclic creep rates significantly lower than the static rates.

The mechanism proposed by Derham & Thomas (1977) to account for the very high cyclic creep rates was that bond rupture (probably of crosslinks) occurred during straining due to stress concentration arising from the presence of crystallites in strain crystallizing rubbers such as natural rubber. On subsequent relaxation followed by further straining the crystallites melted and reformed in different locations, causing further bond rupture. Further work (Pond and Thomas, 1979; Pond 1989) on a range of crystallizing and non-crystallizing rubbers supported strain crystallization as contributing to the high cyclic creep rates although for certain non-crystallizing rubbers (polystyrene butadiene and EPDM) the rates were still much higher than comparable static creep rates, suggesting some sort of mechanism, akin to strain crystallization, was operating. Swelling measurements supported breakage of crosslinks as the cause of a significant part of the creep.

McKenna and Zapas (1981) compared cyclic creep and cyclic stress relaxation rates with the static rates for a filled polybutadiene and found that the stress relaxation data showed far less emphatically the effect of Derham and Thomas (1977). Davies et al (1996), however, reported broadly similar behaviour to that of Derham and Thomas (1977) for cyclic creep and stress relaxation for natural rubber containing various loadings of carbon black and a filled polystyrene butadiene, though they did not attempt quantitative comparisons.

1.4.9 *Linear viscoelasticity theory*

Stress relaxation and creep, as examples of viscoelastic behaviour, may be described in terms of a theory of viscoelasticity.

For linear viscoelastic behaviour the stress at the present time may be expressed as the sum (or integral) of the stresses resulting from all previously applied strains. This is the Boltzmann superposition principle. For the case of simple shear, linear viscoelastic behaviour is described by the equation (Ferry, 1970):-

$$\tau(t) = \int_{-\infty}^{t} G(t - t') \dot{\gamma}(t') dt' \qquad (1.70)$$

where τ is the shear stress at time t, G(t-t') is the relaxation modulus, $\dot{\gamma}$ is the shear strain rate and the integral is carried out over all past time. The theory is approximately applicable to unfilled rubbers at moderate strains which show linear stress-strain behaviour in simple shear.

1.4.10 *Dynamic behaviour*

As rubber is frequently used in applications such as vibration isolation, its behaviour when subjected to cyclic deformations is of interest. For example, if a sinusoidally varying shear stress is applied to rubber, the shear strain will also vary sinusoidally but will lag behind the stress by a constant phase angle, δ. Tanδ is a measure of the energy loss or hysteresis or damping of the material. Hence for linear stress-strain behaviour, the stress τ, resulting from a sinusoidal strain of amplitude γ_o and angular frequency ω, given as a function of time t, as:-

$$\gamma = \gamma_o \sin(\omega t) \qquad (1.71)$$

is:-

$$\tau(t) = \gamma_o (G' \sin \omega t + G'' \cos \omega t) \qquad (1.72)$$

where G' represents the ratio of stress in phase with the strain to the strain (the in-phase modulus) and G" represents the stress out of phase with the strain to the strain (the out of phase modulus). Equation (1.72) is often written in complex number notation as:-

$$\tau(t) = \mathrm{Re}\left\{\gamma_o (G' + iG'') e^{i\omega t}\right\} \qquad (1.73)$$

with the complex modulus, G*, defined as:-

$$G^* = G' + iG'' \tag{1.74}$$

Equation (1.72) represents a sinusoidally varying stress, out of phase with the strain. Thus, it may be written as:-

$$\tau(t) = \tau_o \sin(\omega t + \delta) \tag{1.75}$$

where σ_o is the stress amplitude and δ the phase angle. Expanding (1.75) gives:-

$$\tau(t) = \tau_o(\sin\omega t \cos\delta + \cos\omega t \sin\delta) \tag{1.76}$$

comparison of equations (1.72) and (1.76) gives:-

$$G' = (\tau_o/\gamma_o)\cos\delta \tag{1.77}$$

$$G'' = (\tau_o/\gamma_o)\sin\delta \tag{1.78}$$

and

$$\frac{G''}{G'} = \tan\delta \tag{1.79}$$

One important consequence of the theory of linear viscoelasticity is that it enables interrelations between the relaxation modulus, creep compliance, loss and storage moduli to be derived (Ferry, 1970; Tschoegl, 1989)

In general G' and G" are not constants but depend on the frequency and amplitude of the vibration. The amplitude dependence of the modulus has already been discussed (Section 1.4.3). The effect of frequency on the modulus of filled rubbers was studied over a fairly small range of frequencies by Fletcher and Gent (1953). Warnaka (1963) looked at a filled polystyrene butadiene over a frequency range of 50 to 150Hz and Payne & Whittaker (1971) studied a filled polybutadiene. All report little effect of frequency on the modulus but Mullins (1950) reports an increase in dynamic modulus with increasing frequency, especially at low temperatures. More extensive measurements by

Ahmadi and Muhr (1992) over a frequency range of 5 to 400Hz showed a small increase in dynamic shear modulus with frequency for low damping rubbers such as unfilled natural rubber. A larger increase was seen for epoxidized natural rubber and polybutadiene. The addition of filler caused a large increase in the magnitude of the shear modulus, as expected, but no significant increase in its frequency dependence.

It has been shown (Williams et al., 1955) that a decrease in frequency has the same effect on the viscoelastic parameters of a rubber as an increase in temperature.

1.4.11 *Viscoelastic behaviour in filled rubbers*

As indicated in Section 1.4.3 filled rubbers exhibit markedly non-linear stress-strain behaviour and recoverable softening at small strains following a deformation. Such behaviour means that the theory of linear viscoelasticity is not applicable. Various non-linear theories of viscoelasticity have been developed, such as that of Bernstein et al. (1963) who report success in modelling the stress relaxation behaviour of an unfilled polybutadiene with an equation containing three fitted time-dependent functions, though since they do not compare their results with those predicted from a linear theory of viscoelasticity, it is not clear whether their approach offers any advantage over simpler models. Neither is the applicability of this or other such theories to the more non-linear behaviour of filled rubbers well established.

1.4.12 *Modelling of viscoelastic behaviour of rubbers*

The behaviour of a viscoelastic material may be considered as comprising a perfectly elastic response (modelled as a Hookean spring) and a viscous response (modelled as a dashpot). By means of many elements of either the Maxwell type (a spring in series with a dashpot) or the Voigt type (a spring in parallel with a dashpot) with appropriately chosen values for the spring stiffnesses and dashpot viscosities a good description of the actual behaviour may be obtained.

A simple model of the spring and dashpot type, is shown in Figure (1.11) and predicts qualitatively stress relaxation, creep and dynamic behaviour in unfilled rubbers. k and η are not constants but depend on frequency and amplitude as outlined in Section 1.4.10.

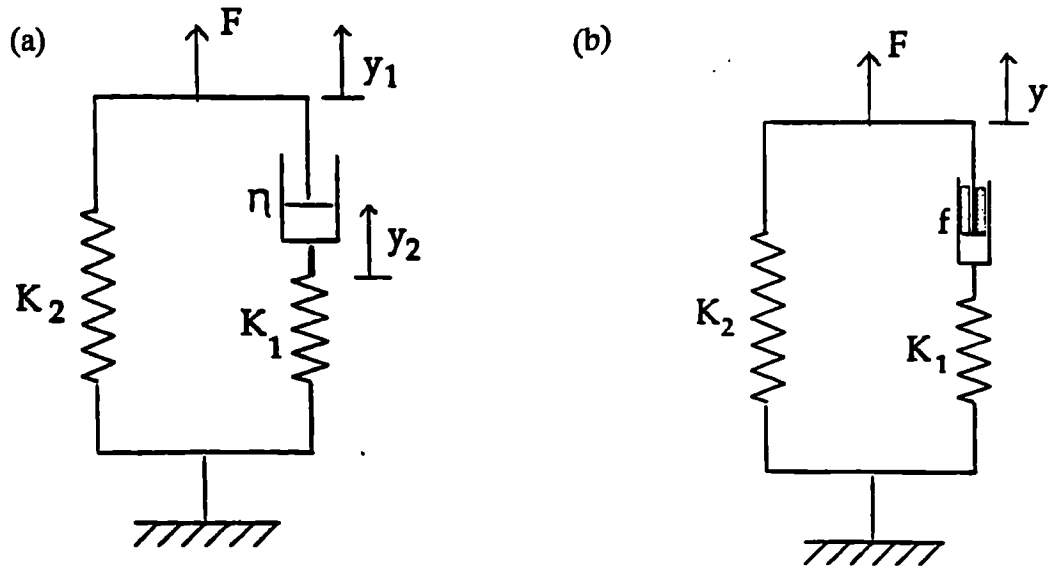

Figure 1.11 Models of rubber viscoelasticity. (a) spring and dashpot model, (b)spring and friction pad model.
(From Muhr, 1991)

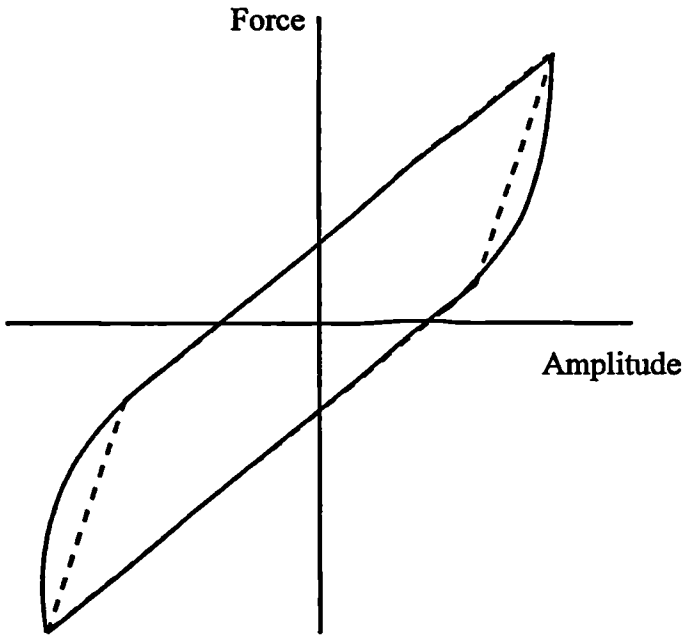

Figure 1.12 Schematic diagram to illustrate the difference between the hysteresis loops predicted by the spring and friction pad model of Figure 1.10 (-------), and the behaviour of a fillled natural rubber vulcanizate (——).

The presence of only one dashpot leads to a single relaxation time which results in a much sharper peak in damping as a function of frequency than is seen in practice.

For filled rubber, the strong amplitude dependence of the modulus means that the stress resulting from a sinusoidal strain is not sinusoidal. Also, the dynamic/static ratio is greater than one (see section 1.4.3). The simplest model to take account of these features is a combination of two springs and a friction pad (Figure 1.11); though the qualitative predictions of the model are sensible, the details, such as the predicted shape of the hysteresis loops, are too idealised (Figure 1.12).

The use of frictional sliders and springs was developed as a "triboelastic" model by Coveney et al. (1995) in order to reduce the excessive frequency sensitivity of conventional spring and dashpot models and to model nonlinear effects such as amplitude dependence of dynamic stiffness (see also Ahmadi and Muhr, 1997)

1.5 Crystallization in rubber

As outlined in Section 1.1 two types of phase transition may take place in rubber, the glass transition and crystallization. In both cases, the rubbery material loses its hyperelasticity and its modulus increases by several orders of magnitude.

1.5.1 *Thermodynamics of phase transitions*

Crystallization may be described formally as a first order phase transition; that is there are discontinuities in the values of properties such as volume or enthalpy. Thus the melting temperature is ideally infinitely sharp and independent of the amount of material in each phase. The glass transition, on the other hand, is a second order phase transition, that is the rate of change of enthalpy (or volume) with temperature is discontinuous, and the glass transition temperature is dependent on the kinetics of the system and cannot be defined purely as a thermodynamic quantity.

For a first order phase transition at constant pressure, the change in Gibbs free energy of melting is given by:-

$$\Delta G = G_a - G_c \tag{1.80}$$

$$\Delta G = \Delta H - T\Delta S \tag{1.81}$$

where G_a and G_c are the Gibbs free energies of the amorphous and crystalline phase respectively, ΔH is the enthalpy of melting, T is the temperature and ΔS is the entropy of melting. At equilibrium the free energies of the two phases are equal, thus $\Delta G = 0$ and equation (1.81) becomes:-

$$T_m = \frac{\Delta H_m}{\Delta S_m} \tag{1.82}$$

where T_m is the equilibrium melting temperature. The dependence of ΔH and ΔS on temperature is generally rather weak and at small undercoolings the Gibbs free energy change increases with decreasing temperature, T, approximately as

$$\Delta G = \Delta H_m\left(1 - \frac{T}{T_m}\right) \tag{1.83}$$

For a sharp, well-defined melting temperature to be observed experimentally a perfect arrangement of the crystal phase is required. Also, the crystals must be large to minimize additional contributions to the free energy arising from the surface energies of crystals. In rubbery materials such conditions are seldom observed. Moreover, the thermodynamic analysis takes no account of kinetics. In rubbers, the crystallization kinetics may be extremely slow and appreciable rates occur only at temperatures well below T_m. For crystallization to be favourable the free energy of the crystalline phase, G_c, should be as small as possible relative to the amorphous free energy G_a. It can be seen from equations (1.80), (1.81) and (1.83) that the thermodynamic driving force for crystallization increases as the temperature is reduced, the difference in the enthalpy between the crystalline and amorphous phase is as large as possible and the entropy change as small as possible.

1.5.2 *Kinetics*

A plot of crystallization with time is typically sigmoidal in shape (Figure 1.13). At first,

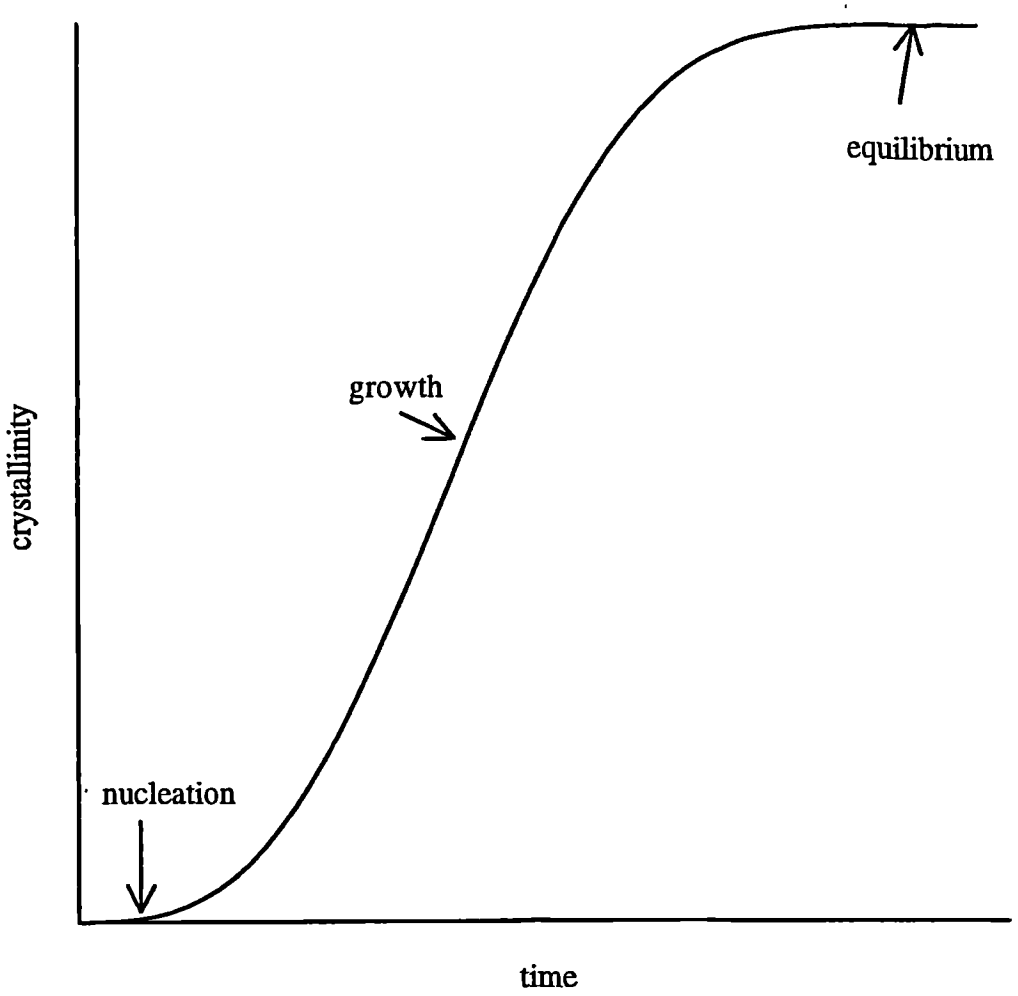

Figure 1.13 **Typical crystallization curve.**

while crystals are nucleating, crystallization is slow. During the next stage, the growth phase, crystallization proceeds much faster. Finally the crystallization rate slows down as an "equilibrium" state is approached; for polymers this limit is often well short of 100%.

(i) Nucleation

In most circumstances, the free energy barrier for heterogeneous nucleation is lower than the free energy barrier for homogeneous nucleation. Heterogeneous nucleation requires an effective nucleating agent such as impurities, solid precipitates or randomly occurring regions of aligned rubber chains (see Section 1.5.4). Gent (1954a) and Stevenson (1983) found that preheating testpieces for up to two hours at 90°C resulted in a longer and more reproducible nucleation time.

For crystallization to proceed it is necessary for the nuclei to reach a critical size. Below this size, growth is thermodynamically unfavourable; that is the free energy loss of the melt in transforming into crystal is less than the free energy gain of forming new surfaces. These sub-critical size nuclei will disappear through normal random motion of the molecules. Above the critical size nucleus growth will take place. For nuclei to reach the critical size relies on the random movements of the polymer chains to result in a sufficiently large ordered region. The larger the critical size and the less mobile the polymer chains, the longer will be the nucleation time. As the energy requirement to create new surfaces is a hindrance to crystal formation, additions to the crystal nucleus will occur preferentially at incomplete corners and edges.

Some degree of undercooling usually occurs before polymer crystallization takes place in order to overcome the barrier caused by the formation of the free surfaces: as the temperature decreases the rate of nucleation increases. However, as the glass transition temperature is approached, diffusion of molecules across the phase boundary becomes slower thus reducing the rate of nucleation. Therefore the rate of nucleation has a maximum somewhat below the thermodynamic melting temperature.

(ii) Growth

The rapid rate of crystallization during the growth phase is a consequence of a plentiful

supply of stable nuclei and crystallites providing surface onto which to add new material and a plentiful supply of mobile amorphous material available for crystallization.

Based on these two factors, the volumetric growth rate may be described by the equation due to Avrami (1940):

$$V_c(t) = 1 - \exp(-kt^n) \qquad (1.84)$$

where V_c is the volume fraction of the crystalline phase at time t and k and n are constants. The theory assumes a complete transformation from the amorphous to crystalline state, a condition not applicable for polymers. For example, the maximum crystallinity in natural rubber is about 30% (Roberts and Mandelkern, 1955). A modification of equation (1.83), allowing for an equilibrium volume fraction of crystallinity, V_e, has been used by Gent (1954a) (see Section 1.5.5):

$$V_c(t) = V_e\left(1 - \exp(-kt^n)\right) \qquad (1.85)$$

The value of the parameter n depends on the type of crystal growth. For the case where growth from a constant density of nuclei is assumed, n = 3 for the growth of spherical crystals at a constant radial rate and n = 1 for linear growth at a constant rate. For the case of a constant nucleation rate and spherical crystal growth, n = 4. The constant k is a measure of the rate of crystallization (Avrami, 1940).

(iii) Final amount of crystallinity

Eventually the availability and mobility of amorphous material diminishes and crystallization slows down or ceases. The final amount of crystallinity in natural rubber has been measured by X-ray diffraction, enthalpy changes and density changes (from a value for the density of the crystalline region, determined from the unit cell dimensions (Bunn, 1942). In all cases, the equilibrium degree of crystallinity has been found to be around 30% (Roberts and Mandelkern, 1955).

The amount of crystallinity may also be obtained from a measure of the heat absorbed

during melting, using a standard value for the heat of melting for the perfect crystal. This has been measured as 64.0 J/g for natural rubber from the depression of the melting point of rubber/diluent mixtures (Roberts and Mandelkern, 1955) using the theory of Flory (1953). Later, Kim and Mandelkern (1972) deduced a value of 65.3 J/g by measuring the heat of fusion by differential scanning calorimetry (DSC) for a sample whose crystallinity had been calculated from the volume change. These two values are in good agreement.

Other workers, however, (Burfield, 1984; Zemel and Roland, 1992) have obtained values of about 38% for the final crystallinity in unstrained natural rubber from DSC measurements; significantly higher than the 30% found more generally.

1.5.3 *Effect of temperature on crystallization*

Wood and Bekkedahl (1946) measured the temperature dependence of the overall rate of crystallization for unstrained unvulcanized natural rubber. They monitored the change in volume in order to quantify the amount of crystallization. They found that appreciable rates of crystallization occurred for temperatures between 0°C and -50°C with the maximum rate at about -25°C. Russell (1951) confirmed a similar temperature dependence for vulcanized rubber.

For a purified natural rubber, the equilibrium amount of crystallization was found to be about 15% higher at 0°C than at -40°C (Gent, 1955). This may be accounted for by the formation of fewer larger and more structurally perfect crystals at lower degrees of undercooling. For an unpurified rubber very little dependence of the equilibrium amount of crystallization on the crystallization temperature was observed, suggesting that the morphology was controlled by instantaneous nucleation at the start of crystallization.

The melting behaviour of unvulcanized natural rubber was investigated by Wood and Bekkedahl (1946) who found that the melting temperature depended on the temperature of crystallization. Moreover, the melting point was not sharp, nor did it coincide with the temperature of crystallization, typically beginning 5 to 10°C above the crystallization temperature and taking place over a range of about 10°C (Figure 1.14). The conditions

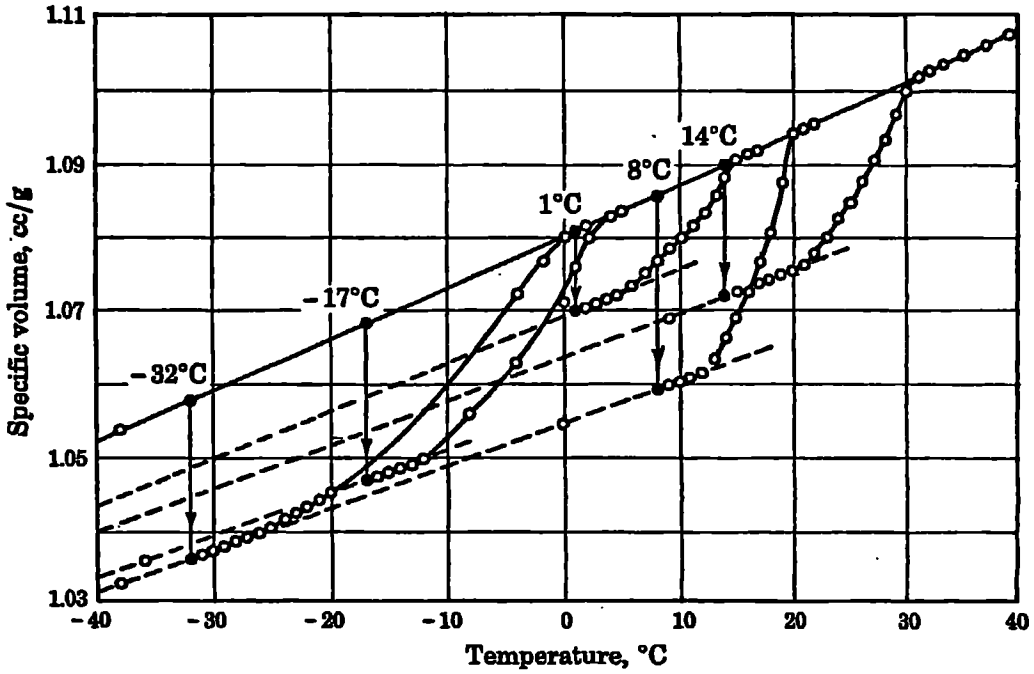

Figure 1.14 Melting range of natural rubber as a function of the temperature of crystallization. The change of specific volume on crystallization is indicated by the vertical lines joining the dark circles. Open circles show the specific volume during slow melting. The initial crystallization was not always to equilibrium.
(From Wood and Bekkedahl, 1946)

applicable to equation (1.82) are an infinitely slow rate of heating in order to allow for the development of near-perfect crystals. Imperfect crystals are likely to melt at a temperature well short of the thermodynamic melting point, T_m. Roberts and Mandelkern (1955) adopted a very slow heating rate of 1 °C per 24 to 48 hours in order to measure T_m for natural rubber and obtained a figure of 28 °C for a purified rubber crystallized at 14 °C. For rubbers crystallized at lower temperatures they were unable to achieve such a high melting temperature, presumably due to imperfections in the crystal structure.

1.5.4 *Effect of compounding on crystallization*

The rate and amount of crystallization are strongly dependent on the degree of crosslinking. Order of magnitude reductions in rate may be achieved with moderate levels of crosslinking, along with a more modest (about 10%) reduction in the final amount of crystallinity (Gent, 1955). Bristow and Tiller (1970) found that vulcanizing systems which caused a large amount of main chain modification in natural rubber were very effective in retarding crystallization. Gent (1954b) investigated the effect of various additives on the nucleation period in natural rubber and found that acetone extraction of smoked sheet increased the half-life of crystallization roughly fourfold. Additives which markedly increased the crystallization rate included stearic acid and paraffin wax. Gent noted that substances with long molecules which crystallized readily were particularly effective at increasing the crystallization rate. On the other hand, carbon black filler was found to inhibit slightly the rate of crystallization in unstrained natural rubber (Gent, 1954c).

Any irregularity in the chemical structure of the polymer which inhibits the molecules from forming into a regular close-packed structure is likely to inhibit crystallization. Thus certain polymers, such as polystyrene-butadiene and polyacrylonitrile butadiene are inherently resistant to crystallization. Synthetic cis-polyisoprene is more crystallization resistant then natural rubber (also cis-polyisoprene) due to the higher trans-polyisoprene content of the synthetic material. Blending a crystallizable rubber with another miscible polymer may also inhibit crystallization. For example, blends of natural rubber with atactic high vinyl polybutadiene has been found to retard crystallization (Zemel and

Roland, 1992).

1.5.5 *Effect of strain on crystallization*

The high strength properties of natural rubber and certain synthetic rubbers have often been attributed to their ability to crystallize rapidly at room temperature under high strains. Strain crystallization has also been postulated as a cause of higher hysteresis and stiffness.

Gough (1805) reported that a sample of unvulcanized rubber pulled to a high extension lost its retractive force until it was heated at which point it sprang back to its original length. Further investigations were carried out by Treloar (1941) who measured changes in birefringence and density. He found a smaller equilibrium amount of crystallinity and faster rate for increasing strains. The effect of temperature is interesting; at 0°C Treloar (1941) found that crystallization was possible even at low (or zero) strain but was very slow, whereas at 25°C or 50°C, although negligible crystallization occurred at small or moderate strains, at larger strains crystallization proceeded rapidly. This is explained by the fact that the equilibrium melting temperature, T_m, increases with an applied strain due to the reduction in entropy of the amorphous material (see Section 1.5.1). At higher temperatures the molecules are more mobile so, for a given degree of undercooling, crystallization proceeds more quickly.

Measurements on vulcanized natural rubber were carried out at -26°C by Gent (1954a) who calculated the degree of crystallization in stretched samples from the amount of stress relaxation using the thermodynamic theory of Flory (1947). Although Flory's (1947) theory contained assumptions which were not strictly valid, Gent (1954a) showed good correlation between the stress relaxation behaviour and the crystallinity calculated more directly from the change in density. He (Gent, 1954a) fitted his data to equation (1.85) and found reasonable agreement. The value of n was strongly dependent on strain and suggested a transformation from spherical crystal growth at a constant radial rate for unstrained rubber to linear growth at a constant rate for rubber strained to 300%. This is consistent with the observation that the crystal morphology changes from spherulitic to fibrillar with increasing strain. (Andrews, 1964; see Section 1.5.7) though later

workers (Kim and Mandelkern, 1968; Stevenson, 1983) suggested that n could take values outside the range of 1 to 3 implying that the assumptions in equation (1.85) are not strictly valid. Kim and Mandelkern (1968), who also measured stress relaxation, reported an increase in the rate of crystallization with increasing strain whereas Stevenson (1983) found that the growth rate decreased with increasing strain although the nucleation time was shorter. Stevenson's (1983) measurements were of the modulus change and he assumed a linear relationship between modulus change and crystallinity. For unstrained, unvulcanized rubber it is known (Leitner, 1955) that this is only approximately correct (see Figure 1.15) though it is not apparent that such discrepancies would have altered Stevenson's conclusions. Also, Kim and Mandelkern (1968) adopted an approximation of equation (1.84) valid for small amounts of crystallinity in evaluating their data, whereas Stevenson (1983) designated early data points as being part of the nucleation stage and calculated the Avrami rate constant from the central part of the modulus-time curve. Stevenson (1986) showed that the mode of deformation was relatively unimportant in determining the crystallization kinetics from measurements in uniaxial tension, uniaxial compression and simple shear.

Stevenson (1983) found no systematic dependence of the equilibrium degree of crystallinity on the strain, which suggests that the crystal morphology is unimportant in determining the equilibrium degree of crystallinity. In contrast to unstrained rubber, small amounts of crosslinking promote crystallization (Morrell and Stern, 1952). This is attributed to the reduced creep of vulcanized rubber compared to unvulcanized rubber, resulting in a greater molecular strain. For high extents of crosslinking the behaviour is similar to unstrained rubber and crystallization is retarded.

For rubbers containing carbon black fillers, Gent (1954c) found that the crystallization rate was increased by the application of a strain in a similar way to that observed for unfilled rubbers (Gent, 1954a) once the effect of strain amplification (Mullins and Tobin, 1954) had been taken into account. The effect of previous stretching was interesting; for samples crystallized under strain a previous larger strain caused a reduction in the crystallization rate, whereas for samples crystallized unstrained the reverse effect was seen (Gent, 1954c). For the case of crystallization under strain Gent suggested that the

previous stretching had caused breakage of some rubber-filler attachments in accordance with the proposal of Mullins and Tobin (1954), (see Section 1.4.5), thus reducing the average extension in the rubber and causing a reduction in the crystallization rate. However, in view of subsequent re-evaluation of the mechanisms of strain softening (see Section 1.4.5) some doubt is cast on the accuracy of this mechanism. The increase in crystallization rate between a previously unstrained testpiece and one that had been previously strained to 360% was about a factor of three. Gent (1954c) suggested that some elements of the rubber matrix remain in a strained state after the testpiece is relaxed and cites the anisotropic tearing behaviour seen in similarly treated testpieces as evidence of residual orientation. Derham (1973) found a similar effect of pre-stressing on reducing stress relaxation rates and suggested that molecular chain entanglements were pulled through the network in a manner which prevented their return to the equilibrium position once the strain was removed. Swelling and de-swelling appeared to return the rubber to its original state. A similar mechanism could lead to the residual strain implied by Gent's (1954c) experiments.

1.5.6 *Effect of crystallization on mechanical properties*

A very large increase in the stiffness of rubber and loss of elasticity accompanies crystallization. Leitner (1955) quantified the change in Young's modulus with the degree of crystallization, measured by changes in density, for an unvulcanized unstrained sample of natural rubber (Figure 1.15). She noted that the hundred-fold increase in modulus for a crystallinity of about 24% was remarkably high and could not easily be accounted for in terms of a simple filler reinforcing effect; an aspect ratio of 36 would be needed in the Guth (1945) equation (equation 1.69) to achieve this level of reinforcement. However, it has been suggested (Halpin and Kardos, 1972) that partially crystalline polymers may be modelled as fibre reinforced composites for which high aspect ratios are appropriate. Quantitative data on the modulus-crystallinity relationship for vulcanized rubber is lacking in the literature and is addressed in Chapter 9.

The effect of cyclic deformations on the mechanical behaviour of partially crystalline natural rubber has been studied by Pettifor and Coveney (1989). In contrast to the effect of static strains (Section 1.5.5) cyclic strains greater than 5% inhibited crystallization.

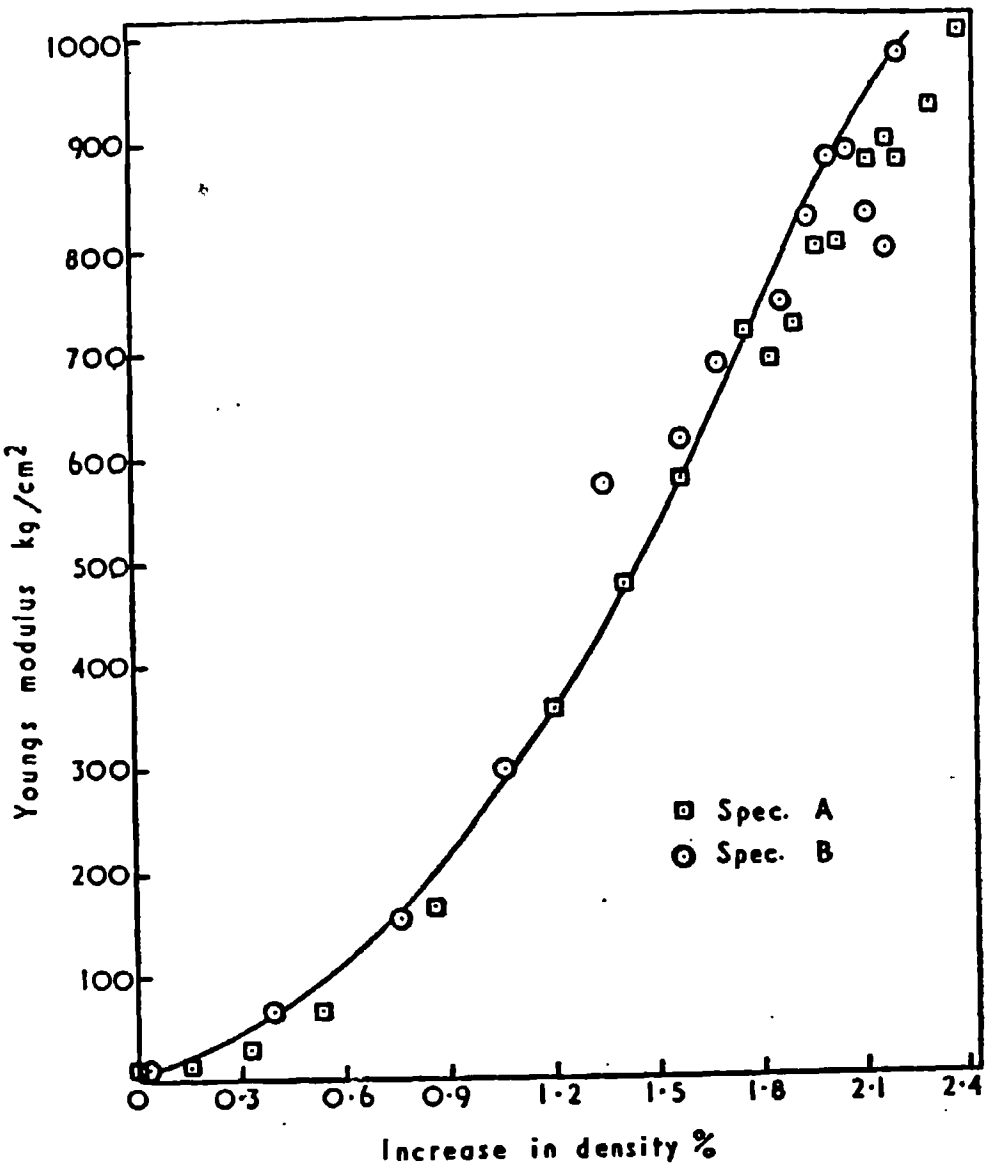

Figure 1.15 Young's modulus as a function of crystallization as measured by the change in density for unvulcanized natural rubber.
(From Leitner, 1955)

The application of a large stress to a partially crystalline polymer causes plastic yielding. This effect, which is well known in conventional partially crystalline polymers such as polyethylene (Gent and Madan, 1989), has also been observed in natural rubber (Pettifor and Coveney, 1989) (Figure 1.16). The principal features were a very high initial modulus up to a yield strain of around 20%, followed by a substantial further increase in strain with little or no additional force (cold drawing). In some cases a drop in stress was seen immediately after yielding. The subsequent second cycle stress-strain behaviour was approximately linear and much softer than the initial modulus of the partially crystalline polymer, though still substantially stiffer than the amorphous material. If the yielded rubber remained at a low temperature re-stiffening occurred at a greater rate than the original rate of crystallization, suggesting that the softening due to yielding was not equivalent to melting. However, Gent and Madan (1989) calculated that the energy of yielding was similar to the free energy of melting for a selection of partially crystalline polymers and proposed that yielding involved a stress-induced disruption of the crystallites which was equivalent to melting.

1.5.7 *Crystal morphology*

X-ray diffraction methods have enabled the arrangement of atoms in the unit cell of crystalline polymers to be deduced. Bunn (1942) determined the unit cells of natural rubber and polychloroprene in this way. Keller and O'Connor (1958) observed by electron microscopy on polyethylene that the crystals comprised thin, flat platelets (lamellae) and proposed chain folding to account for the fact that the crystals were thinner in the direction of the molecule (Figure 1.17). Keller (1959) also observed in Nylon bundles of lamellae radiating from a single point to form a structure called a spherulite. Neighbouring spherulites impinged on one another so that all available space was occupied. Electron microscopy of thin films of unvulcanized natural rubber was carried out by Andrews (1962) who also observed lamella-type crystals and spherulites (Figure 1.18). The lamella thickness was found to be dependent on the crystallization temperature, with thicker crystals resulting from higher crystallization temperatures (Andrews et al, 1971). Both crystalline and amorphous material coexisted within the spherulites.

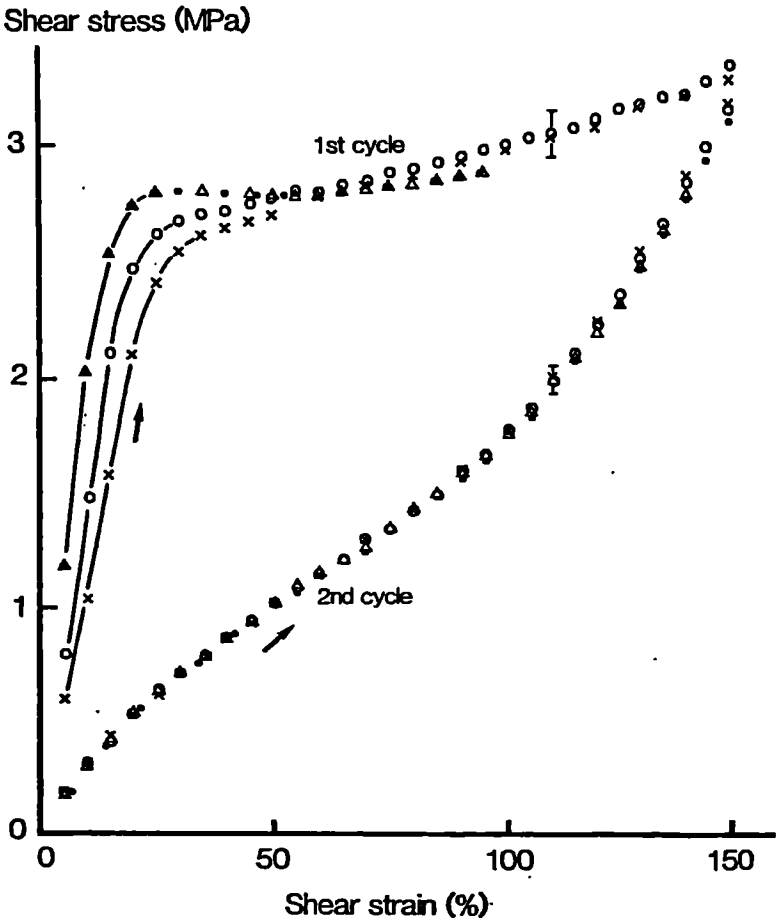

Figure 1.16 Stress-strain behaviour at -25°C of crystallized natural rubber. Conditioning strain amplitudes: ●0.01, ▵ 0.05, ○ 0.10, × 0.15. (From Pettifor and Coveney, 1989)

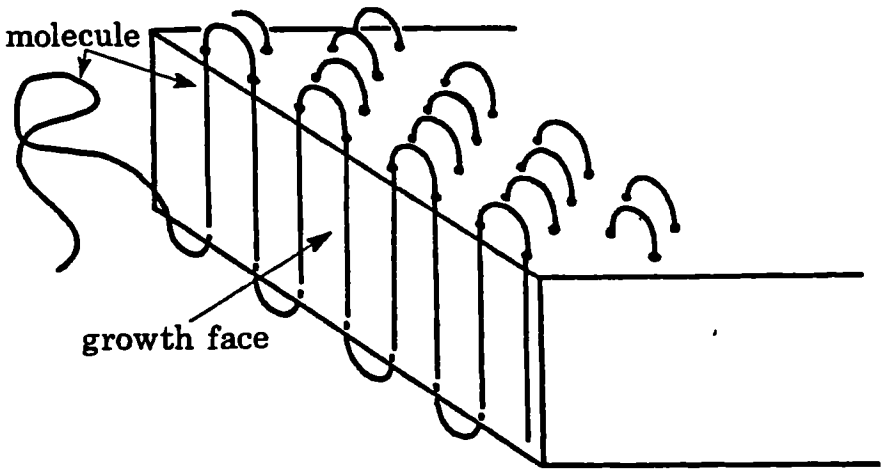

Figure 1.17 Molecular chain folding in a polymer lamellar crystal. (From Andrews et al, 1971)

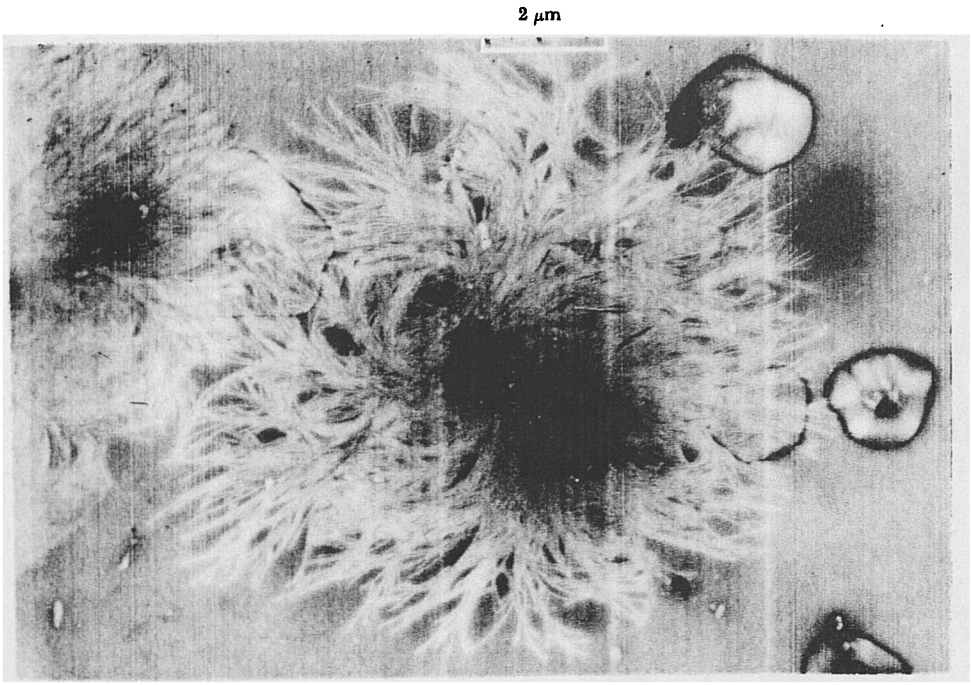

Figure 1.18 Single spherulite in a thin film of cis-polyisoprene. Stained with OsO_4. (From Andrews et al, 1971)

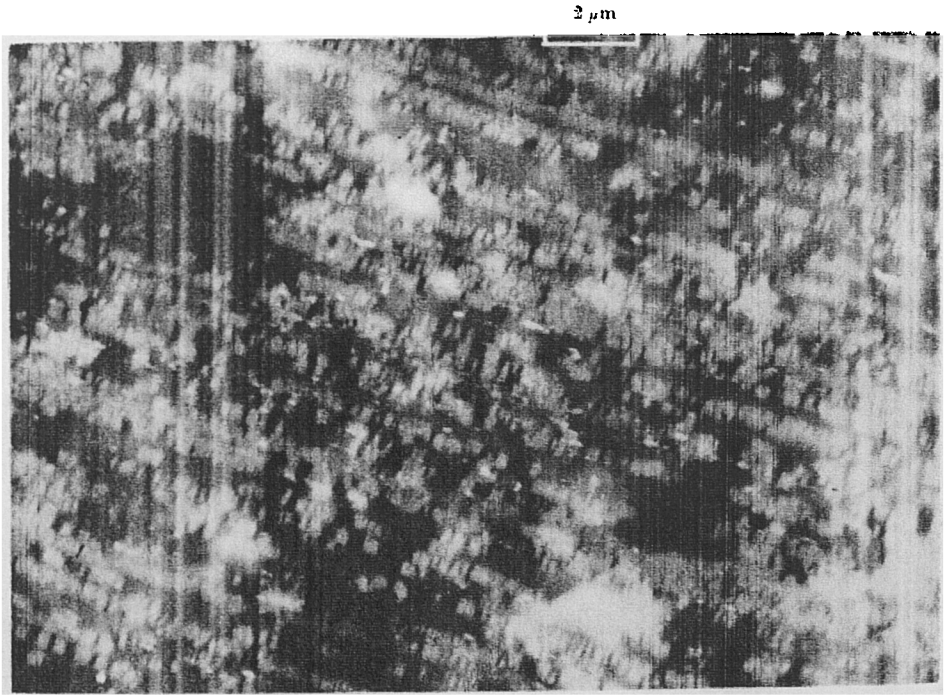

Figure 1.19 Row nucleated 'shish-kebab' morphology in cis-polyisoprene crystallized at 200% strain.
(From Andrews et al, 1971)

Andrews (1964) investigated the effect of a uniaxial tensile strain on the crystal morphology of unvulcanized natural rubber. At strains above about 100%, the isotropic spherulitic structure gradually changed to a fibrillar structure in which the crystal lamella grew with their thin direction in the strain direction. At very high strains (greater than 300%) crystallization occurred too rapidly to allow for crystal growth and the morphology consisted of chains of nuclei growing along the strain axis (Figure 1.19). More detailed investigations, in which similar morphologies were seen, were carried out for trans-polyisoprene (Davies and Ong 1977).

1.6 Aims of this thesis

In the preceding sections factors affecting the mechanical behaviour of amorphous and crystalline rubber have been described, and methods of characterising them, for example for finite element analysis, have been discussed. The purpose of this thesis is to investigate further some features of the mechanical behaviour of rubbers. The emphasis is mainly on natural rubber, although in Chapters 2, 5 and 8 certain synthetic rubbers are studied.

In Section 1.3.6, theoretical equations relating the compression stiffness of bonded pads to the bulk and shear moduli of the rubber were reviewed. In Chapter 2, in order to obtain an assessment of the accuracy of these equations, a critical comparison of them is made alongside an experimental study of a polyurethane rubber containing a compressible filler. Finally, a theory reviewed in Section 1.3.3 is used to obtain an estimate of the volume fraction of the filler.

The remaining chapters consider only materials which may be regarded as incompressible. The aim of Chapters 3 to 8 is to characterise filled and unfilled rubbers in order to obtain appropriate models for use in finite element analysis of elastomeric components. In Chapter 3 a novel pure shear technique, in which both non-zero principal stresses are measured, is developed as a simple alternative to the general biaxial experiments reviewed in Section 1.2.3. This technique is then used to characterise, in terms of a strain energy function, the first loading cycle of a series of natural rubbers

containing a range of loadings of carbon black filler. The treatment is extended to synthetic rubbers in Chapter 5 with a special emphasis in comparing the non-linear behaviour of filled natural rubber with the non-linear behaviour seen in some unfilled rubbers. In Chapter 4, experimental assessment of various forms of strain energy function, reviewed in Section 1.2.4, is carried out by evaluating the theoretical predictions of the equations in various modes of deformation and comparing them to experimental data obtained on the same series of natural rubbers used in Chapter 3. Chapter 6 concerns an alternative to the split pure shear technique based on a simple shear deformation which was considered as a way of eliminating some experimental difficulties associated with the pure shear technique. Complications arising from the boundary conditions in simple shear caused this alternative technique to be rejected. However, finite element analysis was used to determine the effect of unconstrained edges in conventional simple shear testpieces on both the apparent shear modulus and the behaviour in the thickness direction. The next two chapters consider the characterization of rubbers which exhibit departures from elastic behaviour of the types described in section 1.4. In Chapter 7 it is shown by an experiment that even some aspects of the behaviour of such materials which do not involve strain retraction, time-dependent or history effects cannot be appropriately described by a strain energy function. In Chapter 8, models for Mullins' effect and time dependent stress relaxation are assessed by experiment.

Finally, the behaviour of crystalline, rather than amorphous, rubber is studied in Chapter 9. The aim of this work is to establish a relationship between the amount of crystallization and the mechanical properties, in particular the modulus and the yielding behaviour.

Overall, the aim is to develop a broad view of the character of all of the contributions to the stress-strain behaviour of rubbers, whether they arise from rubber elasticity, 'hard' regions of copolymers, compressible or rigid fillers or crystalline regions.

CHAPTER 2

Behaviour of a rubber containing a compressible cellular filler

2.1 Introduction

It is often reasonable to regard a solid rubber material as incompressible since its bulk modulus is over one thousand times its shear modulus. However, rubbers containing voids or compressible fillers are likely to exhibit a significant degree of compressibility. Compressible fillers are sometimes used deliberately to reduce the effect of 'shape factor', discussed in Section 1.3.6, on the compression stiffness. A typical example would be rail pads; the specified low compression stiffness cannot be achieved using a plain pad of incompressible rubber because the area and thickness are constrained to have values set by other design considerations.

Discussion of how to design pads loaded with compressible fillers to achieve specified compression stiffness does not seem to be available in the literature. This chapter aims to address this shortcoming, first by a critical comparison of the alternative equations given in Section 1.3.6, and second through an experimental study for a material containing compressible filler. The bulk and shear moduli for the compressible material are obtained both from measurements in constrained compression by use of one of the equations given in Section 1.3.6 and by direct measurement, thus providing an assessment of the accuracy of the theoretical treatment.

Finally, a theory reviewed in Section 1.3.3 is used to estimate the volume fraction of voids from the experimentally determined bulk and shear moduli.

2.2 Comparison of theoretical equations for the compression of bonded blocks

In the next section experiments to measure the compression modulus of bonded blocks of a compressible rubber with different shape factors are reported. An appropriate relationship will be needed in order to obtain values for the bulk and shear moduli. Several possible equations exist in the literature as reviewed in section 1.3.6. In this section the predictions of these equations are compared so that a suitable choice for

fitting the experimental data may be made.

Making use of expressions derived from classical elasticity theory, the equations were rearranged to give expressions for E_c/G as a function of G/K and S^2.

Comparison of equations

(i) Gent and Lindley (1959) - Equation (1.63)

Substitution from equations (1.56) to (1.58) and equation (1.60) in equation (1.63) yields:-

$$\frac{E_c}{G} = \frac{(3+4G/K)(1+2S^2)}{(1+G/3K)(1+4G/3K)+3G(1+2S^2)/K} \qquad (2.1)$$

(ii) Lindley (1979) - equations (1.65)

Substitution from equation (1.57) yields:-

$$\frac{E_c}{G} = 2 + \frac{1-2G/3K}{G/3K+1}\left(1 + 6S^2\frac{(1-2G/3K)}{G/3K+1}\left(1 - \frac{32GS^2/K}{4G/3K+4+33GS^2/K}\right)\right) \qquad (2.2a)$$

for $S < S_a$

$$\frac{E_c}{G} = \frac{K}{G} + \frac{4}{3} - \frac{K(1-2G/3K)^2}{15G(1+G/3K)}\left(\frac{S_a}{S}\right)\left(8 - \frac{S_a}{S}\right) \qquad \text{for } S \geq S_a \qquad (2.2b)$$

where

$$S_a^2 = \frac{4}{15}\left(\frac{1+G/3K}{G/K}\right) \qquad (2.3)$$

(iii) Chalhoub and Kelly (1986) - equation (1.66)

(iv) Chalhoub and Kelly (1986) - equation (1.67)

(v) Conversey (1967) - equation (1.68) where C_4 was obtained from tabulated values (Conversey, 1967) for the case of a square cross-section.

These five equations were compared for various degrees of compressibility (ratios of

G/K) by plotting E_c/G against S^2 in Figure 2.1.

It is clear from Figure 2.1 that the approximate equation (1.66) becomes unusable at large values of shape factor, especially at significant degrees of compressibility. The condition imposed on its validity, $S \leq (K/12G)^{1/2}$ seems insufficient; at G/K = 1/1000 equation (1.66) should work up to $S^2 = 83$ but Figure 2.1 suggests that it fails at lower values of S^2 than this. The other equations plotted in Figure 2.1 are in reasonable agreement (within about 20%). Equations (2.1) and (2.2) diverge significantly as S increases especially at intermediate values of G/K although, at very high shape factors, they reconverge since, for both equations,

$$E_c/G \rightarrow K/G + 4/3 \text{ as } S \rightarrow \infty$$

For incompressible materials (G/K = 0) equations (2.1) and (2.2) are identical:

$$E_c/G = 3(1 + 2S^2) \tag{2.4}$$

and equations (1.66) and (1.67) are identical:

$$E_c/G = 6S^2 \tag{2.5}$$

Equations (2.4) and (2.5) are applicable to circular cross-sections. For the incompressible material, equation (1.68) becomes:

$$E_c/G = 6.75S^2 \tag{2.6}$$

for a square cross-section. For large shape factors, these equations approximate to those of Gent and Lindley (1959) and Gent and Meinecke (1970) for circular and square cross-sections respectively, (equations (1.60) and (1.62)). Thus the use of shape factor as a parameter is limited as the actual shape of the cross-section as well as its shape factor affects the modulus.

Experimental data for a foam rubber with G/K = 0.24 are available in the literature (Lindley, 1968). Also, tabulated data from numerical analysis are available for certain compressibilities. Thus, for the particular case of G/K = 0.24, further comparison of the

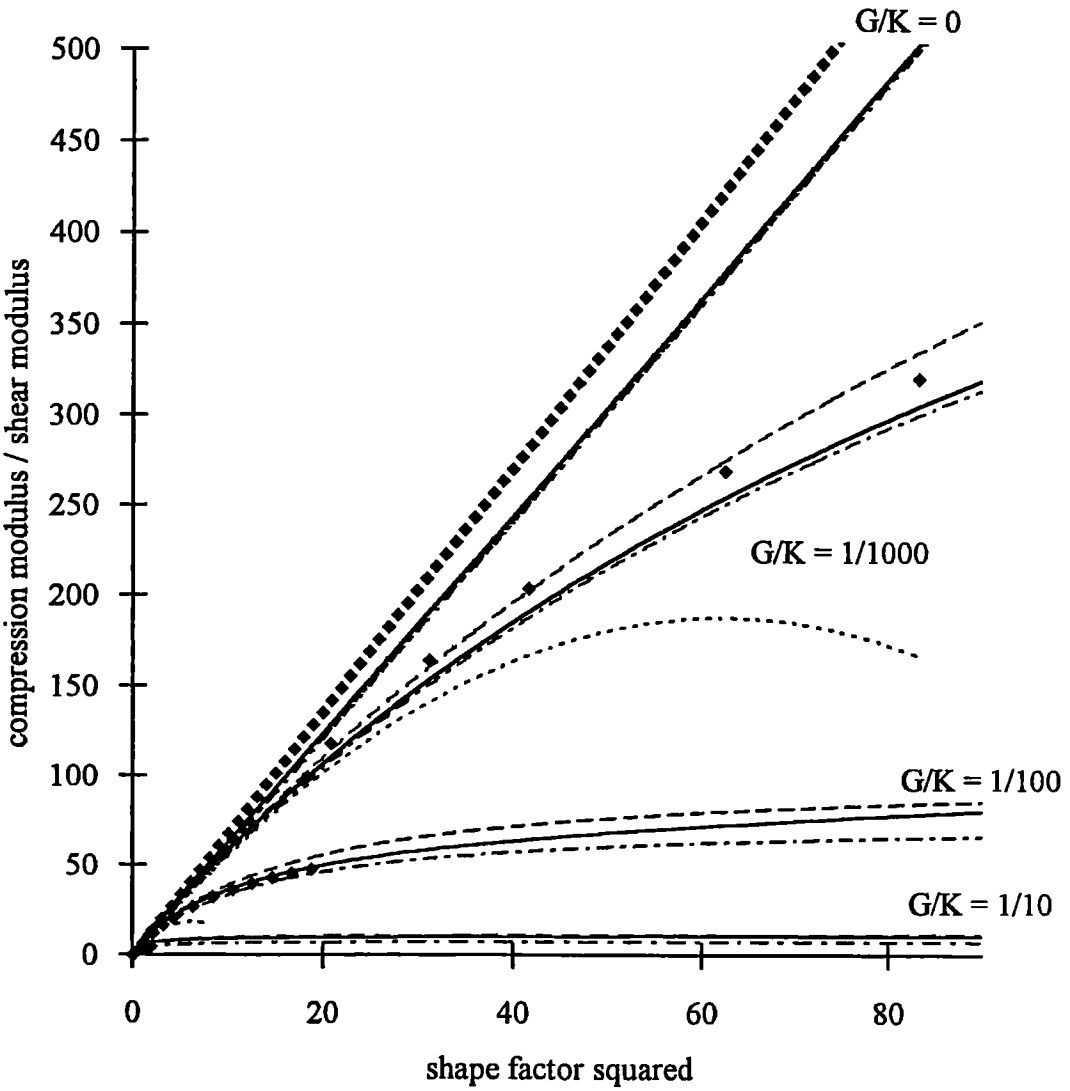

Figure 2.1 Comparison of equations relating the apparent compression modulus to the shape factor and compressibility.

- – – equation 2.1 (Gent and Lindley, 1959)
- —— equation 2.2 (Lindley, 1979)
- ····· equation 1.66 (Chalhoub and Kelly, 1986)
- – · – · equation 1.67 (Chalhoub and Kelly, 1986)
- ◆ equation 1.68 (Conversey, 1967)

equations was made with the following additional information.

(vi) Moghe and Neff (1971)

Moghe and Neff's computations for G/K = 0.24 were utilized.

(vii) Lindley and Teo (1978)

Numerical values for E_c/G obtained from a finite element analysis of a bonded disc were provided by Lindley and Teo for various shape factors and certain values of Λ/G. Appropriate values for G/K = 0.24 ($\Lambda/G = 3.54$) were obtained by interpolation.

(viii) Lindley (1968)

Experimental values of E_c were obtained by Lindley (1968) for a foam rubber with $\upsilon = 0.39$ (equivalent to G/K = 0.24).

A plot of E_c/G as a function of S^2 for G/K = 0.24 is given in Figure 2.2. The limiting values for low and high shape factors, given by E and E_∞ in equations (1.56) and (1.58) respectively, are also shown in the figure.

At G/K = 0.24 (Figure 2.2) equations (2.1) and (2.2) are virtually indistinguishable from the results of finite element analysis and the more precise analytical form of Moghe and Neff (1971), though giving slightly higher values of E_c/G than the experimental data of Lindley and Teo (1978). Equation (1.67) however, seems to seriously underestimate E_c/G. At such a low value of G/K the shape factor has virtually no effect on the stiffness except at very low values.

Taking into account both accuracy and ease of computation equations (2.1) and (2.2) would appear to offer the best estimate of the compression of bonded blocks over a wide range of shape factors and compressibilities. Equations (1.66) and (1.67), though straightforward to use, show inaccuracies at high shape factors and for very compressible materials respectively, and the forms due to Moghe and Neff (1971) and Conversey (1967) require more sophisticated computations.

2.3 Material

The material on which the experiments were carried out was a castable polyurethane

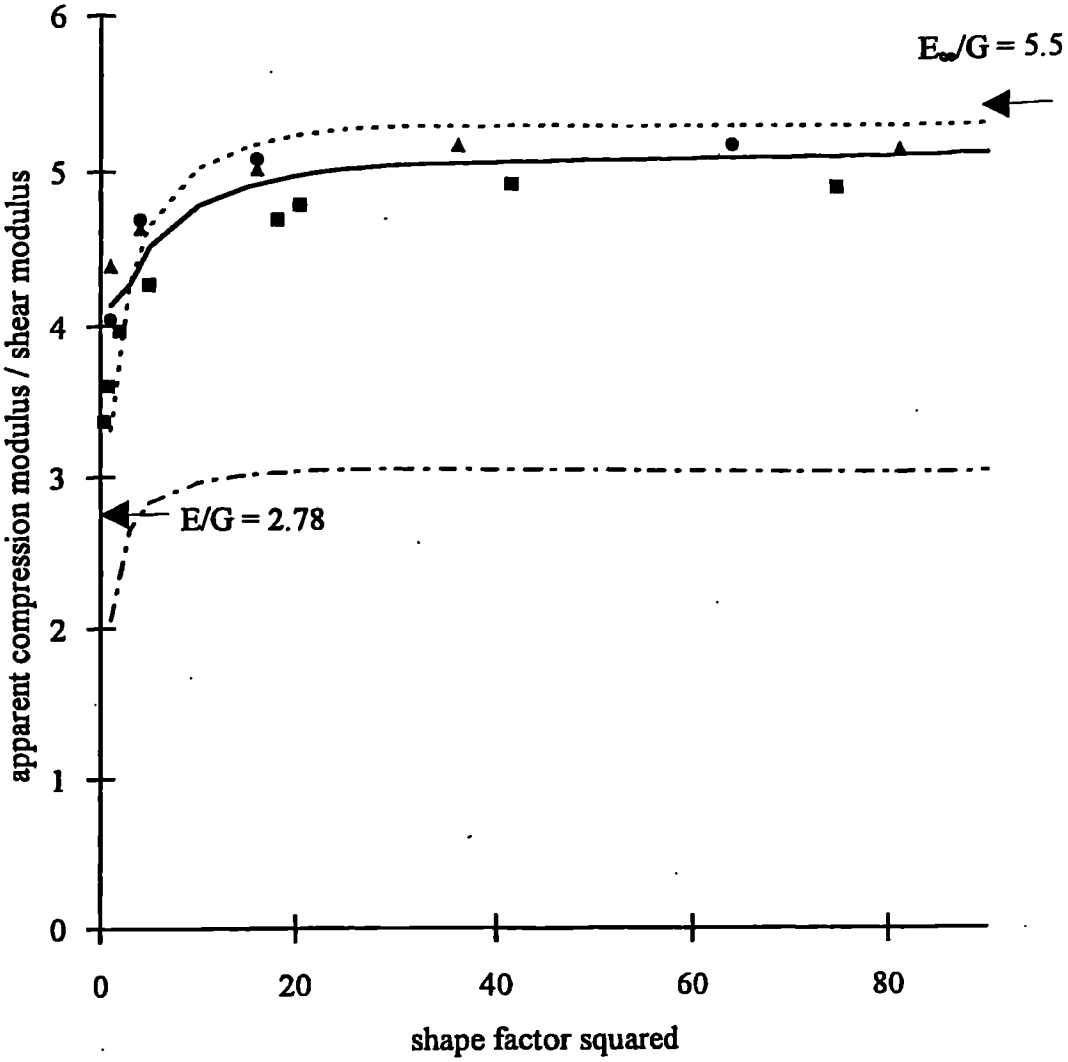

Figure 2.2 Comparison of equations relating the apparent compression modulus to the shape factor at G/K = 0.24. ($E_\infty/G = 5.5$, $E/G = 2.78$).
■ experimental data (Lindley, 1968)
▲ numerical analysis (Moghe & Neff, 1971)
● Finite element analysis (Lindley and Teo, 1978)
------- equation 2.1 (Gent and Lindley, 1959)
——— equation 2.2 (Lindley, 1979)
–·–· equation 1.67 (Chalhoub and Kelly, 1986)

elastomer containing an unknown volume fraction of particles of a compressible filler. It was supplied in the form of a rectangular block of nominal dimensions 300x300x25mm by Sika Chemie GmbH and was a commercial compound developed to provide a light rail track fixing system with low noise and vibration.

2.4 Measurement of compression modulus for square blocks of different shape factor

2.4.1 *Experimental method*

A pad of the material of nominal dimensions 300x300x25mm was bonded between two 1mm thick sheets of steel with a thick, even layer of Sikaflex-221 sealant in order to prevent slippage between the sample and the platens during testing. The pad was compressed in a Schenck POZ 1050 servohydraulic test machine. The force was measured with a 400kN load cell mounted beneath the lower platen. The displacement was measured between the upper platen and the base with an LVDT. A self-aligning device was inserted between the top platen and the machine load cell to ensure that the force was applied uniformly across the area of the pad. The pad was first subjected to three conditioning compression cycles up to a stress of 1320kN/m^2. Quasistatic data were obtained from a fourth cycle at a rate of 0.8mm/min to the same stress. The force-deflection data were plotted directly onto chart recorder paper. The dynamic compression stiffness was also obtained from a Solartron 1250 frequency response analyser connected to the load and displacement transducers. A 5% prestrain was applied and measurements were made at a dynamic amplitude of 0.4mm (= 1.6% strain) and frequencies of 1, 2 and 5Hz.

50mm strips were cut off opposite sides of the pad to leave a pad of dimensions 250x250mm which was tested as above. The size of the square pad was repeatedly reduced by removing further 50mm strips from all sides and re-tested. The smallest pads, of side lengths 50 and 25mm, were tested on a 7kN Schenck VHF servohydraulic test machine since the load-cell capacity was more appropriate. The test procedure was otherwise identical to that described for the larger machine except that the levelling device was not used. As a further check of the accuracy of the two machines, the pads of side length 150, 100, 75 and 50mm were tested also on a 100kN screw driven Zwick

test machine. A check of the homogeneity of the pad was made by testing four 50mm x 50mm pads cut from each side of the original pad, labelled A, B, C and D (Figure 2.3) on the 7kN Schenck machine. The platen temperature was measured and found to be within 22±3°C for all tests.

2.4.2 *Results*

Typical quasistatic force-deflection plots for the fourth cycle are shown in Figure 2.4 for pads of different shape factors. The compression stiffness was obtained from the tangent to the plots at 1% strain which equals 0.25mm deflection since the pad was 24.9mm thick. The tangent stiffness was chosen in preference to the secant stiffness to avoid uncertainty around the zero point due to "lead-in" caused by the platens not being perfectly parallel to the pad. The lead-in was noticeable only in tests conducted on the 7kN Schenck where the levelling device was not used. Since the stress-strain plots were virtually linear up to strains above 1%, the difference between secant and tangent stiffness and change of stiffness with strain were small.

Table 2.1: Quasistatic stiffnesses and apparent compression moduli, E_c at 1% strain

pad size mm x mm	S^2	stiffness (kN mm^{-1})	E_c (MNm^{-2})	Test Machine
304 x 299	9.16	76.9	21.1	400kN Schenck
249 x 251	6.30	52.0	20.7	"
199 x 199	3.99	28.0	17.6	"
150 x 150	2.27	14.0	15.5	"
150 x 150	2.27	14.2	15.7	Zwick
100.9 x 100.5	1.02	5.2	12.8	40kN Schenck
100.9 x 100.5	1.02	5.0	12.3	Zwick
75.5 x 75.9	0.58	2.46	10.7	400kN Schenck
75.5 x 75.9	0.58	2.33	10.1	Zwick
50.0 x 50.0 (centre)	0.25	0.77	7.7	7kN Schenck
50.0 x 50.0 (centre)	0.25	0.86	8.6	Zwick
50.2 x 54.4 (A)	0.27	0.80	7.3	7kN Schenck
50.2 x 50.4 (B)	0.26	0.75	7.4	"
49.8 x 49.5 (C)	0.25	0.75	7.6	"
49.8 x 49.5 (C)	0.25	0.82	8.3	Zwick
49.6 x 49.7 (D)	0.25	0.75	7.6	7kN Schenck
24.1 x 25.2	0.061	0.14	5.9	"
24.3 x 25.2	0.062	0.15	6.3	"

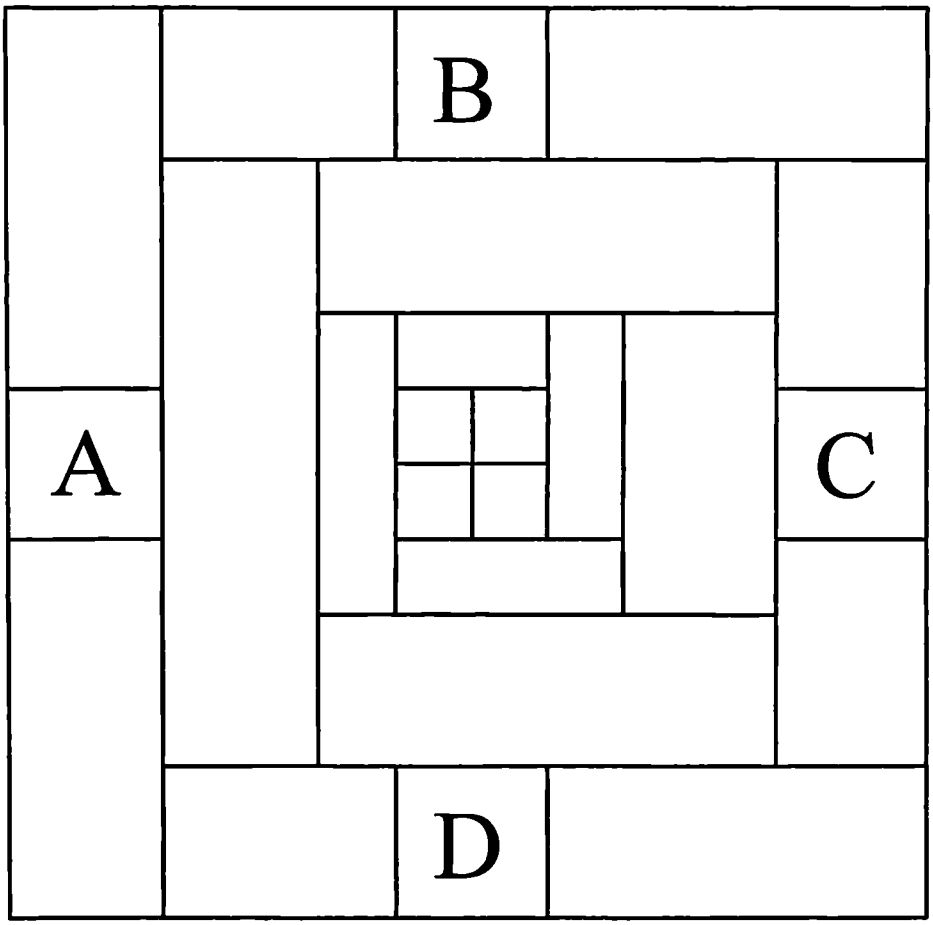

Figure 2.3 Method of sawing pad to provide pads of different shape factor.

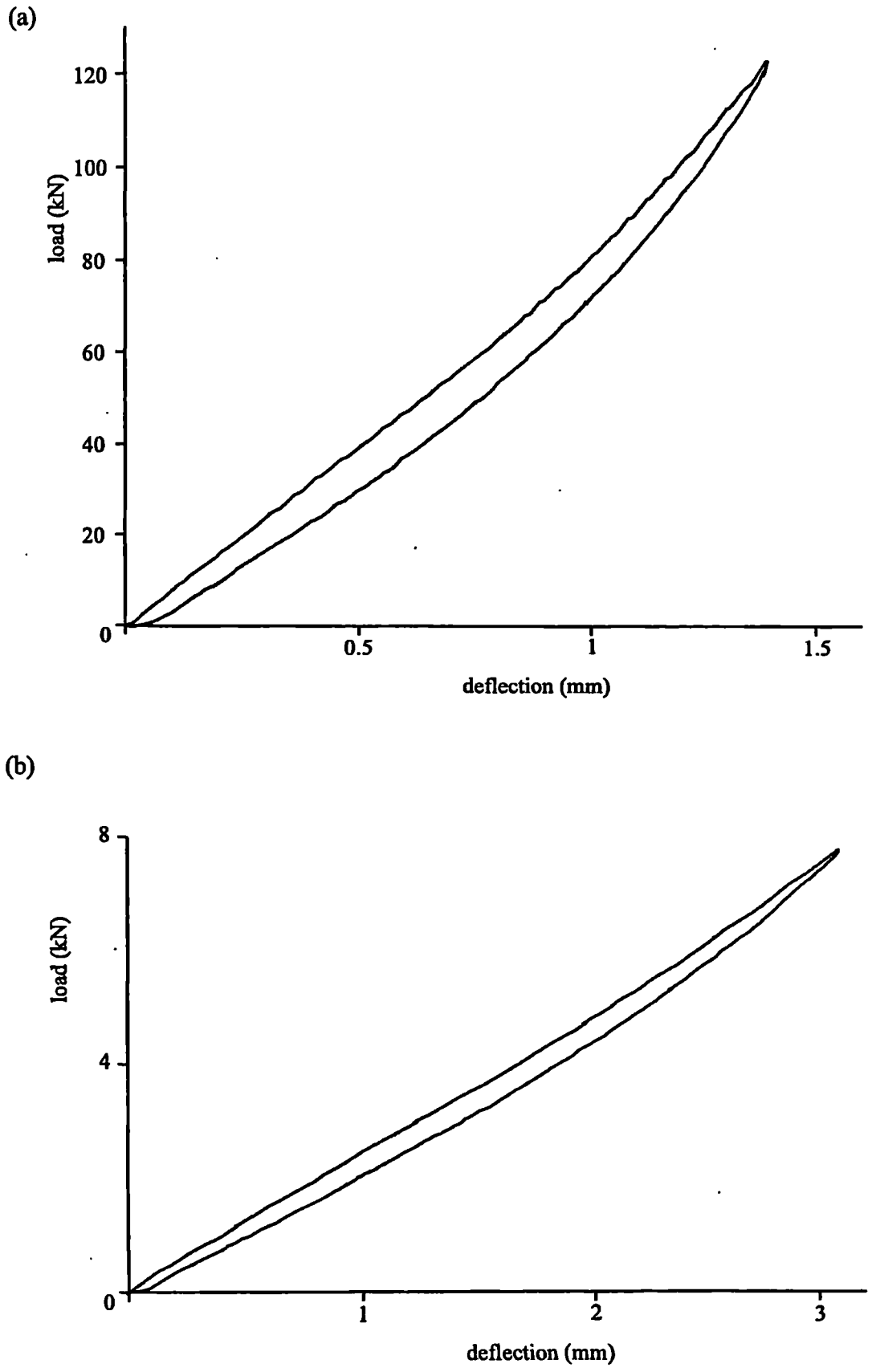

Figure 2.4 Typical fourth cycle force-deflection plots for bonded pads. (a) pad size 304×299mm, (b) pad size 76.5×75.9mm

The compression modulus, E_c, was calculated from:

$$E_c = \frac{kh}{A} \tag{2.7}$$

where k is the stiffness, h the height and A the area of the pad.

The quasistatic stiffnesses and compression moduli are given in Table 2.1. Comparison of the plots for all four quasistatic cycles for one of the tests indicated that the stiffness was not detectably altered by cycling. The dynamic stiffnesses, obtained directly from the frequency response analyser, and compression moduli, calculated from equation (2.7), are given in Table 2.2.

Table 2.2: Dynamic stiffnesses and compression moduli at 5% prestrain and 0.4mm dynamic amplitude

pad size (mm x mm)	Stiffness (kN/mm) at frequency (Hz)			E_c (MN/m$^{2)}$ at frequency (Hz)		
	1	2	5	1	2	5
304 x 299	150	162	176	41.0	44.4	48.1
249 x 251	94.7	103.6	113.5	37.7	41.3	45.2
199 x 199	49.3	53.6	59.0	31.0	33.7	37.1
150 x 150	22.5	24.3	27.2	24.9	26.8	30.1
100.9 x 100.5	7.23	7.75	8.62	17.8	19.0	21.2
75.5 x 75.9	3.37	3.62	4.04	14.7	15.7	17.6
50.0 x 50.0	1.07	1.14	1.27	10.7	11.4	12.6
50.2 x 54.4	1.10	1.17	1.28	10.0	10.7	11.7
50.2 x 50.4	1.00	1.06	1.16	9.8	10.4	11.4
49.8 x 49.5	1.03	1.10	1.22	10.4	11.1	12.3
49.6 x 49.7	1.02	1.09	1.20	10.3	11.0	12.1
24.1 x 25.2	0.212	0.228	0.254	8.4	9.0	10.1
24.3 x 25.2	0.222	0.239	0.268	9.0	9.7	10.9

E_c, obtained from both the quasistatic and dynamic data, is plotted against S^2, as defined in equation (1.61), in Figure 2.5.

2.4.3 *Calculation of bulk and shear moduli*

It was concluded in Section 2.2 that the most reliable and easily computed equations available to relate the compression modulus, E_c to the shear and bulk modulus were equations (2.1) and (2.2). For this work a fit of the data to equation (2.2a) was made with the aid of STATISTICA curve fitting software. For the sizes of pad where more

than one measurement had been made one average value was used for the curve-fitting so that the data was weighted reasonably evenly across the range of values of S^2 investigated. The values of G_{eff} and K_{eff} obtained from the curve-fit are given in Table 2.3 and the best fit curves are shown in Figure 2.5. Values for Poisson's ratio, υ, were computed by using the relationship derived from classical elasticity theory, equation (1.59).

Table 2.3: Values of shear modulus G_{eff}, bulk modulus, K_{eff} and Poisson's ratio υ calculated to fit the experimental values of E_c as a function of S^2 using an equation of Lindley (1979)

Frequency	prestrain (%)	G_{eff}(MPa)	K_{eff} (MPa)	υ
Quasistatic	1	2.01	23	0.460
1Hz	5	2.48	61	0.480
2Hz	5	2.65	67	0.481
5Hz	5	3.00	70	0.480

2.5 Direct measurement of the shear and bulk moduli

2.5.1 *Introduction*

Confidence in the use of Lindley's (1979) equation (2.2a) to provide an estimate of G_{eff} and K_{eff} would be improved by comparing the value obtained in the previous section with more direct measurements. The shear modulus was measured by shearing a pair of 50 x 50 x 25mm pads. The bulk modulus was obtained by compressing a cylinder of the compressible rubber in a way which prevented any lateral expansion. This type of deformation is not exactly bulk compression which requires an equal stress in all directions. Classical elasticity theory relates the constrained unidirectional compression modulus, E_∞ to the bulk modulus K by (see equations (1.57) and (1.58)):

$$K = E_\infty - 4G/3 \qquad (2.8)$$

2.5.2 *Direct measurement of shear modulus*

2.5.2.1 Experimental method

Two of the 50x50mm pads tested in Section 2.4 (those denoted C and D) were bonded with cyanoacrylate adhesive to suitable metal end pieces and bolted in a double shear

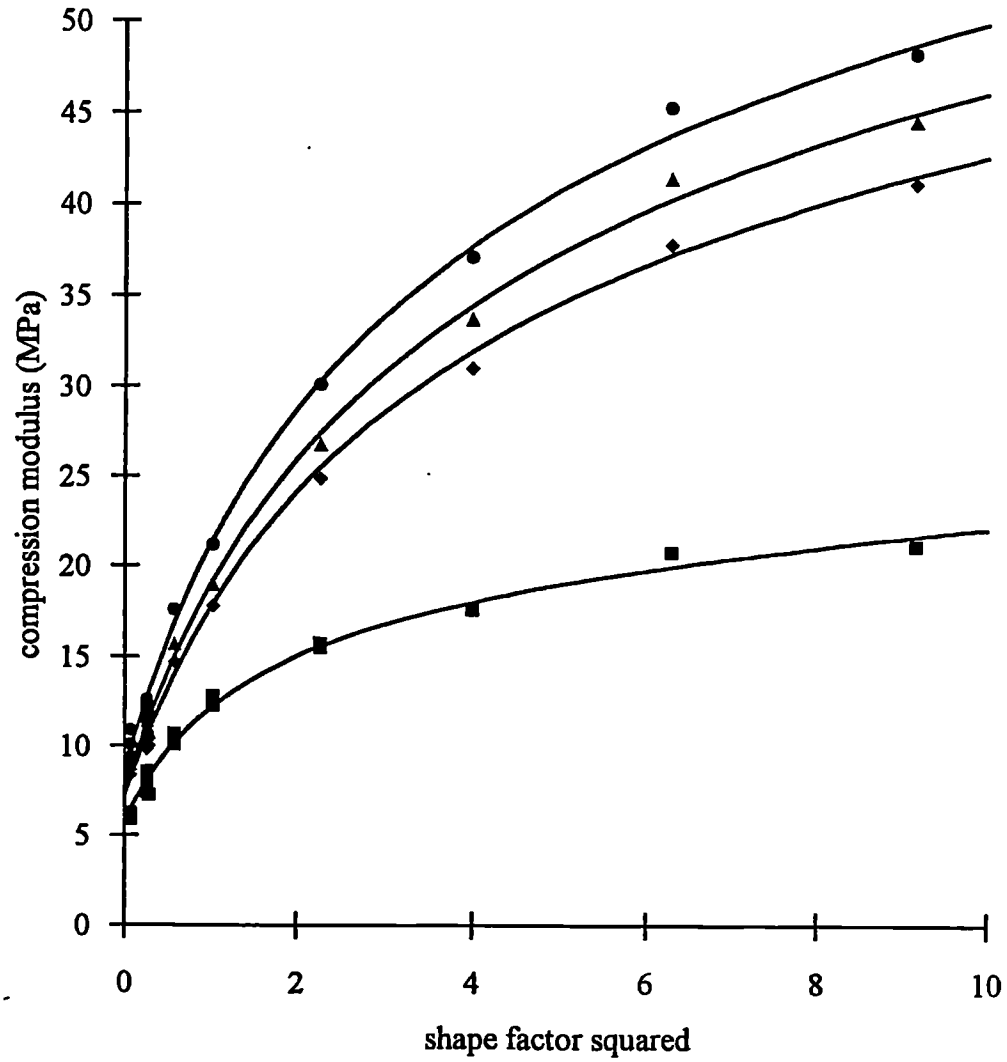

Figure 2.5 Plots of apparent compression modulus, E_c as a function of shape factor squared. The symbols represent experimental points: ■ quasistatic, ◆ 1 Hz, ▲ 2 Hz, ● 5 Hz. Solid lines are fits to equation (2.2a) with the parameters given in Table 2.3.

arrangement (Figure 2.6). A shear force was applied with a 10kN Zwick screw-loaded test machine. The shear displacement was measured with an LVDT mounted on the stationary part of the jig and bearing against the crosshead of the machine.

The rate was calculated to be consistent with the quasistatic measurements in bonded compression by ensuring an equal rate of increase of strain energy. Thus:

$$\frac{1}{2}G\gamma^2 = \frac{1}{2}E_c e^2 \qquad (2.9)$$

where γ is the shear strain and e the strain in bonded compression. Taking $E_c/G = 2$ for pads of this shape factor (see Figure 2.5 and Table 2.3) gives, from equation (2.9) $\gamma = 2e = 1.6$mm/minute.

The shear force and shear displacement were plotted on chart recorder paper. The platen temperature was 10.5°C. Since this was significantly lower than during the bonded compression tests and a long time had elapsed since these tests (Section 2.4), one of the bonded pads (pad A) was retested at the lower temperature on the Zwick test-machine fitted with a 10kN load-cell following the procedure described in Section 2.4.1. E_c at 1% strain was found to be 7.6MPa. Comparison with Table 2.1 indicates that this was similar to the value obtained using the 7kN Schenck machine. It was thus assumed that the effects of temperature and ageing were not significant.

2.5.2.2 Results and calculations

The shear force deflection plot is given in Figure 2.7. Debonding between the rubber and the steel plates to which they were bonded (see Section 2.4.1) was observed at a shear strain of about 5%. Below this point the force deflection curve was linear. The apparent shear modulus, G_{app}, for this was calculated from the stiffness of this linear portion from:-

$$G_{app} = \frac{kh}{2A} \qquad (2.10)$$

where k is the shear stiffness for the pair of pads, h the height and A the cross-sectional area of the testpieces. This yielded $G_{app} = 1.63$MPa. Since the testpiece height to breadth ratio was high a correction to allow for bending was applied, given by (Rivlin and Saunders, 1949):-

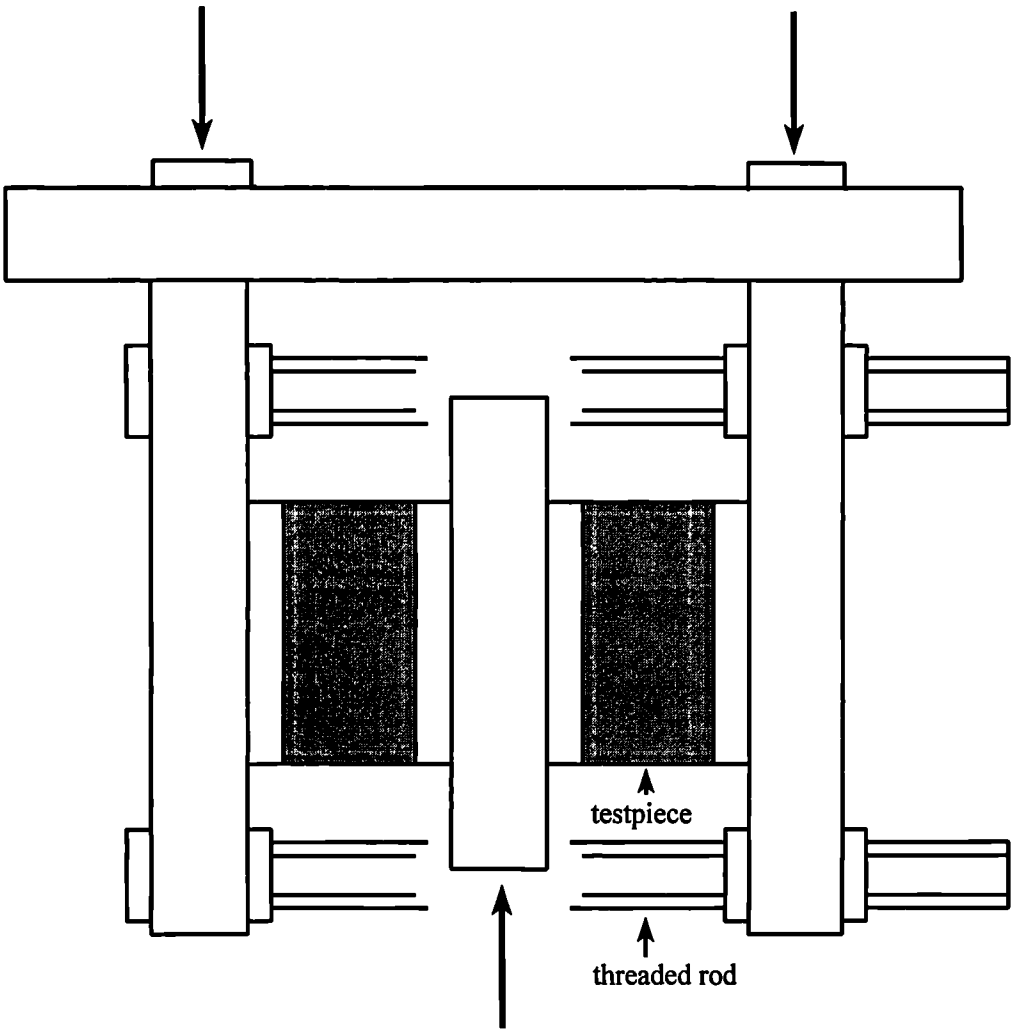

Figure 2.6 Schematic diagram of jig for measuring shear stiffness of pads.

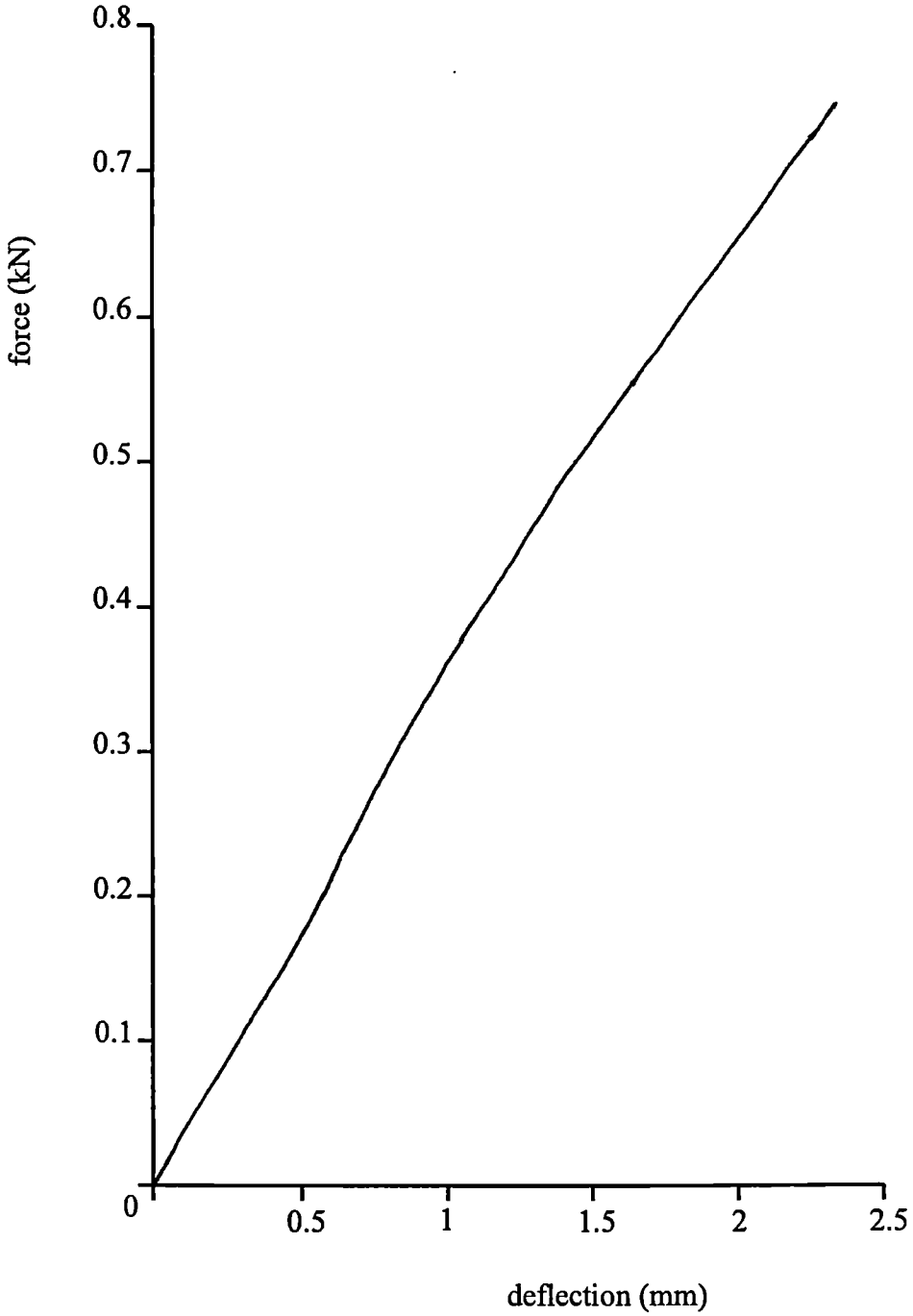

Figure 2.7 force-deflection plot for a pair of compressible pads in shear.

$$G_{eff} = G_{app}\left(1 + \frac{h^2}{3A}\right) \qquad (2.11)$$

for a square block where G_{eff} is the effective shear modulus deduced for the "composite" material. This yielded G_{eff} = 1.77MPa.

2.5.3 *Measurement of bulk modulus*

2.5.3.1 Experimental method

A cylinder of the elastomer of nominal height 25mm and diameter 27mm was cut with a cork borer. It was found that standard cork borers produced a slightly tapered sample due to strains developing in the elastomer as the borer becomes embedded in the rubber. In order to produce a sample of uniform diameter, a cork borer was constructed with a thin wall thickness (~0.5mm) and with the cutting edge at the centre of the wall thickness. The cork borer was liberally lubricated with detergent before cutting the sample.

The sample was lubricated with silicone fluid and fitted tightly into a thick-walled steel cylinder with a close-fitting piston (Figure 2.8). For measurements on a virtually incompressible homogeneous rubber, a tight fit is not necessary as shear deformation of the material to fill the cavity does not significantly affect the bulk modulus. For this material, however, such shear deformation could cause a significant distortion of the cellular filler particles with a consequent effect on the bulk compression behaviour. The apparatus was compressed in a Zwick 100kN screw-driven test machine at a rate of 10mm/minute. This rate was expected to result in an approximately adiabatic deformation. The displacement was recorded from an auxiliary LVDT placed directly between the platens. Smooth passage of the piston into the cylinder was ensured by use of a device incorporating a ball bearing as a point contact between the piston and the top platen.

In order to facilitate comparison with the quasistatic data of Section 2.4 the testpiece was subjected to four cycles of compression to progressively increasing loads of 9.2kN, 10kN, 22.5kN and 50kN. The force-deflection plots were obtained directly from the load-cell and LVDT outputs.

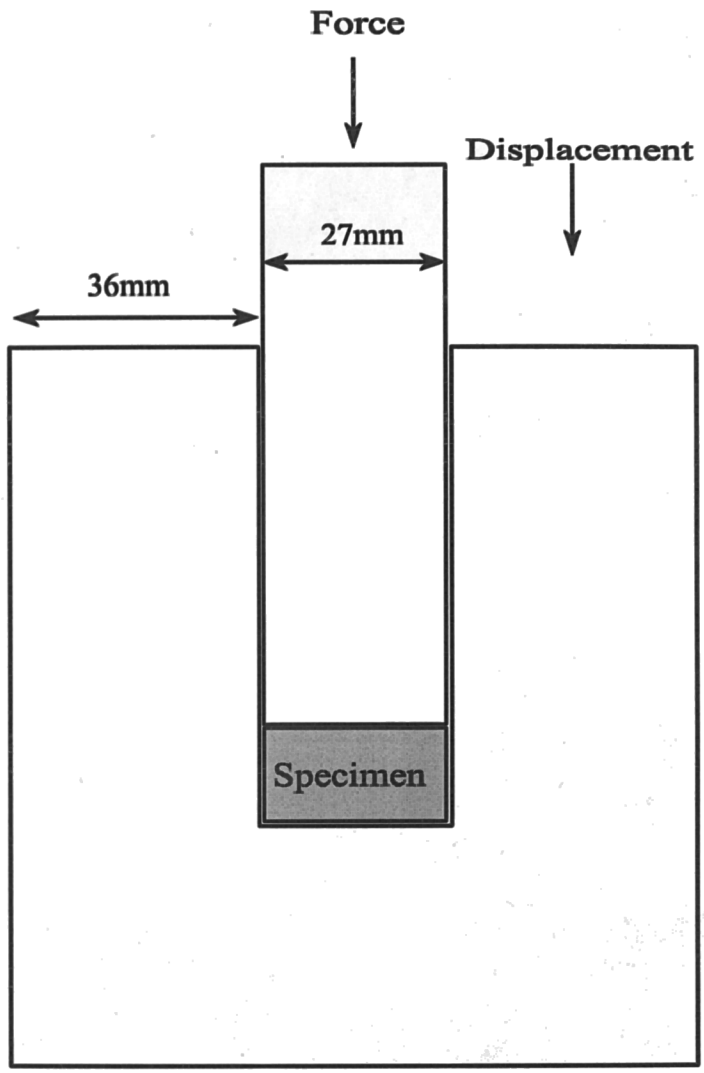

Figure 2.8 Schematic diagram of the bulk compression apparatus

2.5.3.2 Results and discussion

The first and fourth cycle force-deformation plots are shown in Figure 2.9. A very large increase in stiffness was seen at a compression of about 12% on all four cycles. Away from this point the force deformation behaviour was approximately linear. The constrained compression modulus was calculated from:-

$$E_{\infty} = \frac{kh}{A} \qquad (2.12)$$

where k is the stiffness, h the height and A the cross-sectional area of the testpiece.

The modulus in the region below the sharp upturn was calculated at about 1% strain from all four cycles, yielding 43MPa, 41MPa, 39MPa and 41MPa for the 1st, 2nd, 3rd and 4th cycles respectively. Since these values show no systematic change, and the sharp upturn occurred at the same strain on all four cycles it was concluded that the material was reversible, and thus differences of strain history between samples subjected to different tests were not important.

The stiffness above the sharp upturn was obtained from the fourth cycle, since the maximum of the first three cycles occurred before a clear linear region was reached. Thus:

$$E_{\infty} (1\% \text{ strain}) = 41 \pm 2\text{MPa}$$

$$E_{\infty} (15\% \text{ strain}) = 2700\text{MPa}$$

are representative of the linear regions below and above the sharp upturn respectively. The results of section 2.5.2 suggest that $G_{eff} \simeq 1.8$MPa. Thus $E_{\infty} >> G_{eff}$ and use of equation (2.8) shows that $K_{eff} \simeq E_{\infty}$.

2.6 Comparison of experimentally determined values of K_{eff} and G_{eff}

A solid rubber has, typically, a bulk modulus of around 2000MPa and a Poisson's ratio of 0.4998 (Holownia, 1975). The presence of the compressible filler, even in modest quantities, appears to cause a marked increase in compressibility.

The experiments have provided different estimates of K_{eff} and G_{eff} for this material. For the experiments in bonded compression, the higher moduli for the dynamic compared to the quasistatic data would be expected both due to the viscoelastic nature of the

(a)

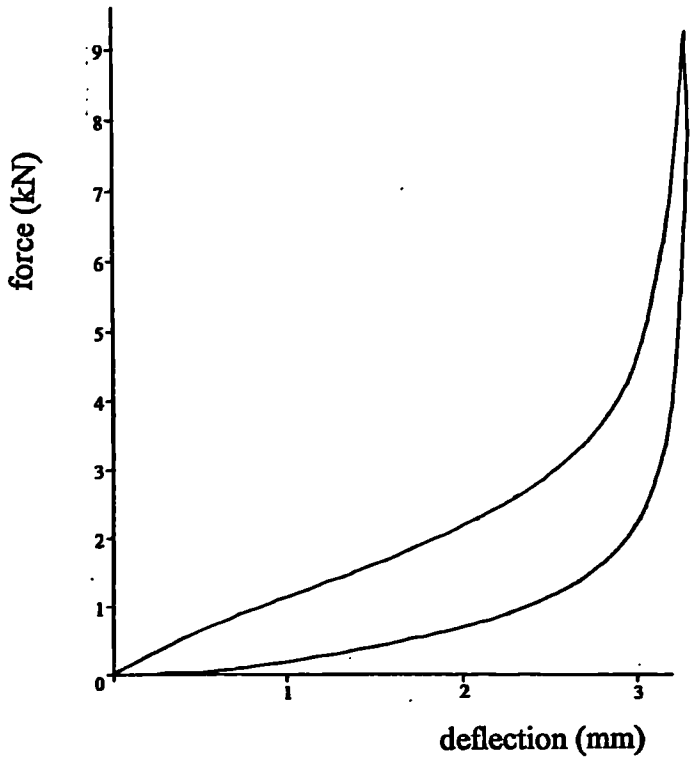

(b)

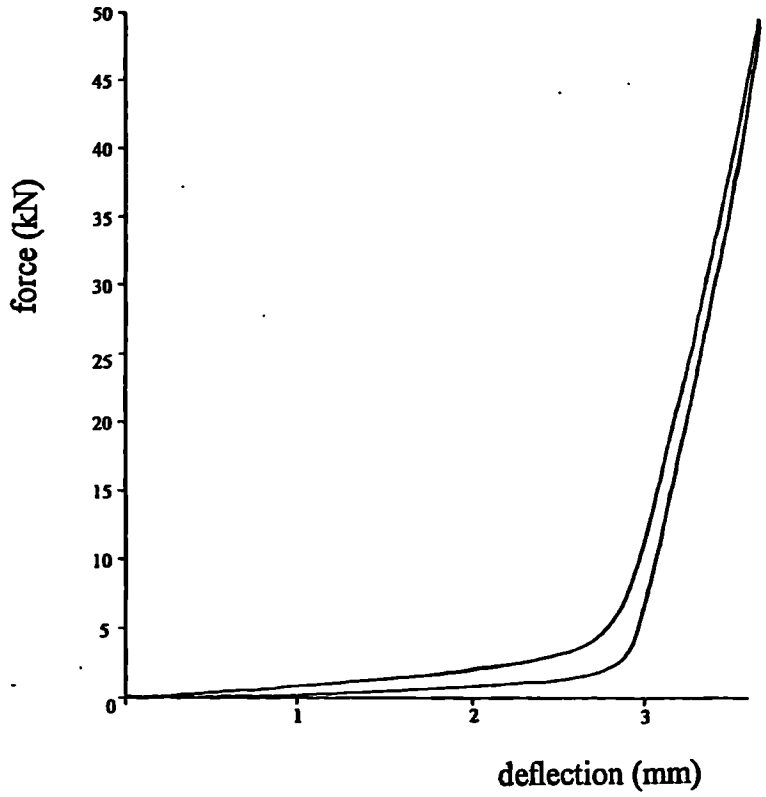

Figure 2.9 Force-deflection plot for confined compression.
(a) first cycle, (b) fourth cycle.

material and as a consequence of the 5% static strain imposed during the dynamic tests; it is apparent from figures 2.4 that the material is stiffer at 5% strain where the dynamic measurements were made than at 1% strain where the quasistatic measurements were made. The increase in stiffness with frequency is also typical of viscoelastic behaviour.

Comparison of the quasistatic value of K_{eff} calculated from bonded compression (23MPa) is somewhat lower than that determined by direct measurement (41MPa). Some of the discrepancy may be due to differences in strain rate in the two experiments as it is clear from Table 2.3 that K_{eff} is rate dependent. Also it is possible that the compressibility of the filler particles is influenced by the type of deformation: their stiffness for a deformation where lateral expansion is permissible may be lower than where it is prevented due to the nature of the buckling of the cellular material.

The value of G_{eff} obtained directly is about 10% lower than that obtained from calculation from bonded compression. No clear explanation for this is apparent although, since the results of Table 2.1 indicate a significant difference in the compression stiffnesses measured with different test machines, the prediction from bonded compression will contain a significant margin of error.

The following features of the deformation behaviour are indicative of the presence of a compressible filler. The increase in stiffness with strain apparent in the compression deformation of bonded pads (Figure 2.4) could be attributed to the collapse of filler particles at higher loads, though geometric effects would cause a similar force-deflection behaviour of incompressible bonded rubber pads. The higher values of Poisson's ratio from the dynamic compared to the quasistatic measurements could also be a consequence of collapse of filler particles under the 5% strain imposed during dynamic measurements. The sharp upturn in stiffness at a well-defined strain of about 12% in the bulk compression measurement may be attributed to complete collapse of the cellular filler. The bulk modulus above this strain (2700MPa) is of the magnitude expected for a solid rubber (Holownia, 1967). Also, K_{eff} increases with dynamic frequency in a similar way to G_{eff} (see Table 2.3). This suggests that a shear mechanism is involved in the deformation such as a shear distortion in the rubber induced by the shrinkage of filler particles. Bulk compression of a homogeneous solid rubber would not be expected to be very frequency dependent.

2.7 Estimation of the volume fraction of voids

Theoretical calculations of the compressibility caused by voids were reviewed in Section 1.3.3. An estimate of the volume fraction of voids due to the cellular filler in this material was made using Thomas's (private communication) theory; equation (1.50). The assumptions inherent in this equation are that the voids are well-spaced and spherical, and that the matrix surrounding them is incompressible. Although strict adherence to these is unlikely, they are reasonable for an approximate calculation and modest departures are not likely to have a large influence on the compressibility in any case. Obviously, the volume fraction of filler would be somewhat larger than the volume fraction of voids for a given stiffness.

Equation (1.50) requires a value for the shear modulus of the rubber matrix, rather than the filled material. Equations are available in the literature (McKenzie, 1950; Kerner, 1956) which relate the shear modulus, G_{eff}, of a solid containing spherical holes or inclusions to the shear modulus, G, of the matrix. The expressions differ slightly; that of McKenzie (1950) reduces to:-

$$G_{eff} = G\left(\frac{3 - 2v}{3 + 3v}\right) \approx G\left(1 - \frac{5}{3}v\right) \qquad (2.13)$$

for an incompressible matrix containing spherical holes, whereas that of Kerner (1956) becomes:-

$$G_{eff} = G\left(\frac{3 - 3v}{3 + 3v}\right) \approx G(1 - 2v) \qquad (2.14)$$

under the same conditions. However, for modest values of v, the difference between equations (2.13) and (2.14) is small.

Substitution of equation (2.13) in equation (1.50) and neglecting powers of v^2 gives:-

$$v = \frac{4G_{eff}}{3K_{eff} - 4G_{eff}} \qquad (2.15)$$

Thus, assuming the rubber containing cellular filler behaves like an incompressible material containing some effective volume of voids, the volume fraction of voids may

be estimated from equation (2.15). Use of the quasistatic values of K_{eff} and G_{eff} given in Table 2.3 indicates a volume fraction of voids of about 13% whereas use of the directly measured values of K_{eff} and G_{eff} gives a volume fraction of voids of about 6%.

The position of the sharp stiffness upturn under bulk compression (Figure 2.9) indicated a volume fraction of voids of about 12%. This value would be expected to be greater than that found by application of (2.15) because a significant pressure is no doubt needed to reduce the volume of the compressible filler whereas the theory assumes no such volumetric stiffness for the voids and so will underestimate their volume for a given K_{eff}. This suggests that the value of v derived from bonded compression using Lindley's (1979) equation (2.2a) is rather high. However, the value obtained from the direct measurements seems somewhat low.

2.8 Conclusions

Measurements were made of the small strain compression modulus of pads containing a compressible filler, where lateral expansion of the surfaces normal to the compression was prevented. The results supported the use of Lindley's (1979) equation to obtain a reasonable prediction of the effective bulk compression modulus and shear modulus of a compressible material.

A simple model (Thomas, private communication) gave a plausible estimate of the volume fraction of filler for this material of around 10%.

CHAPTER 3

Measurement of $\partial W/\partial I_1$ and $\partial W/\partial I_2$ from a split pure shear technique for a series of filled natural rubber formulations

3.1 Introduction

Comprehensive evaluation of the strain energy function, W, where $W=W(I_1,I_2)$, requires the use of an experimental technique in which the strain energy derivatives, $\partial W/\partial I_1$ and $\partial W/\partial I_2$, may be calculated from stress-strain data obtained for all possible combinations of I_1 and I_2. Such measurements require a full biaxial test where the extension in two perpendicular directions may be varied freely. Two experimental arrangements have been exploited by previous workers to obtain such data; the biaxial extension of a flat sheet and the simultaneous extension and inflation of a thin-walled tube. (See Section 1.2.3). The possible combinations of I_1 and I_2 were shown in Figure 1.5, together with a set of solid lines which represent the biaxial experiments of Rivlin and Saunders (1951).

A number of difficulties with the full biaxial tests are apparent. The experiments themselves may be difficult or costly to perform, requiring a specially constructed biaxial test rig to enable simultaneous expansion of the rubber sheet in two directions along with accurate measurement of the extensions and forces. The experimental difficulties are exacerbated by the high sensitivity of the expressions for $\partial W/\partial I_1$ and $\partial W/\partial I_2$ to small errors at low values of I_1 and I_2. For this reason, Rivlin and Saunders (1951) were unable to obtain data with confidence for values of I_1 or I_2 less than about 5. Subsequent modifications of Rivlin and Saunders' (1951) technique have been liable to increase the problem. For example, Kawabata et al (1981) experienced difficulty with force measurements due to friction. Perhaps of more importance is the difficulty of dealing with the departures from elasticity, especially in filled rubbers. A particular problem is the influence of previous strain history on the stress-strain behaviour. Some workers (see Section 1.2) have attempted to eliminate the effect of previous strain history by subjecting the testpiece to several large prestrains before beginning measurements. Others (Rivlin and Saunders, 1951) have designed their experiments such that one of I_1 and I_2 increases whilst the other remains the same as a way of

minimizing any softening due to previous strains. Whatever the procedure adopted, only a limited number of experiments can be carried out, thus one is forced to assume that particular choices of combinations of I_1 and I_2 are representative.

The split pure shear technique was developed as a way of obtaining sufficient information to calculate $\partial W/\partial I_1$ and $\partial W/\partial I_2$ in the particular case that $I_1 = I_2$ without the need for full biaxial tests. Both non-zero principal stresses were measured, thus providing more information than is possible from uniaxial tests.

Since $I_1 = I_2$, some of the difficulty of dealing with the effects of strain history is avoided since straining the pure shear testpiece will cause I_1 and I_2 to rise together. This loss of generality compared to full biaxial tests could be seen as an advantage. For the purposes of this work other strain history effects are avoided by considering only the first loading curve of previously unstrained testpieces.

3.2 **Development of the experimental technique**

3.2.1 *Basic description of apparatus*

The split pure shear apparatus is shown in Figure 3.1. It was fitted in an Instron screw-driven tensile test machine such that the main force was obtained from the machine's load cell. The transverse force was also measured by means of cantilever load cells incorporated in the bottom part of the apparatus. Slits, approximately 1mm wide, were made in the bottom clamp to accommodate the small movements necessary for the correct functioning of the load cells. The longitudinal displacement was usually obtained from an auxiliary LVDT bolted to the lower part of the apparatus and bearing against a small plate attached to the upper part. The load cell and displacement readings were recorded by plotting directly onto a multiaxial chart recorder.

The testpiece comprised a strip of rubber of nominal dimensions 200 x 20 x 1 mm bonded during moulding along the long edges to 1mm thick steel strips to facilitate fixing in the clamp. (Figure 3.2). The steel strips contained slits coinciding with the slits in the lower clamp for accommodating the transverse load cells. The dimensions of the rubber and the position of the load cells were chosen such that the rubber could be

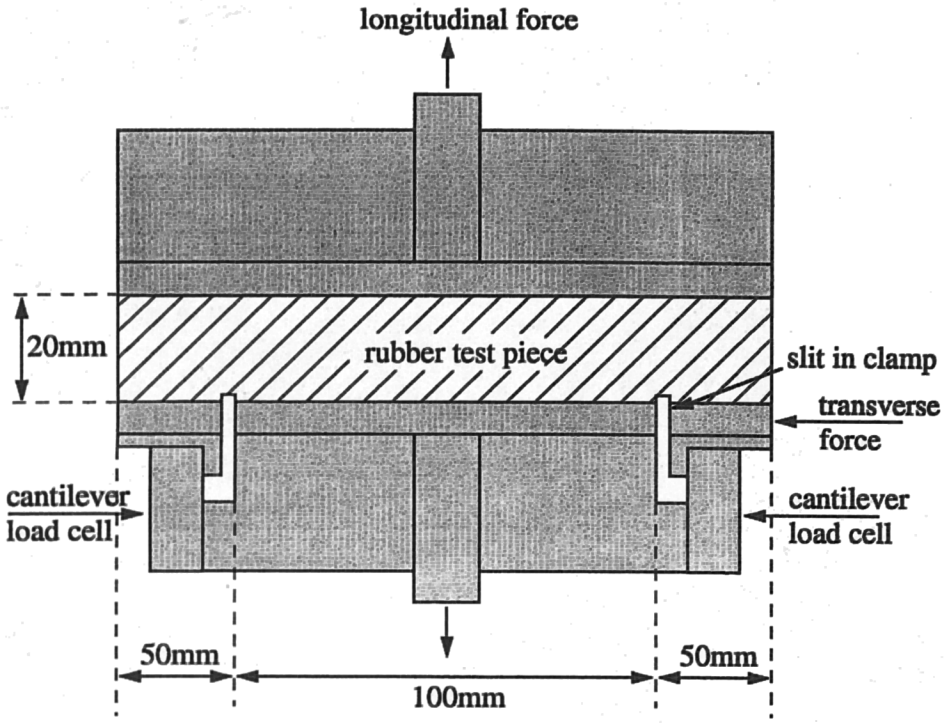

Figure 3.1 Split pure shear apparatus

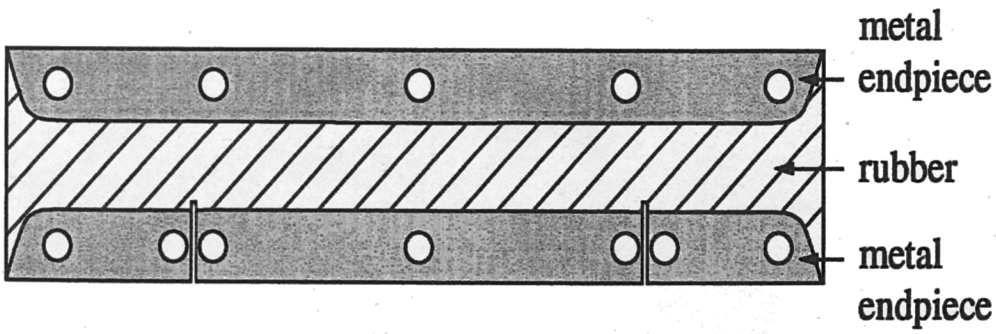

Figure 3.2 Bonded pure shear testpiece

assumed to be in pure shear (see Section 3.2): there was no strain in the transverse direction. The testpiece height was measured with vernier callipers graduated to 0.01mm from which the height of the metal strips was subtracted. The thickness was measured with a spring loaded dial gauge also graduated to 0.01mm. The width was measured with a steel ruler graduated to 0.5mm.

3.2.2 *Preliminary checks*

During development of the apparatus various experimental difficulties were identified.

(i) Because the main force was around 50 times greater than the force registered by one transverse load cell, misalignment of the bottom part of the apparatus such that it was not exactly perpendicular to the line of action of the main force resulted in a very large spurious component in the measured transverse force.

(ii) Failure to ensure correct orthogonal separation of the top and bottom clamps resulted in a spurious simple shear component in the measured transverse force. Also the screw-drive to the test machine crosshead lacked linear bearings, resulting in a small periodic oscillation from side to side. This caused a periodic undulation in the measured transverse force.

(iii) If the top and bottom parts of the apparatus were not exactly parallel the strain varied across the width of the testpiece. The main force was automatically averaged across the width of the testpiece, whereas the measured transverse force was applicable to the strain at the position of the slit.

These three alignment problems were tackled in two ways. Firstly, two cantilever load cells were incorporated in the bottom part of the apparatus. These registered equal and opposite errors due to (i) and (ii) above and also helped to reduce (iii). An average of the readings from the two load cells was thus deemed to be correct. Secondly, two levelling devices were constructed to fit above and below the top and bottom parts of the apparatus. These enabled fine adjustments to the position and tilt of the clamps to be made by turning a set of thumb screws. The setting-up procedure adopted was to level the bottom clamp carefully, checking its position with a sensitive spirit level, then to lower the top clamp until it was resting against the bottom clamp under its own weight and fix it in this position by tightening the screws in the upper levelling device. This ensured that the clamps were exactly parallel. The testpiece was bolted into

position after this levelling procedure had been carried out.

(iv) The cantilever load cells are subjected to large forces perpendicular to their direction of operation due to the action of the main force which is about 50 times the transverse force. The possibility that this affected the measurement was investigated by checking the calibration of the load cells with and without a 9.8N weight hung from them to simulate the action of the main force. The test was repeated four times and the load cell was carefully levelled with a spirit level between readings. The differences in the readings with and without the 9.8N weight were 0.010N, 0.016N, 0.035N and -0.015N. Since these values showed no systematic deviation from zero and were equivalent to a misalignment of about 0.1° it was assumed that the main force would cause no significant error in the measurement of the transverse force.

(v) Effect of slit size

Experimental checks

During preliminary experiments, rather than being bonded to steel strips, the testpieces were cut from a sheet of rubber. Slits were cut in the testpieces to coincide with the slits in the clamp accommodating the action of the cantilever load cells and the rubber was clamped directly. Various problems were encountered; in particular rubber was squeezed out during the clamping procedure. This led to uncertainty in the unstrained length of the testpiece and tended to obstruct the slit, preventing the free operation of the cantilever load cells. It was also found that if the slit in the rubber was over long and extended beyond the clamping edge into the testpiece a significant reduction in the measured transverse force was seen - about 5 to 10% reduction per millimeter extension of the slit into the testpiece.

Finite element analysis

The error in the transverse force due to the slit was also estimated from MARC finite element analysis. The rubber was modelled as a neo-Hookean material with a shear modulus of 0.5MPa. Due to the vertical line of symmetry down the centre of the testpiece it was only necessary to model half of the testpiece. A mesh was constructed containing a greater number of quadrilateral elements in

the vicinity of the slit. (Figure 3.3a). The slit was modelled by duplicating a node on each of the bottom two rows of elements, thus enabling two pairs of elements to separate. (Figure 3.3b). The combined height of these elements was $^1/_{10}$ of that of the testpiece, thus the slit was modelled as if it protruded $^1/_{10}$ of the way into the testpiece which was a rather longer distance than was likely in actual experiments. The width of the slit, for simplicity, was zero.

Boundary conditions were set up such that the nodes along the top, bottom and one side of the model were constrained from moving horizontally, simulating the constraint of the metal strips and the centre line symmetry. A vertical deformation of 100% was applied in 10 increments. The elements were modelled in plane stress. The transverse force registered by one cantilever load cell was calculated as the sum of the horizontal reaction forces on the nodes between the bottom of the slit and the bottom corner of the free side of the testpiece. This represents the horizontal force supported by one load cell.

By introducing additional duplicated nodes, slits of $^1/_5$ and $^3/_{10}$ of the length of the testpiece were modelled. The deformed meshes are shown in Figures 3.3c and 3.3d. Also, the cases for no slit and a slit running the entire length of the testpiece were modelled (Figure 3.3e). The results are given in Table 3.1.

Table 3.1: Finite element predictions of reduction of transverse force due to protruding slit

slit length as fraction of testpiece length	horizontal reaction force (MPa)	reduction in reaction force compared to no slit
0	0.0375	0
$^1/_{10}$	0.0332	11%
$^2/_{10}$	0.0286	24%
$^3/_{10}$	0.0240	36%
1	0	100%

The dimensions of the model were of a testpiece of length 0.2 and width 2. For a neo-Hookean material with a shear modulus of 0.5MPa in pure shear, the theoretical reaction force is given by equation (3.1b) (see Section 3.3.4) with $2\partial W/\partial I_1 = 0.5$MPa and $\partial W/\partial I_2 = 0$. These results suggest that, for a testpiece

(a)

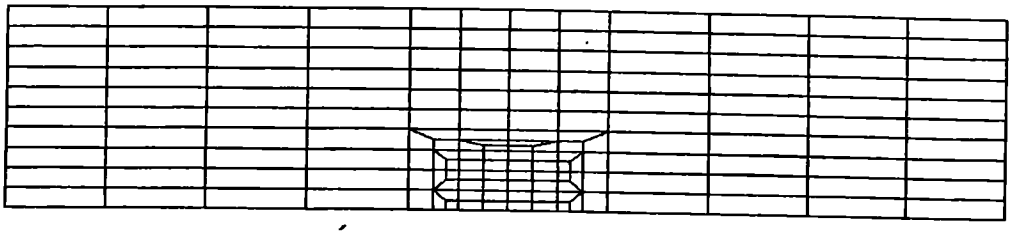

(b)

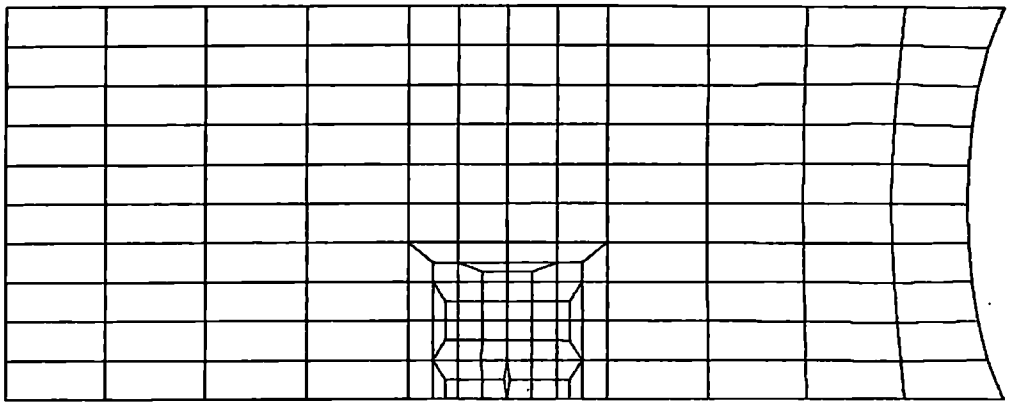

(c)

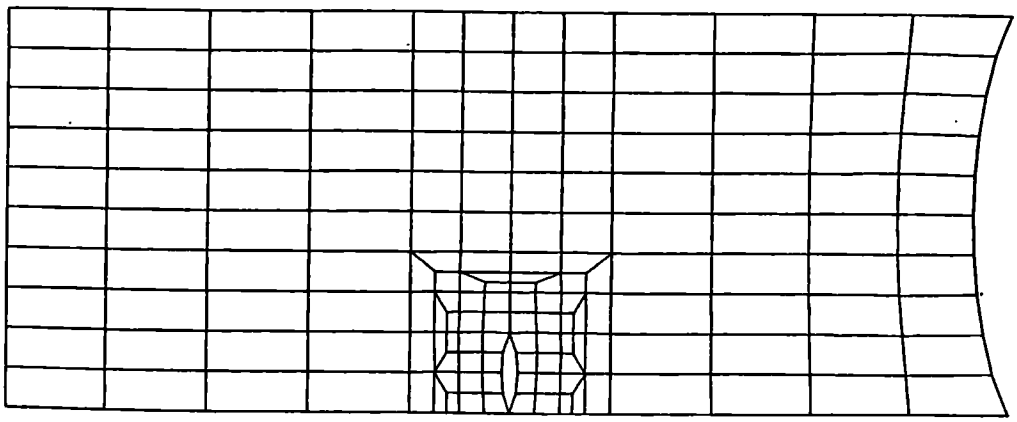

(d)

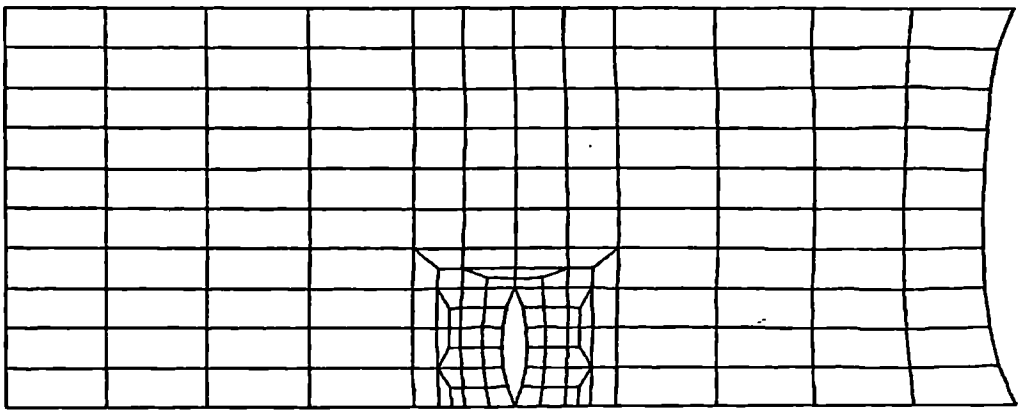

(e)

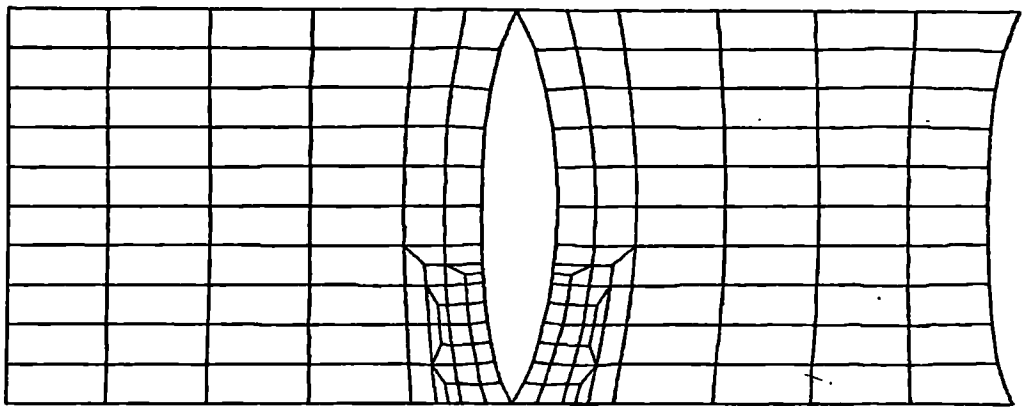

Figure 3.3 Finite element mesh for modelling of the slit in the pure shear clamp. (a) undeformed mesh. (b) to (e) deformed mesh after 100% strain in the y direction for slits of (b) $^1/_{10}$, (c) $^1/_5$, (d) $^3/_{10}$ and (e) the entire height of the testpiece.

20mm high, the transverse force is reduced by approximately 5% for each mm protrusion of the slit into the testpiece, consistent with experimental observations.

Use of the bonded type of testpiece ensured that protrusion of the slit into the testpiece was minimal - less than about 0.5mm and that the conditions near the slit were as reproducible as possible. The main difficulty was ensuring that the slits were free from rubber which could hinder the movement of the cantilever load cells.

(vi) Deviations from pure shear geometry

For a pure shear deformation in an incompressible material, the extension ratios are related such that $\lambda_3 = 1/\lambda_1$ and $\lambda_2=1$. This may be achieved experimentally by stretching a sheet of rubber whilst preventing lateral contraction. The testpiece shown in Figure 3.2 approximates to this because the width is much greater than the length, thus contraction parallel to the clamping edge is virtually eliminated. However, the rubber near the unbonded edges of the testpiece is not constrained and will therefore not be in pure shear. In order to provide an estimate of the size of the region which deviates from pure shear and the corresponding error in the main load the testpiece was modelled using MARC finite element analysis. It was important to ensure that the cantilever load cells were positioned sufficiently far from the ends of the clamp that no appreciable deviation from pure shear occurred at the slit.

The finite element mesh, material properties and boundary conditions were as in (v) above except that no refinement of the mesh near the slit was needed. The undeformed mesh is shown in Figure 3.4a. A 100% vertical strain was applied in 10 increments. The deformed mesh is shown in Figure 3.4b. The main force was calculated as twice the sum of the vertical reaction forces along the top edge since only half of the testpiece was modelled. The transverse force was obtained by summing the horizontal reaction forces along the length of a horizontal edge equivalent to the distance between the slit in the clamp and the unbonded edge of the testpiece. These numerical values were then compared to the theoretical

(a)

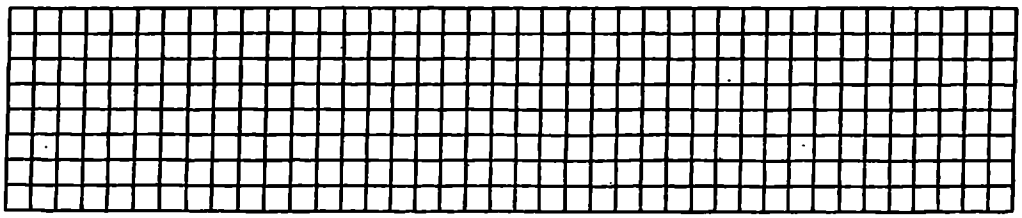

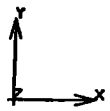

(b)

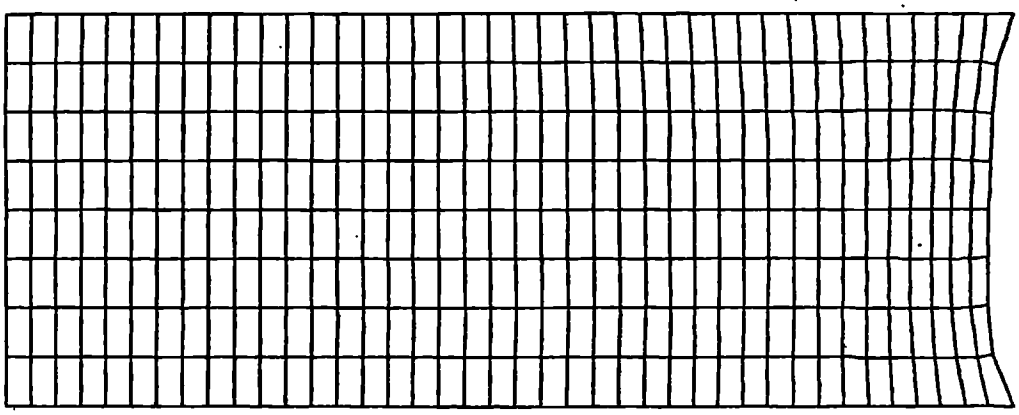

Figure 3.4 Finite element mesh for modelling the edge effect in the pure shear testpiece. (a) undeformed mesh, (b) mesh after 100% shear strain in the y direction.

forces which would be exerted if the testpiece was entirely in pure shear. The theoretical forces were calculated both from equations (3.1) and (3.2) with $\partial W/\partial I_1 = 0.25$MPa and $\partial W/\partial I_2 = 0$ and, as a check, by constraining the free edge in the finite element model to remain vertical. The errors due to deviations from pure shear were thereby calculated to be about 0.5% in the main force and 0.1% in the transverse force. They were disregarded in all subsequent calculations.

3.3 Investigation of a series of natural rubber formulations with a range of filler contents

3.3.1 *Materials*

The rubber formulations are given in Table 3.2 and were taken from the Engineering data sheets (EDS)(MRPRA, 1980). They differ only in content of black and process oil. All the testpieces were cured to maximum rheometer torque at 140°C.

Table 3.2: Natural rubber formulations. Ingredients expressed in parts per hundred of rubber by mass.

EDS number	19	14	15	16
natural rubber, SMRCV60	100	100	100	100
carbon black, HAF (ASTM N-330)	1	15	30	45
process oil[1]	-	1.5	3	4.5
zinc oxide	5	5	5	5
stearic acid	2	2	2	2
antioxidant/antiozonant[2]	3	3	3	3
antiozonant wax	2	2	2	2
accelerator, CBS[3]	0.6	0.6	0.6	0.6
sulphur	2.5	2.5	2.5	2.5
vulcanization time (minutes at 140°C)	40	38	40	40
nominal hardness (IRHD)	43	52	60	71

1. low viscosity naphthenic oil
2. N-(1,3-dimethylbutyl)-N'-phenyl-phenylenediamine
3. N-cyclohexylbenzothiazole-2-sulphenamide

3.3.2 *Experimental method*

The test set-up was as described in Section 3.2.1. The machine crosshead speed was 2.5mm/minute. The testpieces were previously unstrained and were pulled to failure.

3.3.3 *Stress-strain behaviour*

The nominal main and transverse stresses were calculated from the measured forces. It must be noted that the transverse load cells register half the transverse force since it is assumed that there is an equal component in the top clamp. The stress-strain plots are shown in Figures 3.5 and 3.6. The curves show the usual features associated with filled rubbers, namely a high modulus at low strain which at first decreased, then increased as the strains became large. The rubbers with high loadings of filler are stiffer at all strains and the upturn with high strains occurs sooner.

3.3.4 *Magnitude of the transverse force in pure shear*

For pure shear, $\lambda_2 = 1$, $\lambda_3 = 1/\lambda_1$ and $\sigma_3 = 0$, thus equations (1.17) become:

$$\sigma_1 = 2(\lambda_1^2 - \lambda_1^{-2})\left(\frac{\partial W}{\partial I_1} + \frac{\partial W}{\partial I_2}\right) \tag{3.1a}$$

$$\sigma_2 = 2(1 - \lambda_1^{-2})\left(\frac{\partial W}{\partial I_1} + \lambda_1^2\frac{\partial W}{\partial I_2}\right) \tag{3.1b}$$

From the geometry of the testpiece it is known that

$$f_1 = \frac{wt\sigma_1}{\lambda_1} \tag{3.2a}$$

$$f_2 = ht\sigma_2 \tag{3.2b}$$

where f_1 and f_2 are the main and transverse forces respectively and w, t and h are the unstrained width, thickness and height of the testpiece respectively. It is often useful to express the stresses as nominal rather than true stresses. Equation (3.2a) gives

$$s_1 = \frac{\sigma_1}{\lambda_1} \tag{3.3}$$

where s_1 is the nominal stress. Substitution into equation (3.1a) gives

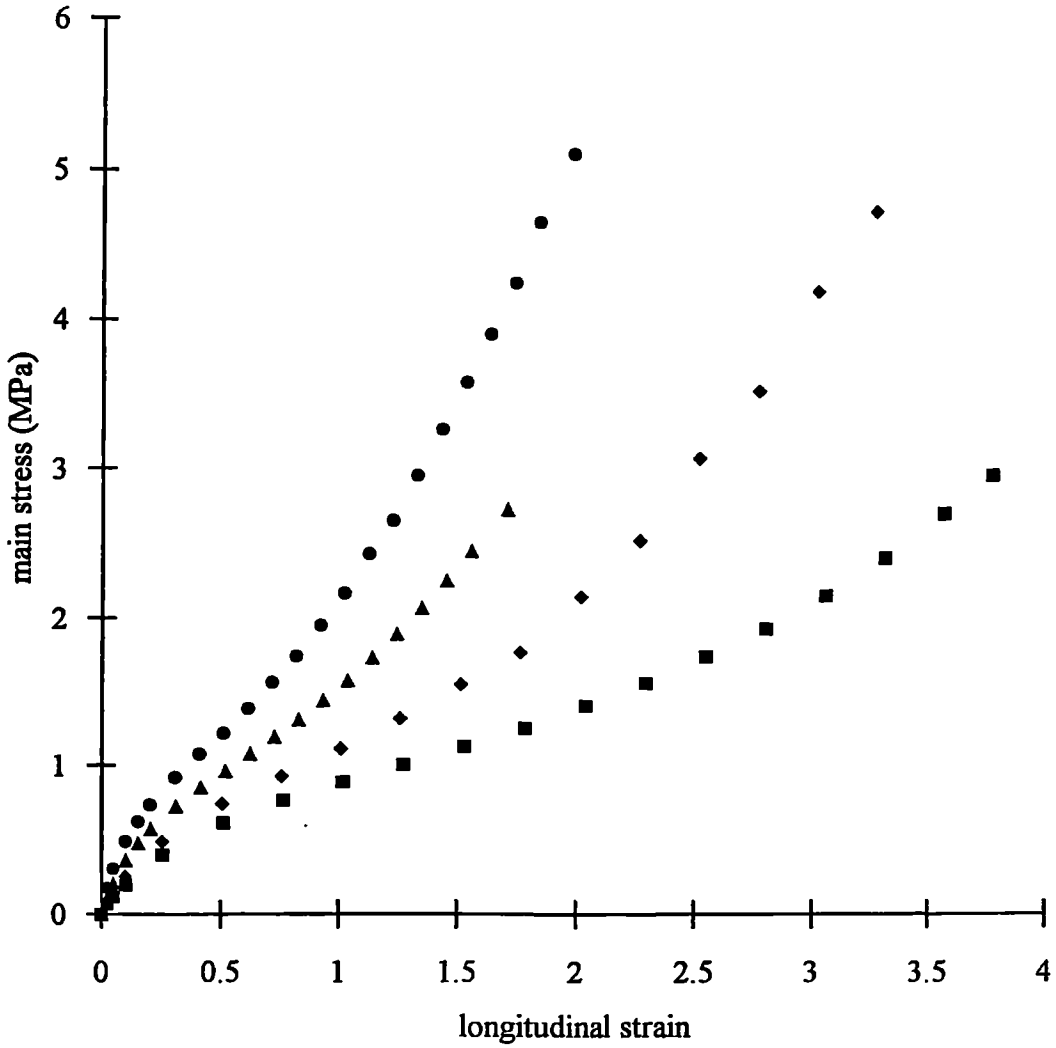

Figure 3.5 Stress-strain plots for the main stress obtained with the split pure shear technique for a series of black filled rubbers.: ■ EDS19 (0), ◆ EDS14 (15), ▲ EDS15 (30), ● EDS16 (45). Filler loadings given in brackets Formulations given in Table 3.2.

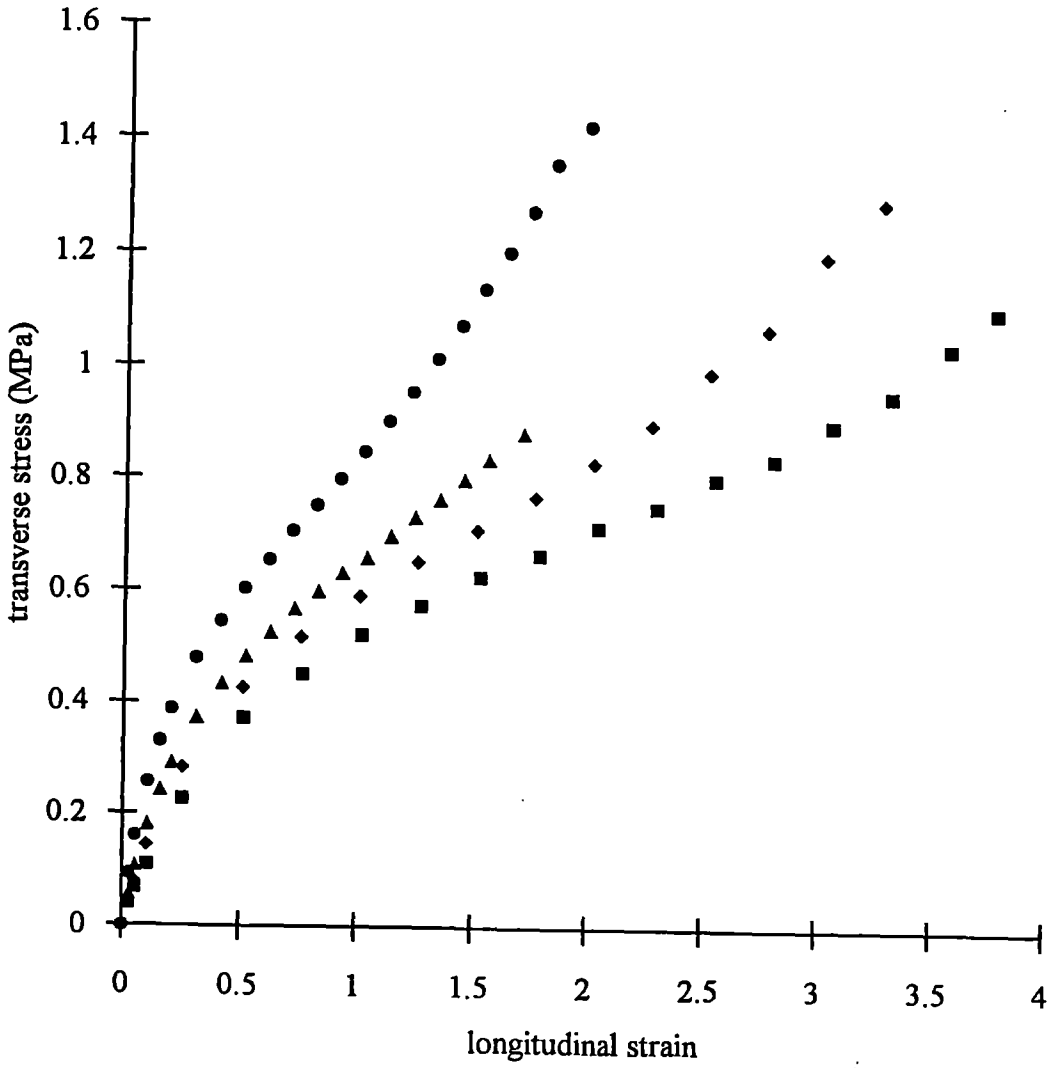

Figure 3.6 Stress-strain plots for the transverse stress obtained with the split pure shear technique for a series of black filled rubbers: ■ EDS19 (0), ◆ EDS14 (15), ▲ EDS15 (30), ● EDS16 (45). Filler loadings given in brackets. Formulations given in Table 3.2.

$$s_1 = 2(\lambda_1 - \lambda_1^{-3})\left(\frac{\partial W}{\partial I_1} + \frac{\partial W}{\partial I_2}\right) \tag{3.4}$$

A useful check of the experimental accuracy may be made as follows. Substitution from equations (3.1) into equations (3.2) gives:

$$\frac{f_2}{f_1} = \frac{h\lambda\sigma_2}{w\sigma_1} = \frac{h\lambda_1}{w(\lambda_1^2 + 1)}\left(\frac{\partial W/\partial I_1 + \lambda_1^2 \partial W/\partial I_2}{\partial W/\partial I_1 + \partial W/\partial I_2}\right) \tag{3.5}$$

$$\rightarrow \frac{h}{2w} \text{ at small strain since } \lambda_1 \rightarrow 1$$

Gregory (1979) and others (see Section 1.2.4) have found that $\partial W/\partial I_2$ is close to zero for black filled rubbers which suggests that the term in brackets in equation (3.5) is close to unity. Thus

$$\frac{f_2}{f_1} \approx \frac{h\lambda_1}{w(\lambda_1^2 + 1)} \tag{3.6}$$

In Figure 3.7, f_2/f_1 obtained from the experimental measurements is plotted as a function of λ_1 and compared with equation (3.6). As required by the small strain approximation of equation (3.5) the experimental points and theoretical curve all converge to h/2w at $\lambda_1 = 1$ although the experimental scatter at small strains is large. This is an indication that the experimental accuracy of the transverse force measurement is reasonably good. At larger values of λ_1 the agreement between the theoretical line and the experimental points for the three filled rubbers remains good in agreement with Gregory's (1979) hypothesis. The results for the unfilled rubber deviate from equation (3.6) indicating a significant $\partial W/\partial I_2$ term.

3.3.5 *Evaluation of $\partial W/\partial I_1$ and $\partial W/\partial I_2$*

The fact that both of the non-zero principal stresses have been measured provides enough information for the evaluation of expressions for $\partial W/\partial I_1$ and $\partial W/\partial I_2$ for the specific condition of pure shear, that is for $I_1 = I_2$. Solving equations (3.1) for $\partial W/\partial I_1$ and $\partial W/\partial I_2$ gives:

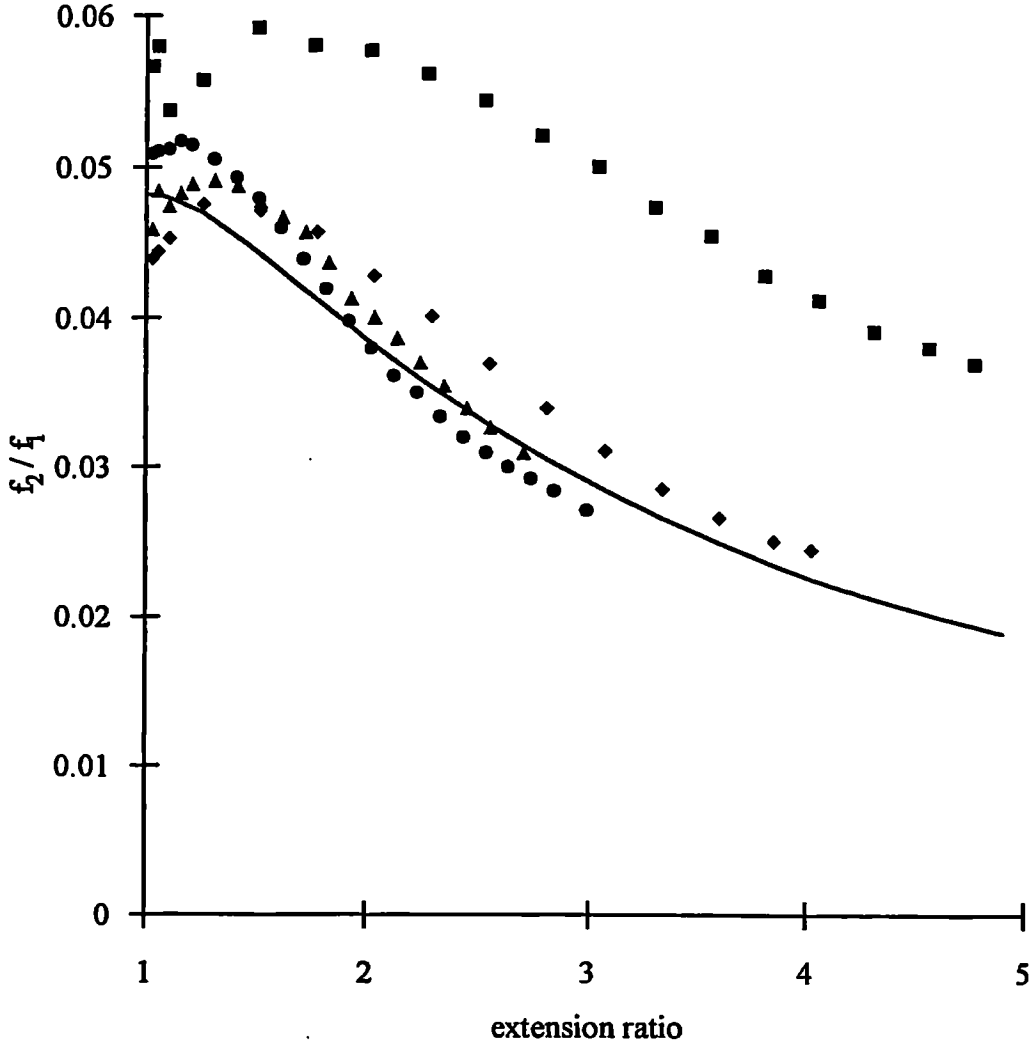

Figure 3.7 Ratio of forces obtained from split pure shear technique for a series of black filled rubbers. Solid line calculated from equation (3.6): ■ EDS19 (0), ◆ EDS14 (15), ▲ EDS15 (30), ● EDS16 (45). Filler loadings given in brackets. Formulations given in Table 3.2.

$$\frac{\partial W}{\partial I_1} = \frac{\sigma_1(\lambda_1^2 - 1) - \sigma_2(\lambda_1^2 - \lambda_1^{-2})}{2(\lambda_1^2 - \lambda_1^{-2})(\lambda_1^2 + \lambda_1^{-2} - 2)} \tag{3.7a}$$

$$\frac{\partial W}{\partial I_2} = \frac{\sigma_2(\lambda_1^2 - \lambda_1^{-2}) - \sigma_1(1 - \lambda_1^{-2})}{2(\lambda_1^2 - \lambda_1^{-2})(\lambda_1^2 + \lambda_1^{-2} - 2)} \tag{3.7b}$$

Plots of $\partial W/\partial I_1$ and $\partial W/\partial I_2$ as functions of $(I_1 - 3)$, which equals $(I_2 - 3)$ for pure shear, are shown in Figure 3.8. In all cases $\partial W/\partial I_1$ is much greater than $\partial W/\partial I_2$ and, since $\partial W/\partial I_2$ appears to decrease while $\partial W/\partial I_1$ increases with increasing loadings of filler, Gregory's (1979) conclusion that it is reasonable to assume that $\partial W/\partial I_2 = 0$ for filled natural rubbers is confirmed. This simplification is very useful as it enables W to be obtained from a simple uniaxial test since, in equation (1.17), $\partial W/\partial I_1$ is now the only unknown quantity.

The form of $\partial W/\partial I_1$ and $\partial W/\partial I_2$ as a function of I_1 (for $I_1 = I_2$) is less clear. As $I_1 \rightarrow 3$ (equivalent to $\lambda_1 \rightarrow 1$) it can be seen from equations (3.7) that $\partial W/\partial I_1$ and $\partial W/\partial I_2$ become indeterminate. At higher strains $\partial W/\partial I_1$ rises with increasing strain, especially for the filled rubbers, and $\partial W/\partial I_2$ falls slightly. It is unsafe to place any confidence in the data at small strains; the rapid changes in $\partial W/\partial I_1$ and $\partial W/\partial I_2$ may arise from small experimental inaccuracies, for example in measuring the unstrained length or width of the testpiece or in determining the point of zero strain. The latter is likely to lead to the largest errors, estimated to be of the order of 10% of of $\partial W/\partial I_1$ at I_1-3=0.2 (λ=1.25), reducing to about 1% at I_1-3=2.25 (λ=2), and of equal numerical magnitude but opposite sense in $\partial W/\partial I_2$. Errors in the thickness measuement, likely to be less than 5%, will cause corresponding errors in $\partial W/\partial I_1$ and $\partial W/\partial I_2$ at all strains.

Rivlin (1948b) has shown that, for an incompressible material, the secant shear modulus is given by

$$G = 2\left(\frac{\partial W}{\partial I_1} + \frac{\partial W}{\partial I_2}\right) \tag{3.8}$$

Hence the sum of each pair of lines for each rubber in Figure 3.8 is simply half the shear modulus. The shear moduli thereby obtained are plotted in Figure 3.9. A rise in either $\partial W/\partial I_1$ or $\partial W/\partial I_2$ or both with strain for filled rubbers at moderate to high strains is necessary for consistency with the increase in shear modulus. In a similar way, one of

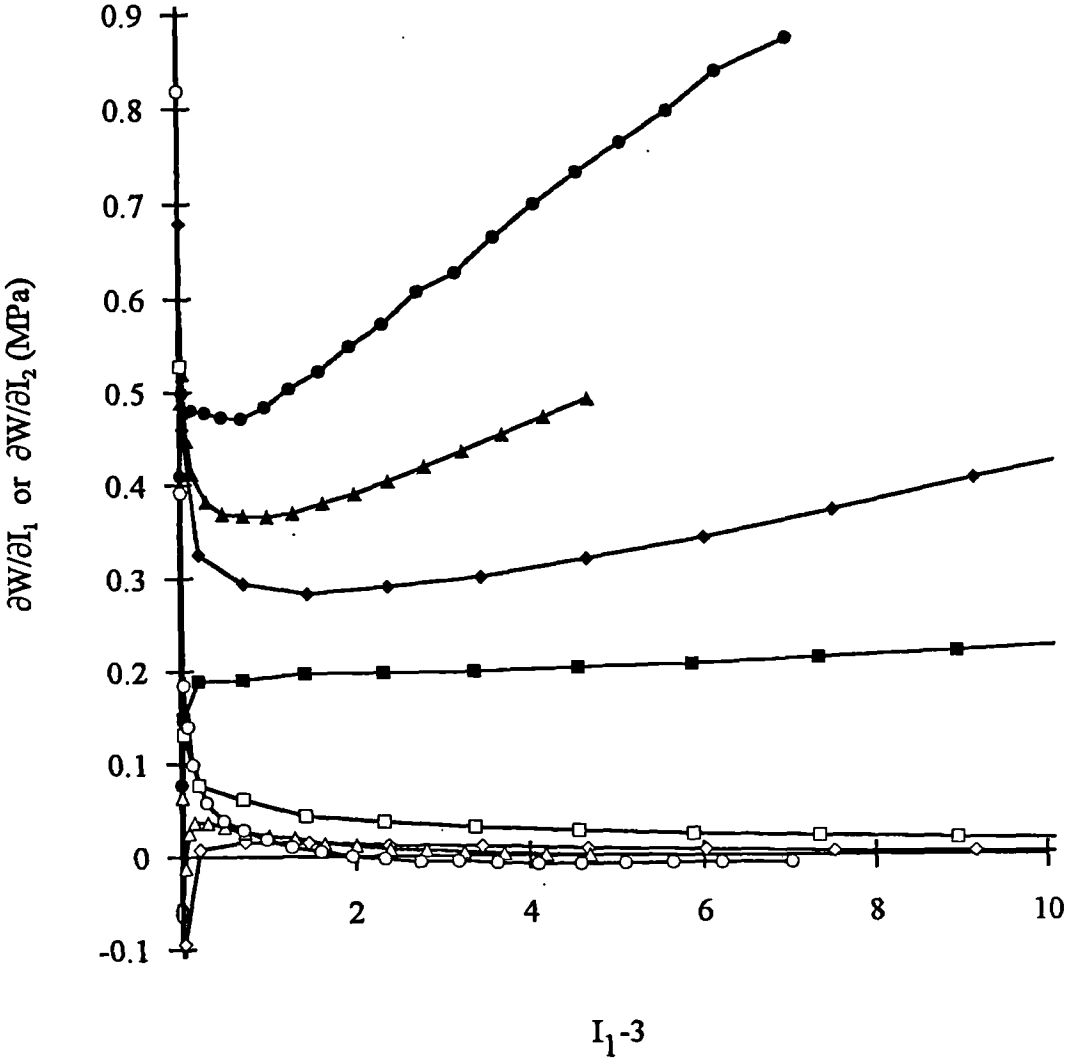

Figure 3.8 Strain energy derivatives, $\partial W/\partial I_1$ (filled symbols) and $\partial W/\partial I_2$ (open symbols), obtained from the split pure shear technique.
■ □ EDS19 (0), ◆ ◇ EDS14 (15), ▲ △EDS15 (30), ● ○ EDS16 (45). Filler loadings given in brackets. Formulations given in Table 3.2.

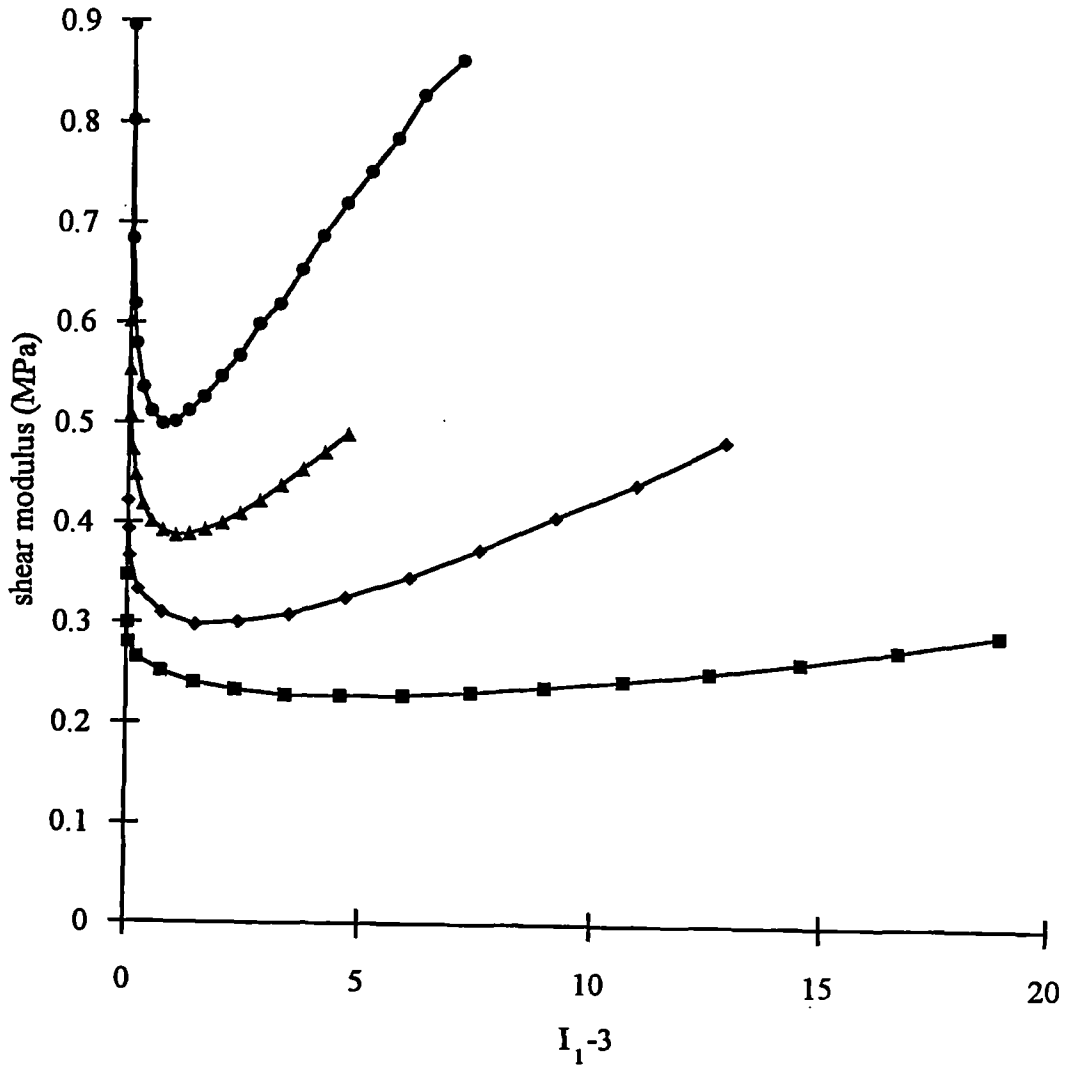

Figure 3.9 Shear modulus calculated from pure shear data using equation (3.8): ■ EDS19 (0), ◆ EDS14 (15), ▲ EDS15 (30), ● EDS16 (45). Filler loadings given in brackets. Formulations given in Table 3.2.

$\partial W/\partial I_1$ or $\partial W/\partial I_2$ must fall with increasing strain at small strains although no clear trend as to which emerges from the data shown in Figure 3.8 due to the uncertainty in the data at small strains. The form of equations (3.7) mean that errors in σ_1, σ_2 or λ_1 will lead to equal and opposite errors in $\partial W/\partial I_1$ and $\partial W/\partial I_2$ so, although separating the behaviour into $\partial W/\partial I_1$ and $\partial W/\partial I_2$ terms is problematic, measurement of the physically more meaningful parameter of shear modulus is much less susceptible to error.

The magnitudes of $\partial W/\partial I_1$ and $\partial W/\partial I_2$ for the unfilled rubber are in reasonable agreement with those of Rivlin and Saunders (1951). The dependence of $\partial W/\partial I_1$ and $\partial W/\partial I_2$ on strain is broadly consistent with other results reported in the literature, such as those of Fukahori and Seki (1992), also for pure shear. Detailed comparison with other workers is hindered by differences in the combinations of I_1 and I_2 investigated and strain histories of the testpieces. More worthwhile, in view of the restricted nature of the pure shear test, is an investigation of the applicability of these results to more general strains. This is the purpose of Chapter 4, where predictions based on these pure shear results are compared to experiments in other modes of deformation.

3.4 **The effect of anisotropy**

3.4.1 *Introduction*

Many polymers are manufactured from the melt by extrusion or injection moulding, where anisotropic flow is likely to occur, and are subsequently cooled rapidly when they become glassy or crystalline. Such materials are likely to be anisotropic. Rubber components are subjected to less severe anisotropic forces during manufacture and are not "frozen" into a particular glassy or crystalline morphology. They are thus less likely to exhibit significant anisotropy in their mechanical properties, although there is the possibility that, in filled rubbers, carbon black structures (see Section 1.4.4) may be anisotropic. However, as the pure shear technique relies on careful measurement of forces in two perpendicular directions and the method of preparation of the testpieces would be likely to lead to any anisotropy being a maximum in these two directions, an experiment to measure the testpiece anisotropy was carried out.

3.4.2 *Experimental method*

Sheets of the unfilled rubber, EDS19, and the most highly filled rubber, EDS16, (see Table 3.2) of nominal dimensions 200 x 20 x 1 mm were compression moulded in exactly the same way as the testpieces used for the pure shear testpieces except that no bonding agent was used. New batches of rubber compound were used because none of the original mixes remained.

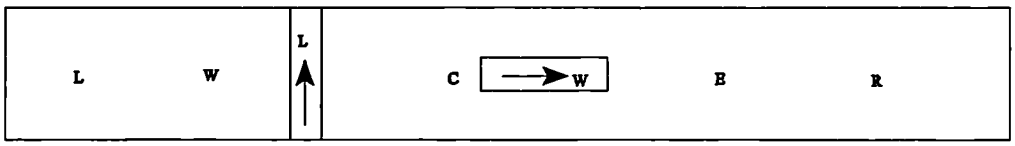

Figure 3.10 Positions and orientations of small strips cut from pure shear testpiece for measurement of anisotropy.

Small strips, of nominal dimensions 20 x 2 x 1 mm, were cut from the sheets with a standard cutter from various positions in the sheet and in two perpendicular directions as shown in Figure 3.10. The letters on Figure 3.10 correspond to a two letter code for each strip; the first letter denotes the location of the strip on the sheet and the second its direction. The thickness of the strips was measured with a spring loaded dial gauge. The strips were pulled in uniaxial tension in a Instron screw-driven test machine with a 100N load cell at a crosshead speed of 10mm/minute. To facilitate comparison of the stiffnesses, the same initial crosshead position was used for all strips from one rubber, thus ensuring that the unstrained length was the same. The absolute length was measured with a cathetometer. The force and deflection were taken from the machine's output and plotted directly. The densities of the strips were measured by the method of hydrostatic weighings and found to vary by not more than 0.2% for each rubber, confirming that the mix was homogeneous.

3.4.3 *Results and discussion*

The testpiece dimensions are given in Table 3.3.

Table 3.3: Dimensions of testpieces for anisotropy measurements			
testpiece rubber and position code (see text and Figure 3.10)		thickness (mm)	length (mm)
EDS19	CW	0.92	14.12
EDS19	RL	0.88	14.14
EDS19	RW	0.90	14.06
EDS19	CL	0.91	14.04
EDS16	EL	0.95	12.11
EDS16	LL	0.97	12.15
EDS16	WL	0.94	12.15
EDS16	CW	0.93	12.11
EDS16	EW	0.93	12.23
EDS16	WW	0.93	12.15

The length variations within each set are most likely due to inaccuracies of measurement rather than actual differences. In any case they are of the order of 1% which is negligible. The thickness variations of up to 4% which may be real or due to measurement uncertainty are of more significance.

The force-deformation plots are given in Figures 3.11 and 3.12. In the case of the unfilled rubber (Figure 3.11) the differences amount to not more than about 3% and show no systematic variation which could be attributed to anisotropy. Thus pure shear measurements on unfilled rubber are not distorted by anisotropy. For the filled rubber (Figure 3.12), however, a clear distinction between the strips cut in different directions is seen, equivalent to the rubber being about 10% stiffer in the direction of the main force than the transverse force in the pure shear experiment.

3.4.4 *Reconsideration of the pure shear data*

If it is assumed that 10% stiffness anisotropy is typical for EDS16, it could be more appropriate to replot Figures 3.7d and 3.8d after increasing the values of the transverse force by 10%. This has been done in Figures 3.13 and 3.14 for the results obtained on two testpieces of EDS16. Figure 3.13 shows that the agreement in the data for the two testpieces is good but the correction for anisotropy brings the experimental points further away from the theoretical curve for strains below about 100%. This is an indication either that the direction of the anisotropy is not always the same or that there are other sources of error of similar magnitude which outweighed the effect of

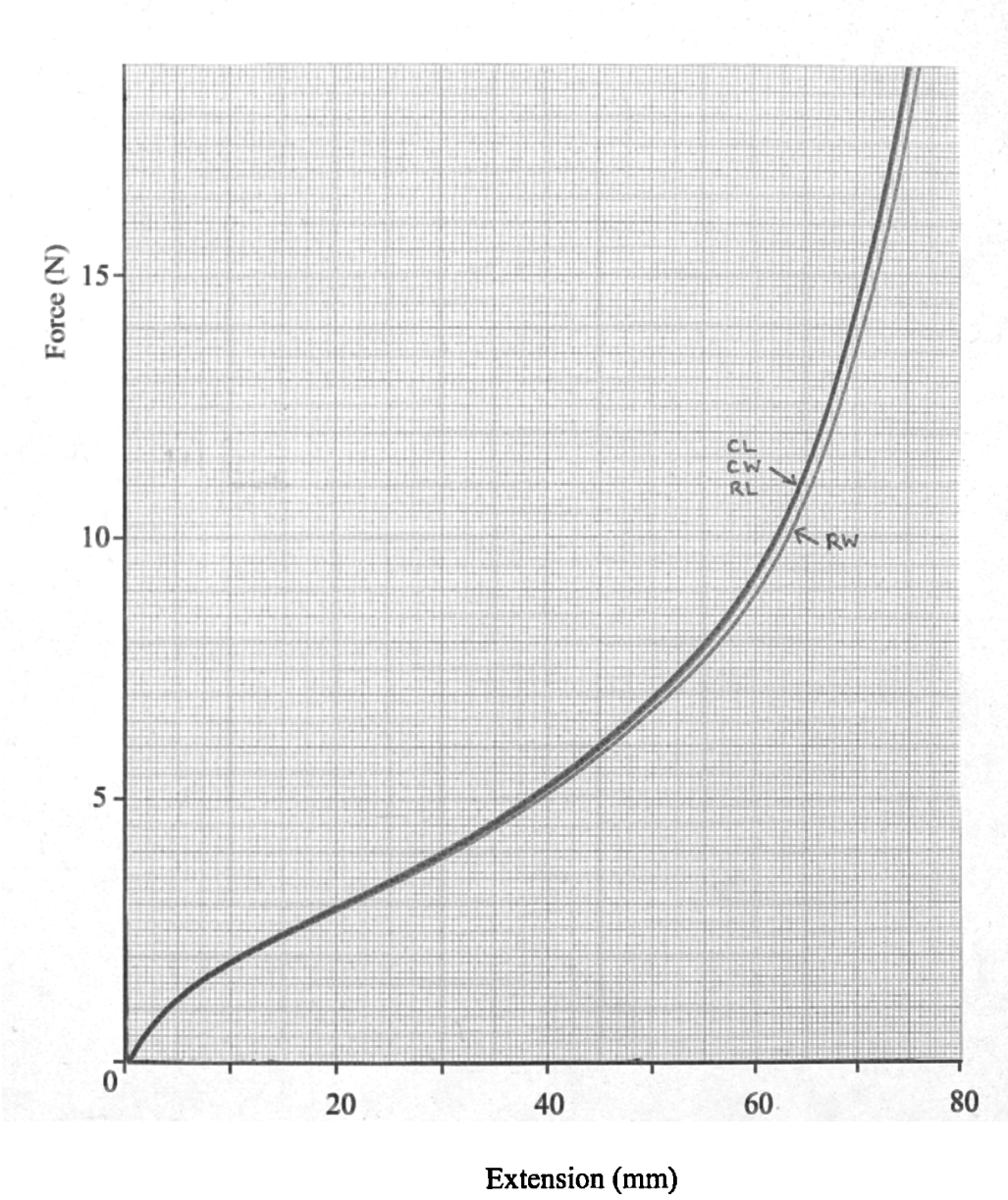

Figure 3.11 Force-deflection plot showing anisotropy of unfilled rubber, EDS19. Locations and orientations of samples are shown in Figure 3.10.

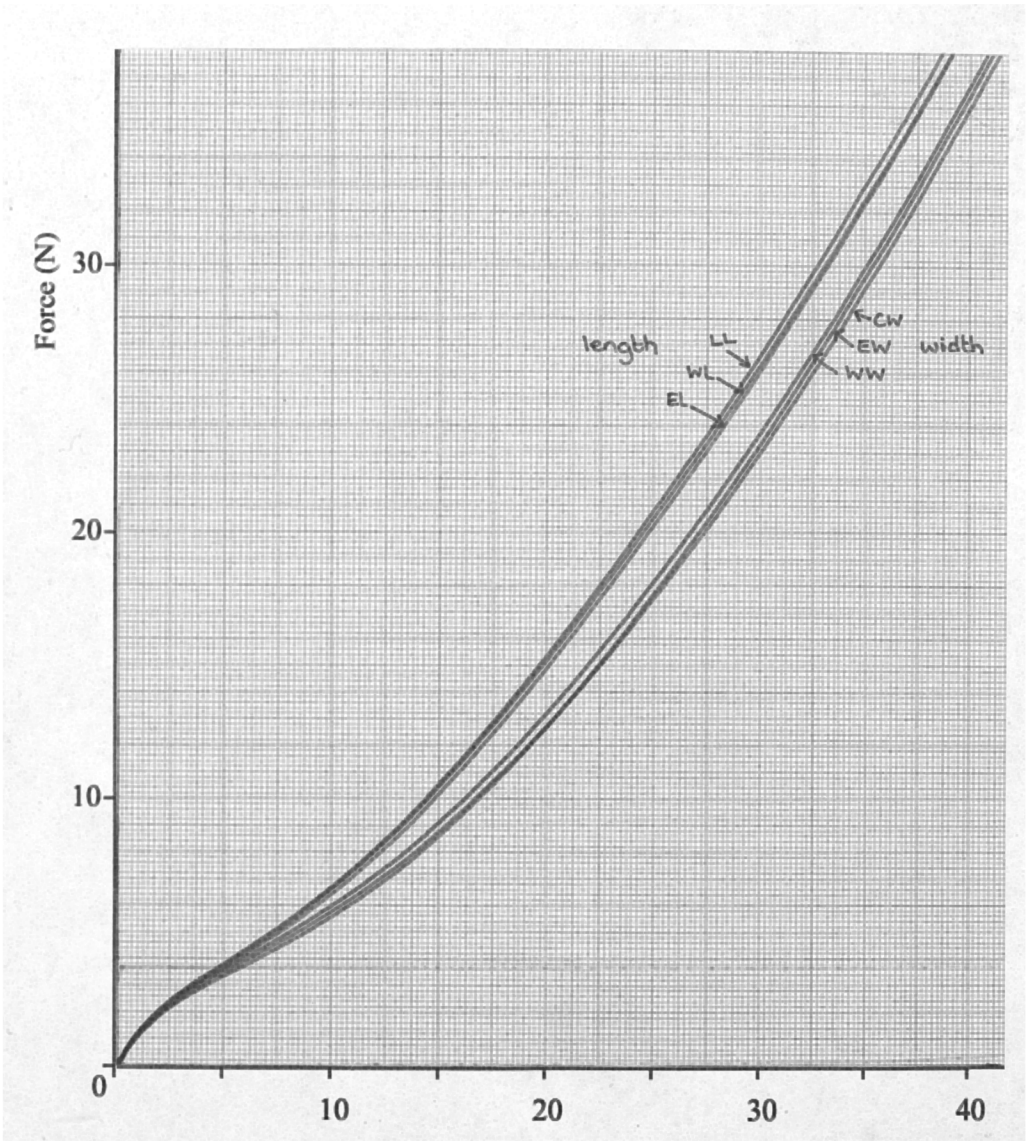

Figure 3.12 Force-deflection plot showing anisotropy of filled rubber, EDS16. Locations and orientations of samples are shown in Figure 3.10.

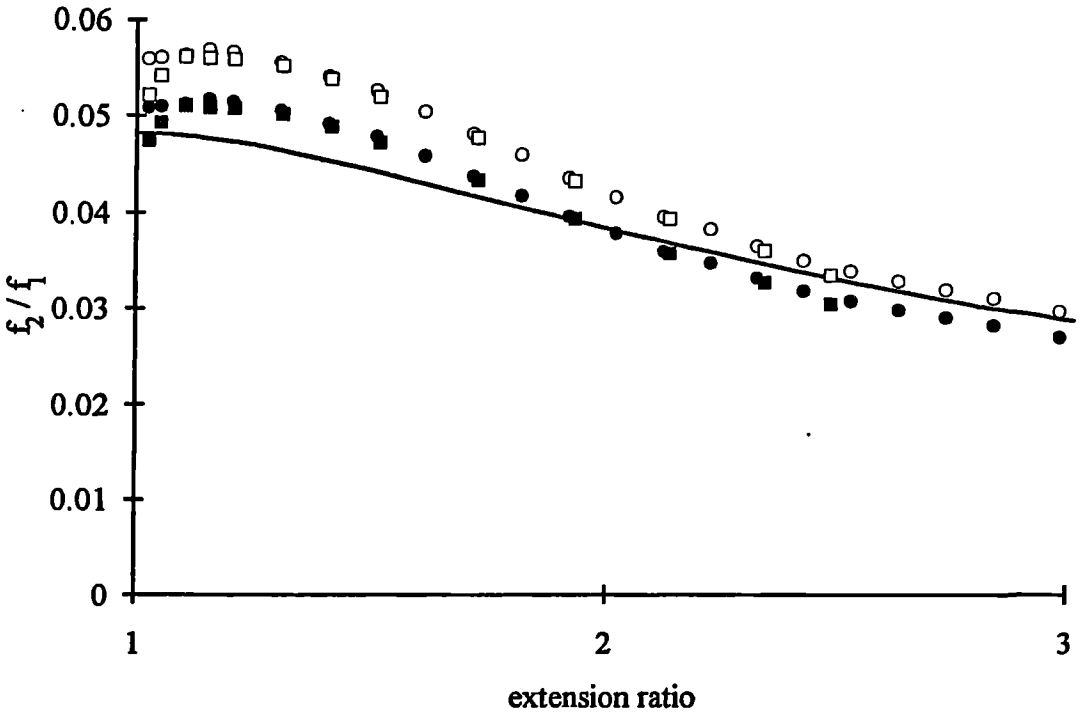

Figure 3.13 Effect of 10% anisotropy in EDS16 (45 parts of black) on the ratio of the transverse to the main force. Filled symbols: "uncorrected" data (for two testpieces); open symbols: data "corrected" by increasing the measured values of the transverse force by 10%. Solid line: theory - equation (3.6).

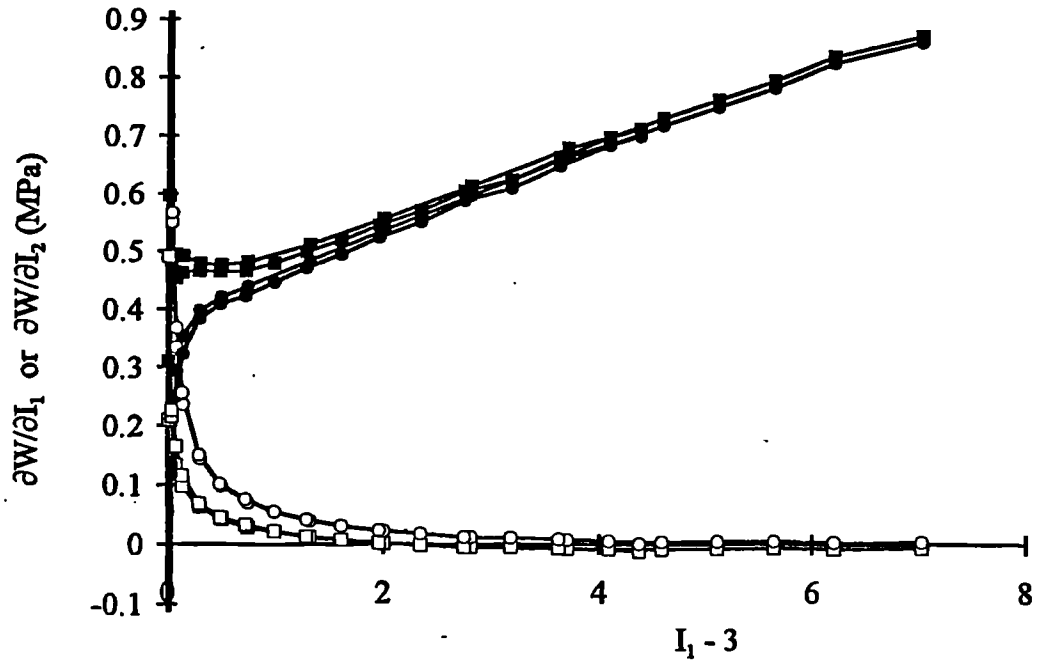

Figure 3.14 Effect of 10% anisotropy in EDS16(45 parts of black) on $\partial W/\partial I_1$ (filled symbols) and $\partial W/\partial I_2$ (open symbols). Squares: "uncorrected" data (for two testpieces); circles: data "corrected" by increasing the measured values of the transverse force by 10%.

anisotropy. Figure 3.14 shows that at small strains the effect of 10% anisotropy is very large, though for strains above about 1, equivalent to I_1-3=2.25, the differences due to anisotropy become insignificant. Thus anisotropy provides another reason for caution in evaluating $\partial W/\partial I_1$ and $\partial W/\partial I_2$ at small strains.

Testpiece anisotropy has not been discussed by previous workers who undertook biaxial strain measurements. In square sheets the anisotropy may arise from milling the rubber blank which would result in maximum anisotropy in two perpendicular directions in the moulded sheet, or due to mould flow which is more likely to cause a radial and tangential anisotropy depending on the shape of the rubber blank. Some engineering components, however, could plausibly exhibit anisotropy of the magnitude reported here, depending on their geometry and method of fabrication. Since it is not feasible to establish the amount and direction of stiffness variations of real components for finite element analysis design purposes, it is perhaps unrealistically ambitious to demand measurement of stiffness to a precision greater than about 5 to 10%.

The reasons for anisotropy in filled rubbers are not well-documented. The carbon black structure is likely to be affected by flow behaviour during moulding (see Section 1.4.4). This possibility is supported by the absence of anisotropy in the unfilled rubber.

3.5 Conclusions

The pure shear technique provides a reasonably straightforward way to characterize the strain energy function of rubber and is sufficiently general for most purposes. It is sufficiently simple to be potentially useful as a means of assessing strain history effects such as stress relaxation (see Chapter 8). Its drawbacks include its sensitivity to errors at low strains, as are the more general full biaxial experiments, and to testpiece anisotropy. For these reasons alternative techniques were considered. One such technique is discussed in Chapter 6.

CHAPTER 4

Use of experiments in various modes of deformation to assess particular functional forms of the strain energy density function, W

4.1 Introduction

The split pure shear technique has enabled evaluation of $\partial W/\partial I_1$ and $\partial W/\partial I_2$ for the particular case of $I_1 = I_2$. It has not been established whether or how these values may be used to obtain good predictions of the behaviour in other modes of deformation. In order to assess the relevance of the pure shear data to general strain it is sensible to investigate as wide a variety of combinations of I_1 and I_2 as possible (Figure 1.5). Therefore the pure shear results from Chapter 3 were used to predict the behaviour in uniaxial tension and lubricated compression (which is equivalent to biaxial extension) and compared with directly measured experimental values on the same rubbers. In order to make these predictions assumptions about W where $I_1 \neq I_2$ are required. These are discussed in Section 4.5. The literature also contains many suggestions of particular functional forms of W (Section 1.2.4). Two of these are examined in Section 4.6.

As a means of assessing the experimental errors associated with obtaining measurements in different deformation modes, the pure shear results are compared with some experimental results obtained in simple shear.

4.2 Experimental methods

The rubbers investigated were as detailed in Section 3.3.1. All measurements were taken from the first loading cycle of previously unstrained testpieces.

4.2.1 *Simple tension*

Strips of rubber of nominal dimensions 180 × 1 × 20mm were cut from one of the mouldings made in the four cavity mould at the same time as the pure shear testpieces used in Chapter 3. They were measured, clamped along their two shortest edges and pulled to failure in an Instron screw-driven test machine at a crosshead speed of 20mm/minute. The force and displacement were plotted directly from the machine's

output.

4.2.2 *Lubricated compression*

Cylindrical testpieces of nominal height 32mm and diameter 25mm were lubricated liberally with detergent and compressed between smooth, flat, parallel plates. The force was obtained directly from the machine's load cell output; the displacement was obtained with an auxiliary LVDT measuring directly between the plates. The crosshead speed was 5mm/minute.

4.2.3 *Simple shear*

Double shear testpieces, comprising two rubber discs of nominal diameter 25mm and thickness 6mm sandwiched between three metal cylinders, were moulded (Figure 4.1). The testpieces were clamped in a jig such that the central metal part moved relative to the outside parts, placing the rubber discs in shear (Figure 4.2). The testpieces were pulled to failure in a Dartec Servohydraulic test machine at a rate of 1.2mm/minute. The force output was obtained directly from the machine output; the displacement was measured with an auxiliary LVDT. The data was recorded in digital form.

It is known that moulding conditions can influence the modulus of rubber testpieces. The testpieces for pure shear and simple tension were obtained from a single compression moulding and the lubricated compression testpieces were also compression moulded. In compression moulding crude blanks of milled rubber sheet are placed directly in the mould cavity and forced into shape under the high moulding temperature and pressure. Double shear testpieces are normally transfer moulded, that is the rubber is initially placed in a separate pot and is extruded into the mould cavity through small holes by a piston. Compression and transfer moulded testpieces were compared by making two sets of double shear testpieces; one by the usual method of transfer moulding and the other by placing discs of unvulcanized rubber directly in position in the mould and then compression moulding.

4.3 Stress-strain behaviour

The nominal stress and strain were calculated from the force and deflection and the

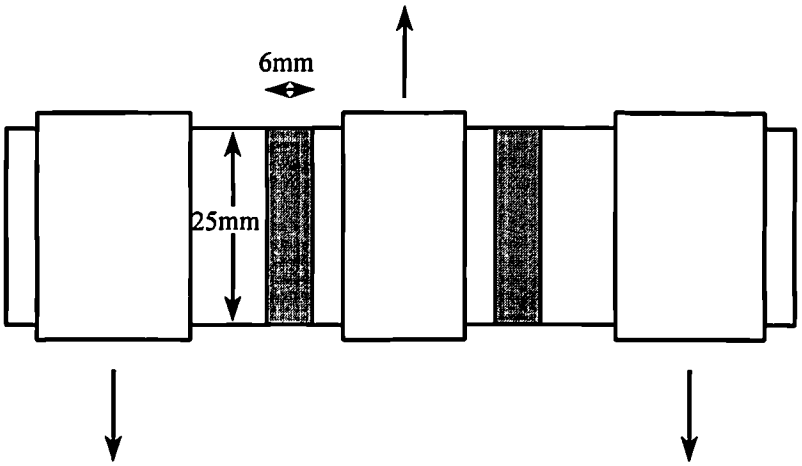

Figure 4.1 Undeformed double shear testpiece. Shaded areas represent rubber discs. White areas are steel.

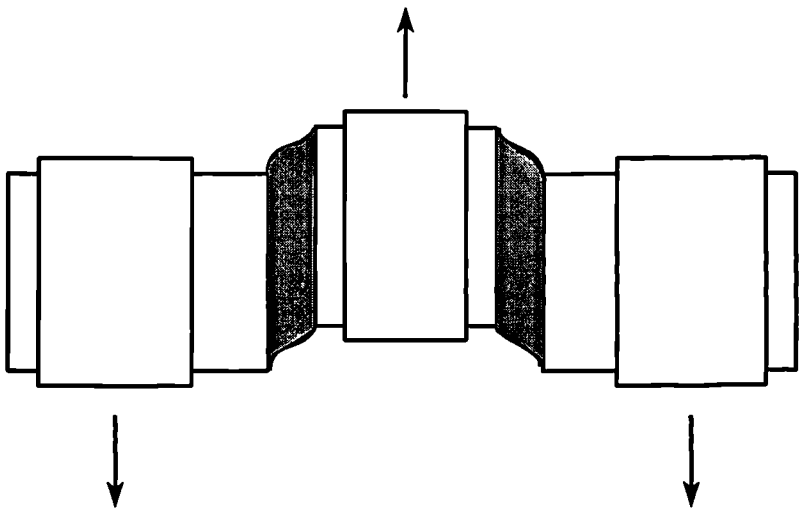

Figure 4.2 Deformed double shear testpiece showing schematically bending of unbonded edges. (see Chapter 6)

measured testpiece dimensions. For double shear testpieces the shear stress, τ, and shear strain, γ, are given by:-

$$\tau = \frac{f}{2A} \tag{4.1a}$$

$$\gamma = \frac{x}{h} \tag{4.1b}$$

where f is the force, x the displacement, A the area of the circular face of one disc and h the disc thickness.

The stress-strain curves for all geometries are shown in Figures 4.3 to 4.5. The features are similar to those seen in pure shear (Figure 3.5 and Section 3.3.3). However, the high initial stiffness does not appear in compression. The unfilled rubber shows approximately linear behaviour in simple shear in accordance with the statistical theory (see equations (1.9) and (1.12.)) Since it was possible to pull the simple shear testpieces to very high extensions without failure the increase in stiffness at high strains is particularly noticeable for this type of deformation.

There was a tendency for the compression moulded simple shear testpieces to be slightly softer than the transfer moulded ones for filled rubbers (Figure 4.6). The discrepancy was never large - about 6% for the most highly filled rubber.

4.4 Comparison of pure shear and simple shear

In simple shear we have, from equation (3.8):-

$$\tau = 2\gamma\left(\frac{\partial W}{\partial I_1} + \frac{\partial W}{\partial I_2}\right) \tag{4.2}$$

Substitution from equation (3.1a) into equation (4.2) gives a relationship between the main stress in pure shear and the shear stress:-

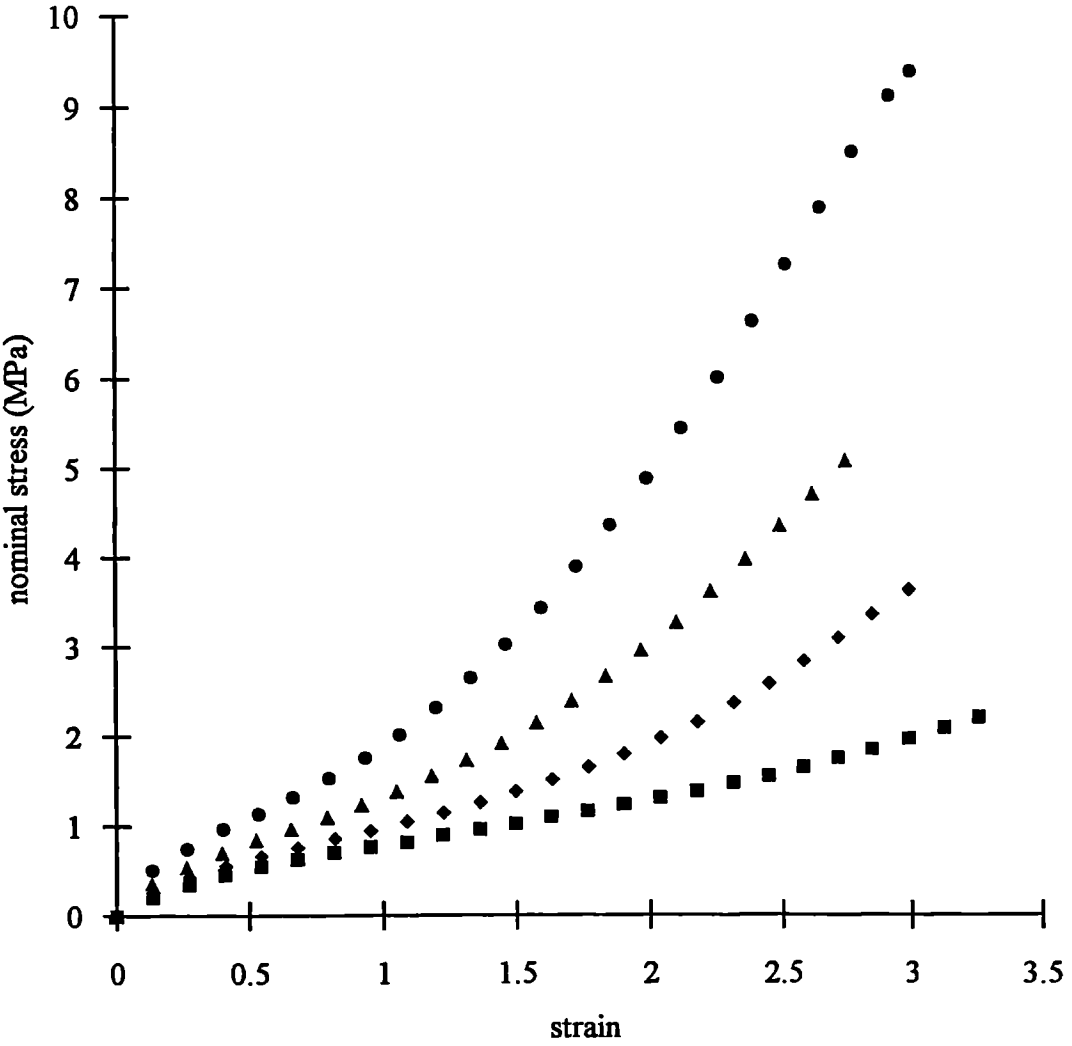

Figure 4.3 Stress-strain behaviour of a series of black filled rubbers in uniaxial tension: ■ EDS19 (0), ◆ EDS14 (15), ▲ EDS15 (30), ● EDS16 (45). Filler loadings given in brackets. Formulations given in Table 3.2.

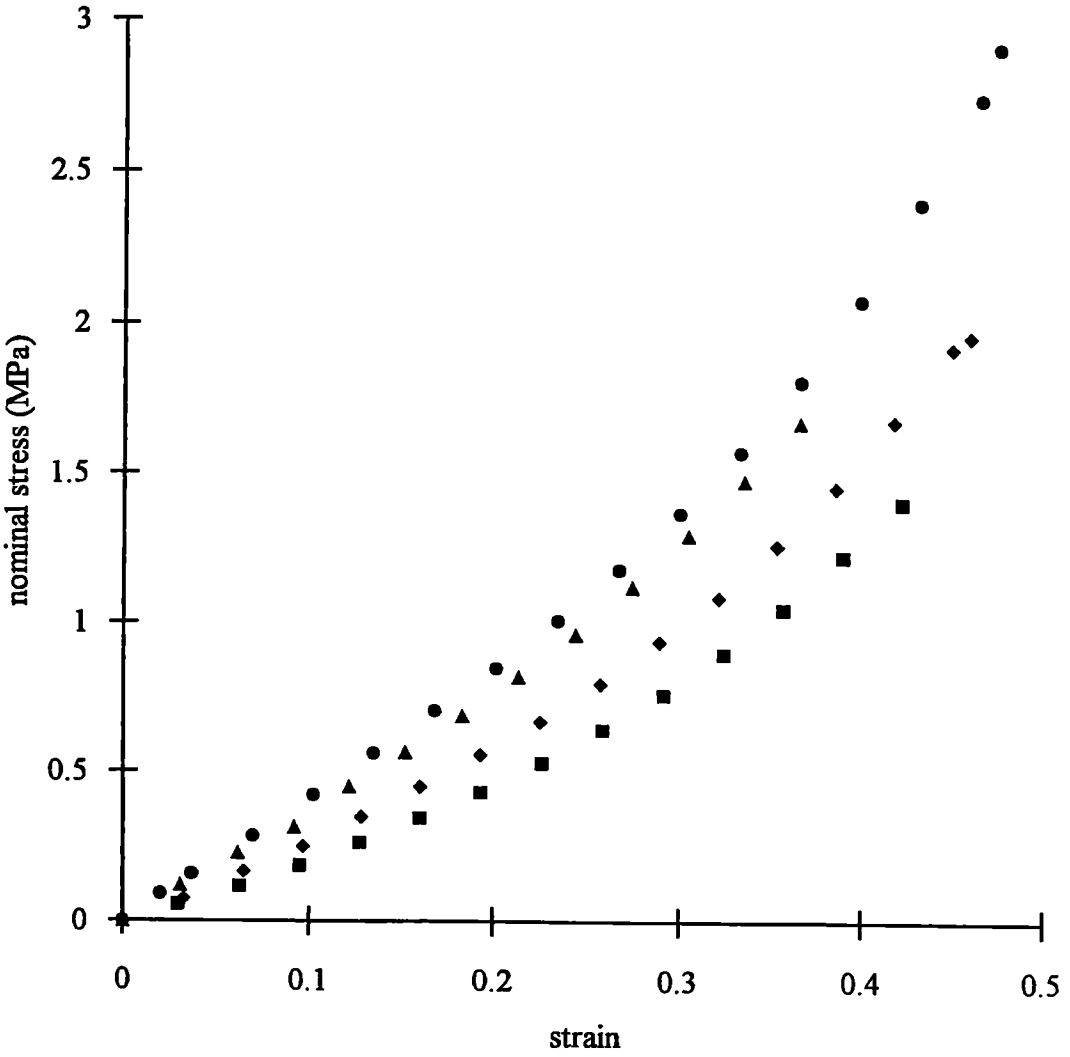

Figure 4.4 Stress-strain behaviour of a series of black filled rubbers under lubricated compression: ■ EDS19 (0), ◆ EDS14 (15), ▲ EDS15 (30), ● EDS16 (45). Filler loadings given in brackets Formulations given in Table 3.2.

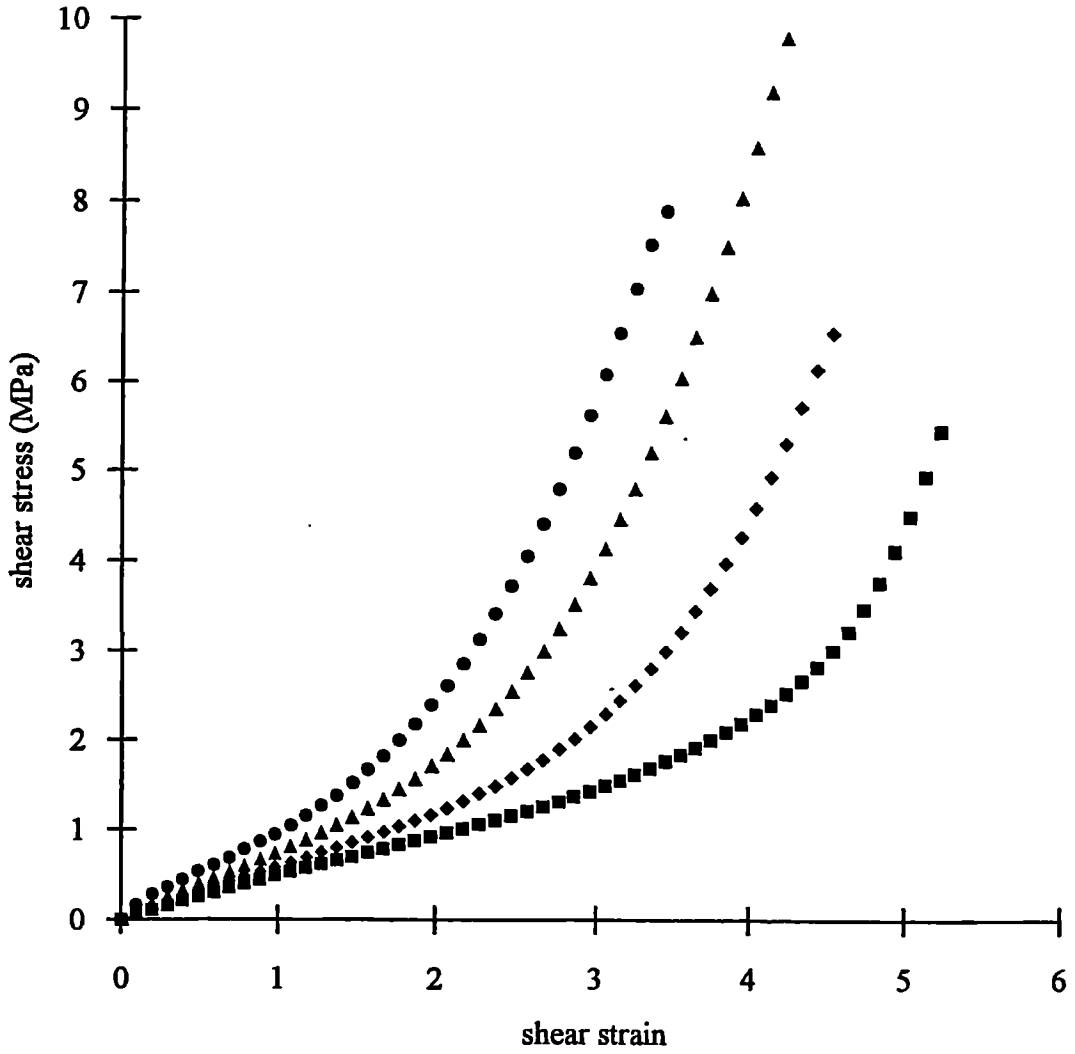

Figure 4.5 Stress-strain behaviour of a series of black filled rubbers in simple shear:
■ EDS19 (0), ◆ EDS14 (15), ▲ EDS15 (30), ● EDS16 (45). Filler loadings given in brackets. Formulations given in Table 3.2.

$$\tau = \frac{\sigma_1 \gamma}{\left(\lambda_1^2 - \lambda_1^{-2}\right)} \tag{4.3}$$

It can be shown that (Treloar, 1975) the shear strain in pure shear is given by:-

$$\gamma = \lambda_1 - \frac{1}{\lambda_1} \tag{4.4}$$

Thus equation (4.3) may be used to calculate $\tau(\gamma)$ from the experimental values of σ_1 and λ_1 obtained in pure shear. This has been done in Figure 4.6 where the shear stress calculated from the pure shear measurements reported in Chapter 3 have been compared to that obtained in simple shear.

The agreement between the simple shear and pure shear measurements is generally very good. The simple shear measurements were not corrected to take account of the free edges in the testpiece which would be expected to lead to the apparent shear modulus, as plotted in the figures, being of the order of 5% lower than the actual shear modulus (see Section 6.3.5). The testpieces were all made at about the same time from the same mixes and the good agreement of the data suggests that a consistent state of cure was achieved between the different mouldings; larger differences between stiffnesses may result from batch variations or the effect of ageing on the unvulcanized rubber. Also, anisotropy of the filled pure shear testpieces could cause discrepancies between pure and simple shear of the order of 10% (see Section 3.4). It is likely, therefore, that the good agreement between the two modes of deformation is partially fortuitous with the various sources of error tending to cancel, rather than reinforce, each other.

It is worth noting that equation (4.3) is independent of the strain energy function. Thus no information about the applicability of any particular form of the strain energy function may be obtained from comparisons between tests in pure and simple shear. This is a consequence of the fact that these two deformations differ only by a rotational component; hence in both cases $I_1 = I_2$ and the strain states are equivalent.

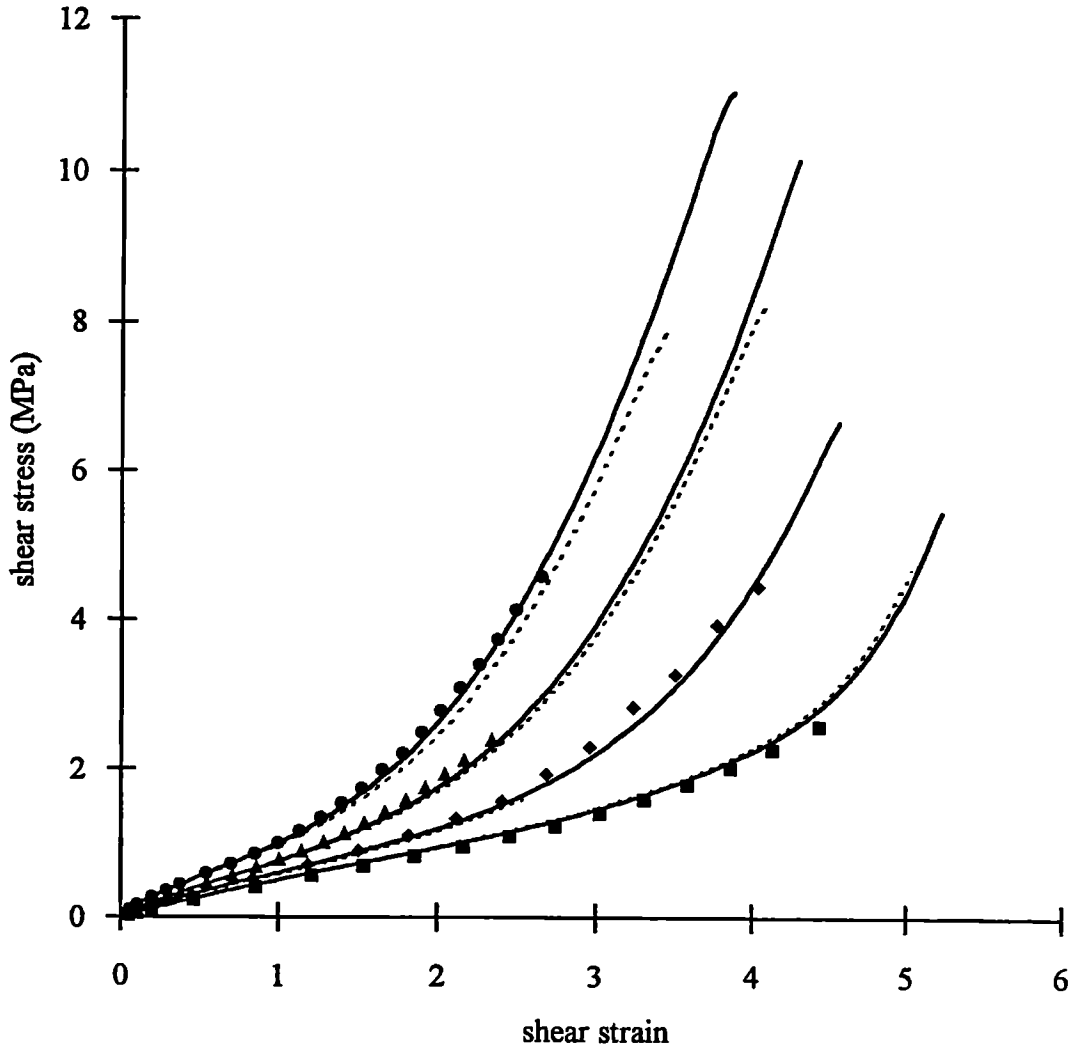

Figure 4.6 Comparison of pure shear and simple shear data. Pure shear: ■ EDS19 (0), ◆ EDS14 (15), ▲ EDS15 (30), ● EDS16 (45). Filler loadings given in brackets. Simple shear: ——— transfer moulded, ····· compression moulded. Formulations given in Table 3.2.

4.5 Simplifying assumptions for the strain energy function W

4.5.1 *Introduction*

The validity of a particular form of W may best be assessed by its ability to make an accurate prediction of the stress-strain behaviour in one type of deformation from measurements obtained in another. For such a check to be reasonably stringent, the chosen deformations should be as different as possible in terms of the combinations of I_1 and I_2 that they cover (see Figure 1.5). Thus a good test is to compare the predictions from shear with actual measurements in uniaxial tension and equibiaxial extension or uniaxial compression. In what follows, the pure shear data reported in Chapter 3 has been used to predict the behaviour in tension and compression by adopting the assumptions on which several particular forms of W are based. The predictions have then been compared to the experimental results.

4.5.2 *Particular assumptions*

(i) Assume $W = F_1(I_1) + F_2(I_2)$

For uniaxial tension and compression, substituting $\lambda_2 = \lambda_3 = 1/\sqrt{\lambda_1}$ and $\sigma_2 = \sigma_3 = 0$ in equations (1.17) gives:-

$$\sigma_T = 2\left(\lambda^2 - \lambda^{-1}\right)\left(\frac{\partial W}{\partial I_1} + \frac{1}{\lambda}\frac{\partial W}{\partial I_2}\right) \tag{4.5}$$

where σ_T is the true stress in tension or compression and the subscript 1 has been dropped from λ. It is conventional to plot nominal, rather than true stresses; for tension and compression, the nominal stress:-

$$s_T = \frac{\sigma_T}{\lambda} \tag{4.6}$$

hence:-

$$s_T = 2\left(\lambda - \lambda^{-2}\right)\left(\frac{\partial W}{\partial I_1} + \frac{1}{\lambda}\frac{\partial W}{\partial I_2}\right) \tag{4.7}$$

The split pure shear experiment has yielded sets of values for $\partial W/\partial I_1$ and $\partial W/\partial I_2$ for $I_1 = I_2$. In order to use these in equation (4.7) some assumption about the dependence of $\partial W/\partial I_1$ and $\partial W/\partial I_2$ where I_1 is not equal to I_2 is required. The assumption must be consistent with the condition that:-

$$\frac{\partial^2 W}{\partial I_1 \partial I_2} = \frac{\partial^2 W}{\partial I_2 \partial I_1} \tag{4.8}$$

A straightforward possibility, which is consistent with the general biaxial data of Rivlin and Saunders (1951), is that $\partial W/\partial I_1$ is independent of I_2 and $\partial W/\partial I_2$ is independent of I_1. Hence $W = F_1(I_1) + F_2(I_2)$. By taking the pure shear values of $\partial W/\partial I_1$ and $\partial W/\partial I_2$ at the values of I_1 and I_2 respectively applicable to each value of λ for tension and compression, equation (4.7) may be used to obtain a prediction of s_T from the data for pure shear.

(ii) Assume $\partial W/\partial I_2 = 0$ (Gregory 1979)

For filled rubbers, the results in pure shear, as well as those of previous workers (Gregory, 1979; Yeoh, 1990; Fukahori and Seki, 1992; Davies et al., 1994) suggest that $\partial W/\partial I_2 \simeq 0$. If the assumption is made at the outset that $\partial W/\partial I_2 = 0$, equation (3.1a) for pure shear may be rearranged to give an expression for a modified $\partial W/\partial I_1$ term which incorporates a component for $\partial W/\partial I_2$ if the latter is non-zero:-

$$\left.\frac{\partial W}{\partial I_1}\right|_m = \frac{\sigma_p}{2(\lambda^2 - \lambda^{-2})} \tag{4.9}$$

where σ_p is the true stress in the straining direction in pure shear and the subscript 1 has been dropped from λ.

The behaviour in tension and compression may then be predicted from pure shear from equation (4.7) which becomes:-

$$s_T = 2(\lambda - \lambda^{-2}) \left.\frac{\partial W}{\partial I_1}\right|_m \tag{4.10}$$

where $\partial W/\partial I_1|_m$ is evaluated at the I_1 - 3 appropriate to tension or compression.

(iii) Assume $W(\lambda_1, \lambda_2, \lambda_3) = \omega(\lambda_1) + \omega(\lambda_2) + \omega(\lambda_3)$ (Valanis and Landel 1967)

As explained in Section 1.2.4, this separable form of the strain energy function provides a way of characterizing the material from an experiment in pure shear provided both non-zero principal stresses are known. Equations (1.30) may be used to calculate $\phi(\lambda)$ over a range of λ from $1/\lambda_{max}$ to λ_{max} where λ_{max} is the maximum value of λ_1 achieved in a pure shear experiment. Plots of $\phi(\lambda)$ obtained from the pure shear data are given in Figure 4.7. For tension and compression, equation (1.29) gives:-

$$\sigma_T = \lambda\omega'(\lambda) - \lambda^{-\frac{1}{2}}\omega'(\lambda^{-\frac{1}{2}}) \qquad (4.11a)$$

$$= \phi(\lambda) - \phi(\lambda^{-\frac{1}{2}}) \qquad (4.11b)$$

Thus σ_T may be obtained by substitution of values for $\phi(\lambda)$ obtained in pure shear, and s_T calculated using equation (4.6).

4.5.3 *Comparison of predictions*

The stress-strain curves in uniaxial tension and compression are shown in Figure 4.8, together with the predictions from pure shear based on the three forms of W considered above. For all rubbers, the difference in the predictions by the three methods are very small - less significant than the difference between any of the predictions and the experimental data, though in all cases the agreement was good. Thus the disparity between predictions and experiment is more likely to be due to experimental errors than to the inadequacy of any of the simplifying assumptions needed to make the predictions. Characterization of a rubber using the Valanis-Landel hypothesis requires a technique such as split pure shear in order to provide experimental data for two non-zero principal stresses, and thus offers no advantage over the simplifying assumption that $\partial W/\partial I_1$ is independent of I_2 and $\partial W/\partial I_2$ is independent of I_1. If one adopts Gregory's assumption, however, a straightforward uniaxial test suffices. In view of the lack of evidence for any increased accuracy resulting from the use of either $W = F_1(I_1) + F_2(I_2)$ or the Valanis-Landel hypothesis, except possibly for the unfilled rubber, it seems sensible to adopt Gregory's approximation that $\partial W/\partial I_2 = 0$.

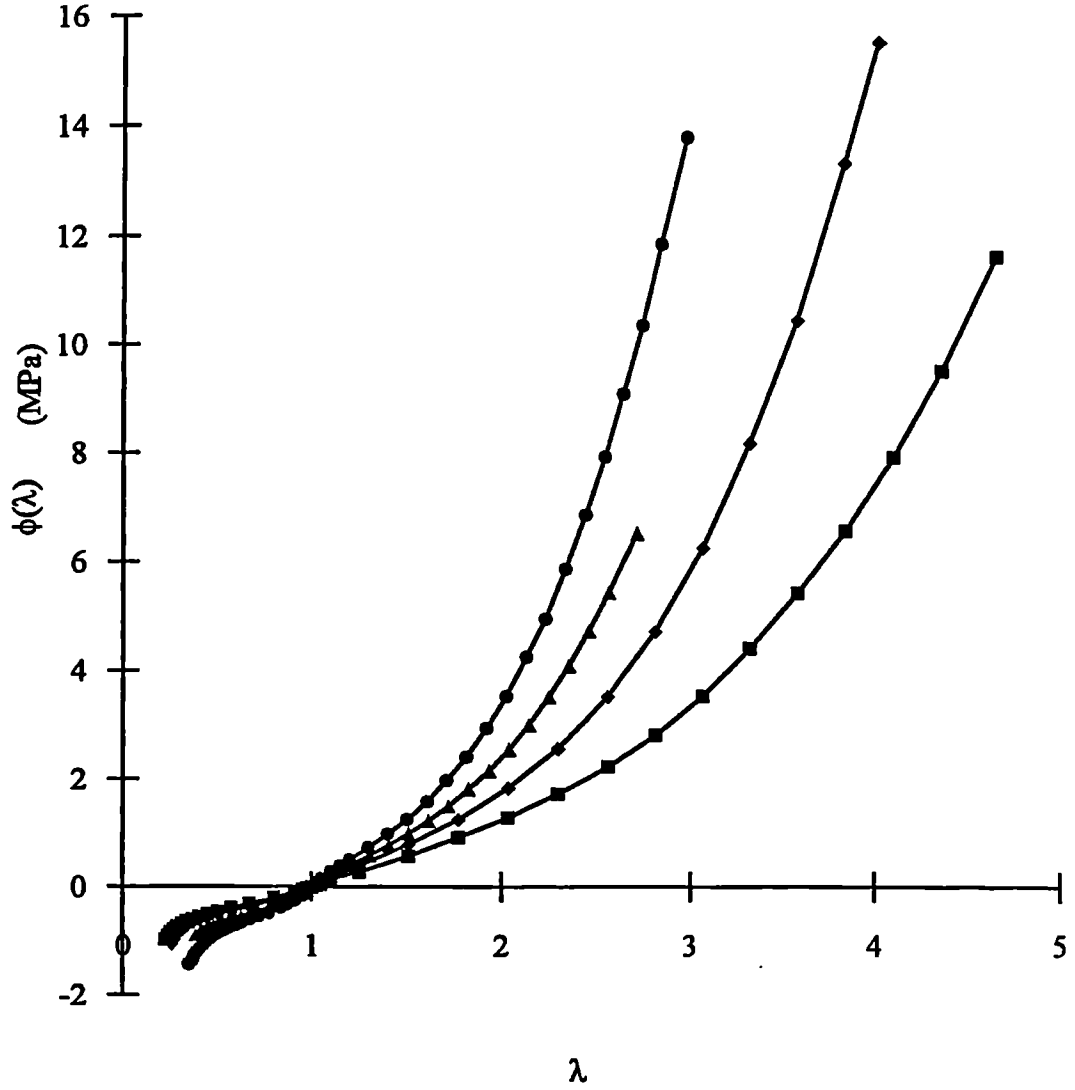

Figure 4.7 Plots of $\phi(\lambda)$, obtained from the split pure shear data using equation (1.30): ■ EDS19 (0), ◆ EDS14 (15), ▲ EDS15 (30), ● EDS16 (45). Filler loadings given in brackets. Formulations given in Table 3.2.

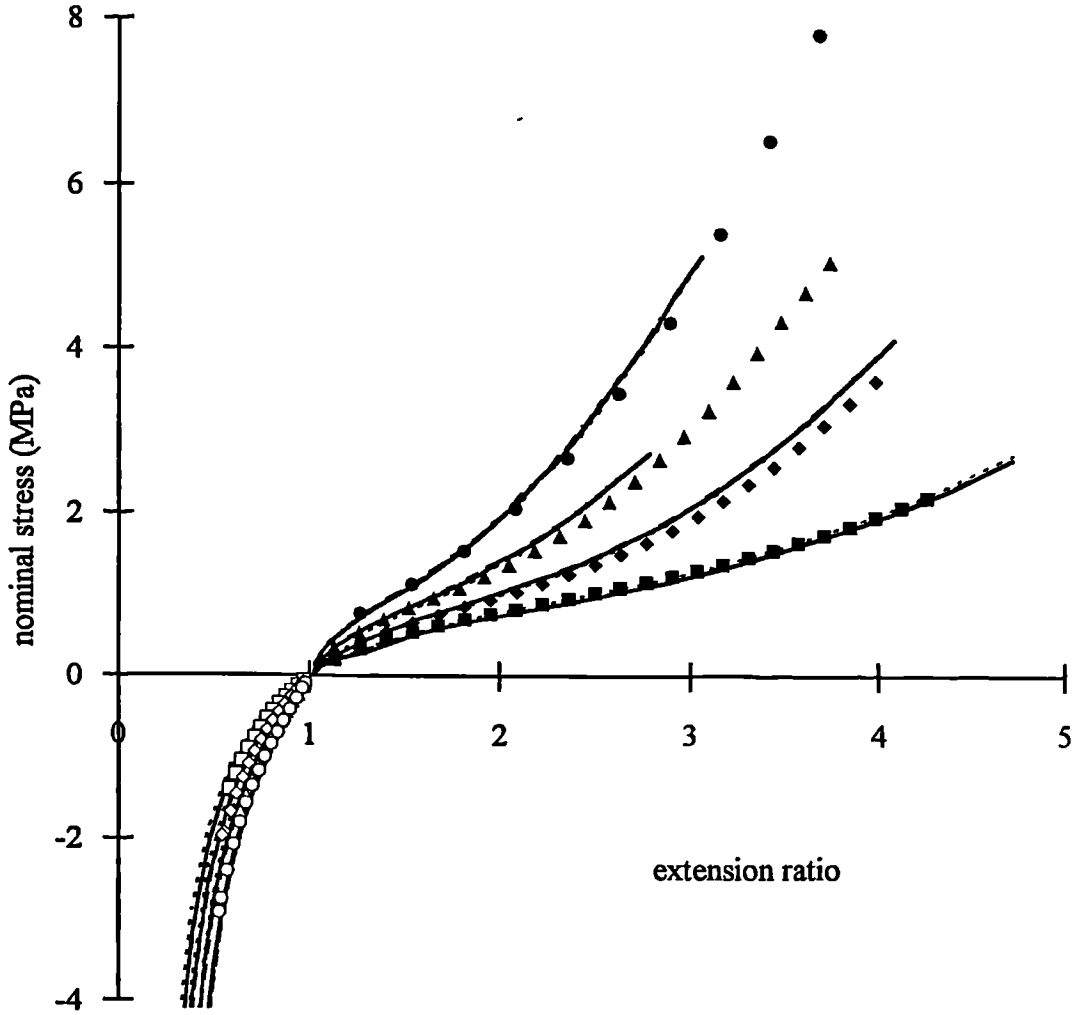

Figure 4.8 Comparison of the predictions from the split pure shear data with the experimental results for tension and compression.
Experimental data: ■ EDS19, ◆ EDS14, ▲ EDS15, ● EDS16.
Predictions from pure shear: ····· $\partial W/\partial I_2 = 0$ (Gregory, 1979),
– – – – – $W = w(\lambda_1) + w(\lambda_2) + w(\lambda_3)$ (Valanis and Landel, 1967),
———— $\partial W/\partial I_1$ is independent of I_2 and $\partial W/\partial I_2$ is independent of I_1.

4.6 Evaluation of particular functional forms for W

For many purposes, characterization of the rubber in the form of stress-strain plots or tabulated data is acceptable. In some circumstances, it is useful to be able to express the information in the form of an equation, for example where a finite element package requires such input or for compactness. Also, an explicit functional form will give explicit expressions for $\partial W/\partial I_1$, and $\partial W/\partial I_2$, thereby enabling the rubber to be characterized from a single uniaxial test, for example by using equation (4.7) in the case of characterisation in tension.

4.6.1 *Fit of experimental data to Yeoh (1990) equation*

Differentiation of equation (1.25) yields:-

$$\frac{\partial W}{\partial I_1} = C_{10} + 2C_{20}(I_1 - 3) + 3C_{30}(I_1 - 3)^2 \qquad (4.12a)$$

$$\frac{\partial W}{\partial I_2} = 0 \qquad (4.12b)$$

For simple shear, substitution into equation (4.2) gives:-

$$\frac{\tau}{2\gamma} = C_{10} + 2C_{20}(I_1 - 3) + 3C_{30}(I_1 - 3)^2 \qquad (4.13)$$

Thus, in a plot of $\tau/2\gamma$ against $(I_1 - 3)$ a best fit quadratic will provide best-fit values for C_{10}, C_{20} and C_{30} for simple shear. The values so obtained are given in Table 4.1.

Table 4.1: Fits of Yeoh equation to simple shear data

	C_{10}(MPa)	C_{20}(MPa)	C_{30}(MPa)
EDS 19	0.275	-0.00556	0.000235
EDS 14	0.325	-0.00428	0.000473
EDS 15	0.426	0.000266	0.000802
EDS16	0.559	-0.00323	0.00176

These constants may be substituted into equation (4.12a) to provide expressions for $\partial W/\partial I_1$, and $\partial W/\partial I_2$ which may in turn be substituted into equations (4.7) and (3.4) to provide fits to the data in tension and compression and pure shear respectively:-

$$s_T = 2\left(\lambda_T - \lambda_T^{-2}\right)\left(C_{10} + 2C_{20}(I_{1T}-3) + 3C_{30}(I_{1T}-3)^2\right) \quad (4.14)$$

$$s_P = 2\left(\lambda_P - \lambda_P^{-3}\right)\left(C_{10} + 2C_{20}(I_{1P}-3) + 3C_{30}(I_{1P}-3)^2\right) \quad (4.15)$$

where the subscripts T and P refer to the main straining directions in tension/compression and pure shear respectively.

Plots of the fits are given in Figures 4.9 to 4.11. The low strain sections of these figures have been expanded and are shown in Figures 4.12 to 4.14.

4.6.2 *Fit of experimental data to Gregory, Muhr and Stephens (1997) equation*

As outlined in Section 1.2.4, various workers (Yeoh, 1990; Othman and Gregory, 1990; Davies et al., 1994; Gregory et al., 1997; Yeoh and Fleming, 1997) have proposed empirical equations to model the rapid decrease in stiffness with increasing strain at small strains. Equation (1.26) (Gregory et al. 1997) enables a reasonably straightforward fitting procedure to be used and thus was considered worth investigating.

Differentiating equation (1.26) with respect to I_1 gives:-

$$\frac{\partial W}{\partial I_1} = \frac{A}{2}\left(I_1 - 3\right)^{-n/2} + \frac{B}{2}\left(I_1 - 3\right)^{m/2} \quad (4.16)$$

Substitution into equations (4.2), (4.7) and (3.4) gives expressions for the nominal stresses:

simple shear

$$\tau = \gamma\left[A\left(I_1 - 3\right)^{-n/2} + B\left(I_1 - 3\right)^{m/2}\right] \quad (4.17)$$

tension and compression

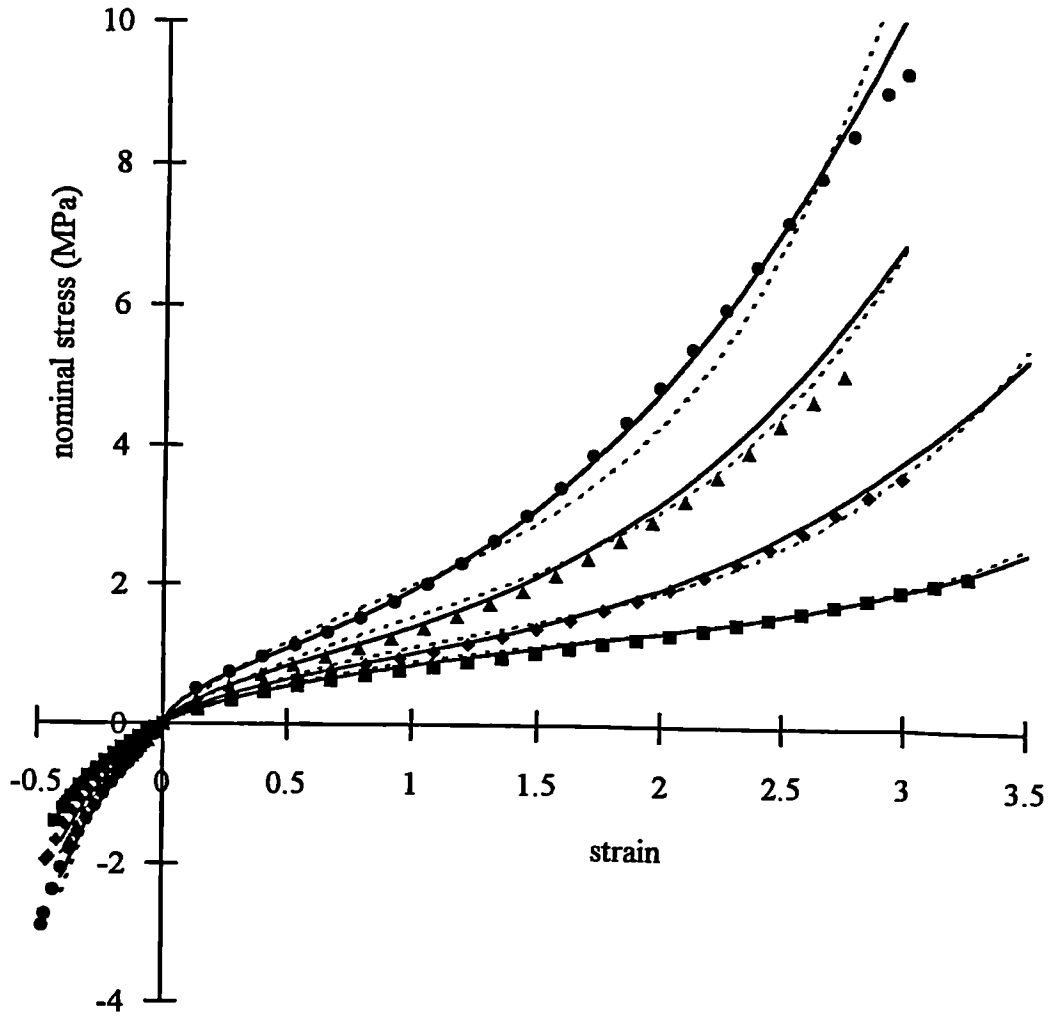

Figure 4.9 Comparison of the experimental data in tension and compression with fits to the equations of Yeoh (1990) and Gregory et al (1997).
Experimental data: ■ EDS19, ◆ EDS14, ▲ EDS15, ● EDS16.
Fits to equations: ------- Yeoh, equation (4.12a) with equation (4.7) and constants given in Table 4.1; ——— Gregory et al, equation (4.18) with constants given in Table 4.2.

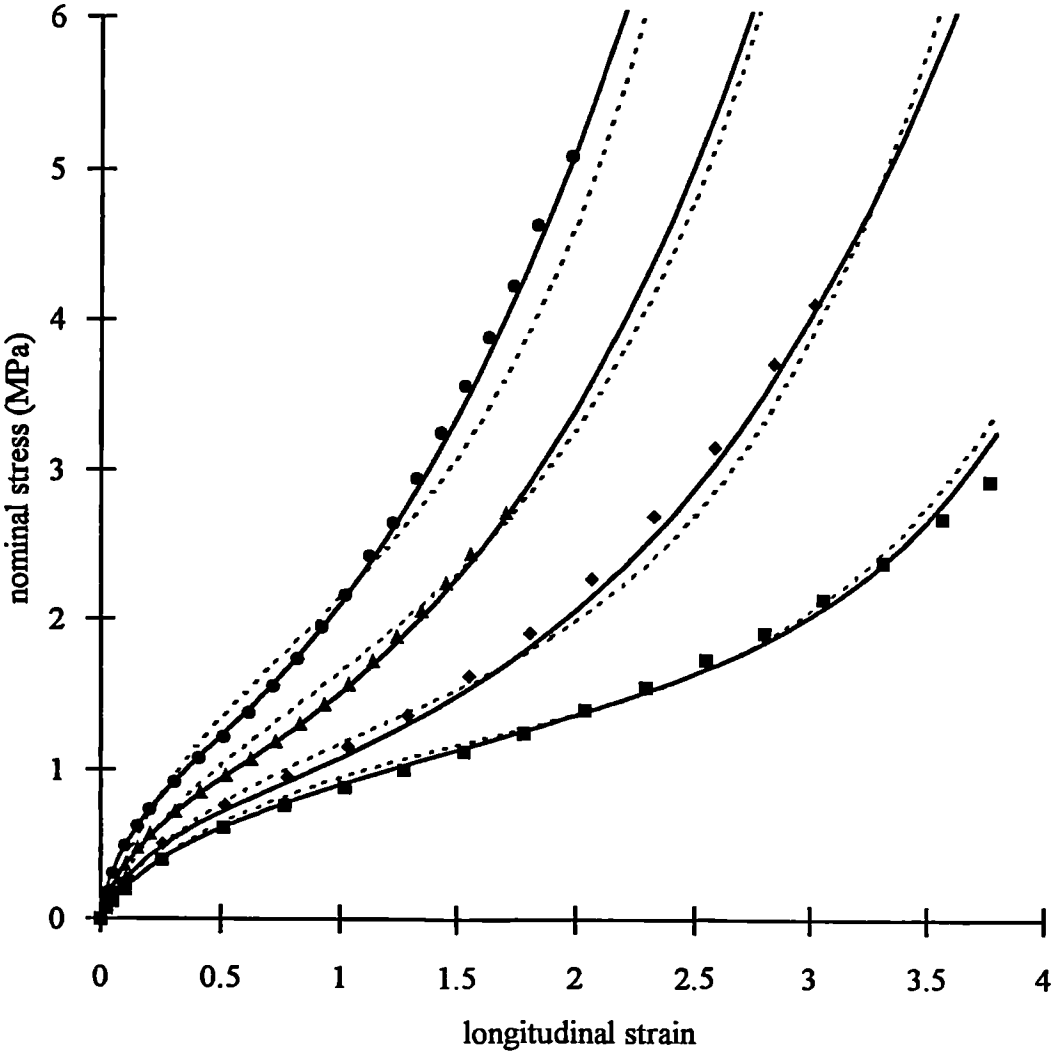

Figure 4.10 Comparison of the experimental data in pure shear with fits to the equations of Yeoh (1990) and Gregory et al (1997).
Experimental data: ■ EDS19, ◆ EDS14, ▲ EDS15, ● EDS16.
Fits to equations: ------- Yeoh, equation (4.12a) with equation (3.4) and constants given in Table 4.1; ——— Gregory et al, equation (4.19) with constants given in Table 4.2.

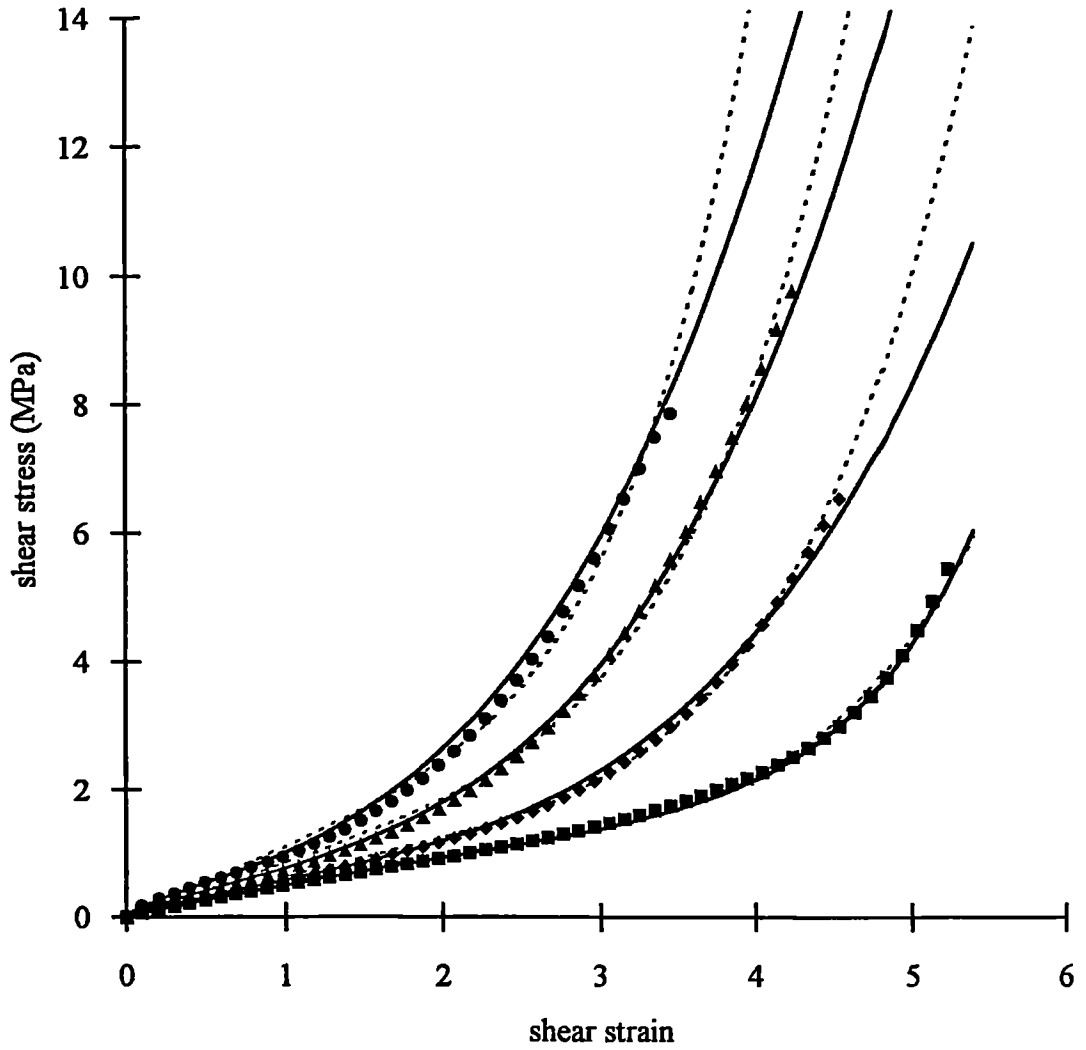

Figure 4.11 Comparison of the experimental data in simple shear with fits to the equations of Yeoh (1990) and Gregory et al (1997).
Experimental data: ■ EDS19, ◆ EDS14, ▲ EDS15, ● EDS16.
Fits to equations: ------- Yeoh, equation (4.13) with constants given in Table 4.1; ——— Gregory et al, equation (4.17) with constants given in Table 4.2.

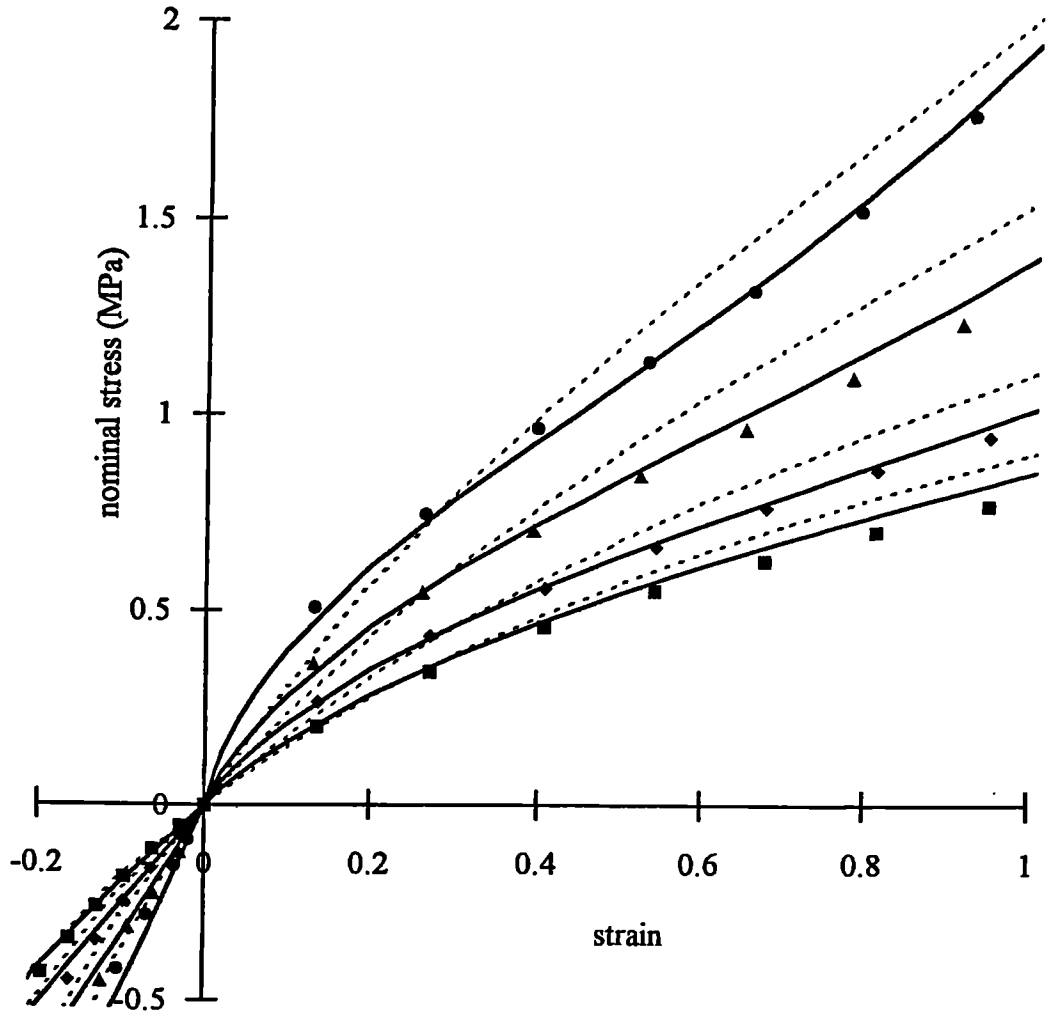

Figure 4.12 Enlargement of the small strain region of Figure 4.9. Comparison of the experimental data in tension and compression with fits to the equations of Yeoh (1990) and Gregory et al (1997).
Experimental data: ■ EDS19, ◆ EDS14, ▲ EDS15, ● EDS16.
Fits to equations: ------- Yeoh, equation (4.12a) with equation (4.7) and constants given in Table 4.1; ——— Gregory et al, equation (4.18) with constants given in Table 4.2.

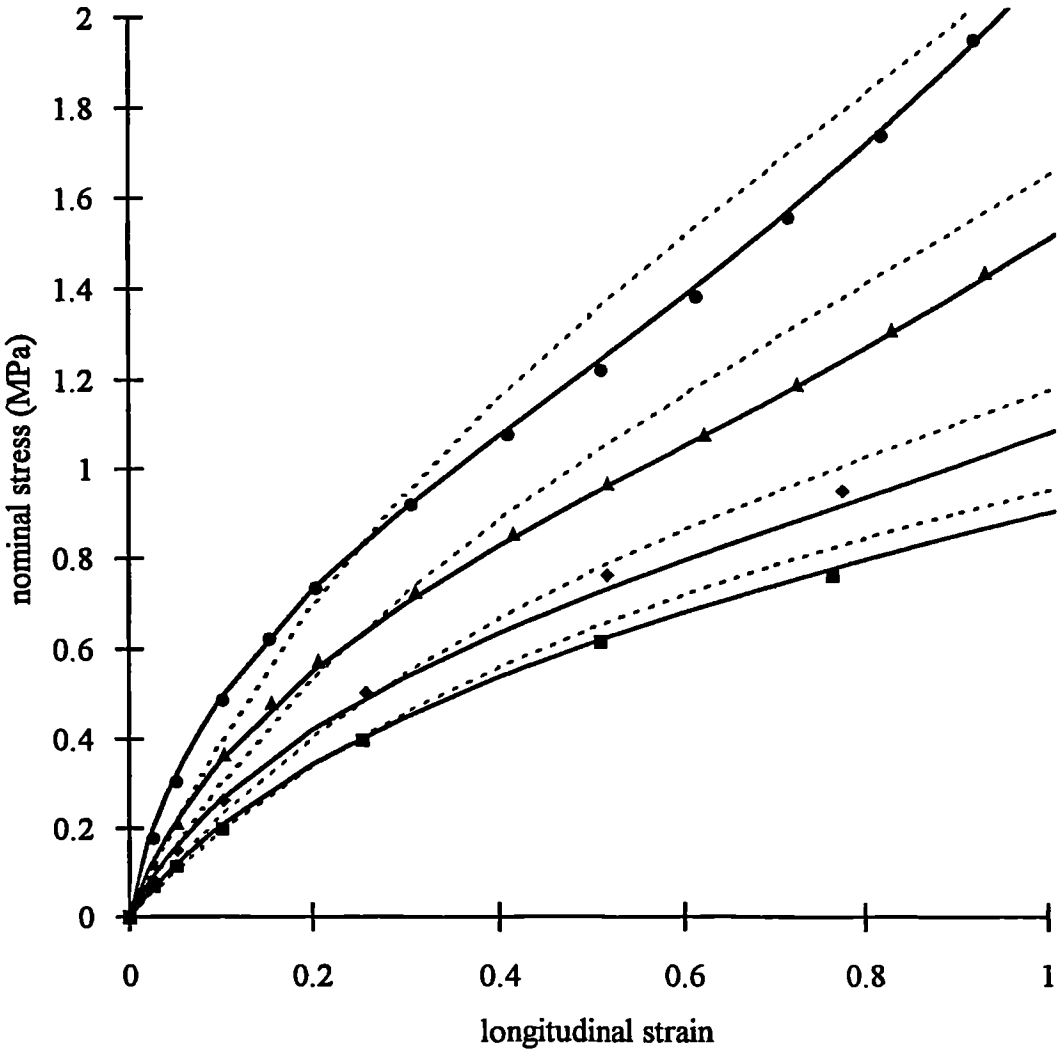

Figure 4.13 Enlargement of the small strain region of Figure 4.10. Comparison of the experimental data in pure shear with fits to the equations of Yeoh (1990) and Gregory et al (1997).
Experimental data: ■ EDS19, ◆ EDS14, ▲ EDS15, ● EDS16.
Fits to equations: ------- Yeoh, equation (4.12a) with equation (3.4) and constants given in Table 4.1; ——— Gregory et al, equation (4.19) with constants given in Table 4.2.

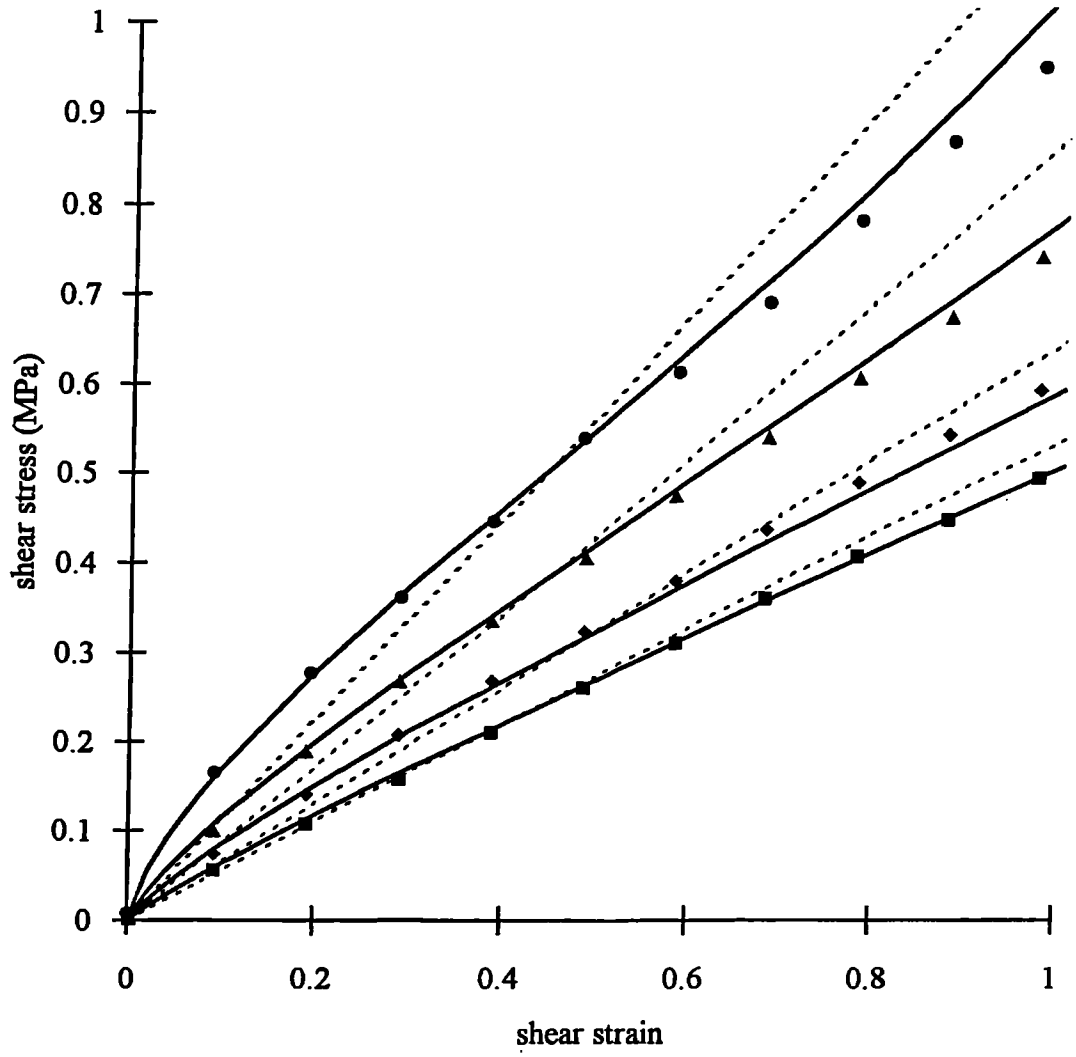

Figure 4.14 Enlargement of the small strain region of Figure 4.11. Comparison of the experimental data in simple shear with fits to the equations of Yeoh (1990) and Gregory et al (1997).
Experimental data: ■ EDS19, ◆ EDS14, ▲ EDS15, ● EDS16.
Fits to equations: ------- Yeoh, equation (4.13) with constants given in Table 4.1; ——— Gregory et al, equation (4.17) with constants given in Table 4.2.

$$s_T = (\lambda - \lambda^{-2})\left[A(I_1 - 3)^{-n/2} + B(I_1 - 3)^{m/2}\right] \qquad (4.18)$$

pure shear

$$s_P = (\lambda - \lambda^{-3})\left[A(I_1 - 3)^{-n/2} + B(I_1 - 3)^{m/2}\right] \qquad (4.19)$$

Substitution of $I_1 = 4$ into equations (4.17) to (4.19) gives expressions relating to the stress and strain which are independent of n and m. Thereby, a quick check may be made of the applicability of equation (1.26) and the consistency of the testpieces between different deformation modes by seeing whether self-consistent values of A +B may be obtained for the strains applicable to $I_1 = 4$, before embarking on a more extensive fitting procedure.

Equation (1.26) has been expressed so that positive values are expected for all of the constants, thus at small strains the first term on the right-hand side of equation (1.26) dominates and at large strains the second term dominates. Hence, equation (4.18) may be written as:-

$$\log\left(\frac{s_T}{\lambda - \lambda^{-2}}\right) \simeq \log A - \tfrac{1}{2}n\log(I_1 - 3) \qquad (4.20a)$$

for small λ and:-

$$\log\left(\frac{s_T}{\lambda - \lambda^{-2}}\right) \simeq \log B + \tfrac{1}{2}m\log(I_1 - 3) \qquad (4.20b)$$

for large λ.

Straight line fits of equations (4.20) to the tension and compression data at small and large strains were used to obtain values for A, B, n and m. However, it was found that the strain range of the data was insufficient for good fits to be obtained using equations (4.20). The parameters were therefore adjusted manually until a good fit was obtained. The values obtained are given in Table 4.2.

Table 4.2: Fits of Gregory, Muhr and Stephens equation				
	A(MPa)	B(MPa)	n	m
EDS 19	0.5	0.000017	0.1	6.3
EDS 14	0.57	0.014	0.17	2.78
EDS 15	0.72	0.053	0.2	2.4
EDS 16	0.85	0.17	0.3	1.9

These values were then substituted into equations (4.17) to (4.19) to obtain stress-strain plots which are shown in Figures 4.9 - 4.14 alongside the experimental data and fits to Yeoh's (1990) equation.

4.6.3 *Direct comparison of different deformation modes*

If W can be expressed as a function of I_1 only then equations (4.2), (4.7) and (3.4) may be rearranged to give expressions for the "modulus", equal to $2\,\partial W/\partial I_1$. In this way the stress-strain data for all modes of deformation collapse onto a single curve on a graph of modulus versus $I_1 - 3$. Such a procedure was used by Gregory (1979). Plots of this type for the current data are given in Figures 4.15a-d. Also plotted on Figures 4.15 are the theoretical curves for the Yeoh (1990) and Gregory et al. (1997) equations, given by twice equations (4.12a) and (4.16) with coefficients from Tables 4.1 and 4.2.

4.6.4 *Discussion*

It is clear from Figures 4.12 - 4.14 that the Yeoh (1990) equation is unable to model the rapid decrease in modulus with strain at small strains, especially for the more highly filled rubbers, EDS 15 and EDS 16. The same problem is illustrated even more clearly in the "modulus" plots (Figures 4.15a-d). Yeoh (1990) suggested the addition of an empirical exponential term to overcome this difficulty. However, a further difficulty with the use of a limited number of terms of the series expansion for W (equation 1.21) is the likelihood of unrealistic behaviour being predicted outside the range of the fit. This is caused by the presence of terms of high powers of $(I_1 - 3)$ becoming very large at high $(I_1 - 3)$. This difficulty has been limited in the present work by fitting to the mode of deformation where the highest strains were achieved (simple shear), but the potential for serious discrepancies between actual behaviour and equations of this type is apparent from Figure 4.11 where the theoretical stiffness rises more sharply at high strains than the experimental points.

(a)

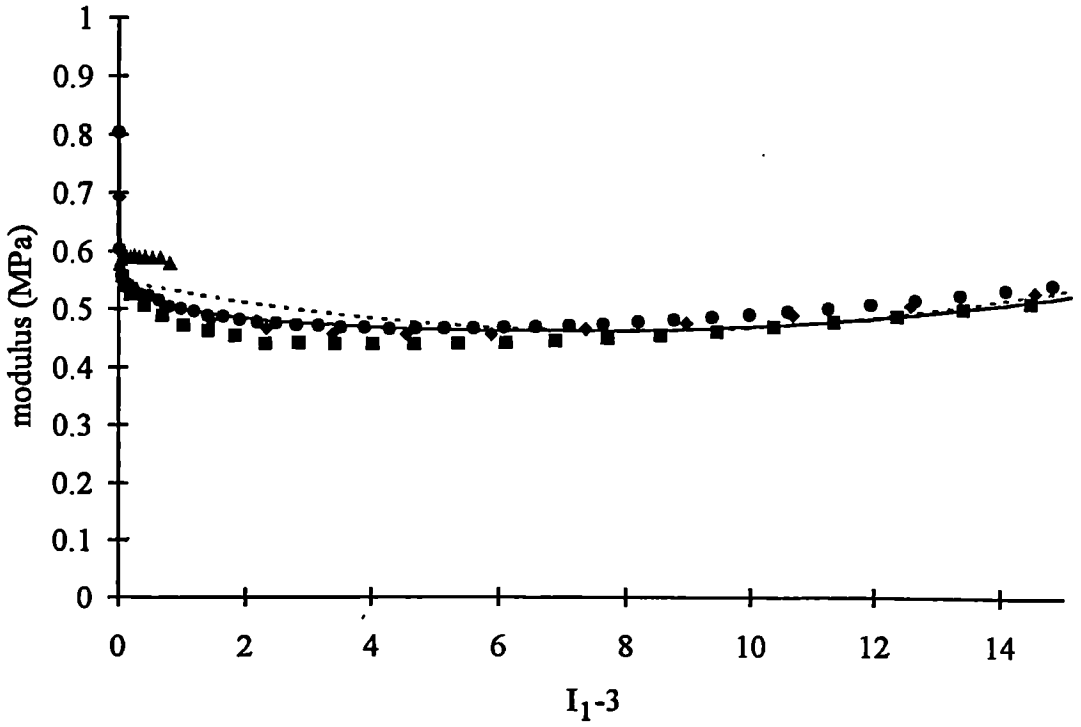
modulus (MPa)
1
0.9
0.8
0.7
0.6
0.5
0.4
0.3
0.2
0.1
0
0
2
4
6
8
10
12
14
I1-3

(b)

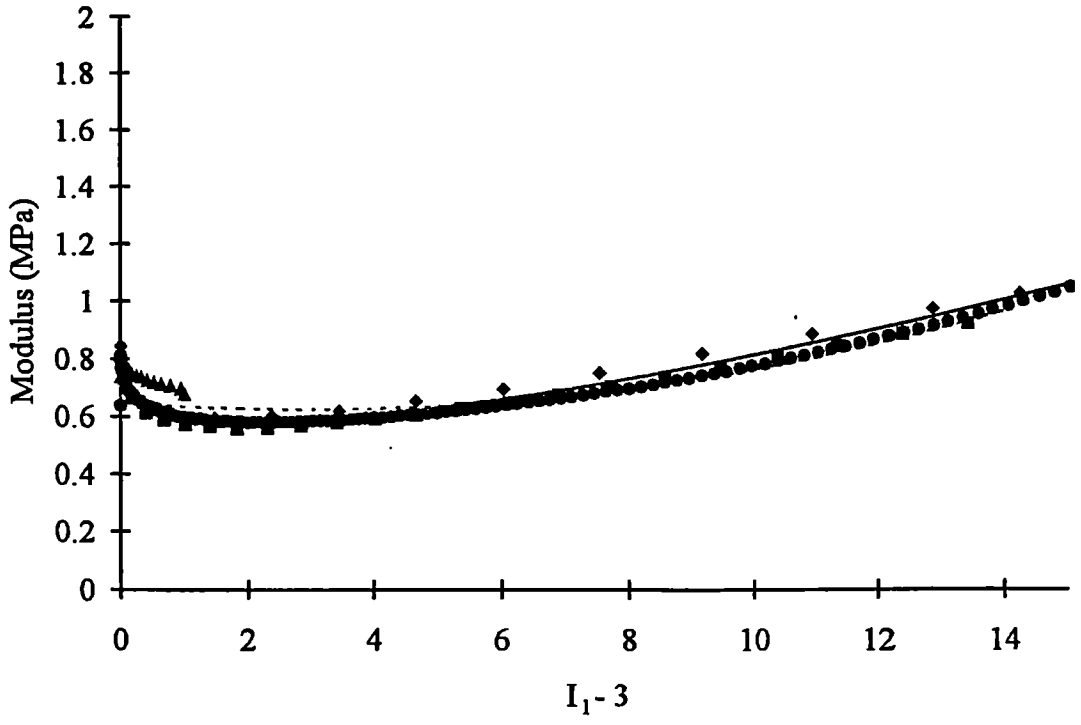
Modulus (MPa)
2
1.8
1.6
1.4
1.2
1
0.8
0.6
0.4
0.2
0
0
2
4
6
8
10
12
14
I1 - 3

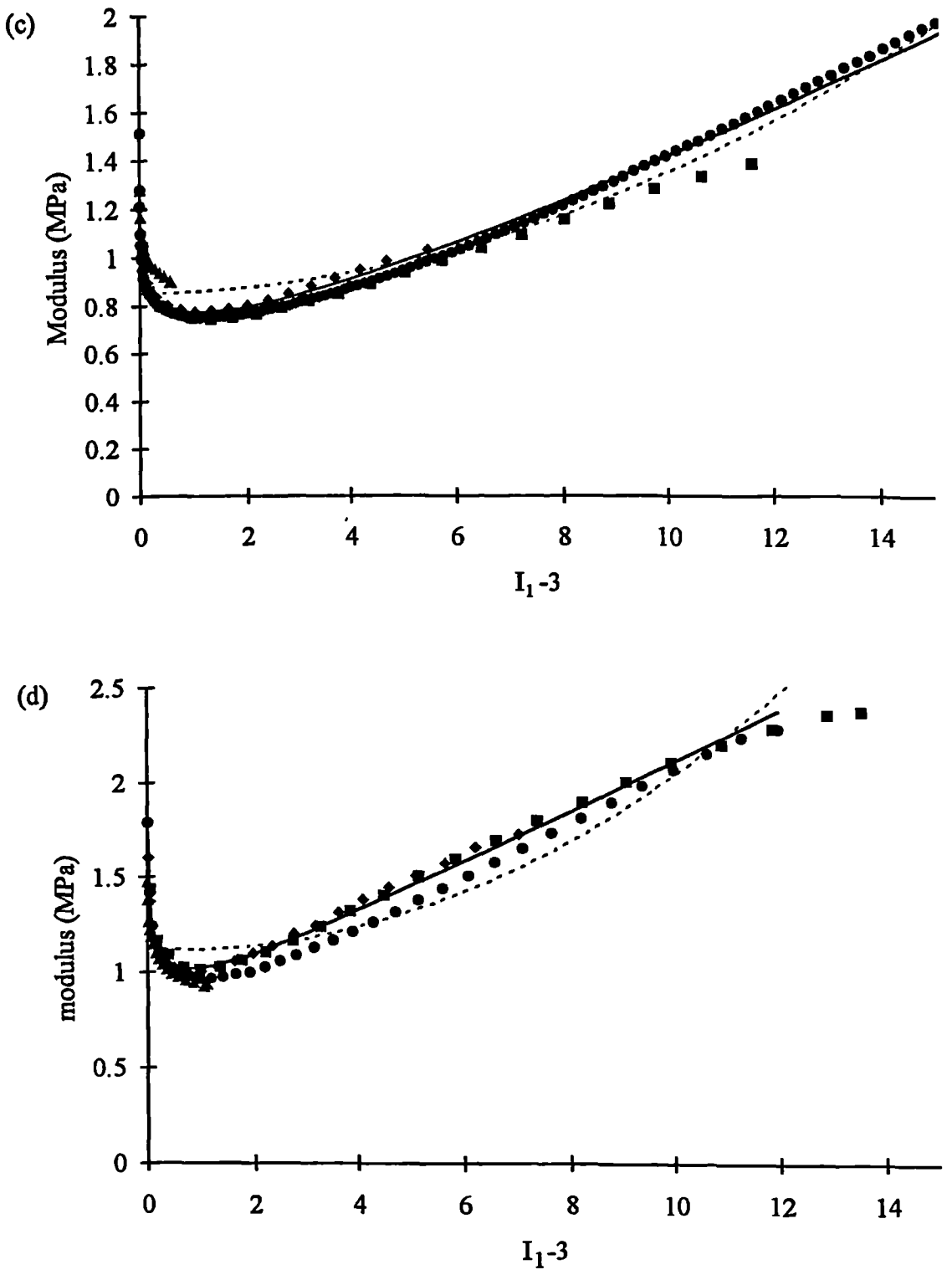

Figure 4.15 Plots of modulus, defined as $2\partial W/\partial I_1$ for $W=W(I_1)$
(a) EDS19, (b) EDS14, (c) EDS15, (d) EDS16
■ tension, ▲ compression, ◆ pure shear, ● simple shear.
------- theoretical fit to equation (1.25), Yeoh (1990).
——— theoretical fit to equation (1.26), Gregory et al (1997).

The equation of Gregory et al. (1997) is more capable of capturing the sharply decreasing modulus at low strains. Also, there is less likelihood of unrealistic behaviour being predicted beyond the range of the fit.

A failure of data to collapse onto a single curve in Figures 4.15 would be an indication, either that the assumption that $\partial W/\partial I_2$ is negligible is wrong or that testpieces from different deformation modes possess different moduli. The results reported in Chapter 3 indicated that $\partial W/\partial I_2 \simeq 0$ for the filled compounds. This is generally confirmed by Figures 4.15b-d and the discrepancies are most likely to be due to testpiece differences, as was concluded in Section 4.5.3. Even for the unfilled rubber, EDS 19, the discrepancies due to assuming $\partial W/\partial I_2 = 0$ are not large.

4.7 Conclusions

Characterization of black filled rubbers may be simplified by:-

(i) Measuring both stresses in pure shear, and defining the behaviour in other modes of deformation by following either the Valanis and Landel (1967) hypothesis that $W = w(\lambda_1) + w(\lambda_2) + w(\lambda_3)$ or by assuming $W = F_1(I_1) + F_2(I_2)$.

(ii) Measuring the stress-strain behaviour from any mode of deformation and assuming $W = W(I_1)$.

Since (ii) above requires simpler experimentation it is the preferred option.

If it is necessary to define W in the form of an explicit equation, that of Gregory et al. (1997) has been found to be reasonably appropriate and straightforward to use. The power series expansions of $W(I_1,I_2)$, frequently incorporated in finite element packages are less able to model the sharp downturn in stiffness at low strains and may be unreliable if a single uniaxial test is used to obtain the fitting constants and if extrapolating beyond the strain range of the experimental data (see Section 1.2.4).

CHAPTER 5

First loading cycle stress-strain behaviour of synthetic rubbers

5.1 Introduction

The emphasis, both in the literature and in this thesis, has been on examining the behaviour of natural rubber or conventional synthetic rubbers such as polybutadiene. Both of these, when unfilled, are known to exhibit almost ideal elastic behaviour with low hysteresis and a linear stress-strain curve in simple shear. They are thus ideal for evaluating the predictions of theoretical models of rubber elasticity. The departures from elastic behaviour when filler is added have also been discussed.

Detailed evaluation of the stress-strain behaviour of most synthetic rubbers is lacking in the literature. However, non-linear stress-strain behaviour has been observed in rubbers of the block copolymer type, such as polyurethane, even when unfilled (Speckhard and Cooper, 1986). Furthermore, Cook (1994) has reported that the dynamic shear modulus of unfilled polyacrylonitrile-butadiene (NBR) is dependent on the shear strain in a similar way to carbon black filled natural rubber. These observations suggest that certain unfilled synthetic rubbers show some of the stress-strain characteristics of filled natural rubber.

In order to make more thorough comparisons with natural rubber the split pure shear technique described in Chapter 3 was used to evaluate $\partial W/\partial I_1$ and $\partial W/\partial I_2$ from the first cycle stress-strain behaviour of three synthetic rubbers. Two were unfilled copolymers. The third, a filled silicone rubber, was known to exhibit a very large first cycle hysteresis and Mullins' effect (Muhr et al, 1999). It was thus chosen as a suitable material on which to compare the magnitude of changes in the main and transverse directions using the split pure shear technique.

5.2 Materials

5.2.1 *Nitrile rubber*

Nitrile rubber, that is polyacrylonitrile butadiene (NBR), is a copolymer of butadiene,

CH_2=CH–CH=CH_2 and acrylonitrile, CH_2=CHCN. It is available in various grades with differing acrylonitrile contents between about 18% and 40%. The higher the acrylonitrile content, the more polar is the elastomer, giving nitrile rubber its most useful characteristic - resistance to swelling in oils. Grades with a high acrylonitrile content are also known to have increased hardness and hysteresis, properties which are increased in natural rubber by adding reinforcing filler. The simplest explanation for the increase in these properties would be the fact that the glass transition temperature is raised by increasing the acrylonitrile content. Similar changes in the properties of natural rubber may be produced by epoxidation, but unfilled epoxidised natural rubber still has relatively linear stress-strain behaviour in simple shear in contrast to nitrile rubber (Cook, 1994).

For this work a grade of nitrile rubber with a high acrylonitrile content was chosen. The formulation is given in Table 5.1. Its glass transition temperature was measured by differential scanning calorimetry and found to be -20°C.

Table 5.1: Formulation of nitrile rubber. Ingredients expressed in parts per hundred of rubber by mass.

Polyacrylonitrile- butadiene, Breon N41/C45[1]	100
zinc oxide	5
stearic acid	2
sulphur	1.5
accelerator, CBS[2]	0.75
vulcanization time (minutes at 150°C)	60
hardness (IRHD)	46

1. The acrylonitrile content is 41%
2. N-cyclohexylbenzothiazole-2-sulphenamide

Bonded pure shear testpieces of the type shown in Figure 3.2 were moulded. In order to allow sufficient flow of the rubber in the mould the rubber was heated for 10 minutes at 100°C before vulcanizing. Unfortunately the testpieces were found to contain air bubbles, though these were estimated to amount to a volume fraction of not more than 0.005. Testing proceeded on the assumption that the stress-strain behaviour was unlikely to be significantly influenced by this small level of porosity.

5.2.2 *Polyurethane rubber*

Polyurethane rubber is a block copolymer of a diisocyanate with a polyester or polyether and a chain extender. The usual synthesis involves a two stage reaction, firstly between the polyester or polyether (B) and two molecules of the diisocyanate (A) to form a prepolymer: A–B–A. In a subsequent reaction, bonds between the diisocyanate and the chain extender (C) are formed so that the structure of the final polyurethane rubber is $[–A–B–A–C–]_n$. The isocyanate blocks are rigid, whereas the polyester or polyether blocks are flexible. Various chemical structures are used for the chain extender which may be flexible or rigid (Hepburn, 1982). The isocyanate blocks are polar and will bond by dipole-dipole interactions to form rigid regions connecting a number of flexible polymer chains in a similar way to the crosslinks in a conventional rubber (Bonart, 1968). It is also possible, if they comprise a significant volume fraction of the rubber, that the rigid regions will act like a rigid filler.

Often polyurethane mouldings are prepared by reacting the prepolymer and the chain extender at the same time as moulding. As these components are usually liquids this requires different equipment to conventional rubber moulding. However, millable polyurethane rubbers have also been developed which are processed as solids using conventional rubber processing machinery. These polymers are chemically modified to incorporate unsaturated C=C bonds and are crosslinked by vulcanization using similar systems to conventional rubbers.

Table 5.2: Formulation of polyurethane rubber. Ingredients expressed as parts per hundred of rubber by mass.

Polyurethane, Millathane 76[1]	100
zinc stearate	0.5
MBTS[2]/zinc chloride activator (Thanecure)	0.5
sulphur	1.5
accelerator, MBTS[2]	2.0
accelerator, MBT[3]	4.0
vulcanization time (minutes at 140°C)	45
hardness (IRHD)	55

1. A millable polyester based polyurethane
2. Benzothiazole-disulphide
3. 2-mercaptobenzothiazole

For this work a millable polyurethane was used. The formulation is given in Table 5.2. The testpieces were vulcanized to maximum rheometer torque. The glass transition temperature was -34°C as measured by differential scanning calorimetry. Attempts to prepare sufficiently strong bonded pure shear testpieces of the type shown in Figure 3.2 using various propriety bonding agents were unsuccessful, Therefore a 1.5mm thick sheet was moulded from which the testpieces were cut.

5.2.3 *Silicone rubber*

This rubber is based on polymer chains consisting of alternating silicon and oxygen atoms. Various organic side groups, such as the methyl group, CH_3, may be attached to the silicon atoms and many silicone rubbers are based on polydimethylsiloxane. Silicone rubbers generally have a very low glass transition temperature and are also likely to crystallize unless bulky side groups are incorporated to suppress crystallization. They are mechanically weak unless a reinforcing filler, usually fused silica, is added. Crosslinking of so-called liquid silicone rubbers, which have a grease-like consistency before vulcanisation, is carried out at elevated temperatures. The cure systems are different to those used for other rubbers. Very short cure times are required, typically 30 seconds at 150°C. For this work testpieces were cut from a 2mm thick sheet of a liquid silicone rubber, containing about 30 parts by mass of a fused silica filler, supplied by Dow Corning, designated as 9280-50E and of nominal hardness 50IRHD. Its glass transition temperature was measured by differential scanning calorimetry as -127°C.

5.3 Measurement of $\partial W/\partial I_1$ and $\partial W/\partial I_2$

5.3.1 *Method*

As the nitrile rubber was in the form of a bonded pure shear testpiece (see Figure 3.2) it could be clamped in the split pure shear apparatus as described in Section 3.2.1. As the polyurethane and silicone rubbers were in the form of sheets the pure shear apparatus was adapted by replacing the usual clamps with clamps designed to grip rubber sheet. Slits were cut in the rubber sheets, corresponding to the splits in the pure shear clamps. The most reproducible means of making the slits was found to be by punching a 2mm diameter hole in the rubber corresponding to the end of the slit with

a leather punch and removing a strip of rubber with a razor blade. The nominal area of the sheet between the clamps was the same as for the bonded testpieces.

The rubbers were pulled in pure shear in an Instron tensile test machine at a speed of 2.5mm/minute for the nitrile and polyurethane rubbers and 10mm/minute for the silicone rubber. Other test details were as described in Chapter 3.

5.3.2 *Results*

In the nitrile rubber, failure initiated at an air bubble so the strain at failure was rather low, about 200%. The silicone rubber proved difficult to clamp, either slipping or cracking along the clamped edge, thus the maximum strain achieved was about 100%.

The main stress, for the three synthetic rubbers, is plotted as a function of strain in Figure 5.1. For comparison, data from Chapter 3 for a filled and unfilled natural rubber are also shown. Further comparisons of the stress-strain behaviour of the rubbers was made by plotting the shear stress as a function of shear strain, calculated using equations (4.3) and (4.4), in Figure 5.2. To allow for the differing stiffnesses of the rubbers, the shear stresses were normalized by dividing them by their value at 100% shear strain. $\partial W/\partial I_1$ and $\partial W/\partial I_2$ were evaluated from equations (3.7) and are shown in Figure 5.3.

5.4 **Discussion**

The polyurethane showed near linear stress-strain behaviour in simple shear, like that of the unfilled natural rubber, EDS19, also shown in Figure 5.2. This result suggests that the rigid blocks of this copolymer are not acting in the same way as fillers such as carbon black in natural rubber. A further investigation of the stress-strain characteristics of this rubber in uniaxial tension showed that, at moderate strains, its hysteresis was very small (see Figure 8.1d). This also is typical of unfilled, rather than filled, rubber. A much larger hysteresis was seen at strains above 350%. This could be attributed to strain crystallization; it was also observed that the unvulcanized rubber crystallized on storage at room temperature. The linear stress-strain behaviour and low hysteresis are not, however, universal properties of polyurethane rubbers. Speckhard and Cooper (1986) present widely differing stress-strain curves for various polyurethane rubbers

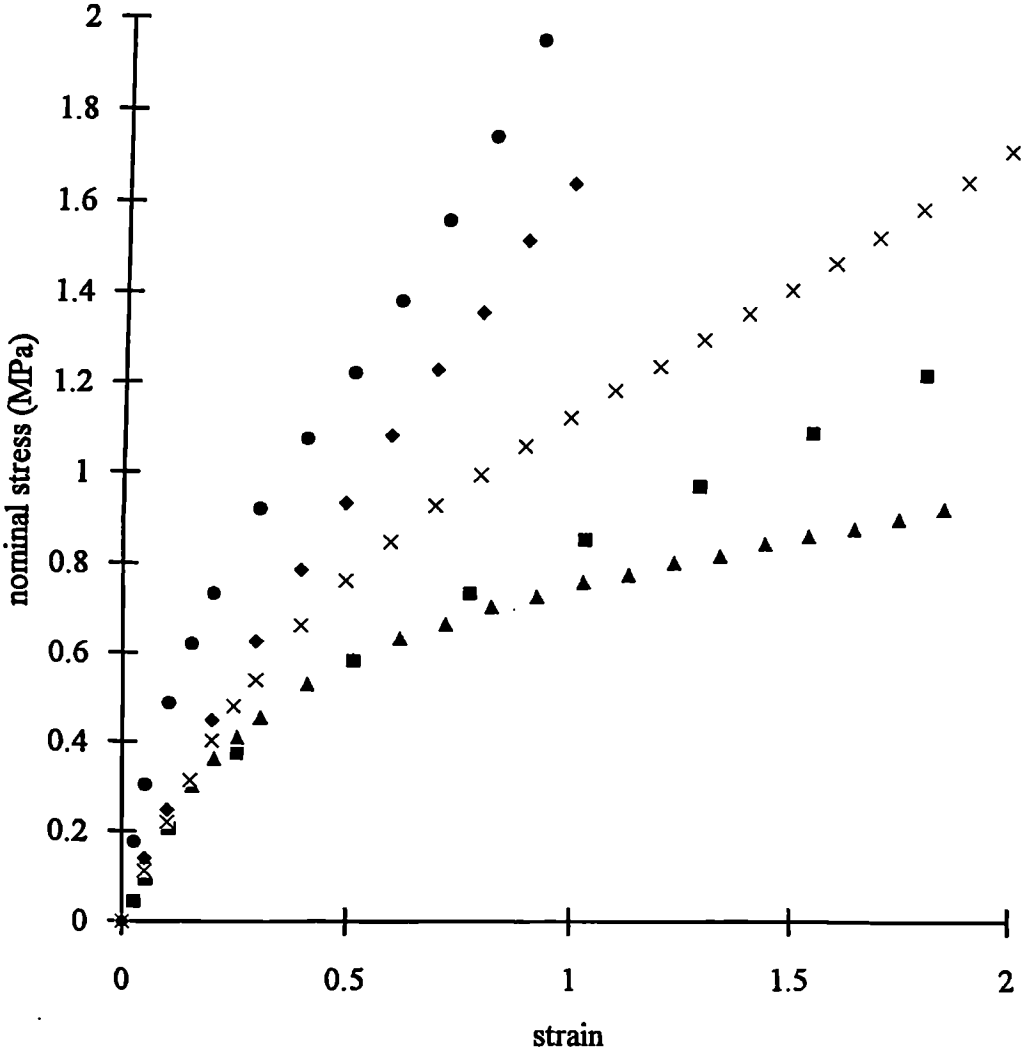

Figure 5.1 Stress-strain behaviour of synthetic rubbers obtained from main stress in pure shear.
▲ nitrile rubber, × polyurethane rubber, ◆ silicone rubber,
■ unfilled natural rubber, EDS19. ● filled natural rubber, EDS16.

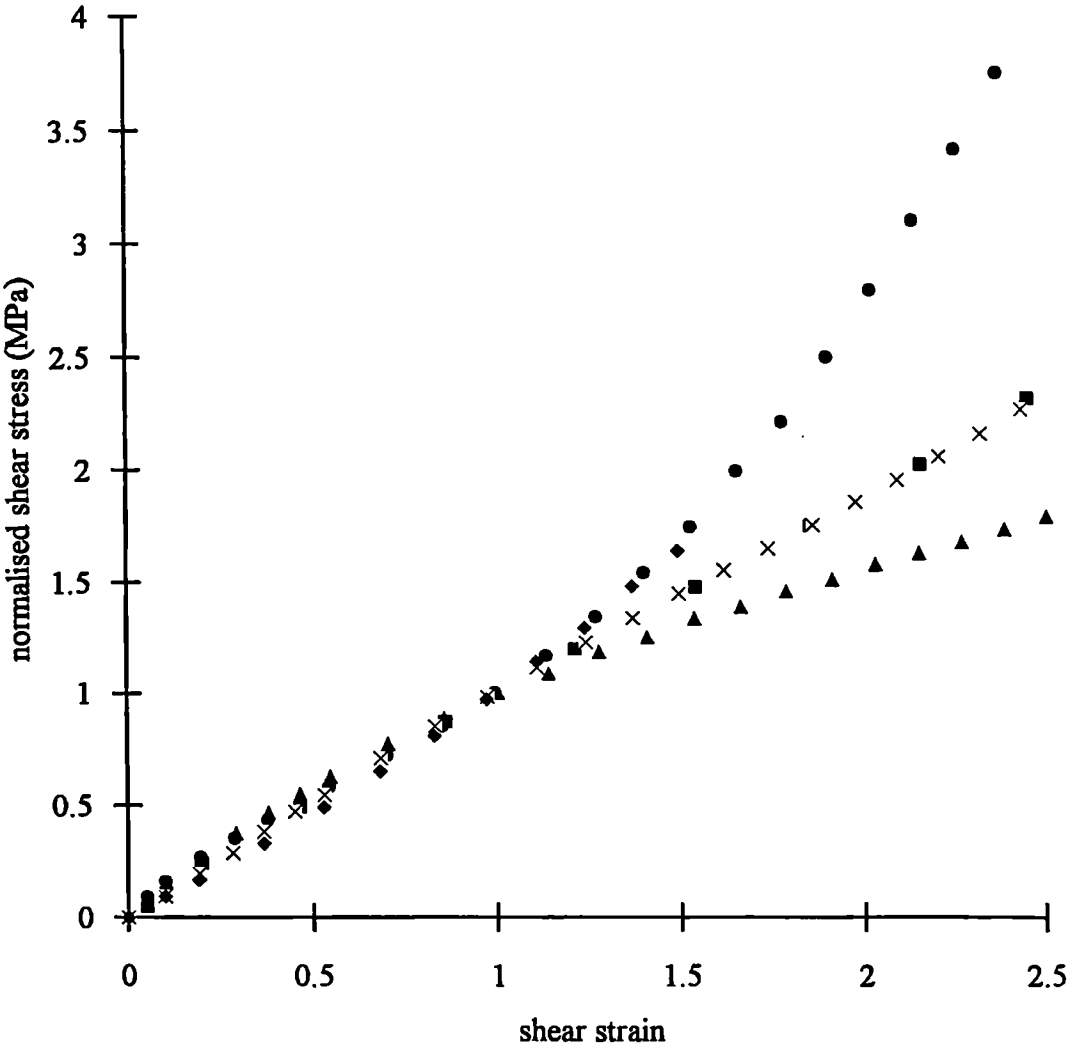

Figure 5.2 Stress- strain data of Figure 5.1 replotted in the form of a normalized shear stress.
▲ nitrile rubber, × polyurethane rubber, ◆ silicone rubber,
■ unfilled natural rubber, EDS19. ● filled natural rubber, EDS16.

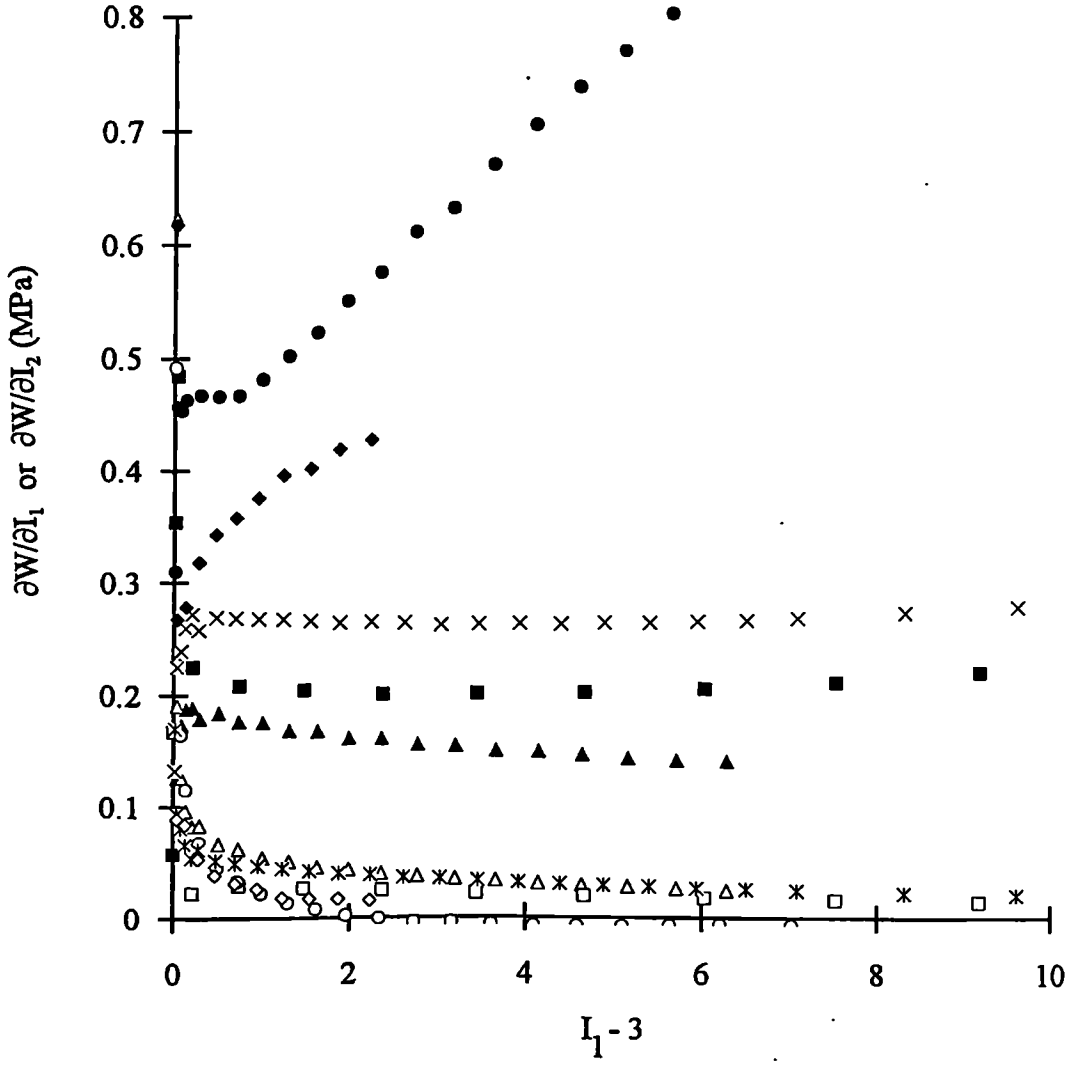

Figure 5.3 Strain energy derivatives, $\partial W/\partial I_1$ and $\partial W/\partial I_2$ for synthetic rubbers. ▲ $\partial W/\partial I_1$ nitrile rubber, △ $\partial W/\partial I_2$ nitrile rubber; × $\partial W/\partial I_1$ polyurethane rubber, * $\partial W/\partial I_2$ polyurethane rubber; ◆ $\partial W/\partial I_1$ silicone rubber, ◇ $\partial W/\partial I_2$ silicone rubber; ■$\partial W/\partial I_1$ unfilled natural rubber, EDS19; □ $\partial W/\partial I_2$ unfilled natural rubber, EDS19; ● $\partial W/\partial I_1$ filled natural rubber, EDS16; ○ $\partial W/\partial I_2$ filled natural rubber, EDS16.

based on different flexible block types. In view of its linear behaviour, it is not surprising that $\partial W/\partial I_1$ and $\partial W/\partial I_2$ for the polyurethane rubber show similar features to the unfilled natural rubber (Figure 5.3).

The nitrile rubber and the silicone rubber, however, show non-linear stress-strain behaviour in shear (Figure 5.2). The silicone rubber stiffens at strains above about 100%, like the filled natural rubber, EDS16. This, perhaps, is not surprising since it is known to contain about 30 parts of a reinforcing filler. $\partial W/\partial I_1$ and $\partial W/\partial I_2$ also behave rather like they do for EDS16, with $\partial W/\partial I_1$ rising with increasing strain while $\partial W/\partial I_2$ is approximately zero.

The non-linearity in the nitrile rubber shows significant differences to that in filled natural rubber. The decrease in modulus with strain at low strain occurred for both materials but no increase in modulus at larger strains was apparent in the nitrile rubber at the breaking strain of about 200% although an upturn at higher strains would be expected. The upturn in filled rubbers occurred at much lower strains. The fall in modulus with strain corresponds to a fall in both $\partial W/\partial I_1$ and $\partial W/\partial I_2$. Also, $\partial W/\partial I_2$ does not fall to zero, suggesting similarities with other unfilled, rather than filled, rubbers. Nitrile rubber is classed as a random copolymer and thus large hard regions, as in block copolymers, would not be expected. However, it is possible that sufficiently large regions of "hard" acrylonitrile exist within areas of "soft" butadiene to cause some non-linear effects. A possible mechanism is that the softening is caused by yielding of the acrylonitrile, analogous to plastic yielding in crystalline polymers. This suggestion is borne out by the significant hysteresis and set of this nitrile rubber (see Figure 8.1e) which is atypical of conventional unfilled rubbers. Yielding behaviour of this sort has been observed in block copolymers (Tang et al, 1980).

5.5 Conclusions

The conclusions about the form of $\partial W/\partial I_1$ and $\partial W/\partial I_2$ for filled and unfilled rubber may be expanded to include some synthetic rubbers. Thus, for materials containing reinforcing fillers, $\partial W/\partial I_2$ is approximately zero, but for unfilled rubbers $\partial W/\partial I_2$ is greater than zero but an order of magnitude smaller than $\partial W/\partial I_1$. Non-linear behaviour

may be accompanied by corresponding changes in both $\partial W/\partial I_1$ and $\partial W/\partial I_2$. The behaviour of synthetic rubbers, such as nitrile rubber, which exhibit non-linear stress strain behaviour when unfilled is different from that of conventional filled rubbers, suggesting that the mechanisms in the two cases are different, and models developed to describe the non-linearity in filled rubbers are therefore not necessarily applicable to non-linear unfilled rubbers. There are a large number of synthetic rubbers and the conclusions drawn from the three materials examined in this chapter may not be representative of all types of synthetic rubber. There is scope for further clarification of these conclusions through examining a wider range of materials.

CHAPTER 6

Behaviour of rubber in simple shear

6.1 Introduction

In Chapter 3, the limitations of the split pure shear technique as a method of characterising rubber were noted. Firstly, as for biaxial straining of a thin sheet, the evaluation of $\partial W/\partial I_1$ and $\partial W/\partial I_2$ is very sensitive to small experimental errors at small strains. Secondly, anisotropy in the testpiece stiffness causes further difficulties in evaluating the data.

In the light of these difficulties, the possibility of obtaining similar information from a different technique was considered. The experiment involved deformation of testpieces of the type shown in Figure 4.1. This deformation, usually referred to as "simple shear", is, in fact, only an approximation. A true simple shear would require the unbonded edges of the testpiece to remain straight, necessitating application of constraining forces which would be very difficult to obtain experimentally. Usually it is assumed that the errors arising from the experimental approximation to simple shear are small enough to be disregarded; the difference between the apparent and actual shear modulus has been estimated from simple equations as being typically of the order of 5% (Rivlin & Saunders, 1949; Gregory & Muhr, 1999).

Rivlin (1948b) has derived the following equations for the components of true stress corresponding to simple shear in the x-direction of the x-y plane:-

$$\begin{aligned}
\sigma_{xy} &= 2\gamma\left\{\left(\partial W/\partial I_1\right) + \left(\partial W/\partial I_2\right)\right\} \\
\sigma_{yz} &= \sigma_{zx} = 0 \\
\sigma_{xx} &= 2\left\{\left(1+\gamma^2\right)\left(\partial W/\partial I_1\right) - \left(\partial W/\partial I_2\right)\right\} + p \\
\sigma_{yy} &= 2\left\{\left(\partial W/\partial I_1\right) - \left(1+\gamma^2\right)\left(\partial W/\partial I_2\right)\right\} + p \\
\sigma_{zz} &= 2\left\{\left(\partial W/\partial I_1\right) - \left(\partial W/\partial I_2\right)\right\} + p
\end{aligned} \qquad (6.1)$$

Thus it can be seen that a shear strain cannot be produced by a shear stress alone but

requires the application of a normal stress.

If we consider the case where there is no normal force acting perpendicular to the shear plane, $\sigma_{zz} = 0$, equation (1) reduces to:-

$$\sigma_{xy} = 2\gamma\left\{\left(\partial W/\partial I_1\right) + \left(\partial W/\partial I_2\right)\right\} \quad (6.2a)$$

$$\sigma_{xx} = 2\gamma^2\left(\partial W/\partial I_1\right) \quad (6.2b)$$

$$\sigma_{yy} = -2\gamma^2\left(\partial W/\partial I_2\right) \quad (6.2c)$$

$$\sigma_{yz} = \sigma_{zx} = \sigma_{zz} = 0 \quad (6.2d)$$

Thus there should be a normal force acting to hold together the bonded surfaces of the testpiece shown in Figure 6.1 the magnitude of which depends only on $\partial W/\partial I_2$. Therefore an experiment in simple shear, with measurement of the normal force, would provide a convenient alternative to the split pure shear technique as a means of characterizing the force-deformation behaviour of rubber.

6.2 **Experimental**

6.2.1 *Method*

Preliminary observations of the behaviour of double shear testpieces suggested that the change in height was in the reverse direction to that predicted by the above theory for simple shear. Thus the experimental arrangement, shown in Figure 6.1, allows for an applied force to prevent a height contraction. Two double shear testpieces (see Figure 4.1) were clamped in quadruple shear. Each disc of rubber in the double shear testpieces was nominally 6mm thick and 25mm in diameter. A 10kN piezo-electric load cell was bolted between the side-pieces of the jig as shown, such that the double shear testpieces were prevented from contracting normal to the shear direction, and the force required to maintain a constant height was measured. The jig was attached to a Zwick screw-loaded test machine. The extension of the testpieces was measured with an LVDT. The piezo-electric load cell is designed primarily for use in high speed experiments, owing to a time dependent decay in charge causing an apparent decay in the force reading. For this quasi-static test, the load cell was set up with the maximum

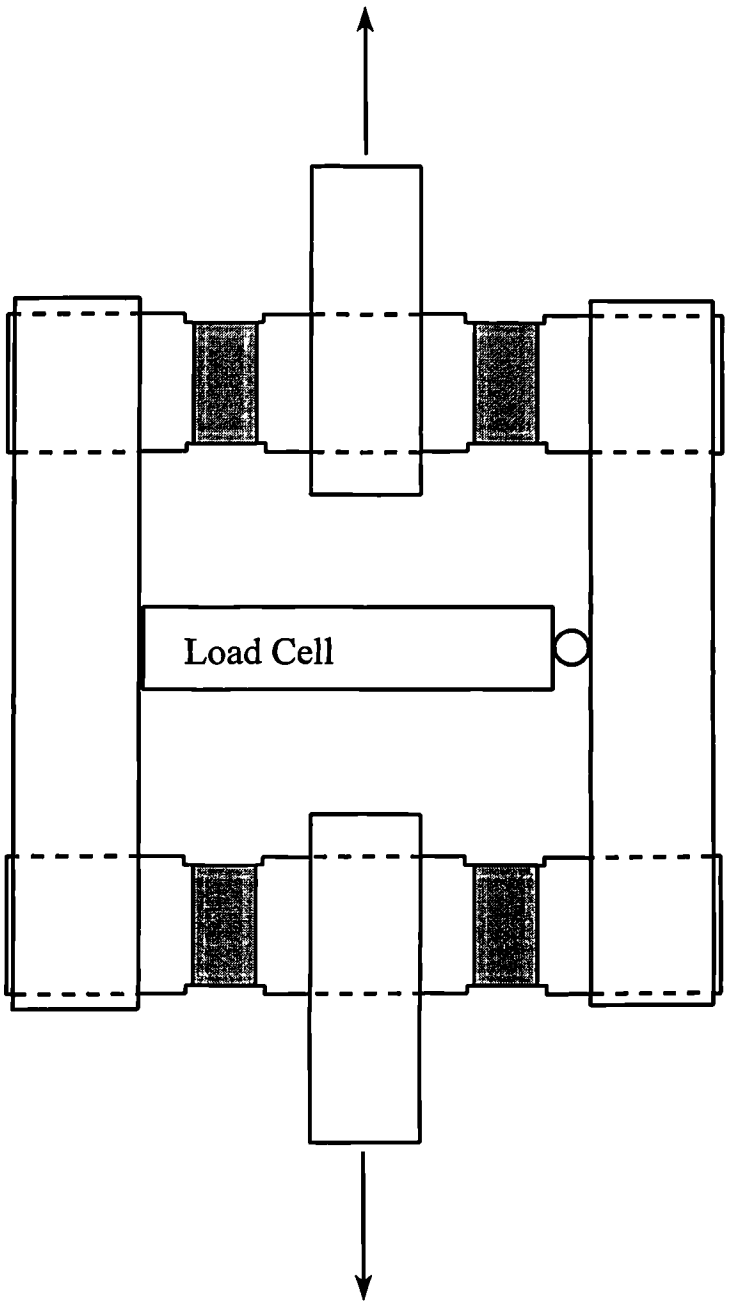

Figure 6.1 Experimental set-up for quadruple simple shear

time constant and the test machine was used to apply a shear displacement of 100mm/minute. Preliminary checks confirmed that the decay in the force reading was negligible over the duration of the experiment. The measurements were done on one unfilled rubber (EDS 19) and one filled rubber (EDS 16). The formulations are given in Table 3.2.

As an additional experiment, the piezo-electric load cell was removed so that the testpiece was permitted to contract in the y-direction. The contraction was measured with an LVDT mounted across the outside sections of the clamping jig. This experiment was done only on the unfilled rubber, EDS 19.

6.2.2 *Results*

The shear and normal stresses are shown in Figures 6.2 and 6.3 respectively. The normal (y-direction) contraction of the unconstrained testpiece is shown in Figure 6.4.

6.2.3 *Discussion*

For a neo-Hookean material, $\partial W/\partial I_2 = 0$, thus no normal force would be expected. For a material where $\partial W/\partial I_2$ is positive, equation (6.2c) suggests that, for the case of exact simple shear, a compressive normal force would be expected or alternatively the testpiece would expand in the y-direction. This is in contrast to the experimental results presented in Figures 6.3 and 6.4 where the force was tensile and the testpiece contracted. It is possible that this contradiction is due to the lack of constraint on the unbonded surfaces of the testpiece allowing it to deviate from true simple shear. A finite element analysis was carried out in order to identify the effect of these deviations from true simple shear on the measurement of the normal force.

6.3 Finite Element analysis of a block in simple shear

The three dimensional case of simple shear of a disc was simplified to two dimensions by considering the simple shear of a rectangle. It was assumed that the stress perpendicular to the shear plane, σ_{zz}, was zero. Thus the elements were in plane stress. The dimensions of the rectangle was chosen so that a block of square cross-section would have approximately the same cross-sectional area and height as one disc in the double shear testpiece.

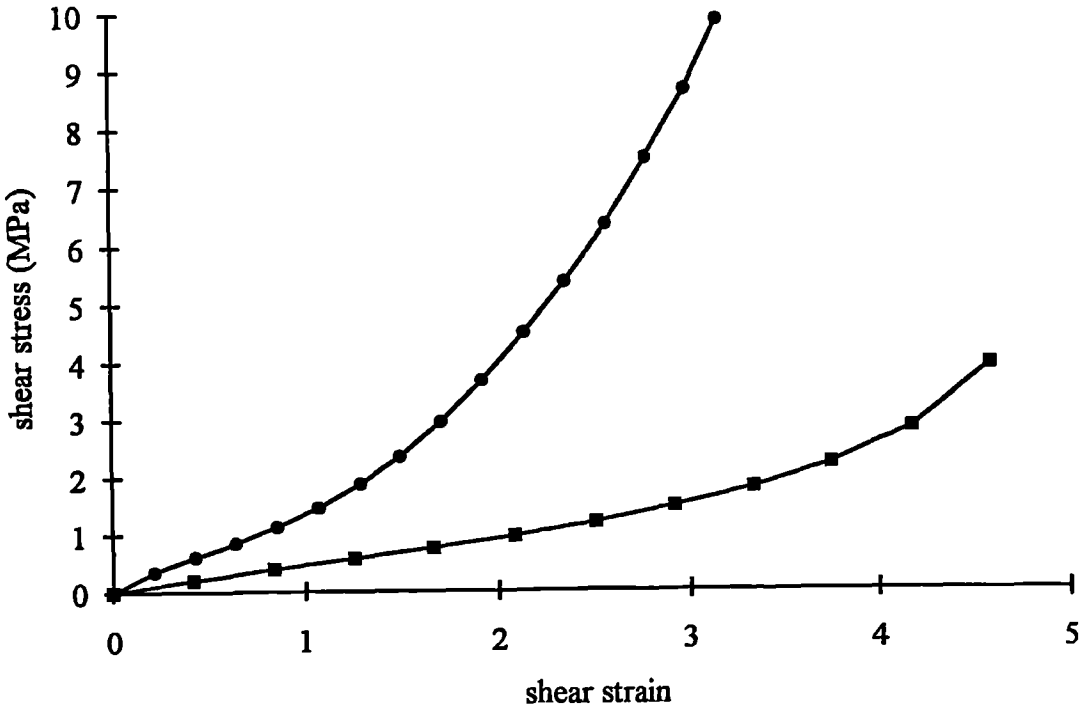

Figure 6.2 Shear stress in simple shear of natural rubber.
■unfilled (EDS19), ● filled (EDS16)

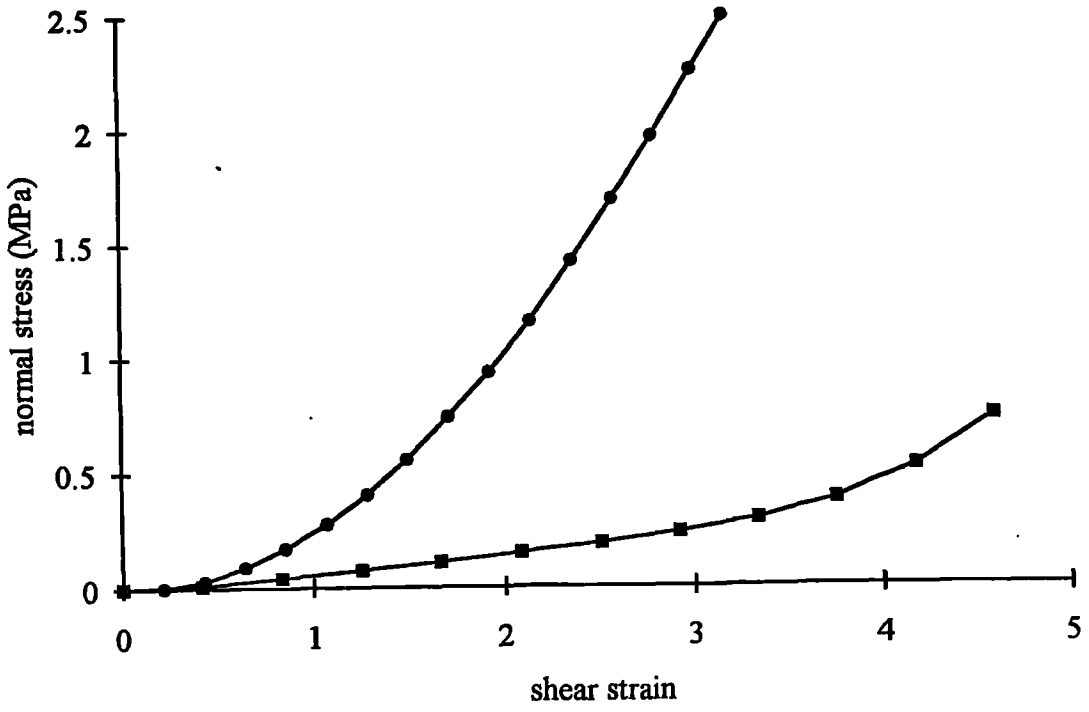

Figure 6.3 Normal stress in simple shear of natural rubber.
■unfilled (EDS19), ● filled (EDS16)

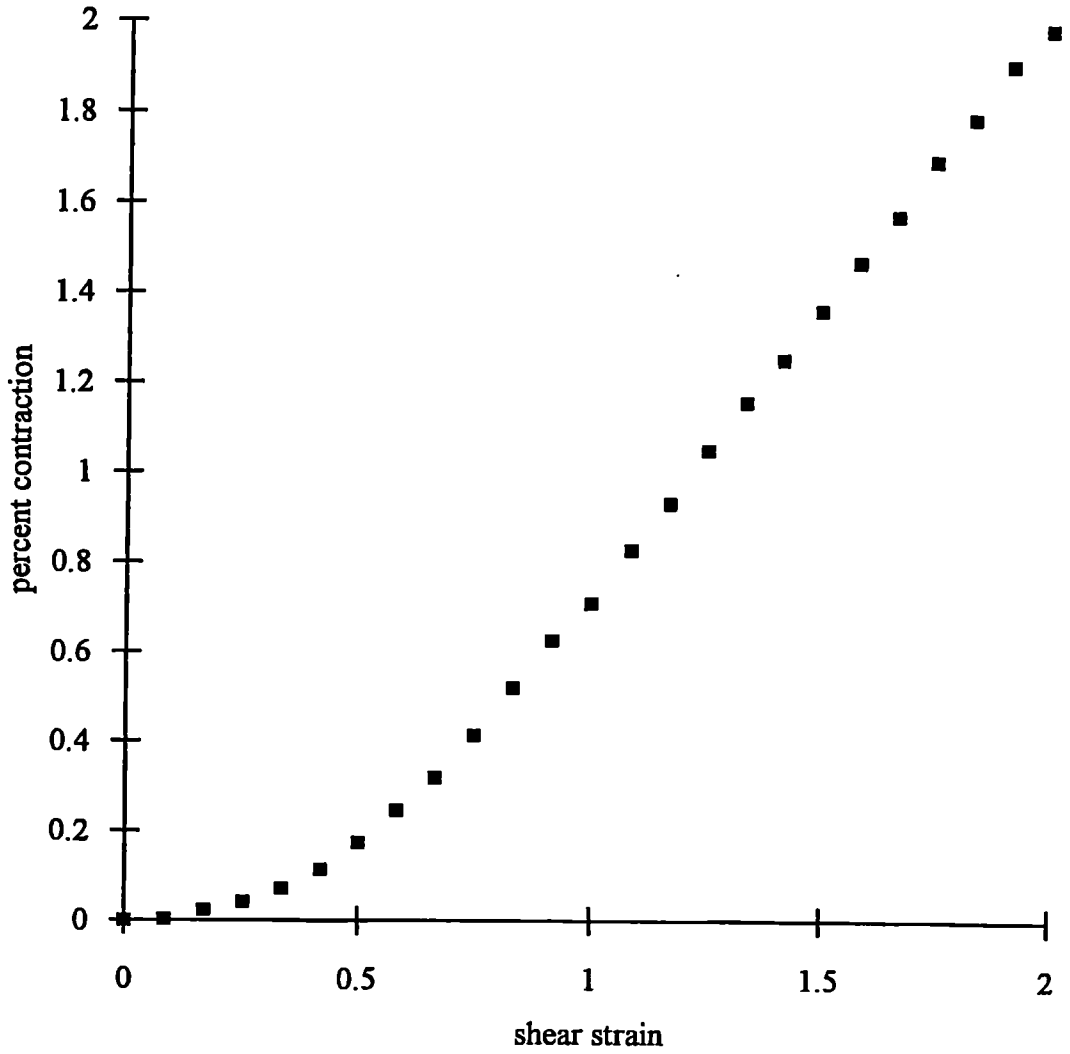

Figure 6.4 Contraction of a simple shear testpiece in the direction perpendicular to the shear plane for unfilled natural rubber (EDS19).

6.3.1 *Rectangle in true simple shear*

Some preliminary checks were carried out on a model where all the requirements for a true simple shear were satisfied. For this a rectangular mesh of height 6mm and width 22mm was used (given later as Figure 6.6a). A neo-Hookean material with a shear modulus of 0.5MPa was modelled in plane stress. Boundary conditions were set up such that no change in height in the y-direction of the rectangle was permitted. The nodes along the vertical edges of the rectangle were linked to the top and bottom corner nodes in such a way as to ensure these edges were constrained to remain straight. The mesh was deformed in 10 increments to a shear of 100% in the x-direction of the xy plane. The reaction forces on the nodes in the x and y direction of the deformed mesh are shown in Figure 6.5a. These may be resolved relative to the undeformed dimensions as shown in Figure 6.5b. The resolution of the forces was obtained by calculating the forces acting on the triangular regions of Figure 6.5a. These were then assumed to act across the vertical edges shown in Figure 6.5b. Owing to the linking technique, all reaction forces on the slanting edges in Figure 6.5a appear as reaction forces on the corner nodes. For example, from the resolved forces shown in Figure 6.5b, the stresses (in MPa) were calculated as:-

$$\sigma_{xy} = 8/16 = 0.5 = G\gamma$$
$$\sigma_{yx} = 3/6 = 0.5 = G\gamma$$
$$\sigma_{xx} = 3/6 = 0.5 = G\gamma^2$$
$$\sigma_{yy} = 0$$

Thus the forces are consistent with the theoretical predictions of equation 6.2.

An equivalent calculation for the same mesh deformed to a shear stress, σ_{xy}, of 0.5MPa was carried out. In this case, the reaction forces on the nodes were half their values for 100% shear strain and the cuboid used for resolution of the forces is 19×6, so that the xy shear force is 0.5×11×(19/22), the xx normal force is 0.5×11×(3/22) and the yx shear force is 0.5×3. Thus the stress calculations become:-

$$\sigma_{xy} = 4.75/19 = 0.25 = G\gamma$$
$$\sigma_{yx} = 1.5/6 = 0.25 = G\gamma$$
$$\sigma_{xx} = 0.75/6 = 0.125 = G\gamma^2$$
$$\sigma_{yy} = 0$$

also in agreement with equation 6.2.

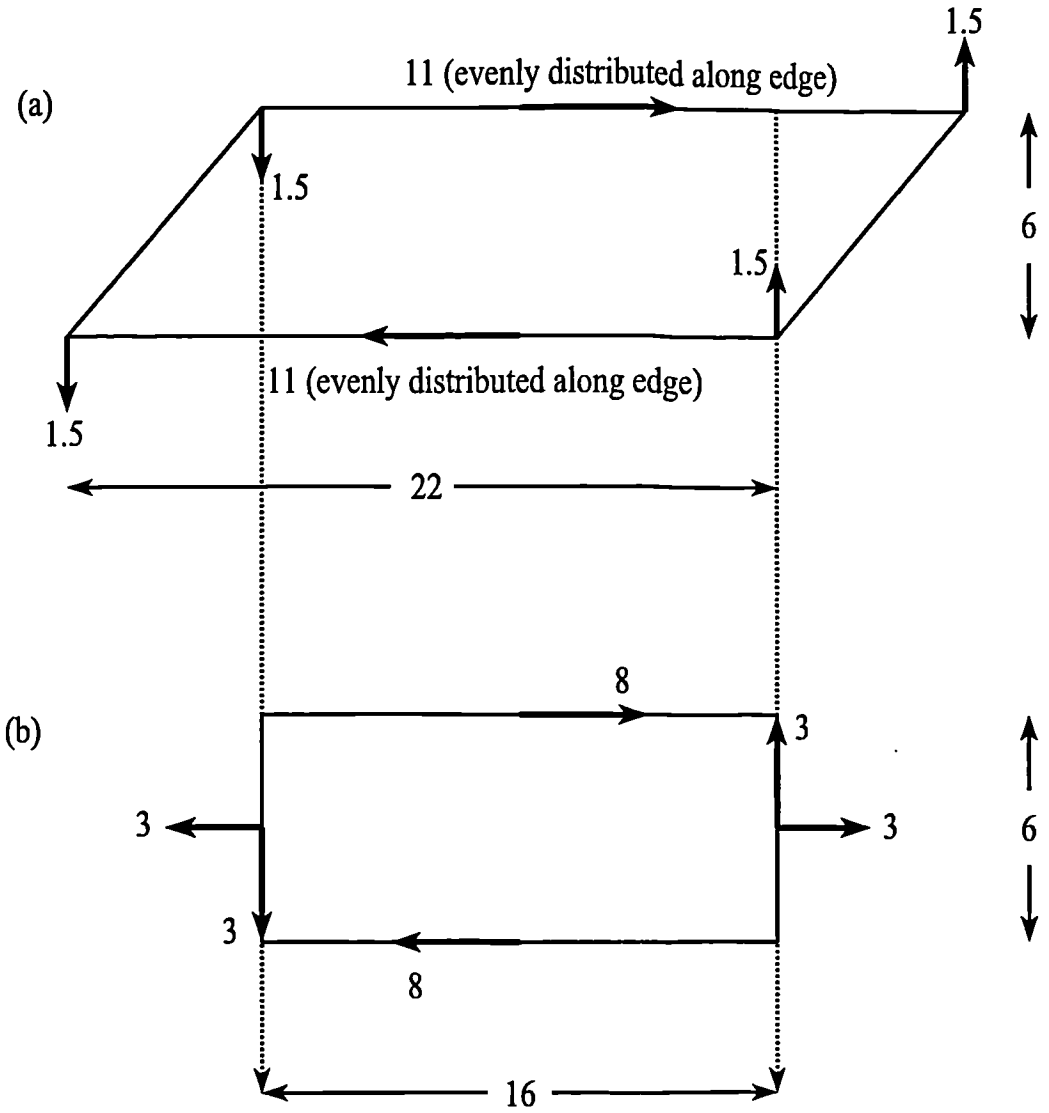

Figure 6.5 Resolution of forces (in N per mm thickness) for a rectangular mesh in plane stress under 100% shear strain. Mesh dimensions in mm. (a) deformed mesh, (b) relative to undeformed shape.

6.3.2 *Construction of the mesh*

For the investigation of the behaviour of a block where the sides were not constrained to remain straight, "approximate" simple shear, meshes with different element densities were compared.

The addition of extra elements in either the x or y directions, especially near the corners led to an increase in the normal force. For example, changing from the mesh shown in Figure 6.6a to the one shown in Figure 6.6b resulted in f_y changing by 18%, from 0.95 to 1.12 N per mm thickness for a neo-Hookean material under 100% shear strain. The corresponding changes in f_x (in N per mm thickness) were 10.42 to 10.38, ie. 0.5%. The large percentage change in f_y is not unexpected since, for a perfect simple shear, f_y = 0, thus small changes in the deformed shape are likely to lead to large percentage changes in f_y. The deformed blocks at 100% shear strain corresponding to the undeformed meshes shown in Figures 6.6 are shown in Figure 6.7.

6.3.3 *Shear and normal force for two materials in approximate simple shear*

In order to limit the errors associated with the mesh, a highly refined mesh (Figure 6.6b) was used for subsequent measurements. It was sheared in 20 increments to a shear strain of 2 under the following boundary conditions:-

(i) no change in height in the y-direction was permitted

(ii) the top edge was free to move in the y-direction.

Two materials were modelled:

(i) A neo-Hookean material with $C_{10} = 0.25$MPa

(ii) A Mooney material with $C_{10} = 0.225$MPa and $C_{01} = 0.025$MPa

The shear and normal forces were obtained by summing respectively the x and y reaction forces along the top edge of the mesh.

Figures 6.8 and 6.9 show the shear and normal force where no change in height was permitted as a function of γ^2 compared to the case of a block in true simple shear, as calculated from equation (6.2). A check that the finite element solution agreed with equation (6.2) was made by shearing the single element rectangle (Section 6.3.1) for

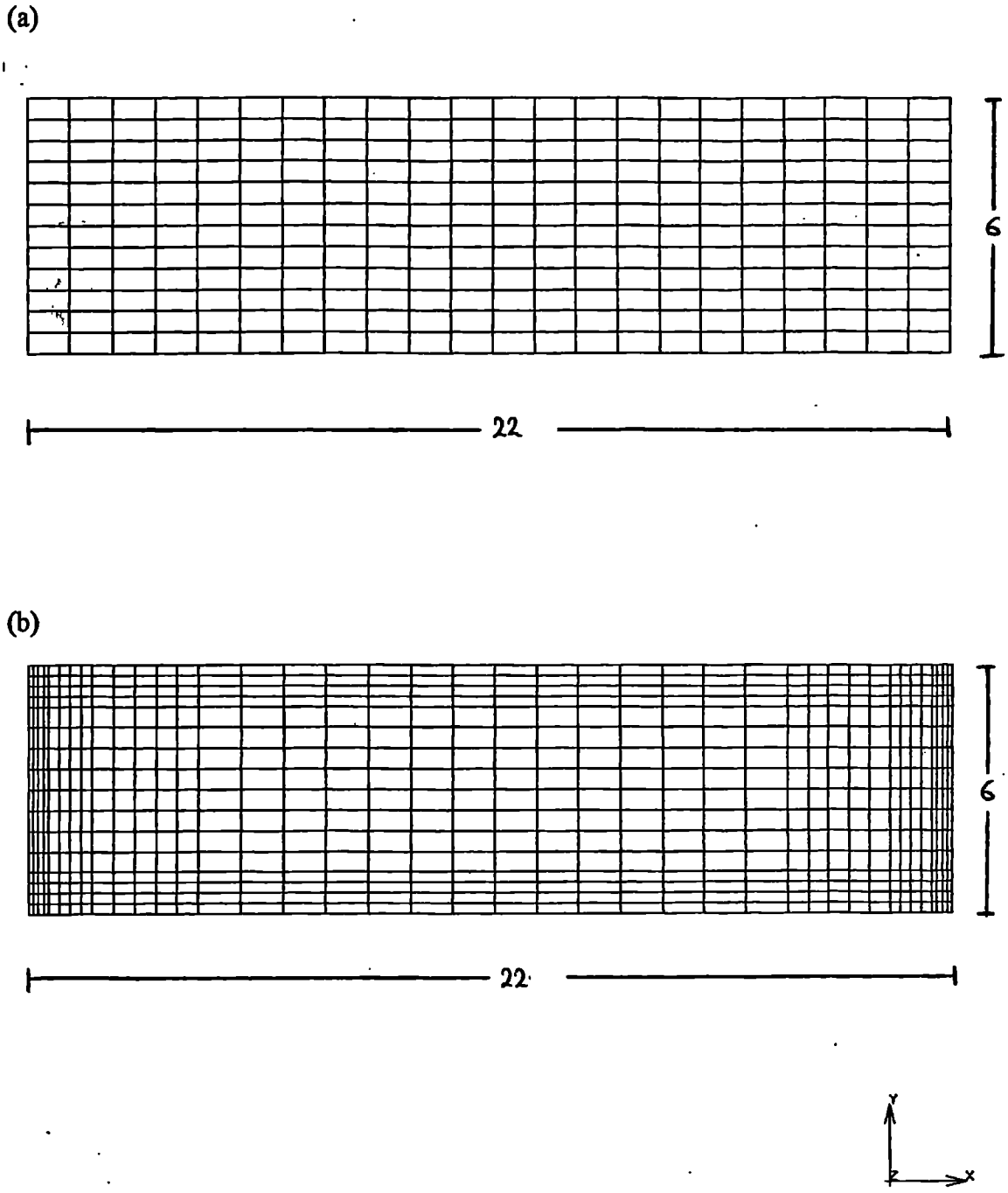

Figure 6.6 Undeformed (a) coarse and (b) refined two-dimensional rectangular mesh.

(a)

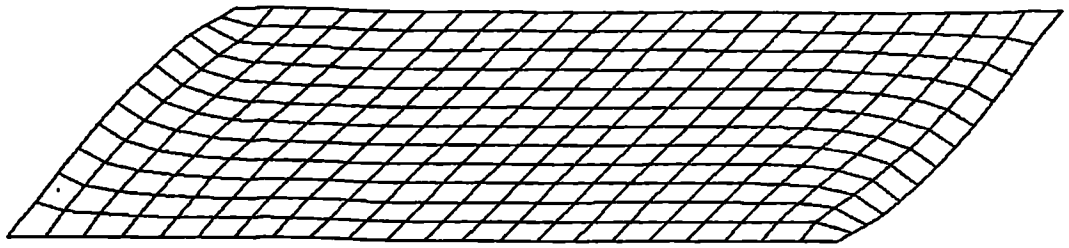

(b)

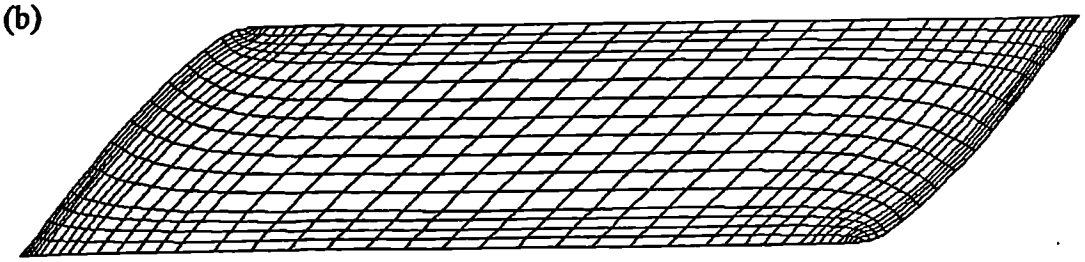

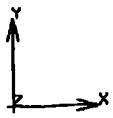

Figure 6.7 Deformed shape, under 100% shear strain for a neo-Hookean material, of a block meshed as shown in Figure 6.6.

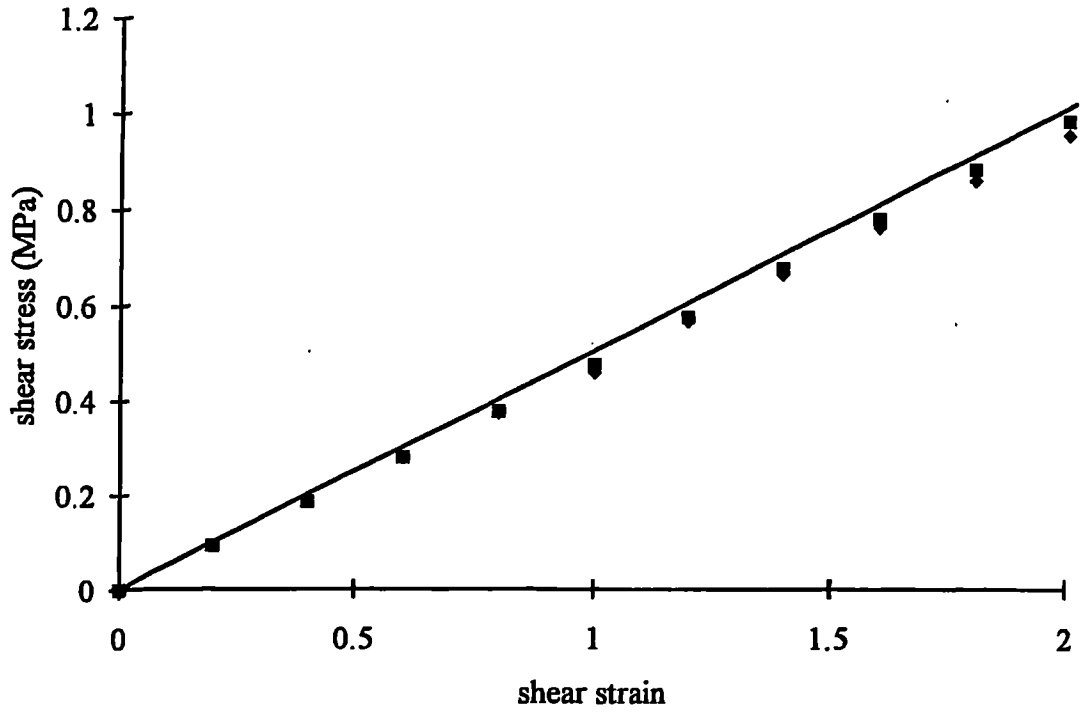

Figure 6.8 Finite element predictions of the shear stress of neo-Hookean and Mooney materials in exact and 'approximate' simple shear. ———— exact simple shear, ■ approximate simple shear for a Neo-Hookean material with G=0.5MPa, ◆ approximate simple shear for a Mooney material with C_{10}=0.225MPa and C_{01}=0.025MPa.

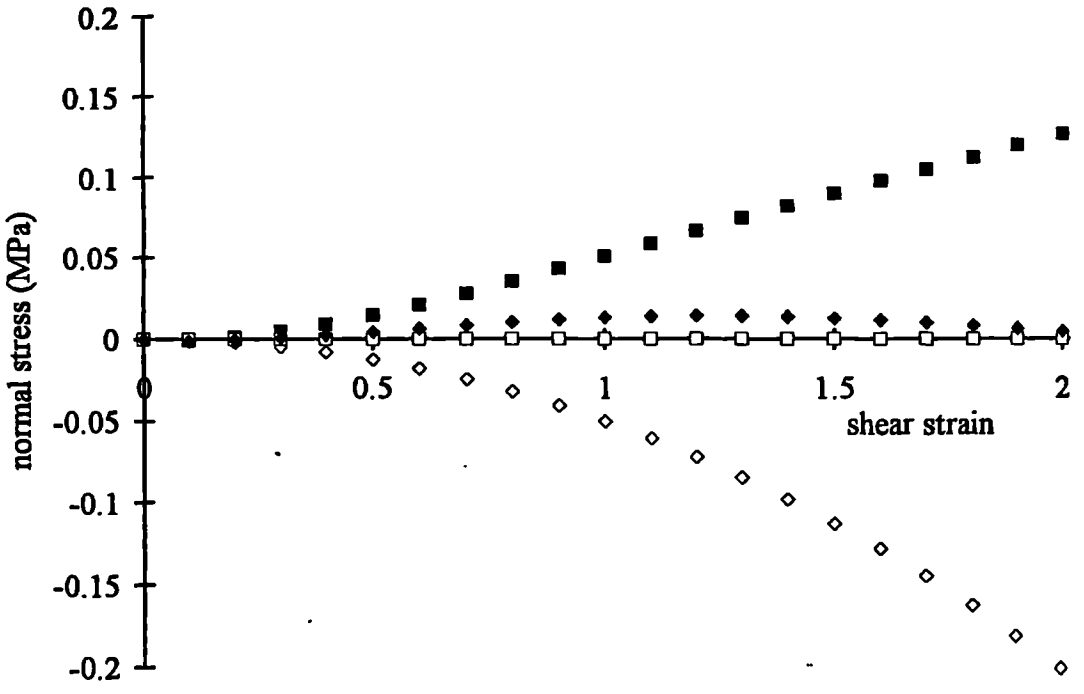

Figure 6.9 Finite element predictions of the normal stress of neo-Hookean and Mooney materials in exact and 'approximate' simple shear. □ exact and ■ approximate simple shear for a neo-Hookean material with G=0.5MPa, ◇ exact and ◆ approximate simple shear for a Mooney material with C_{10}=0.225MPa and C_{01}=0.025MPa.

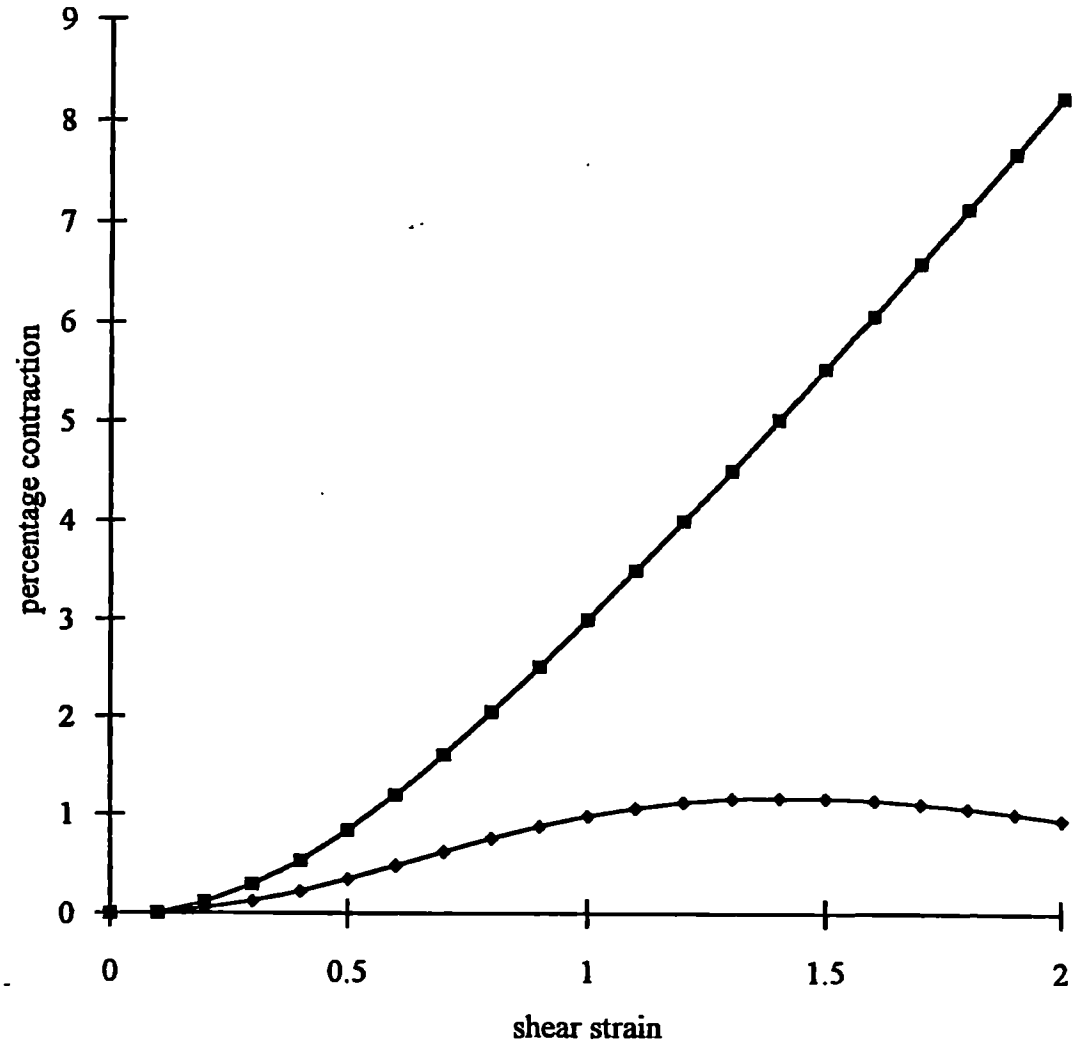

Figure 6.10 Finite element prediction of the normal contraction for an approximate simple shear deformation with permitted height change. ■ neo-Hookean material with G=0.5MPa, ◆ Mooney material with C_{10}=0.225MPa and C_{01}=0.025MPa.

both materials. Figure 6.10 shows the change in height for the case where this was permitted.

The shear stress (Figure 6.8) is reduced by about 5% by failure to constrain the sides. There is a large difference, however, in the size of the normal stress (Figure 6.9) between exact and approximate simple shear. The effect is so great that for the Mooney material, instead of a compressive force being required to prevent normal expansion, as required by equation (6.2), a tensile force is predicted. This behaviour is qualitatively in agreement with experimental observations (Section 6.2). The finite element prediction of a normal contraction (Figure 6.10), also observed experimentally, is consistent with the requirement for a tensile normal force to prevent such a change in the thickness of the block. The finite element results for the neo-Hookean material suggest that the normal force induced by the unconstrained boundary is tensile and roughly proportional to the shear strain, whereas the component due to a constant positive non-zero $\partial W/\partial I_2$ term is compressive and proportional to the shear strain squared (equation (6.2)). Thus where both of these effects are operative a maximum normal stress will occur at some intermediate strain.

Owing to the sensitivity of the normal force to details of the mesh geometry a more quantitative analysis of the behaviour was not attempted. The Mooney material modelled is known to be unrepresentative of real rubbers (see Section 1.2 and Chapter 3) but was selected to assess the effect of a non-zero $\partial W/\partial I_2$ term on the normal force in approximate simple shear. The results of the finite element analysis serve to show why the experimental measurement of the normal force in approximate simple shear deviates so markedly from the predictions of equation (6.2) for the idealized case.

6.3.4 *Effect of aspect ratio on the shear and normal forces*

Distortions from simple shear may be minimised by reducing the height to cross-sectional area ratio. The effect of changing the aspect ratio was modelled by reducing the mesh shown in Figure 6.6b to ones of ½ and ¼ of the original height (Figures 6.11a and 6.12a). These meshes were deformed in shear for a neo-Hookean material as described above. The deformed meshes at 100% shear strain are given in Table 6.1, where they are compared to the values expected for exact simple shear.

(a)

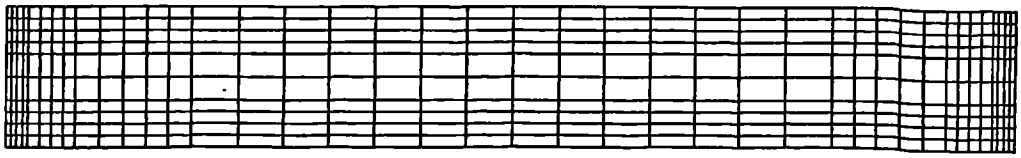

(b)

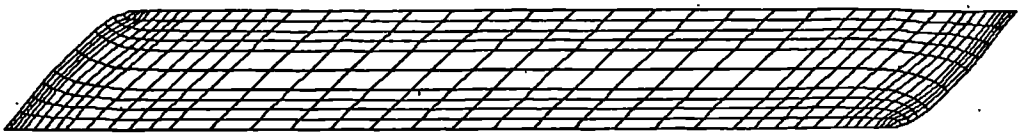

Figure 6.11 Finite element meshes for a rectangle in plane stress with a aspect ratio of 0.136. (a) undeformed mesh, (b) deformed to 100% shear strain.

(a)

(b)

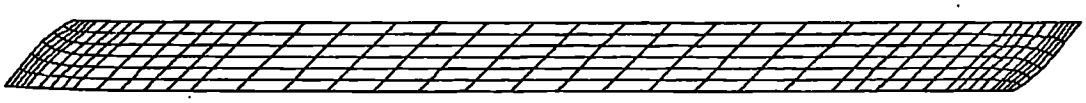

Figure 6.12 Finite element meshes for a rectangle in plane stress with a aspect ratio of 0.068. (a) undeformed mesh, (b) deformed to 100% shear strain.

Table 6.1 Finite element prediction of the effect of aspect ratio on shear and normal stresses in approximate simple shear (plane stress)								
height/width	shear stress (MPa)				normal stress (MPa)			
	strain(%)				strain(%)			
	50	100	150	200	50	100	150	200
0.273	0.231	0.472	0.720	0.971	0.0146	0.0508	0.0896	0.126
0.136	0.241	0.486	0.735	0.986	0.0071	0.0241	0.0426	0.0606
0.068	0.246	0.493	0.743	0.993	0.0034	0.0111	0.0197	0.0282
exact simple shear	0.25	0.5	0.75	1	0	0	0	0

Gregory and Muhr (1999) have derived an approximate equation for the reduction of apparent shear modulus due to the free edge based on an estimation of an effective area around the perimeter of the block not being in simple shear. The size of the effective area was obtained from a finite element analysis of a rectangular block in plane strain, from which an approximate expression for the ratio of actual to apparent shear modulus for short cylindrical blocks was found to be:

$$\frac{G}{G_{app}} \approx 1 + \frac{1}{9}\left(\frac{h}{r}\right) \qquad 0 < h/r < 1 \qquad (6.3a)$$

where h is the height and r the radius of the cylinder. Using the reasoning applied by Gregory and Muhr (1999) the corresponding expression for rectangular blocks in plane strain was calculated as:

$$\frac{G}{G_{app}} \approx 1 + \frac{2}{9}\left(\frac{h}{w}\right) \qquad 0 < 2h/w < 1 \qquad (6.3b)$$

where h is the height and w the width of the block.

Table 6.2 Comparison of finite element predictions of G/G_{app} with equation (6.3b)					
height/width	G/G_{app}				G/G_{app} (equation 6.3b)
	Strain(%)				
	50	100	150	200	
0.273	1.082	1.059	1.042	1.030	1.061
0.136	1.037	1.029	1.020	1.014	1.030
0.068	1.016	1.014	1.009	1.007	1.015

In Table 6.2, G/G_{app} has been calculated from the data in Table 6.1 and compared to the predictions of equations (6.3b). The results indicate that, as expected, the apparent shear and normal stresses approach the true values as the height/width ratio decreases and show reasonable quantitative agreement with equation (6.3b) . However, the results indicate a smaller error at high strains which is not taken into account in equation (6.3). This effect may be purely a consequence of the finite element size in the mesh preventing complete freedom of deformation along the free edges, more pronounced at large strains, resulting in an underestimate of G/G_{app}. Further work was carried out in order to establish whether the strain dependence of G_{app} was genuine or merely an artefact of the mesh size.

6.3.5 *Shear dependence of G_{app}*

In deriving equation (6.3), Gregory and Muhr (1999) used a fairly coarse mesh deformed to 10% in plane strain. As in the above analyses a neo-Hookean material with a shear modulus of 0.5MPa was modelled. In order to see whether the results in Table 6.2 are typical, the analyses were rerun using both of the meshes shown in Figure 6.7 for both the plane stress and plane strain cases. The results are given in Table 6.3

Table 6.3 Finite element predictions of the effect of shear strain on G/G_{app}

mesh	G/G_{app}			
	Strain(%)			
	50	100	150	200
coarse, plane stress	1.074	1.055	1.039	1.029
fine, plane stress	1.082	1.059	1.042	1.030
coarse, plane strain	1.051	1.031	1.017	1.009
fine, plane strain	1.055	1.033	1.018	1.009

In all cases, G/G_{app} is reduced as the shear strain increases. The size of the effect is not strongly dependent on the mesh density and is of a similar magnitude in both plane strain and plane stress. These observations suggest that G_{app} is, indeed, dependent on the shear strain and approaches G with increasing strain.

These results suggest that the approximation to simple shear achieved in the conventional technique for simple shear characterisation would lead to the apparent

shear modulus being about 8% less than the actual shear modulus at a shear strain of 50%. No correction was made to allow for this in the data reported in Chapter 4 and, surprisingly, the simple shear testpieces show no systematic trend to appear softer than those for other modes of deformation (see Figures 4.6, 4.14 and 4.15). This suggests either that the finite element analysis has overpredicted the apparent softening or that features such as differences in the vulcanising conditions or anisotropy in the testpiece stiffness caused discrepancies of a similar magnitude which have masked the edge effect in simple shear.

6.4 Conclusions

The magnitude of the normal force in a conventional experiment in simple shear depends on two things:

(i) The size and form of $\partial W/\partial I_2$ in accordance with the behaviour in exact simple shear.

(ii) The nature of the boundary conditions.

If, as is usual, the unbonded sides of the block are not constrained then the magnitudes of these two effects may be similar although the effect of the unconstrained edge could be reduced by using testpieces with a much higher shape factor (see equation (1.61)) Measurement of the normal force in simple shear using conventional double shear testpieces does not offer a useful way of quantifying $\partial W/\partial I_2$.

Since a positive $\partial W/\partial I_2$ and unconstrained edges of the testpiece have opposite effects on the normal force, the details which determine the magnitude of (i) and (ii) above will also determine the sign of the force.

The approximation to simple shear achieved in the conventional technique for simple shear characterisation will lead to the apparent shear modulus being about 2 to 8% less than the actual shear modulus.

CHAPTER 7

Combined torsion and extension of a cylinder

7.1 Introduction

In Chapters 3 and 4 the behaviour of a series of rubbers was described and discussed in terms of a strain energy function, W. It is well known, however, that black filled rubbers in particular exhibit significant departures from elastic behaviour. These have been reviewed in Section 1.4. The experiment described in this chapter involves the combined torsion and extension of a cylinder. It was devised to show the limitations of the concept of a strain energy function as a way of describing the force-deformation behaviour of filled rubber.

7.2 Theory

Rivlin (1949; with Saunders, 1951) has shown that a particular relationship between the applied normal force and the torsional couple at small angles of twist will hold for any material whose behaviour is describable by a strain energy function W (I_1, I_2), regardless of the form of W.

Consider an unstrained solid rubber cylinder of radius a and height ℓ_o (Figure 7.1). The cylinder is stretched to a length $\lambda\ell_o$, and the top surface is rotated by an angle $\theta = \psi\lambda\ell_o$ relative to the bottom surface. The forces required to maintain this state of strain are a couple, M, and a normal force, N, given by (Rivlin, 1949):

$$M = 4\pi\psi\int_o^a r^3\left(\frac{\partial W}{\partial I_1} + \frac{1}{\lambda}\frac{\partial W}{\partial I_2}\right)dr \qquad (7.1)$$

$$N = 4\pi\left(\lambda - \frac{1}{\lambda^2}\right)\int_o^a r\left(\frac{\partial W}{\partial I_1} + \frac{1}{\lambda}\frac{\partial W}{\partial I_2}\right)dr - 2\pi\psi^2\int_o^a r^3\left(\frac{\partial W}{\partial I_1} + \frac{2}{\lambda}\frac{\partial W}{\partial I_2}\right)dr \qquad (7.2)$$

where the strain invariants are given by:-

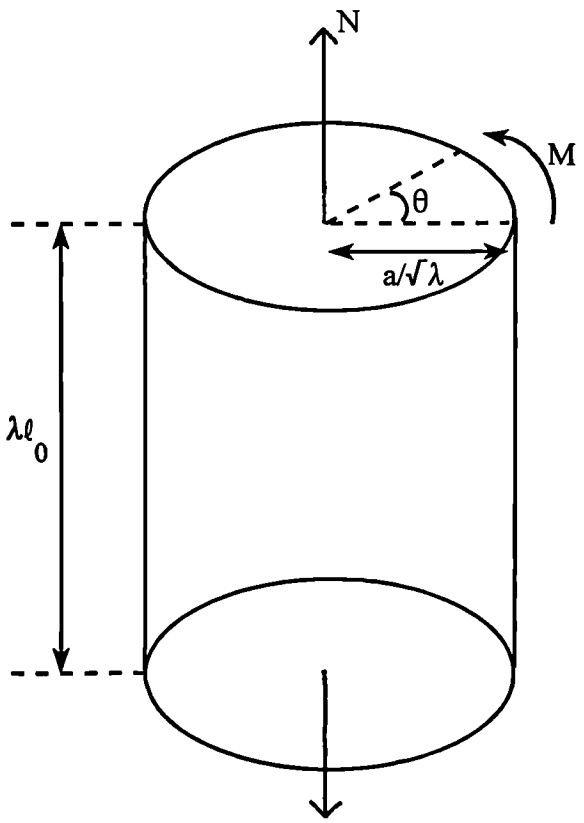

Figure 7.1 Cylinder subjected to combined torsion and extension.

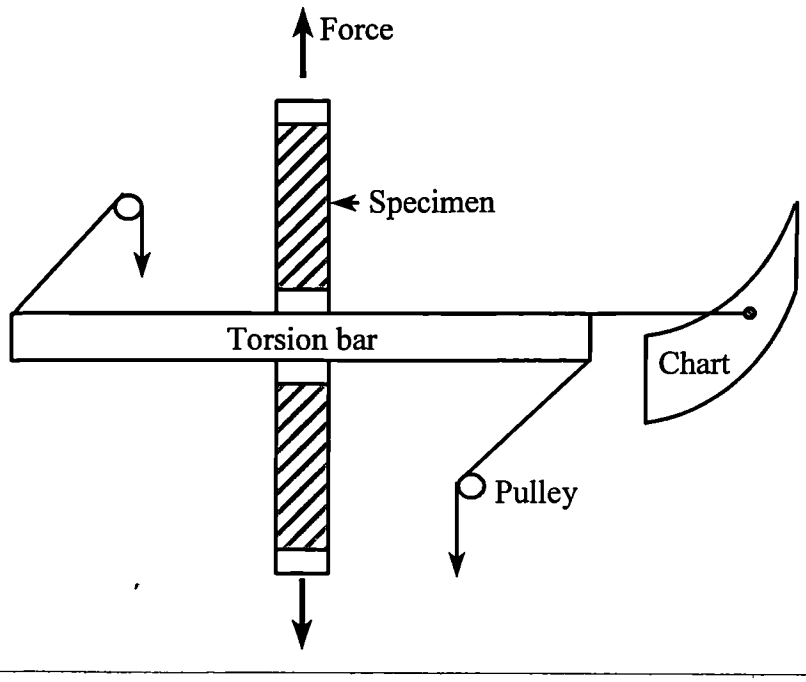

Figure 7.2 Schematic diagram of experimental arrangement for combined torsion and extension of a pair of cylinders.

$$I_1 = \lambda^2 + \frac{2}{\lambda} + \lambda\psi^2 r^2$$
$$I_2 = 2\lambda + \frac{1}{\lambda^2} + \psi^2 r^2 \qquad (7.3)$$

As $\psi \to 0$, terms in ψ^2 become negligible, the strain invariants reduce to $I_1 = \lambda^2 + 2/\lambda$ and $I_2 = 2\lambda + 1/\lambda^2$, and are therefore independent of r. Thus, in equations (7.1) and (7.2), $\partial W/\partial I_1$ and $\partial W/\partial I_2$ may be treated as constants for integration with respect to r. Also, the second term in equation (7.2) vanishes. Thus, integration of equations (7.1) and (7.2) yields:-

$$M_{\psi=0} = \pi\psi a^4\left(\frac{\partial W}{\partial I_1} + \frac{1}{\lambda}\frac{\partial W}{\partial I_2}\right) \qquad (7.4)$$

$$N_{\psi=0} = 2\pi a^2\left(\lambda - \frac{1}{\lambda^2}\right)\left(\frac{\partial W}{\partial I_1} + \frac{1}{\lambda}\frac{\partial W}{\partial I_2}\right) \qquad (7.5)$$

hence:-

$$\frac{N_{\psi=0}}{2(\lambda - \lambda^{-2})} = \frac{M_{\psi=0}}{\psi a^2} \qquad (7.6)$$

Expressing the normal force in terms of a nominal stress

$$s_N = \frac{N}{\pi a^2} \qquad (7.7)$$

gives

$$\frac{s_{N\,\psi=0}}{2(\lambda - \lambda^{-2})} = \frac{M_{\psi=0}}{\psi\pi a^4} \qquad (7.8)$$

Equations (7.6) and (7.8) are independent of the form of W. Thus a comparison of experiment with the predictions of equation (7.8) provides an indication of whether the material may be described by a strain energy function.

7.3 Experimental method

Cylinders of the unfilled rubber, EDS19, and the filled rubber, EDS16, were compression moulded. Details of formulations are given in Table 3.2. The height of each cylinder was nominally 128mm and the diameter 25mm. Threaded end-pieces were bonded to the cylinders during moulding to facilitate clamping.

A pair of identical cylinders was bolted to a Zwick screw-driven test machine with a 10kN load cell. A light aluminium torsion bar was bolted between the cylinders (Figure 7.2). A torsional couple was applied by weights hung from threads attached to each end of the torsion bar which passed over pulleys. The pulleys were rigidly clamped to stands and their height was adjusted for each extension of the cylinders so that they remained level with the torsion bar. The torsion bar had curved ends so that, for the small torsional angles required for the experiment, the strings were always pulling tangentially.

The uniaxial extension of the cylinders was taken to be the crosshead displacement. The angle of twist was measured from the movement of a light pointer, attached to the torsion bar, relative to a fixed curved chart. For all but the first experiment on EDS19 two such pointers were set up - one at each end of the torsion bar.

The extension of the cylinders was increased in stages. After each extension the normal (axial) load, N, and the displacement were recorded. A series of small increasing weights were applied to generate the torsional load and the angle of twist was recorded after each addition. Finally, the normal load was remeasured. For EDS16, for which some stress relaxation was likely to occur over the duration of the measurements, the scatter in the measurements was minimised by allowing two minutes before beginning the torsional measurements following each application of the normal load at a rate of 100mm per minute. The time taken to obtain each set of torsion measurements ranged from 4½ to 7½ minutes. The initial and final normal force measurements were recorded.

The experiment was done twice on a single pair of previously unstrained testpieces of

EDS19. Three days elapsed between these tests. Following the first experiment on EDS16 it became apparent that data at lower normal extensions was required so the experiment was repeated on a new pair of cylinders.

7.4 Results

The normal loads and angular displacements as a function of extension are given in Tables 7.1 to 7.4.

Table 7.1: EDS19 - virgin testpiece
testpiece dimensions: average length of one cylinder=126.8mm; diameter=24.6mm

total extension (mm)	normal load (N)		angular displacement (mm) for following torques (grams force on torque arm)									
	initial	final	0	5	10	15	20	30	40	50	70	90
0	0	0	0	11	23	37	51	78	106	133	180	219
20	61.9		0	14	30	45	60	91	121	149	197	
40	111.4	110.0	0	16	34	51	68	102	134	163	211	
60	152.7	151.5	0	18	37	57	75	112	146	176		
90	205.2	203.7	0	21	43	64	86	127	165	196		
130.2	261.0	258.6	0	24	49	75	99	145	185	217		
170.6	307.4	305.8	0	29	58	86	114	165	206			
209.9	348.2	346.2	0	31	64	95	127	170	214			
250	386.5	384.7	0	35	71	105	139	194				
290	423.4	421.4	0	40	80	117	150	208				
330.4	462.2	458.9	0	42	84	123	161	206				
370.3	498.6	493.9	0	38	93	133	168	228				
410.2	531	529	0	51	99	144	184					
450.1	573	569	0	50	102	149	189					
490	613	607	0	54	106	155	195					

Table 7.2: EDS19 - second loading cycle

total extension (mm)	normal load (N)		angular displacement (mm) for following torques (grams force on torque arm)			
	initial	final	0	5	10	20
0	0	0	0	15, 14	30, 29	60, 59
128.4	261.5	257.7	0	27, 25	54, 50	103, 105
200	332.4	330.2	0	34, 33	67, 66	
300	426.5	424.7	0	43, 41	86, 82	
400	520	517	0	51, 49	102, 98	
500.3	616	613	0	57, 54	118, 121	
600	728	715	0	62, 58	125, 120	
700	839	826	0	66, 61	130, 125	

Table 7.3: EDS16 - virgin testpiece
testpiece dimensions: average length of each cylinder=129mm; diameter=25.1mm

total extension (mm)	normal load (N)		angular displacement (mm) for following torques (grams force on torque arm)							
	initial	final	0	10	20	30	50	70	80	0 (end)
0	0	0	0		7,8		21,22		37,38	3,4
25	220	215	0		14,13		35,35		74,74	14,14
50	345.5	340.5	0		15,17		45,44	65,66		7,8
75	445.5	438.5	0		20,20		54,54		79,79	12,10
100	534	526	0		24,23		62,60			9,8
125	621	613	0		27,26		67,66			7,7
150	708	697	0	14,13	32,29	44,43				7,9
175	804	788	0	14,15	30,29	44,44				5,7
200	906	889	0	16,15	33,30	47,47				6,7
225	1019	998	0	15,16	31,31	47,49				6,7
250	1146	1123	0	12,14	30,30	45,46				5,5
300	1424	1384	0	13,16	30,32	45,48				5,6
350	1732	1681	0	15,14	35,33	48,47				8,7
400	2095	2021	0	16,15	31,30	48,45				9,7
450	2493	2419	0	14,13	29,28	44,43				6,5
500	2919	2826	0	11,13	26,27	41,41				5,5
550	3356	3256	0	13,13	28,27	41,40				6,5
600	3788	3690	0	11,12	27,26	41,39				6,5

Table 7.4: EDS16 - virgin testpiece
testpiece dimensions of each cylinder: average length=129mm; diameter=25.1mm

total extension (mm)	normal load (N)		angular displacement (mm) for following torques (grams force on torque arm)				
	initial	final	0	20	50	70	0(end)
0.0	0	0	0	8, 7	23, 21	33,31	2, 3
2.0	32.0	30.0	0	7, 8	22, 23	32, 34	4, 2
4.0	53.9	51.8	0	8, 9	23, 26	35, 38	4, 5
6.1	74.0	72.0	0	9, 10	24, 27	37, 40	5, 6
9.9	105.7	103.1	0	10, 11	28, 29	42, 43	7, 7
13.2	130.7	128.2	0	9, 11	30, 32	44, 46	7, 6
17.1	157.8	155.0	0	11, 10	31, 31	46, 48	7, 5
22.0	188.9	185.9	0	11, 12	33, 34	49, 52	7, 7
27.0	217.4	214.2	0	13, 14	36, 38	53, 56	8, 8
35.1	260.3	256.2	0	13, 14	38, 38	58, 60	8, 8
42.1	293.2	289.0	0	15, 16	41, 42	64, 66	10, 9
50.1	328.2	324.0	0	16, 16	45, 45	69, 69	11, 8
60.0	367.8	363.8	0	16, 18	47, 50	71, 75	8, 10

The two values given for angular displacement represent readings made on the chart at each end of the torque arm. The distances of the charts from the centre of the torque arm were 348mm and 333mm respectively.

For a torsion bar of length 2z the torsional couple, M, acting on one cylinder is given by

$$M = Qz \tag{7.9}$$

where Q is the weight applied to each end of the torsion bar. The angle of twist per unit length, ψ, is given by

$$\psi = \frac{b}{d\lambda\ell_0} \tag{7.10}$$

where d is the distance from the centre of the torsion bar to the chart and b is the arc-length of the displacement of the pointer.

M was plotted as a function of ψ for each extension ratio. Typical plots are shown in Figure 7.3. In all cases a good straight line passing through the origin was seen for small ψ. M/ψ was obtained from the slope of these lines. s_N was calculated from (7.7) using the average of the initial and final normal forces given in the Tables. $s_N/2(\lambda - \lambda^{-2})$ and $M/\psi\pi a^4$ were plotted against λ in Figure 7.4 to assess the validity of equation (7.8). As a further comparison, the ratio $2M(\lambda - \lambda^{-2})/s_N\psi\pi a^4$ was plotted in Figure 7.5 and compared to the theoretical prediction of equation (7.8), that is unity.

7.5 Discussion

For the unfilled rubber, EDS19, the experimental data agree adequately with the theoretical prediction from equation (7.8) thus supporting the use of a strain energy function as a way of describing the behaviour of rubber. However, the behaviour of the black-filled rubber, EDS16, shows a clear deviation from the theoretical predictions, with the torsional couple larger than the theory predicts from the stiffness in tension. This behaviour is analogous to the behaviour often observed during dynamic tests for small cycles superimposed upon larger strains where the small strain stiffness is larger than that obtained from the underlying large strain. That is, the dynamic to static ratio as defined in Section 1.4.3 is greater than one (Gregory, 1984, 1985). In the case of the present experiment, the torsional stiffness could be interpreted as the small strain stiffness, superimposed upon a larger tensile strain, for which the stiffness is lower.

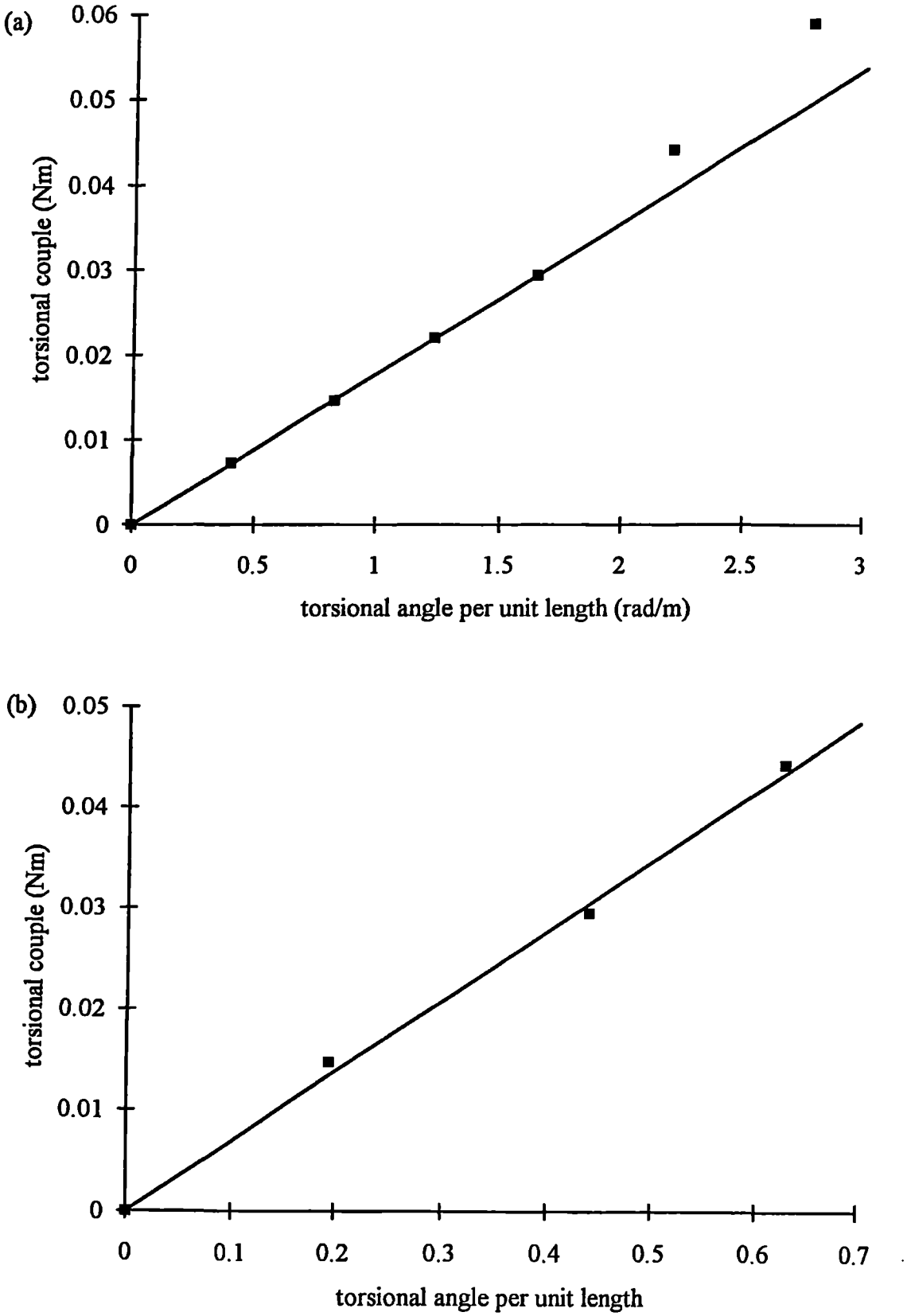

Figure 7.3 Plots relating the torsional couple, M, to the torsional angle per unit length at small angles for the combined torsion and extension of a cylinder. (a) unfilled natural rubber (EDS19) under 83% uniaxial strain, (b) filled natural rubber (EDS16) under 58% uniaxial strain.

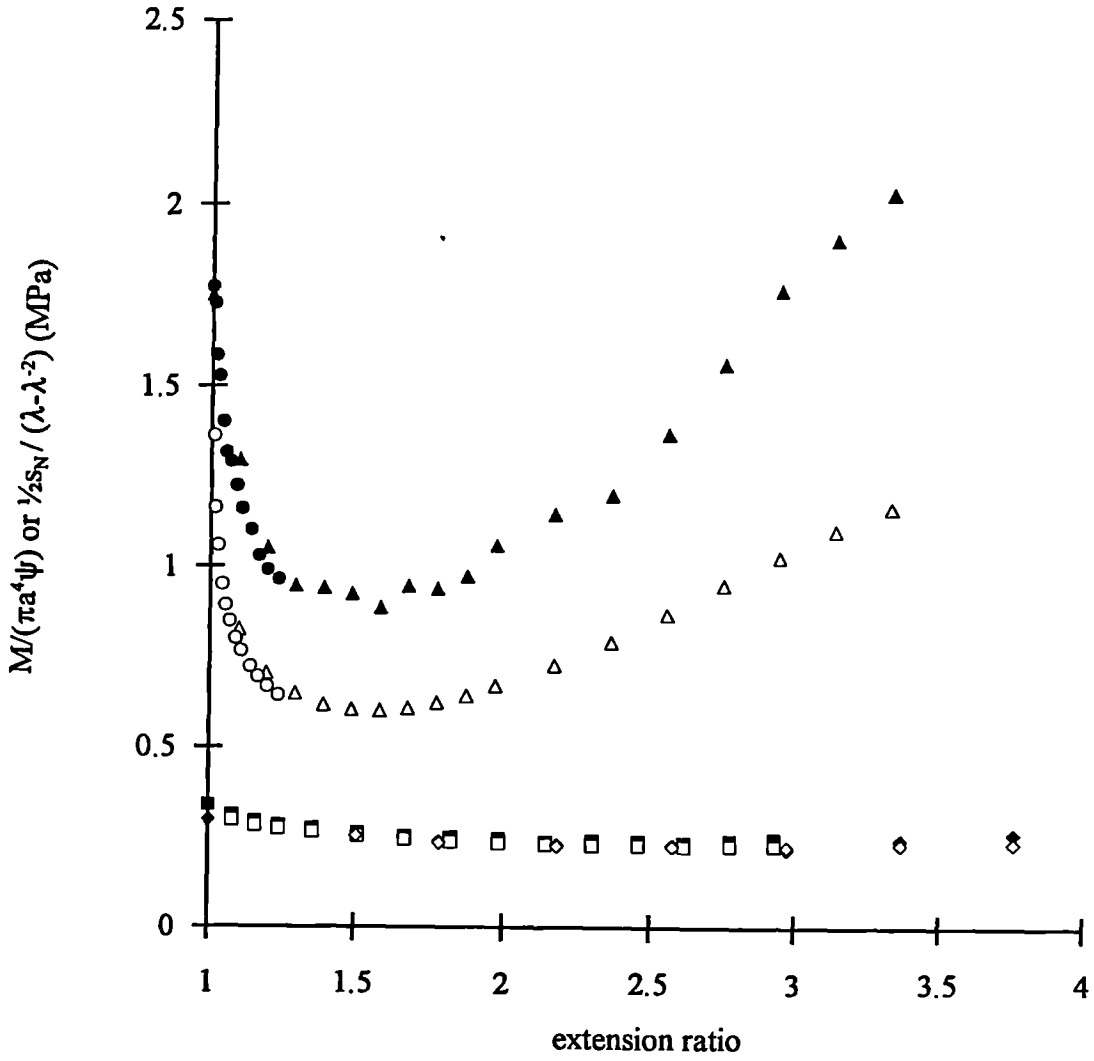

Figure 7.4 Plots of $M/(\psi\pi a^4)$ (filled symbols) and $s_N/(2(\lambda-\lambda^{-2}))$ (open symbols) against the extension ratio, λ for the combined torsion and extension of a cylinder.
■ ◆ unfilled natural rubber EDS19, ▲ ● filled natural rubber EDS16.
Two experiments in each case.

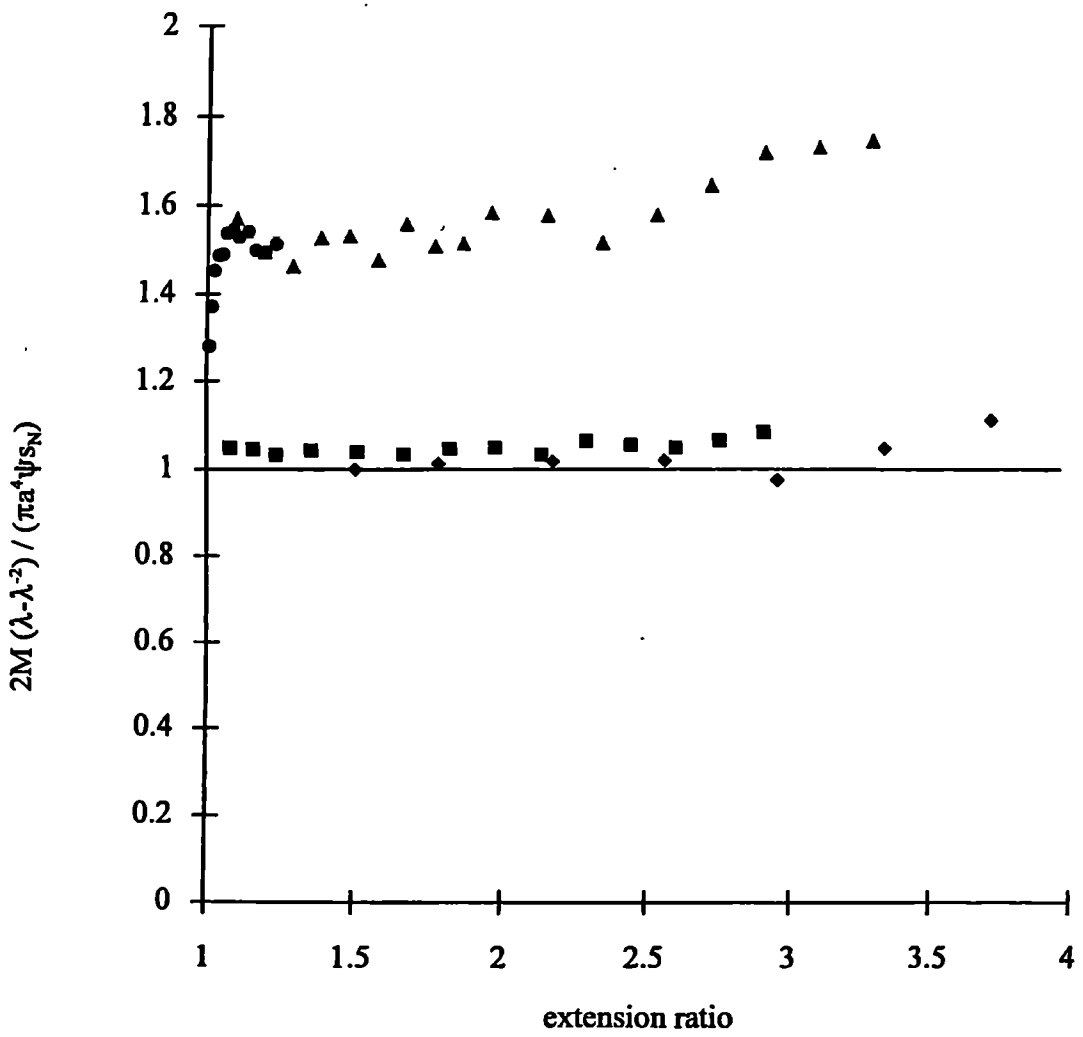

Figure 7.5 Comparison of theory and experiment for the combined torsion and extension of a cylinder. ———— theoretical from equation (7.6), ■ ◆ unfilled natural rubber EDS19, ▲ ● filled natural rubber EDS16. Two experiments in each case.

Figure 7.4 shows that for the unfilled rubber the stiffness in both tension and torsion falls slightly with increasing extension. The stiffness of the filled rubber, however, falls steeply and then rises more slowly. For the normal force term, where the extension was rising, this is the shape expected from the stress-strain behaviour in uniaxial tension. However, it is less obvious what the effect of a tensile strain on the small angle torsional stiffness would be, and it is interesting to see that the shape of the curve is similar, leading to a roughly constant ratio at moderate strains, shown more clearly in Figure 7.5. For the filled rubber both the normal stiffness and the torsional stiffness decrease very rapidly as λ increases for small values of λ. It can be seen from Figure 7.5, however, that the change in the normal stiffness is more pronounced, thus the behaviour of the filled rubber approaches the theoretical predictions close to $\lambda = 1$. This is to be expected in view of the fact that at $\lambda = 1$, both measurements are small strain measurements. It supports the hypothesis that the disagreement with theory is a consequence of the high stiffness for small deformations, which is observed to occur whenever there is a change in the direction of straining, regardless of whether the overall state of strain is large or small.

These results are a clear indication of the inadequacy of the concept of an elastic strain energy function for describing the stress-strain behaviour of filled rubbers. However, a strain energy function may still be useful provided its limitations are recognised and it is not applied in circumstances where inelastic effects are likely to be large. For example, in Chapters 3 and 4, a strain energy function was shown to describe adequately the first cycle quasistatic deformation of filled rubbers. However, its application to finite element modelling of components under dynamic strains of varying magnitude is likely to be problematic.

7.6 Conclusions

The measurement of small torsional couples superimposed upon uniaxial extensions of filled and unfilled rubbers has shown that the use of a strain energy function inadequately describes the behaviour of filled rubbers. Discrepancies of the order of 40% were found between experimental measurement of the stiffness compared with predictions from large strain elasticity theory.

CHAPTER 8

Use of a strain energy function to model inelastic effects

8.1 Introduction

In Chapters 3 and 4 a study of the first cycle force-deformation behaviour of filled and unfilled natural rubber was made and described in terms of a strain energy function, W. In Chapter 5 this treatment was extended to some synthetic rubbers. However, as discussed in Chapter 7, filled natural rubber and synthetic rubbers which do not behave as perfectly elastic materials cannot be described by a strain energy function. One of the most obvious features of imperfect elasticity is the significant hysteresis of many filled rubbers (see Section 1.4.1). An evaluation of the hysteresis of the rubbers used in this work is presented in Section 8.2.

Nevertheless, the concept of the strain energy function has been retained as a means of describing in a restricted way some inelastic features of rubber. Kawabata (1973) examined the relative rates of decay of stress in two directions under various biaxial strains for unfilled peroxide cured rubbers. He found that $\partial W/\partial I_1$ and $\partial W/\partial I_2$ decayed at the same rate, relative to the magnitudes of the two stresses. This relative rate was independent of the magnitudes of I_1 and I_2. He described this behaviour in terms of a time dependent strain energy function, W_t, written in "separable" form as

$$W_t = W_t(I_1, I_2) = \Psi(t)\, W(I_1, I_2) \qquad (8.1)$$

Thus the behaviour for a general strain may be determined after any time t from a characterization of the first cycle stress-strain behaviour, scaled with a suitable function for $\Psi(t)$. More recently, Ogden and Roxburgh (1999) have proposed a concept of pseudo-elasticity in their model of Mullins' effect. On the first cycle loading curve they model the behaviour with a strain energy function. In subsequent cycles this function is appropriately modified by another function to take account of the softening.

The split pure shear technique provides a method of measuring the stress reduction due to stress relaxation or Mullins' effect in two directions. It is therefore a potentially valuable method of assessing the validity of equations such as (8.1) or the predictions

of models such as that of Ogden and Roxburgh (1999). In this Chapter filled silicone rubber is used to investigate Mullins' effect and assess the usefulness of Ogden and Roxburghs' model. The silicone rubber was chosen as being particularly suitable for these experiments as it exhibits a very large Mullins' effect (Muhr et al, 1999). Also, the stress relaxation under both static and cyclic loading conditions for some filled and unfilled natural rubbers is measured using the split pure shear technique in order to assess the applicability of equation (8.1).

8.2 Comparison of hysteresis for rubbers investigated in this work

8.2.1 *Experimental*

The rubbers studied were the natural rubbers, EDS19 (unfilled) and EDS16 (filled), the formulations of which are given in Table 3.2, the nitrile, polyurethane and silicone rubbers investigated in Chapter 5, and two other unfilled natural rubbers used for stress relaxation measurements (see Section 8.4, Table 8.1). These had lower crosslink densities than EDS19. One was peroxide cured and thus contained predominantly direct carbon-carbon crosslinks rather than the more usual mono- and poly-sulphidic ones of sulphur vulcanizates.

A strip of each rubber, with a nominal length of 150mm, width of 5mm and thickness between 1 and 2mm, was measured and clamped along the short edges in an Instron tensile test machine, fitted with a 100N load cell. It was subjected to two cycles in uniaxial extension, the first to 100% strain and the second to 200% strain. The crosshead speed was equivalent to a strain of 0.04/s. The force extension curves for both loading and retraction were plotted directly, from which plots of nominal stress against strain were obtained. These are shown in Figure 8.1.

8.2.2 *Discussion*

The greatest hysteresis, or energy loss as a proportion of energy input (see Section 1.4.1), occurred for the filled rubbers: EDS16 and the silicone rubber. The nitrile rubber, although unfilled, showed significant hysteresis and stress softening and a large permanent set, features which suggest that some plastic yielding took place. This supports the suggestion that plastic yielding was a cause of the non-linearity in the first

(a)

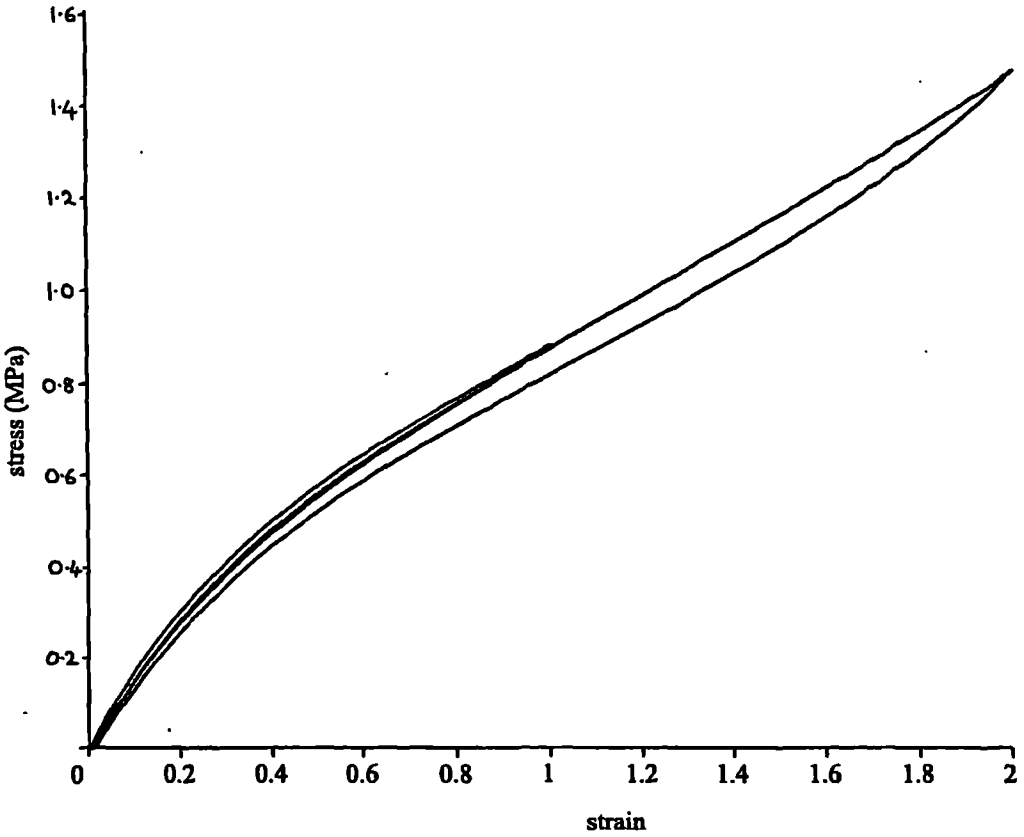
1·6
1·4
1·2
1·0
0·8
0·6
0·4
0·2
stress (MPa)
0
0.2
0.4
0.6
0.8
1
1.2
1.4
1.6
1.8
2
strain

(b)

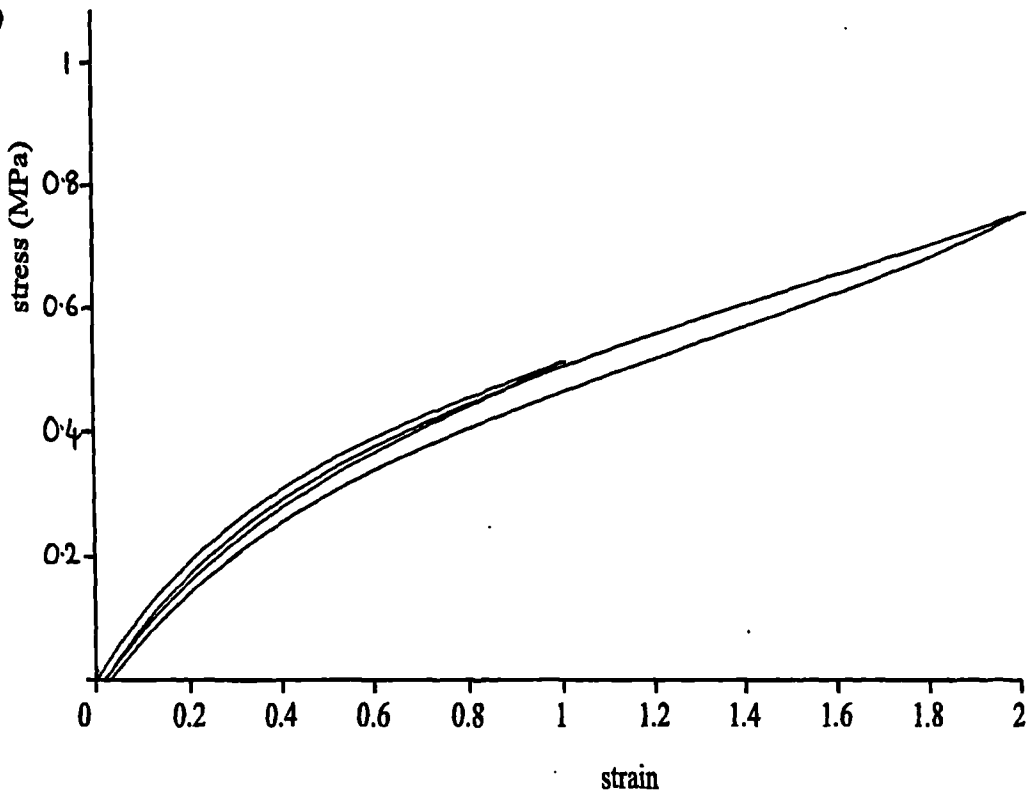
1
0·8
0·6
0·4
0·2
stress (MPa)
0
0.2
0.4
0.6
0.8
1
1.2
1.4
1.6
1.8
2
strain

(c)

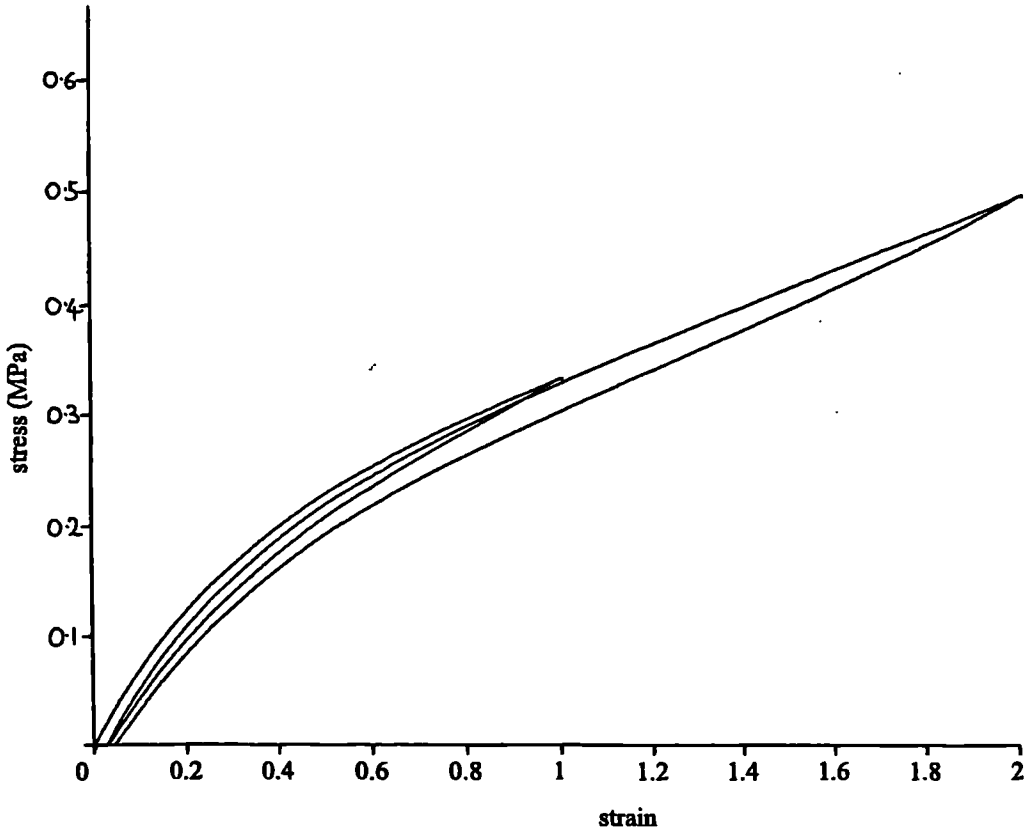
0·6
0·5
0·4
0·3
0·2
0·1
stress (MPa)
0
0.2
0.4
0.6
0.8
1
1.2
1.4
1.6
1.8
2
strain

(d)

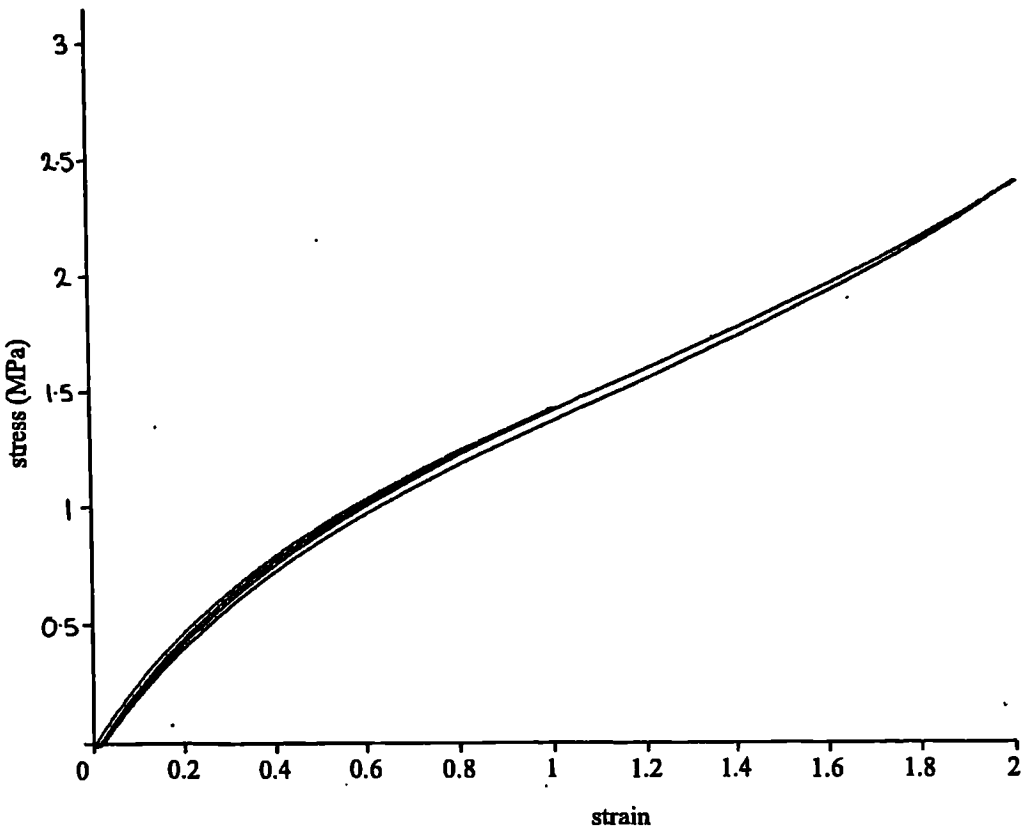
3
2·5
2
1·5
1
0·5
stress (MPa)
0
0.2
0.4
0.6
0.8
1
1.2
1.4
1.6
1.8
2
strain

(e)

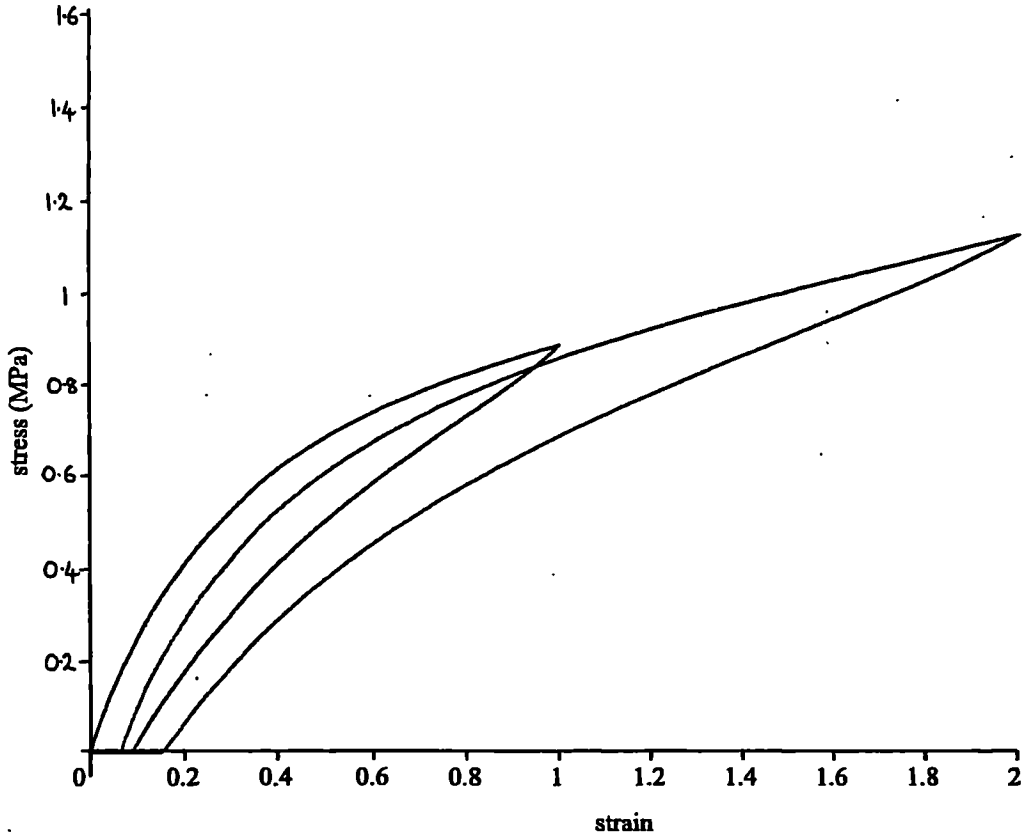
1·6
1·4
1·2
1
0·8
0·6
0·4
0·2
stress (MPa)
0
0.2
0.4
0.6
0.8
1
1.2
1.4
1.6
1.8
2
strain

(f)

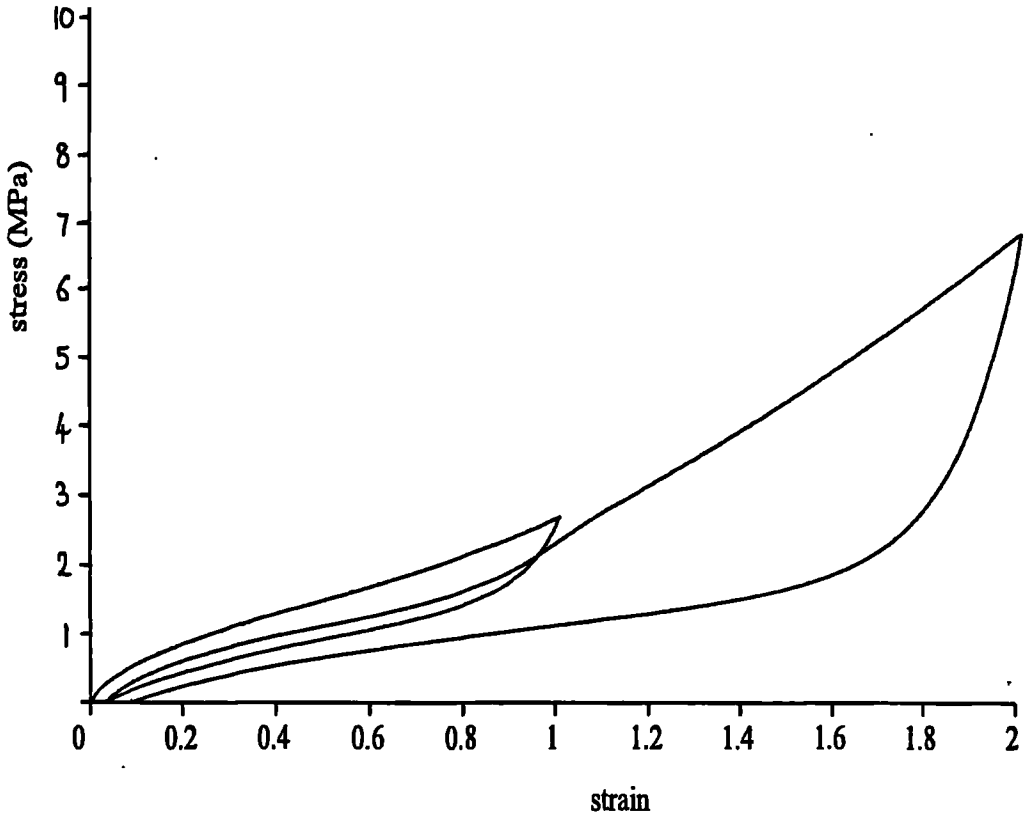
10
9
8
7
6
5
4
3
2
1
stress (MPa)
0
0.2
0.4
0.6
0.8
1
1.2
1.4
1.6
1.8
2
strain

(g)

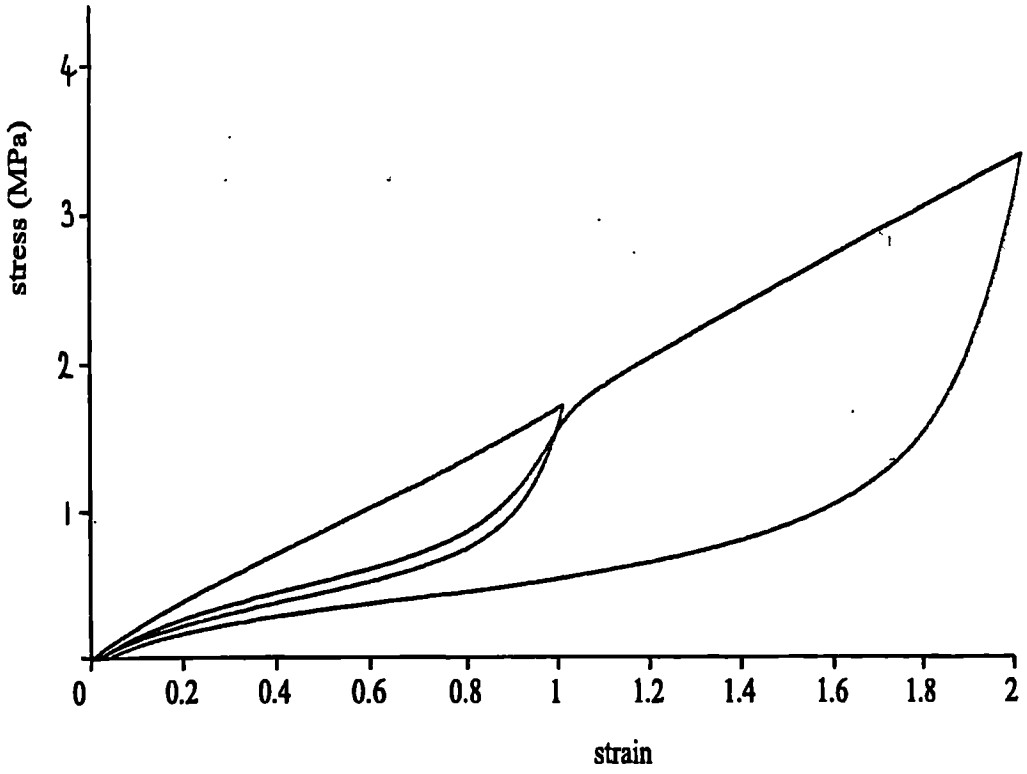

Figure 8.1 Plots of nominal stress against strain for rubbers subjected to one cycle to 100% strain, followed by one cycle to 200% strain in uniaxial tension. (a) unfilled natural rubber, EDS19; (b) unfilled natural rubber, low sulphur; (c) unfilled natural rubber, peroxide-cured; (d) polyurethane rubber; (e) nitrile rubber; (f) filled natural rubber, EDS16; (g) silicone rubber.

loading cycle (see Section 5.4). The other unfilled rubbers showed little hysteresis, especially the polyurethane.

8.3 Mullins' softening in silicone rubber

8.3.1 *Method*

A testpiece of silicone rubber, cut from the same sheet as that tested in Chapter 5, was clamped in the pure shear apparatus as described in Section 5.2. It was subjected to two cycles to 100% extension at a rate of 10mm/minute.

A new strip, from the same sheet of silicone rubber, of dimensions 184.5×2.18×30mm was pulled in uniaxial tension in a Instron tensile test machine to 100% at a rate of 443 mm/minute which is equivalent to a strain rate of $0.04s^{-1}$. It was then clamped in the pure shear apparatus, after cutting off the ends which had been deformed by clamping, and pulled perpendicular to the original straining direction at the same strain rate. Finally the central strip of the pure shear testpiece, now of area 171.5×12.8mm was again pulled in uniaxial tension in the original straining direction at a strain rate of $0.04s^{-1}$.

8.3.2 *Results*

The main and transverse stresses were calculated from the measured forces for the first and second cycles in pure shear. They are plotted in Figures 8.2. The stress-strain behaviour of the testpiece subjected to the sequence of tension, pure shear, tension is shown in Figure 8.3. In this figure the main strain in pure shear has been plotted alongside the strain in tension with no adjustment to allow for the fact that the strain energy at equal values of nominal strain will be different for the two modes of deformation. The equivalent values of λ in pure shear and tension for a given value of I_1 may be calculated from equation (1.14) and it may be seen by comparing equations (3.1a) and (4.5) that the differences in the stresses are small if the dependence of W on I_2 is small, especially as the strain increases. The data for the testpiece subjected to two cycles of pure shear is also shown in Figure 8.3 to facilitate comparisons.

8.3.3 *Discussion*

As expected (Muhr et al, 1999), the rubber shows considerable softening between the

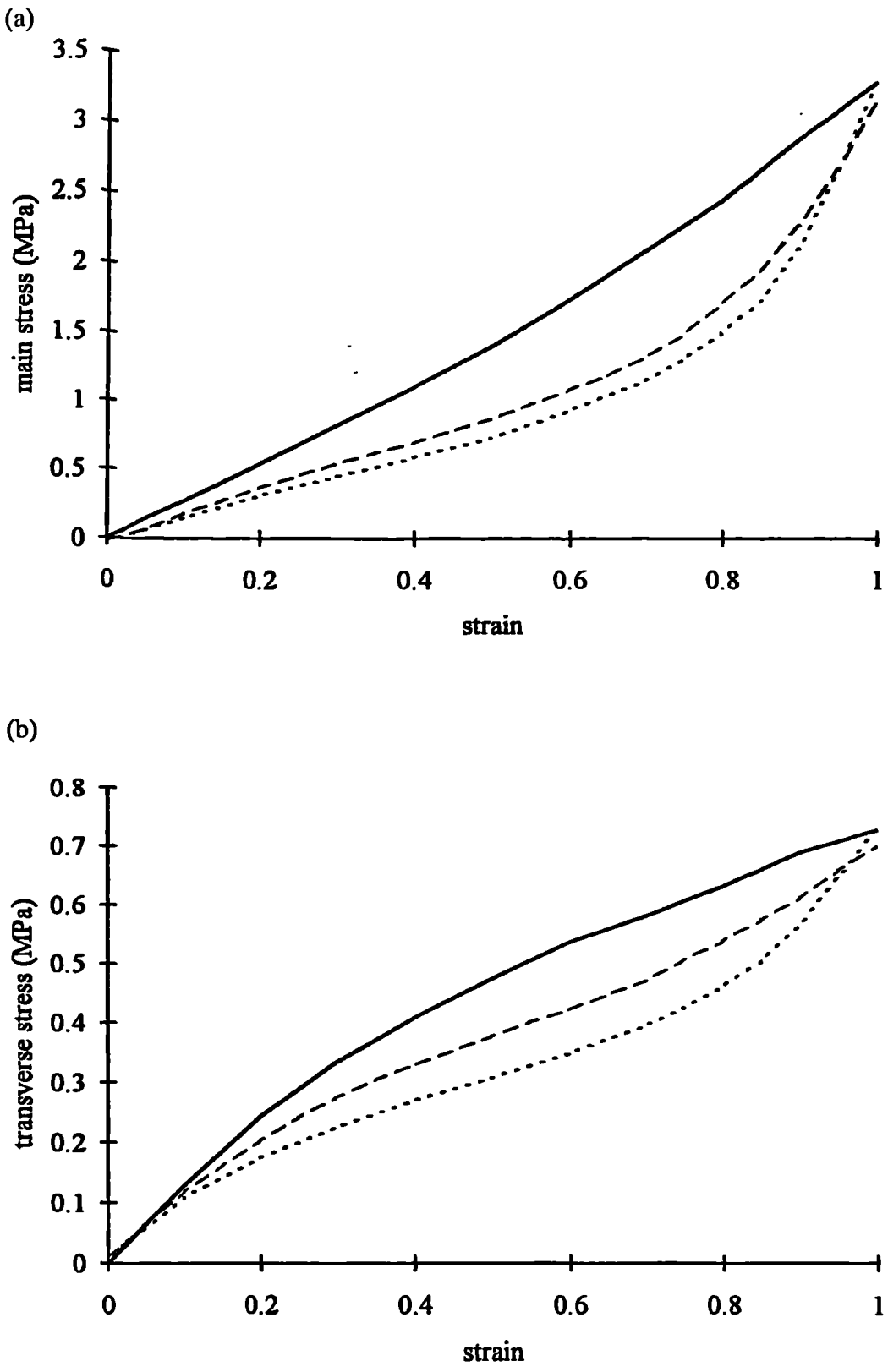

Figure 8.2 Stress-strain plots for filled silicone rubber in pure shear.
———— first cycle loading, -------- first cycle unloading
– – – – second cycle loading.
(a) main stress, (b) transverse stress

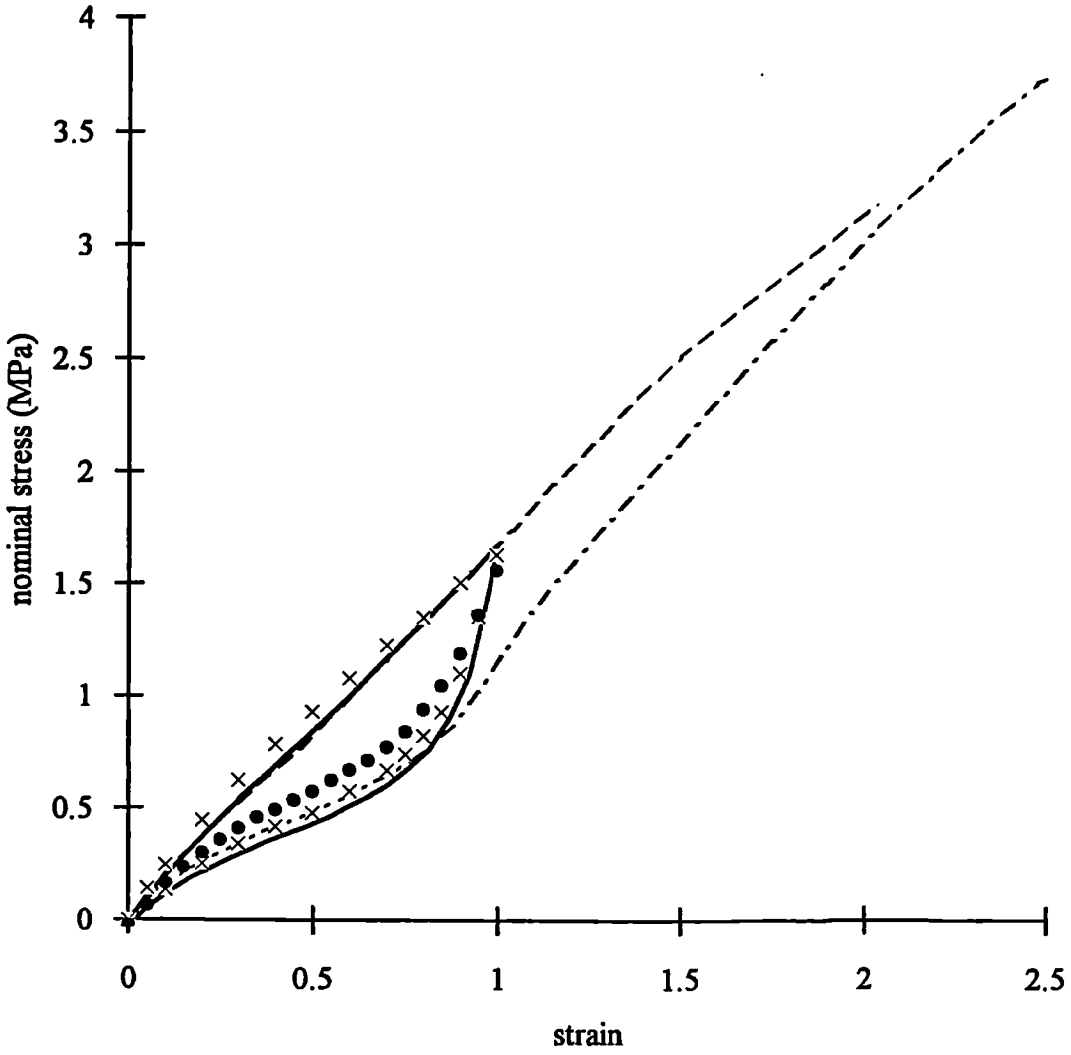

Figure 8.3 Effect of changes in testpiece orientation on Mullins type softening. ——— previously unstrained testpiece in tension, ------- pure shear in orthogonal direction after tension to 100%, – · – · – tension after tension to 100% and orthogonal pure shear to 200%, × previously unstrained testpiece in pure shear, ● pure shear after pure shear to 100%.

first and second loading cycles (Figures 8.2). This softening shows typical features of Mullins' effect with the second cycle stresses approaching their values for the virgin material as the maximum of the previous cycle is reached. This Mullins' type softening is apparent in both the main and the transverse stress. As the rubber began slipping from the clamp at strains slightly above 100%, it is not possible to see the second cycle behaviour above the first cycle maximum. In Figure 8.4, the ratio of the second to first loading cycle stresses in both the main and the transverse directions has been plotted as a function of strain. The two lines do not coincide, with the relative fall in the main stress being greater than that in the transverse stress. The behaviour at low strains is complicated by the presence of permanent set in the main straining direction which was not seen in the transverse direction because no strain occurs in the transverse direction. As the maximum strain is approached the ratio of the stresses becomes one for both stresses, as it must if the second cycle curve is to rejoin the first cycle curve.

Figure 8.3 shows that the Mullins' softening is not seen if the direction of straining is rotated through 90°; the stiffness of the testpiece in pure shear following perpendicular tension is almost as great as for a virgin pure shear cycle. A significant softening in the original straining direction was evident when the final tensile straining was carried out. This was presumably caused by the original tensile strain which was in the same direction. However, in this cycle, the rubber appears to be softer than the virgin material, even at strains above the maximum previous strain in the same direction, suggesting that the pure shear to 200% caused some softening in tension, which was rather more pronounced than the softening in pure shear following tension to 100%.

8.3.4 *Predictions of Ogden and Roxburghs' model*

In the model of Mullins' effect developed by Ogden and Roxburgh (1999), the strain energy function for a hyperelastic material, $W(\lambda_1, \lambda_2)$, is modified with a damage parameter, η, so that

$$W = W(\lambda_1, \lambda_2, \eta) \tag{8.2}$$

In general, η is a function of λ_1 and λ_2. On the virgin loading curve, η is set to be unity so that this curve may be described by a strain energy function

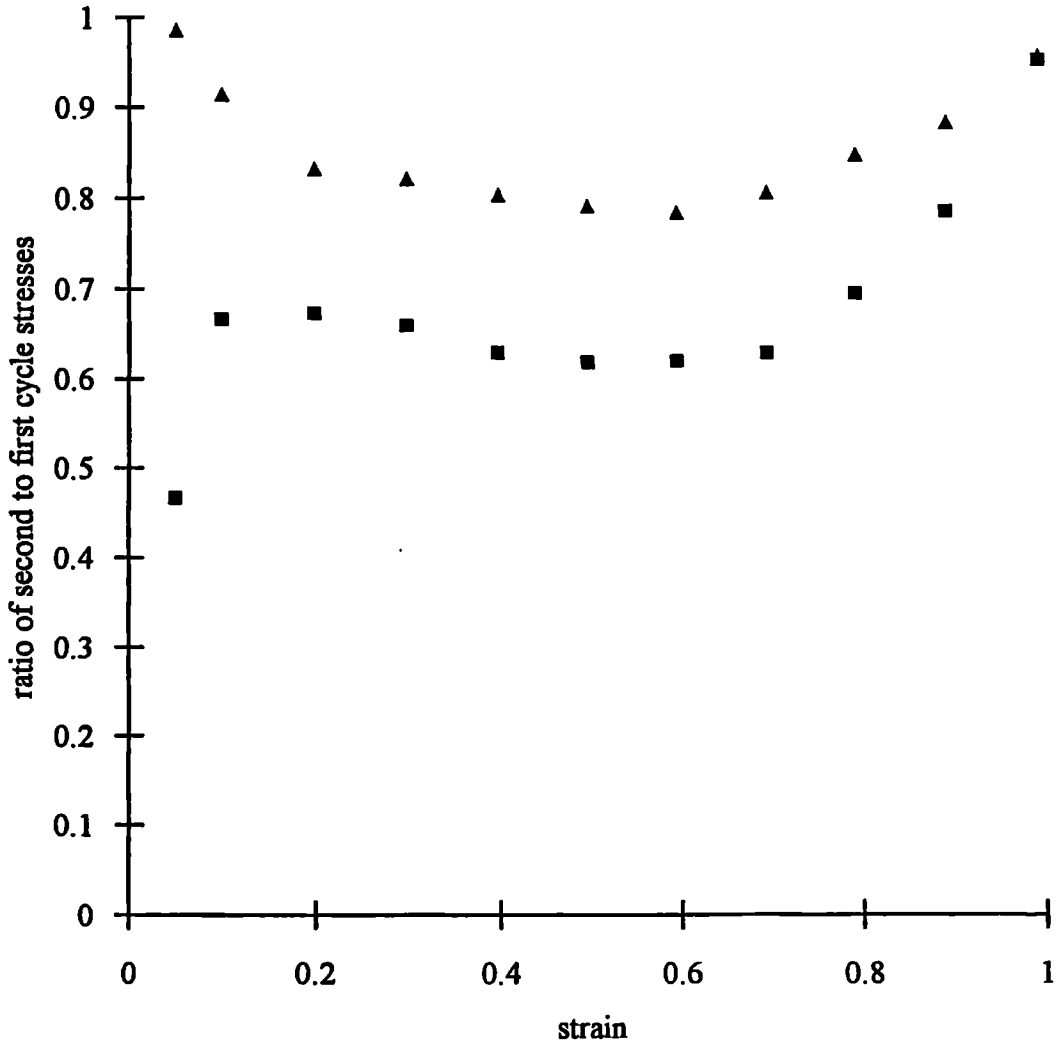

Figure 8.4 Ratio of first and second cycle main and transverse stresses for filled silicone rubber. ■ main stress, ▲ transverse stress.

$$\tilde{W}(\lambda_1, \lambda_2) = W(\lambda_1, \lambda_2, 1) \tag{8.3}$$

where a suitable strain energy function for a hyperelastic material may be chosen for $\tilde{W}$. The particular specialization of equation (8.2) adopted by Ogden and Roxburgh (1999) is

$$W(\lambda_1, \lambda_2, \eta) = \eta \tilde{W}(\lambda_1, \lambda_2) + \phi(\eta) \tag{8.4}$$

from which they obtain the nominal stresses in pure shear in the main and transverse directions respectively:

$$\begin{aligned} s_1 &= \eta \, \partial \tilde{W} / \partial \lambda_1 \\ s_2 &= \eta \, \partial \tilde{W} / \partial \lambda_2 \end{aligned} \tag{8.5}$$

The value of η depends on the maximum principal stretches, λ_{1m} and λ_{2m} previously obtained. It follows from equations (8.5) that for either stress the ratio of the second to first cycle at equal strain will be $\eta_2 (\lambda_1, \lambda_2)$, where η_2 is the value of η on the second loading cycle, since η_1 is defined as unity. The value of this ratio will in general depend on strain but should be the same for both stresses, thus the prediction of this model is for the two lines of Figure 8.4 to coincide. Furthermore, the amount of the softening predicted by the model depends only on λ_{1m} and λ_{2m}, and hence on the maximum strain energy previously attained, but not on the directions of λ_{1m} and λ_{2m}. Thus Ogden and Roxburghs'(1999) model is not sufficiently sophisticated to model either the different relative reductions in the main and transverse stresses (Figure 8.4) or the dependence of the amount of the softening on the direction of previous strains (Figure 8.3). However, it should be borne in mind that the silicone rubber investigated exhibits a particularly large Mullins' effect. For more conventional rubbers, where Mullins' effect is typically much smaller, such limitations in the model are likely to cause only small errors. Improvements in accuracy would require a more complex model, incorporating additional direction dependent parameters and a detailed material characterization. Such an approach is unlikely to be necessary for most practical purposes.

8.4 Stress relaxation in filled and unfilled natural rubber

8.4.1 *Method*

The experiments were carried out on four rubbers. Two were conventional sulphur cured rubbers as used for previous experiments, EDS19 (unfilled) and EDS16 (filled). Their formulations are given in Table 3.2. Two other unfilled rubbers were tested; one was similar to EDS19, but with a lower crosslink density in order to increase the amount of stress relaxation, and the other was a peroxide cured rubber containing direct carbon-carbon crosslinks instead of mono- or poly-sulphidic ones. The formulations of these rubbers are given in Table 8.1.

Table 8.1: Formulations of unfilled rubbers. Ingredients expressed in parts per hundred of rubber by mass.

	low-sulphur rubber	peroxide-cured rubber
natural rubber, SMR CV60	100	100
carbon black, HAF (ASTM N330)	1	1
zinc oxide	5	-
stearic acid	2	-
antioxidant / antiozonant [1]	3	-
antioxidant, Flectol H [2]	-	1
antioxidant/antiozonant wax	2	-
sulphur	1.25	-
accelerator, CBS [3]	0.3	-
dicumyl peroxide	-	1
vulcanization time and temperature	50 minutes at 140°C	60 minutes at 150°C
hardness (IRHD)	33	<28

1. N-(1,3-dimethylbutyl)-N'-phenyl-phenylene-diamine
2. Polymerized 2,2,4-trimethyl-1,2-dihydroquinoline
3. N-cyclohexylbenzothiazole-2-sulphenamide

The testpieces of the low sulphur rubber were cured at 140°C to maximum rheometer torque. The testpieces of the peroxide cured rubber were preformed by heating under pressure in the mould for 10 minutes at 100°C before vulcanizing. This procedure is necessary with peroxide cure systems because they have no scorch time, that is crosslinks begin forming immediately so that the rubber has no time to flow in the mould.

Bonded testpieces (see Figure 3.2) were clamped in the split pure shear apparatus (see Figure 3.1) and pulled in an Instron screw-driven test machine to various strains at a rate such that the required strain was reached in 10 seconds. The time of straining was thus small compared to the time over which the subsequent stress relaxation measurements were taken. The subsequent decay of both the main and transverse forces with time was monitored by plotting on a chart recorder. Since the forces were sensitive to temperature, the experiments were carried out in a temperature controlled cabinet at $29.4 \pm 0.1\,°C$. Each experiment was usually carried out on a new testpiece. However, some of the testpieces which had previously been strained to low strains were subsequently used for experiments at much higher strains as it was assumed that the small strain softening would have negligible impact on the stress relaxation at higher strains.

8.4.2 *Results*

In order to enable direct comparison of the rate of decay of the main and transverse forces, and of experiments carried out at different initial strains, the main and transverse forces were normalized by calculating

$$f_N = \frac{f_t}{f_{300}} \tag{8.6}$$

where f_N is the normalized force, f_t is the force after time t and f_{300} is the force after a arbitrary standard time, chosen to be 300 seconds.

When the rates of decay of the transverse force for the two load cells were compared considerable differences were apparent, especially for EDS16 for which one load cell always recorded relaxation rates much greater than those of the other. For this reason only the more self consistent results have been presented in Figure 8.5. Even so, the relative rates of stress relaxation measured by the two load cells differed by up to a factor of two. For the other sulphur cured rubbers the rates of stress relaxation measured by the two load cells were generally within 25% and often much closer. The results for EDS19 are shown in Figure 8.6 and those for the sulphur cured rubber in Figure 8.7. For the peroxide cured rubber differences of up to 100% were seen. This large percentage error is perhaps a consequence of the very small absolute amounts of

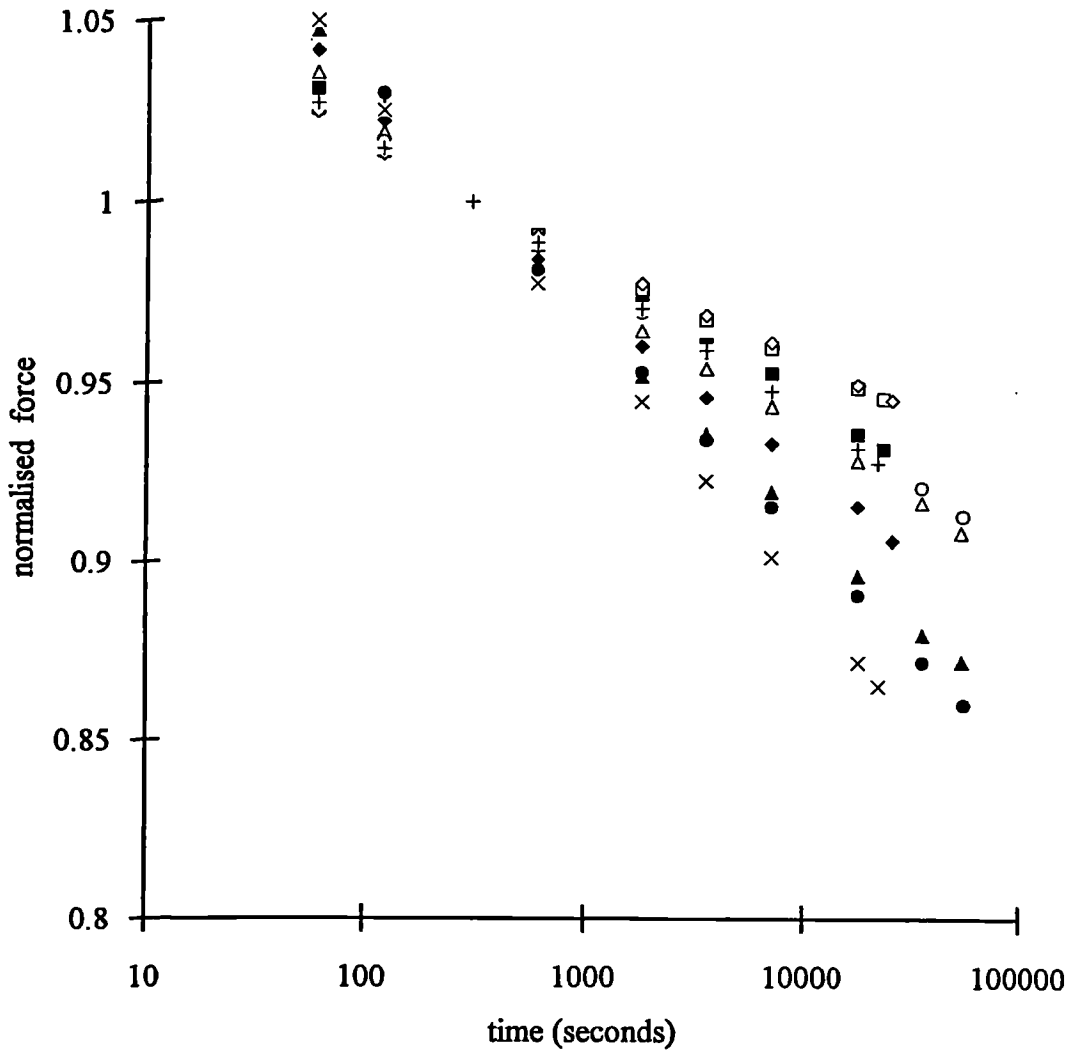

Figure 8.5 Relative stress relaxation rates for the main and transverse force in filled sulphur cured rubber, EDS16.
Filled symbols and ×, main force; open symbols and +, transverse force.
■ □ 40% strain; ◆ ◇ 80% strain; ▲ △ 100% strain; ● ○ 120% strain; × + 140% strain.

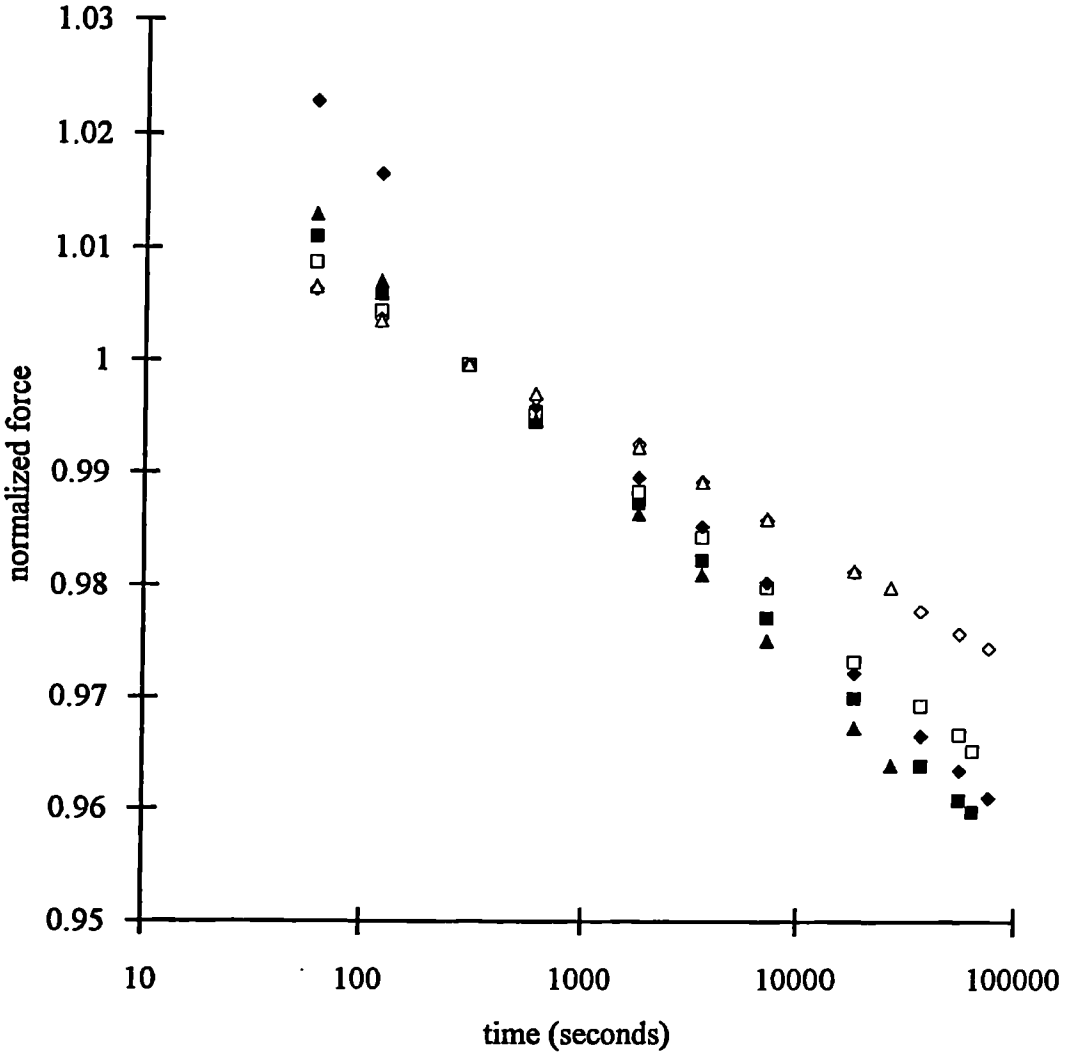

Figure 8.6 Relative stress relaxation rates for the main and transverse force in unfilled sulphur cured rubber, EDS19.
Filled symbols, main force; open symbols, transverse force.
■ □ 42% strain; ◆ ◇ 100% strain; ▲ △ 150% strain.

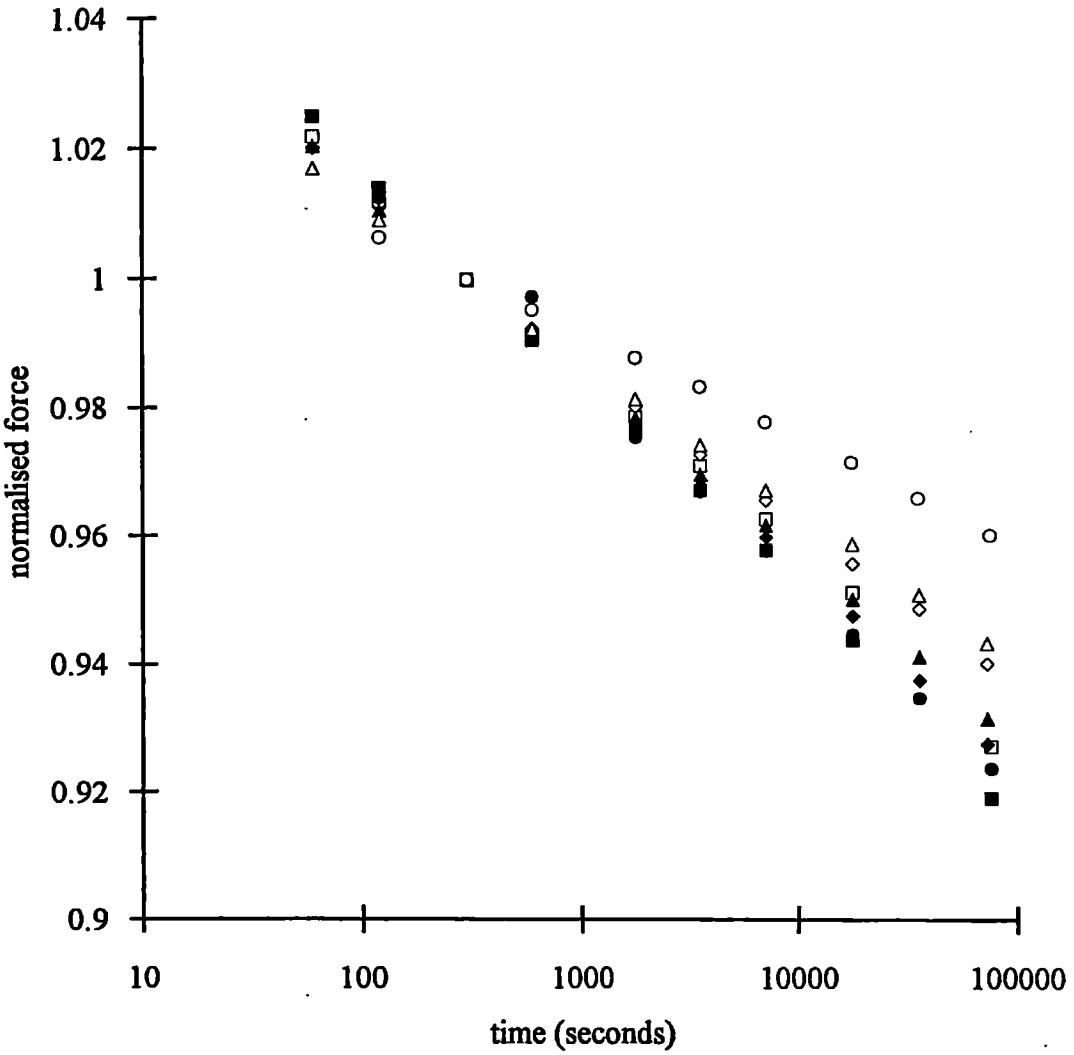

Figure 8.7 Relative stress relaxation rates for the main and transverse force in low crosslink density unfilled sulphur cured rubber (see Table 8.1 for formulation)
Filled symbols, main force; open symbols, transverse force.
■ □ 50% strain; ◆ ◇ 100% strain; ▲ △ 150% strain; ● ○ 265% strain.

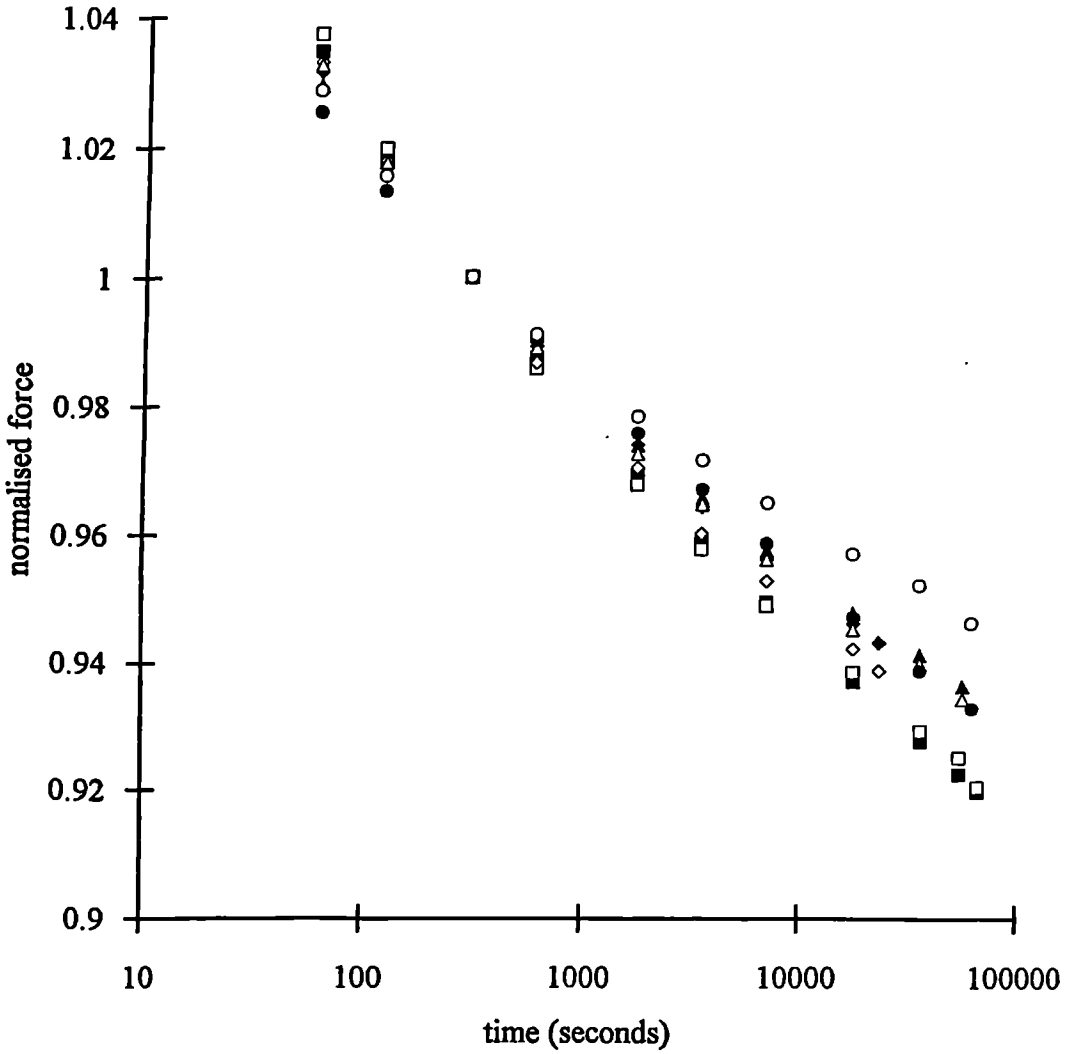

Figure 8.8 Relative stress relaxation rates for the main and transverse force in unfilled peroxide cured rubber.
Filled symbols, main force; open symbols, transverse force.
■ □ 80% strain; ◆ ◇ 120% strain; ▲ △ 150% strain; ● ○ 285% strain.

stress relaxation seen for this rubber. These results are given in Figure 8.8. For all the data presented in Figures 8.5 to 8.8 an average of the two load cell readings has been used, as was the case for all data previously reported using the split pure shear technique.

8.4.3 *Estimation of causes of errors*

Component of main force in transverse force

As pointed out in Section 3.2.2, if the horizontal alignment of the apparatus is imperfect the large main force will introduce an equal and opposite component into the forces measured by the transverse load cells. This was one reason for introducing two load cells and averaging their readings. The effect of misalignment on the normalized transverse forces was calculated as follows. If the forces recorded by the transverse load cells are f_A and f_B respectively then

$$f_A = f + f_m \tag{8.7a}$$

$$f_B = f - f_m \tag{8.7b}$$

where f is the "correct" transverse force reading and f_m is the transverse component of the main force due to misalignment. If the force decays at a rate of ζ per tenfold increase in time, the normalized forces n tenfold increments after the normalizing time are given by

$$f_{NA} = \frac{f - n\zeta f + (f_m - n\zeta f_m)}{f + f_m} = 1 - n\zeta \tag{8.8a}$$

$$f_{NB} = \frac{f - n\zeta f - (f_m - n\zeta f_m)}{f - f_m} = 1 - n\zeta \tag{8.8b}$$

Hence the normalized force from the two load cells is the same and independent of f_m. This suggests that the differences in the normalized forces from the two load cells do not arise from alignment errors.

Additional relaxation due to set-up stresses

Clamping the rubbers tends to exert a significant load on the transverse load cells which was subtracted from readings of the transverse force. The magnitude of this clamping load was typically about 2N for EDS16 and was tensile for the load cell showing the greater rate of decay and compressive for the load cell showing the smaller decay. For the other softer rubbers these clamping forces were much smaller, typically about 0.4N. This clamping load is presumably due to a small side strain exerted on the rubber at the slit which may relax, distorting subsequent measurement of stress relaxation.

An additional experiment was carried out on EDS16 at 80% strain in which a spacer was introduced to increase the width of the slit at the load cell which showed the lower rate of force decay. The results are shown in Figure 8.9, where it can be seen that a much greater rate of decay of the force was observed at this load cell after the spacer was incorporated. Also, a tensile, rather than compressive, force was exerted on the load cell due to clamping. This suggests that the source of the discrepancies in the apparent rate of relaxation could be that, for the load cell with a tensile force offset, relaxation of the offset will tend to increase the apparent relaxation rate whereas the reverse would be true for a compressive force offset.

An estimate of the effect of the clamping force on the measured rate of stress relaxation was made as follows. It was assumed that the rate of stress relaxation of the clamping force was the same as for the main force for the same rubber and that 25 minutes was allowed after clamping but before beginning the experiment for the temperature to reach equilibrium. From this the force loss in the interval from 30 to 60 minutes after clamping (equal to 0.3 tenfold increments of time) was estimated. These values were compared to the actual transverse force loss recorded during this time in the experiment. Typical values are shown in Table 8.2.

These estimates show that the spurious component accounts for not more than about 10% of the registered force drop for EDS16 and rather less for the unfilled rubbers. Thus this source of error is unlikely to be very significant. The cause of the large variation in relative rates of decay from the two load cells for EDS16 remains unresolved.

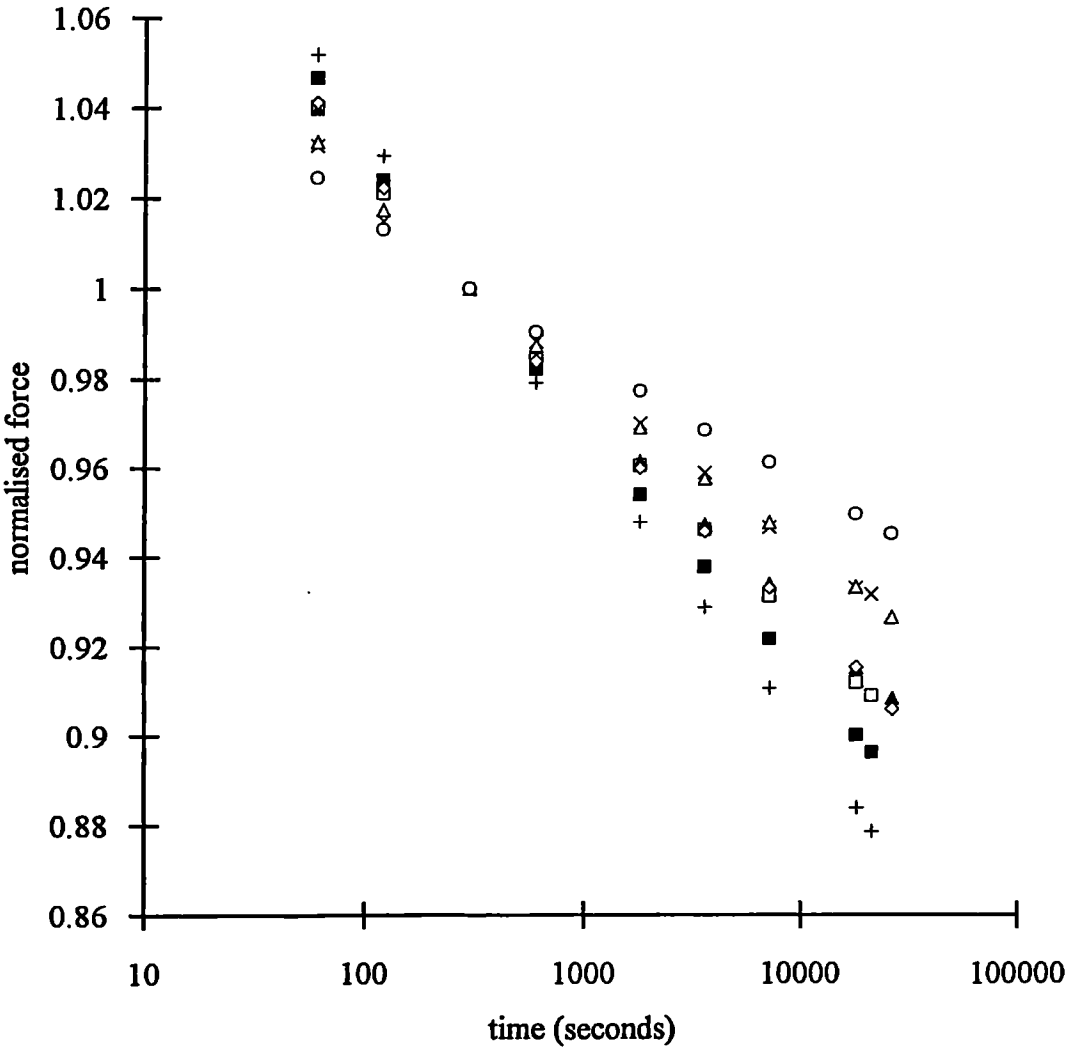

Figure 8.9 Comparison of the relative relaxation rates for two tests at 80% strain on EDS16.

▲ original test, main force; Δ original test, transverse force; ◊ o original test, individual transverse load cells.
■ repeat test, main force; □ repeat test, transverse force; × + repeat test, transverse forces calculated from the individual load cells. (+ denotes data for the load cell with an added spacer.)

Table 8.2: Comparison of actual force drop with estimated spurious force drop				
rubber	relaxation rate estimated from graphs (% per tenfold increase in time)	strain (%)	actual transverse force drop (N) between 5 and 30 minutes	estimate of typical spurious force change (N)
EDS16	3.7	40	0.24	
	5.0	80	0.41	0.02
	6.3	120	0.5	
EDS19	1.7	42	0.05	
	1.8	100	0.06	0.002
	1.9	150	0.07	
low sulphur	3.3	50	0.07	
rubber	3.0	100	0.10	0.003
	2.8	150	0.11	
peroxide	3.5	80	0.04	
cured	3.1	120	0.09	0.004
rubber	3.1	150	0.09	

A check of the quasistatic data presented in Chapter 3 revealed no significant differences in the forces measured by the two load cells. Thus the conclusions drawn in Chapter 3 remain valid. The difficulties with the stress relaxation measurements may be a consequence of the need to measure small force changes over long periods of time.

8.4.4 *Discussion*

It is apparent from Figures 8.5 to 8.8 that the rate of stress relaxation of both the main and the transverse force for all rubbers is linear as a function of log time in agreement with the literature (Gent 1962a). For the unfilled rubbers the rate of stress relaxation was largely independent of the imposed strain. For the filled rubber the amount of stress relaxation increased with increasing strain, at least in the main stress. The amount of stress relaxation of the three unfilled rubbers was smaller than that of the filled rubber. These observations also are in agreement with the literature (Gent, 1962b). The softer unfilled rubbers (low-sulphur and peroxide cured) showed more stress relaxation than EDS19. This is likely to be because in rubbers with a low crosslink density, there is more molecular movement, such as rearrangement of chain entanglements, to relieve

stresses.

In view of the large experimental errors associated with measurement of the decay of the transverse force, especially in EDS16, only tentative conclusions may be drawn about the relative amounts of stress relaxation of the main and transverse forces. There is a trend for the main stress to relax more than the transverse stress in all the sulphur cured rubbers, both filled and unfilled. This is not the case for the peroxide cured rubber, except at the largest imposed strain, which is consistent with the results of Kawabata (1973).

8.5 Cyclic stress relaxation

8.5.1 *Method*

Bonded pure shear testpieces of EDS19 and EDS16 were clamped in the pure shear apparatus. They were continuously cycled between 0 and 100% strain at a rate of 100% strain per minute on an Instron screw-driven test machine. The main and transverse forces were monitored by plotting on a chart recorder.

8.5.2 *Results*

The peak forces in each cycle were normalized in a way analogous to the stress relaxation forces. That is

$$F_N = \frac{F}{F_{10}} \tag{8.9}$$

where, for each cycle, F_N is the normalized peak force, F is the peak force and F_{10} is the peak force on the tenth cycle. The relative rates of decay of the main and transverse peak forces were compared by plotting F_N as a function of the number of cycles on a logarithmic scale. (Figure 8.10). No large differences were observed between the two transverse load cells for either rubber.

8.5.3 *Discussion*

After the first few cycles the decay of the forces became linear with the logarithm of the number of cycles. The non-linearity in the first few cycles has been attributed to the fact

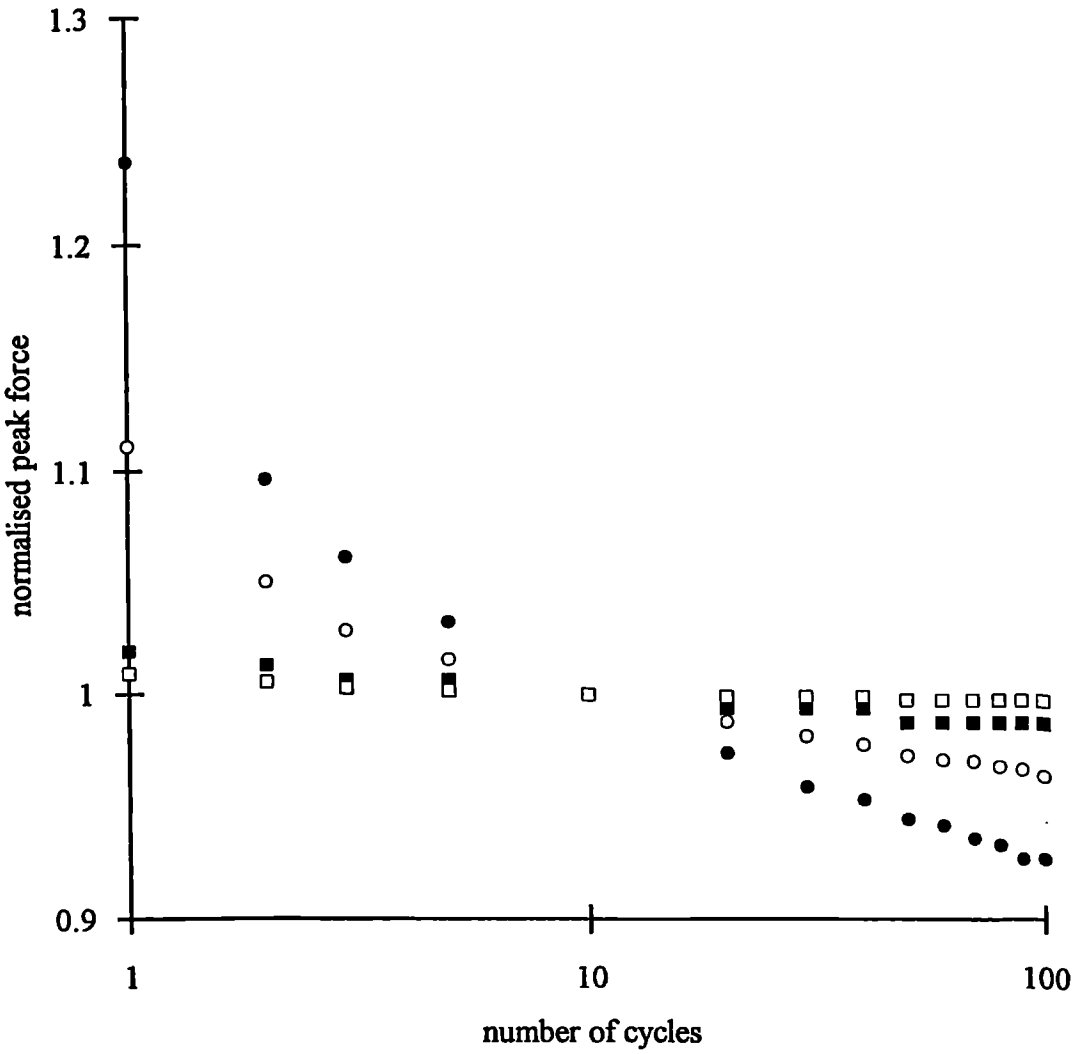

Figure 8.10 Decay of peak force during repeated cyclic straining between 0 and 100% strain.
Filled symbols, main force; open symbols, transverse force.
■ □ unfilled rubber, EDS19; ● ○ filled rubber, EDS16.

that the peak force is recorded after one more loading than unloading strain; thus there is difficulty in defining the number of cycles (Davies et al, 1996). In Figure 8.10 the convention of defining the first peak as the first cycle was adopted.

As for the static stress relaxation experiments, the softening was greater for the filled than the unfilled rubber and the main force decreased by a greater amount than the transverse force.

8.6 Separability of relaxation behaviour

The stress relaxation results indicate that, for a peroxide cured rubber at moderate strains, the main and transverse forces decay at the same rate. Thus, for this rubber, the separability equation (8.1) is satisfied. The results for both the static and cyclic stress relaxation, however, suggest that this may not be true for sulphur cured rubbers, whether filled or unfilled.

Another example of non-separability of the time and strain dependencies in rubber is the increase in the amount of stress relaxation in filled rubbers as the imposed strain is increased, also observed here and reported in the literature (Gent, 1962b; Sullivan and Mazich, 1989). This behaviour is also seen in unfilled rubbers at strains above 200% and has been attributed to strain crystallization (Gent, 1962b). The differing rates of decay in the filled rubber (Figure 8.5) and of the peroxide rubber at 285% strain could be another manifestation of the same molecular processes. However, the differing rates in the unfilled sulphur cured rubbers at strains below those where strain crystallization would occur suggests the existence of some process other than crystallization contributing to the non-separability of time and strain dependencies. The polysulphidic crosslinks which are usually predominant in conventional sulphur cured rubbers are known to be labile and possibly undergo direction dependent reorganization under anisotropic strain to an extent that does not comply with equation (8.1).

Non-separability of the time dependent behaviour is a further example of the limitation of a description of rubber in terms of a strain energy function, even when the strain energy function is modified as in equation (8.1). However, for many rubbers, stress

relaxation is small and thus an approximation such as equation (8.1) could be acceptable.

8.7 Conclusions

Rubbers, especially filled rubbers, are not perfectly elastic materials but exhibit departures from elasticity such as hysteresis, Mullins' effect and stress relaxation. These features limit the use of a strain energy function, which assumes perfect elasticity, in modelling their behaviour. Further complications arise from the fact that anisotropic states of deformation may result in a directional dependency in the softening arising from Mullins' effect and in the relative rates of stress relaxation. Also, the direction of the previous stress was found to influence the amount of stress softening in a filled silicone rubber; there was more softening after previous stresses in the same direction than after stresses in a perpendicular direction. Although these features cannot be modelled simply, models based on a strain energy function but containing additional parameters to allow for Mullins' effect or time dependent stress relaxation, give a reasonable approximation to the behaviour; the additional complexity of anisotropic modelling seems unjustified unless the anisotropic features are especially large or important.

CHAPTER 9

Low Temperature Crystallization

9.1 Introduction

Rubbers are normally used in their amorphous, that is rubbery, phase. Under prolonged periods at low temperatures certain rubbers, such as natural rubber and polychloroprene, crystallize and become much stiffer, seriously impairing their performance in some applications (see Section 1.1). Once crystallized, they also exhibit features in their mechanical properties such as plastic yielding which are typical of other crystalline polymers such as polyethylene and polyamides. Since natural rubber crystallizes slowly it is a suitable material for investigating the effect of the degree of crystallization on the mechanical properties. In this chapter various studies on the mechanical behaviour of partially crystalline natural rubber are carried out.

9.2 Materials

In order to enable experiments to be carried out efficiently a rubber which crystallizes in a convenient length of time was required. Conventional sulphur vulcanized natural rubber formulations crystallize very slowly, even at the temperature of maximum rate which is about -25°C (Bristow and Tiller, 1970; MRPRA engineering data sheets, 1980). The crystallization rate is increased considerably by the use of a low sulphur to accelerator ratio which decreases the number of chemical modifications of the polymer chain. However, the simplest crosslinking system is obtained with peroxide vulcanizing systems where direct carbon to carbon bonds are formed. These compounds crystallize relatively quickly.

One of the experiments undertaken required calculation of the degree of crystallinity from the volume change of a block of rubber. Zinc oxide, which is added as an activator for the accelerator in sulphur vulcanized rubbers, remains as insoluble particles in the rubber compound. As it does not bond to the rubber, voids are liable to form around the zinc oxide particles if the rubber is stretched, distorting volume change measurements (Gee et al, 1950). Peroxide cured rubbers do not contain insoluble additives such as

zinc oxide so voiding is unlikely. Therefore, for the work in this chapter, peroxide cured natural rubber formulations were used with the quantity of peroxide, and hence the degree of crosslinking, chosen such that the rubber crystallized in a few days at -25°C. The formulations are given in Table 9.1.

Table 9.1: Formulations of rubbers for low temperature crystallization. Ingredients expressed as parts per hundred of rubber by mass.

Formulation	A	B	C
natural rubber, SMR CV60	100	100	100
dicumyl peroxide	1	2	2
antioxidant, Flectol H[1]	1	1	-

1. Polymerized 2,2,4-trimethyl-1,2-dihydroquinoline

The testpieces were preformed by heating under pressure in the mould for 10 minutes at 100 to 110°C, then cured at 150°C for one hour.

9.3 Apparatus

The experiments required testpieces to be held at temperatures below ambient for prolonged periods with measurements of the force and displacement made occasionally. Some experiments required continuous cyclic straining to be applied to the testpiece. Two pieces of equipment were developed to enable these experiments to be carried out.

9.3.1 *Strain-gauged jigs*

The jig is shown in Figure 9.1. Each block of rubber in the quadruple shear testpiece (Figure 9.2) was approximately 4mm thick, 21mm in the straining direction and 12mm in the direction perpendicular to the shear plane. Shear strains were applied to the testpiece by turning a screw threaded displacement gauge. The consequent shear force was measured with strain-gauges in a full-bridge arrangement on a cantilever beam below the testpiece. The strain gauges were of a type designed to be self compensating with changes in temperature. The displacement was measured with a small LVDT clamped to one T-piece of the quadruple shear testpiece and impinging against a small plate bolted to the other T-piece. The LVDT was of the spring loaded type with a rubber sleeve which protected its moving parts from becoming iced up. During

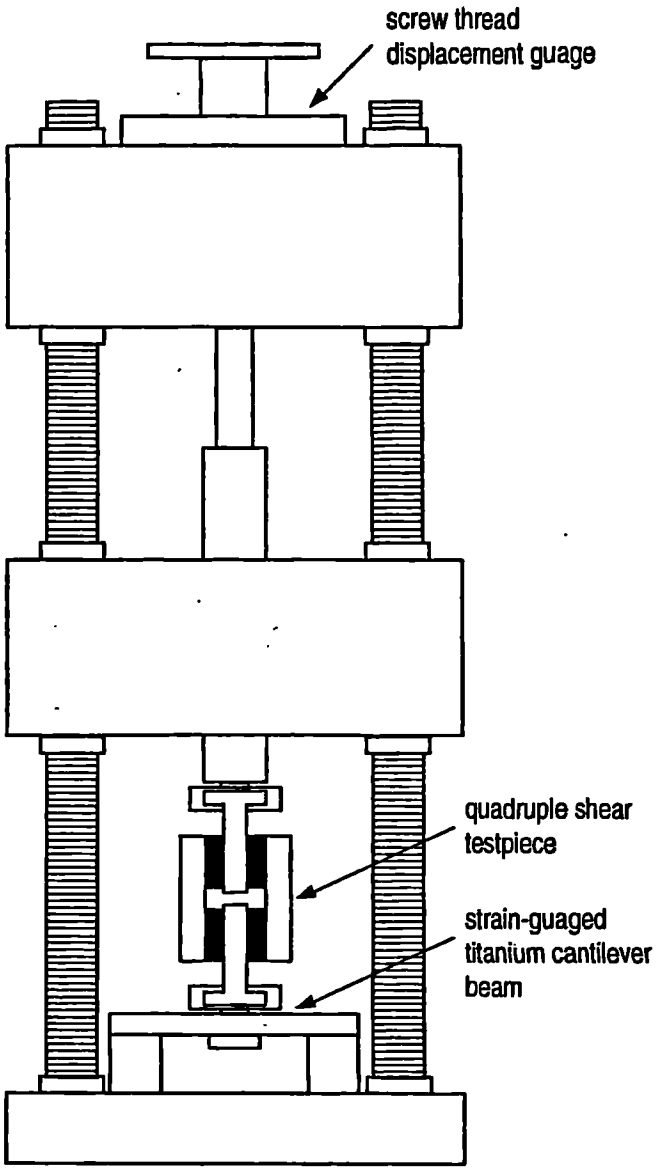

Figure 9.1 Schematic diagram of strain-gauged jig.

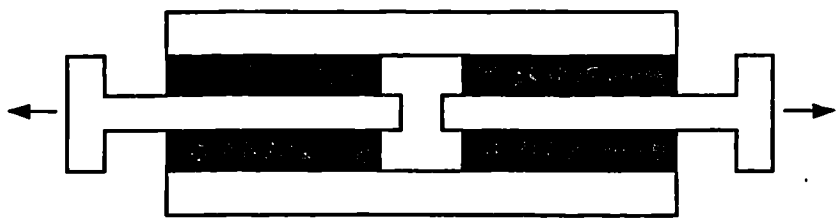

Figure 9.2 Quadruple shear testpiece.

experiments the whole apparatus was enclosed in a polythene bag within the freezer cabinet to minimize temperature fluctuations. The temperature of the freezer was monitored during experiments and maintained within ±1 °C of the required temperature.

The method of making modulus readings was as follows. The initial force and displacement readings were noted. A displacement of 0.16mm, equal to 2% strain, was imposed. The force and displacement after 3 minutes were recorded. The purpose of the 3 minute dwell time was to avoid taking readings when the force was changing rapidly due to stress relaxation of the testpiece. Finally, the strain was removed.

9.3.2 *Slow cycling rig*

The rig is shown in Figure 9.3. A motor, screwjack and gearbox combination provided a vertical displacement of the central column which applied a shear displacement on a double shear testpiece (Figure 4.1). The columns of the jig passed through holes in the roof of the freezer cabinet and were made of insulating Tufnel material at these points. The force was measured with a 10kN load cell mounted in the central column outside the freezer. The displacement was measured with an LVDT mounted on the stationary part of the rig and impinging against the central moving part of the double shear clamp. The LVDT comprised a central core with several millimetres' clearance from the outer coil. This type of LVDT was chosen to avoid sticking due to ice build-up. The motor was controlled with an electronic drive card controlled with a computer. The force and displacement data were collected through an A-D converter and processed via a Keithley Instruments DAS16 data acquisition system controlled with DASYLAB software.

9.4 **Preliminary experiments to assess reproducibility of low temperature crystallization measurements**

9.4.1 *Comparison of nominally identical mixes*

Significant differences were noticed in the crystallization rates of nominally identical mixes. This is shown by the open symbols in Figure 9.4 where the progress of crystallization has been monitored by measuring the increase in hardness with time at

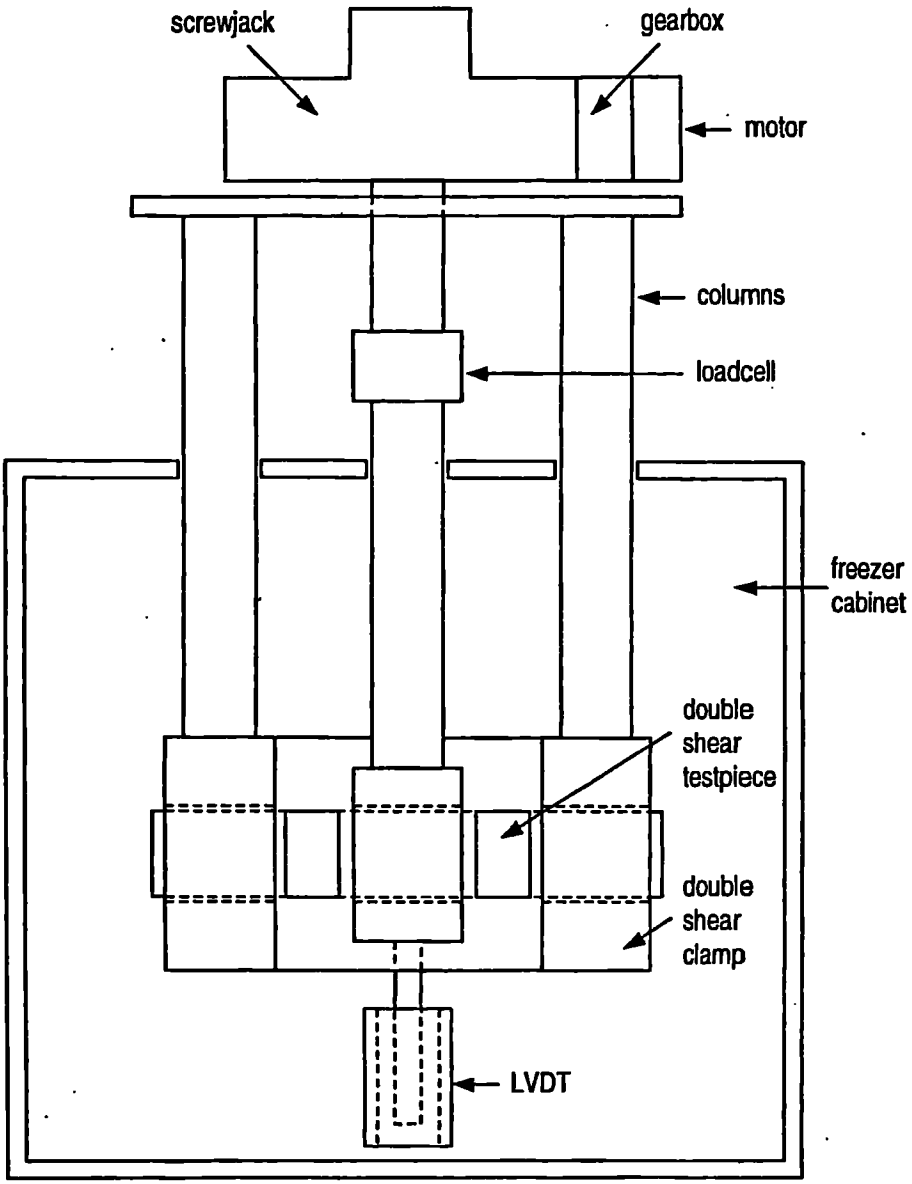

Figure 9.3 Schematic diagram of slow cycling rig.

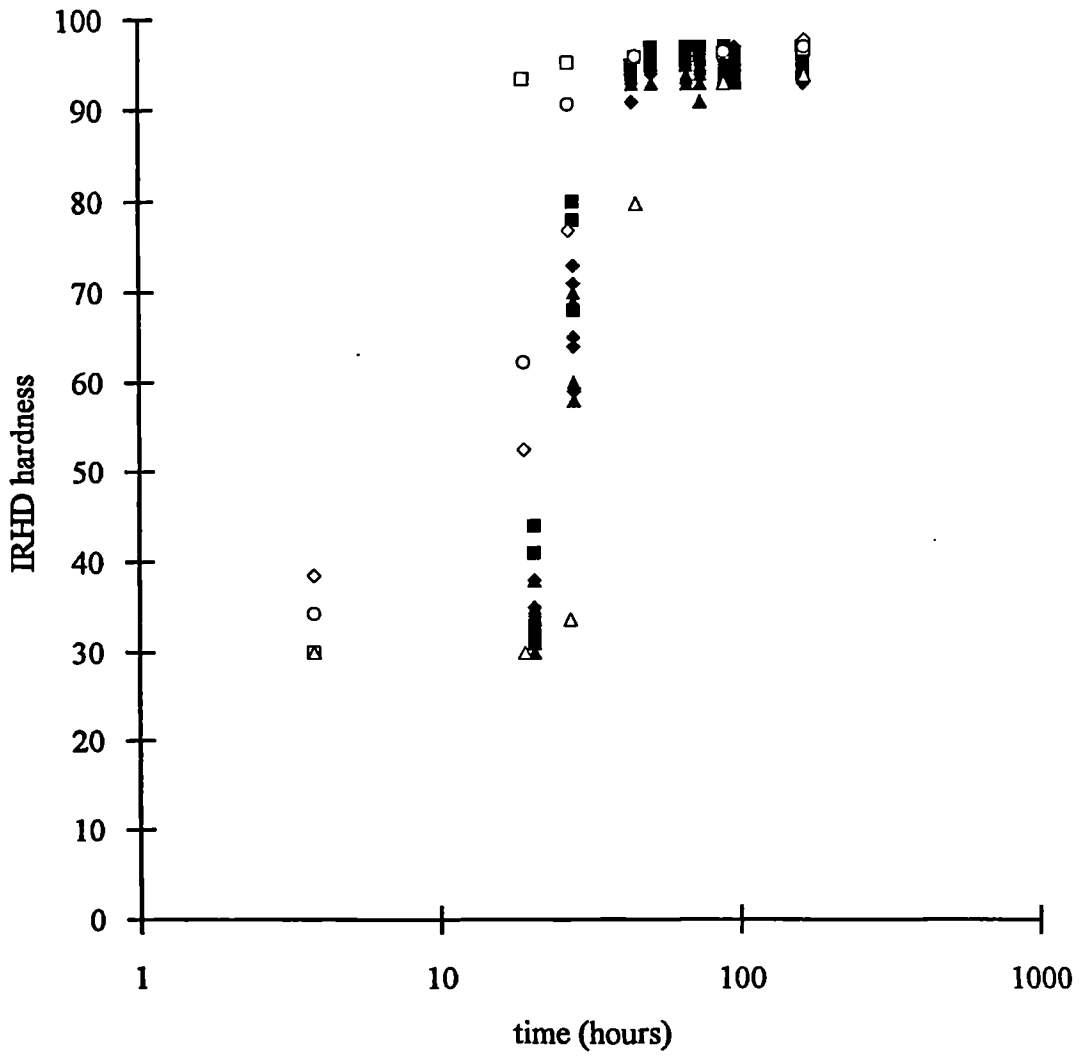

Figure 9.4 Crystallization at -25°C of different testpieces from the same extensively milled mix of natural rubber containing 1 pphr of dicumyl peroxide (filled symbols) compared to those from various other nominally identical mixes (open symbols). The different shapes of the filled symbols represent separate but nominally identical cures. □ mix 3, hardness buttons; ◇ mix 3, quadruple shear testpieces; ○ mix 2, quadruple shear testpieces; △ mix 1, sheet.

-25°C. All the samples received the same conditioning treatment: they were heated at 70°C for one hour before beginning the experiments (see Section 9.4.2).

In order to identify the cause of these differences in crystallization rate, a further three mixes of formulation A were prepared by mill mixing. The dispersion of the curative was assessed by taking small (about 5g) samples from different parts of the mix and measuring the rheometer torque during vulcanization at 150°C. This provided an indication of the crosslink density. Differences of up to 20% were seen between samples from each of the three mixes and between three samples taken from one mix. The mixes were remilled and a further three rheometer samples were taken from each mix. There were still significant variations in rheometer torque for two of the mixes. The third extensively milled mix did show good agreement between rheometer torque measurements, indicating a uniform dispersion of curative throughout the mix. The crystallization rates of different samples from this mix were compared by measuring the low temperature hardness of testpieces prepared in three separate mouldings. The results are shown in Figure 9.4 (filled symbols). Much less scatter is seen in these results than in those shown by the open symbols (corresponding to the other mixes) in Figure 9.4, suggesting that reasonable reproducibility may be obtained by ensuring that all testpieces are taken from one thoroughly prepared mix. Where possible, however, comparisons were made between experiments carried out on a single testpiece which was subjected to a heat conditioning treatment to ensure that complete melting took place between experiments.

9.4.2 *Preconditioning treatments*

Previous workers (Gent, 1954a; Stevenson, 1983) have commented on the need to subject nominally identical testpieces to a heat preconditioning treatment in order to obtain reproducible crystal nucleation rates. In order to establish a suitable procedure, the following series of conditioning treatments was applied to a single double shear testpiece of formulation A:

(i) 30 minutes at 70°C

(ii) 30 minutes at 70°C

(iii) 60 minutes at 70°C

(iv) 60 minutes at 90°C

(v) 60 minutes at 90°C

(vi) 30 minutes at 70°C

After each stage the crystallization was monitored using the slow cycling rig (see Section 9.3.2) to measure the increase in shear modulus as a function of time. This was done by continuously cycling the testpiece to a nominal amplitude of ±2½% and monitoring the peak force and displacement, from which the secant shear modulus was calculated. Strains of such small amplitude were not expected to affect the rate of crystallization (Pettifor and Coveney, 1989). The cycle period was 50 minutes. Between each spell of heating and crystallization the sample was allowed to stand at room temperature for between 30 and 60 minutes.

The results are shown in Figure 9.5. They indicate that an increase in either the time or temperature of the conditioning treatment caused a significant increase in the nucleation time. However, reproducible rates of crystallization were seen for the three tests which followed conditioning for 30 minutes at 70°C, whereas a difference was seen in the rates after 60 minutes at 90°C. It is possible that at higher temperatures or after longer times, chemical changes occur, though this seems unlikely in this case as normally much more severe conditions are necessary for chemical degradation to occur. No systematic effect of conditioning treatment on the final level of crystallinity emerges as there is considerable scatter in the modulus measurement.

For the current work, in which measurement of crystallization rates was of secondary importance, it was concluded that a conditioning treatment at 70°C for a well-defined time between 30 and 60 minutes would suffice.

9.5 Relationship between change in modulus and amount of crystallinity

9.5.1 *Introduction*

Crystallization causes a dramatic increase in the modulus and hardness of rubber and these properties may be used to monitor the progress of crystallization (Stevenson, 1983). Little is known, however, about the exact relationship between the modulus and the level of crystallinity in crystalline polymers. Natural rubber is a convenient material with which to investigate this relationship because it crystallizes sufficiently slowly for

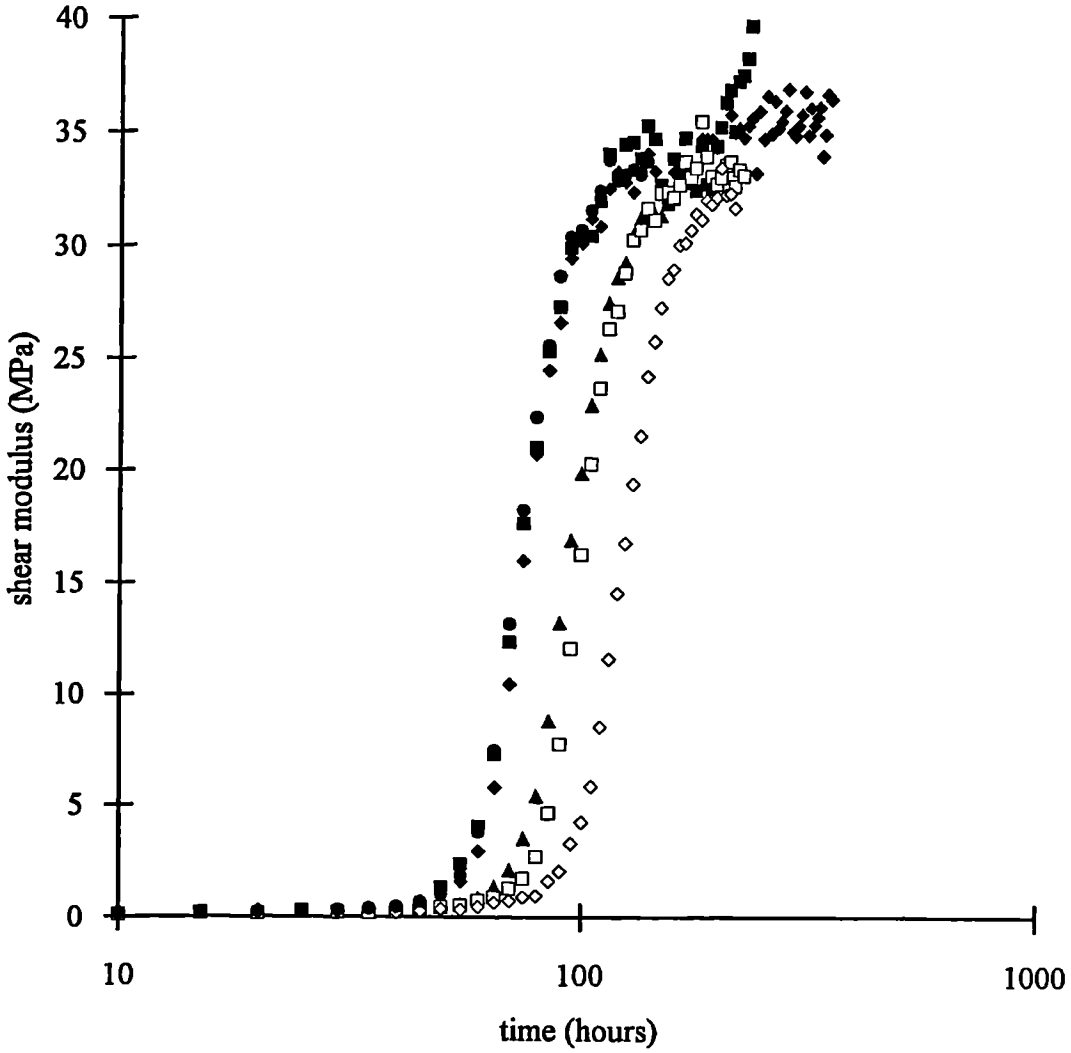

Figure 9.5 Effect of preheating time on the subsequent rate of crystallization at -25°C. All tests carried out on the same sample subjected to the following series of heat treatments between tests: ■ 30 minutes at 70°C, ◆ 30 minutes at 70°C, ▲ 60 minutes at 70°C, □ 60 minutes at 90°C, ◇ 60 minutes at 90°C, ● 30 minutes at 70°C.

its properties to be monitored while crystallization is progressing whereas many other polymers, such as polyethylene, crystallize almost instantaneously when cooled from the melt. Leitner (1955) measured the relationship between Young's modulus and the level of crystallinity, determined from the change in volume, for a sample of unvulcanized natural rubber crystallized at 0°C. In this section the relationship is measured for samples of vulcanized natural rubber with two crosslink densities at three temperatures.

9.5.2 *Calculation of the volume change of a bonded block from a measurement of the change in thickness*

The usual experimental technique employed for volume or density change measurements on natural rubber has been to immerse a sample in a non-swelling liquid in a dilatometer (Wood and Bekkedahl, 1946; Roberts and Mandelkern, 1955) or to use the method of hydrostatic weighings (Gent,1954a; Leitner, 1955). For this work concurrent modulus measurements were needed, making dilatometry measurements inconvenient. Hydrostatic weighings also would have been inconvenient due to the need to maintain the testpiece below ambient temperature while they were carried out. Therefore, the volume change was calculated from measurements of the change in the linear dimension of a bonded block and require an expression for the compression stiffness. The details of the calculation are described below (Thomas, unpublished).

Consider a rectangular block of rubber, bonded to inextensible metal on two opposite faces of area A_0, with a thickness ℓ_0 between the bonded faces (Figure 9.6a). The volume, V_0, is given by

$$V_0 = A_0 \ell_0 \tag{9.1}$$

As crystallization progresses the volume of the block will decrease. The unbonded sides will contract inward producing curved surfaces (Figure 9.6b), and the thickness will also decrease. Now, suppose a force is applied to the bonded surfaces such that the sides become straight (Figure 9.6c).

$$V_0 - \Delta V = A_0 \ell_1 \tag{9.2}$$

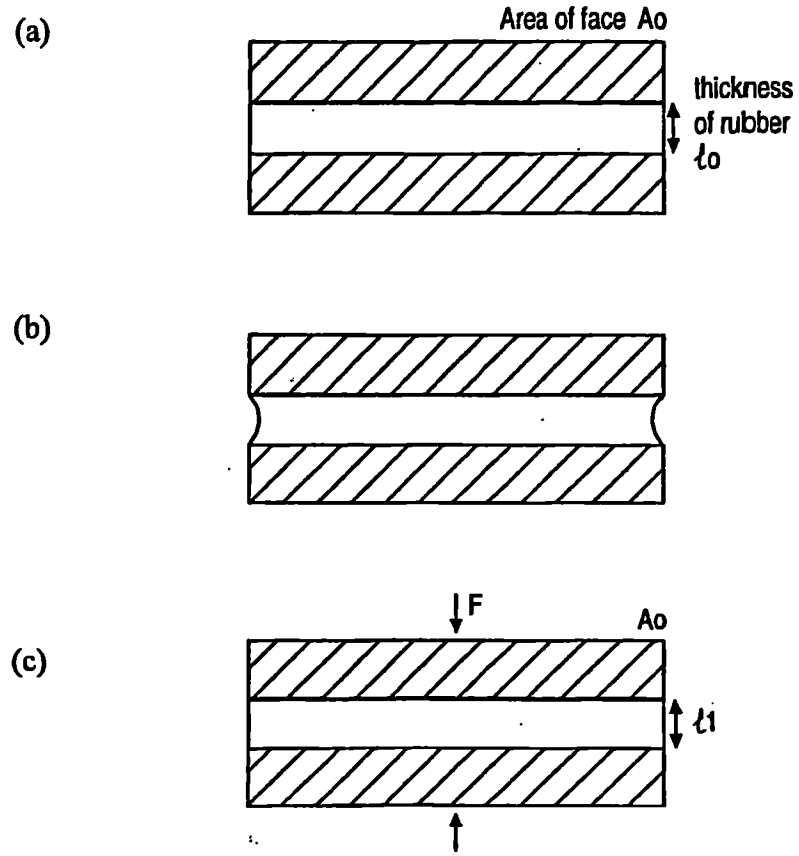

Figure 9.6 Contraction of a block due to crystallization or compression. (a) undeformed block, (b) contraction due to crystallization, (c) compression of the contracted block.

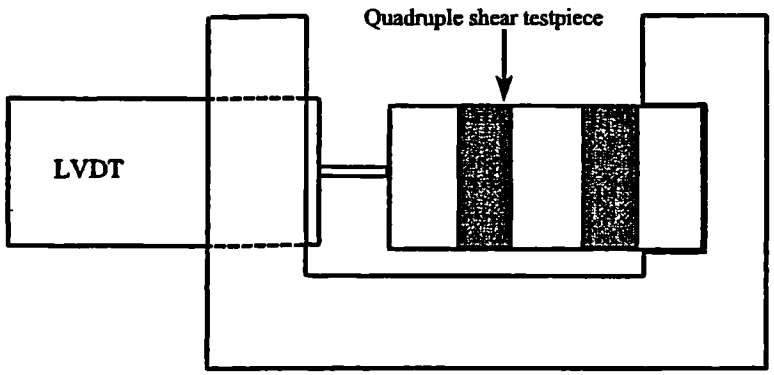

Figure 9.7 Clamp for measuring the change in thickness of a quadruple shear testpice.

where ΔV is the change in volume on crystallization and ℓ_1 is the thickness of the crystalline block. An alternative method of achieving the state shown in Figure 9.6c would be to allow the unbonded rubber block to crystallise and then compress it between lubricated platens. Let the crystalline (but unstrained) block have a cross-sectional area, A_2, and thickness, ℓ_2. Compared to the original amorphous block, the crystalline block has undergone an isotropic contraction. Therefore,

$$A_2 = A_0\left(1 - \frac{2\Delta V}{3V_0}\right) \tag{9.3a}$$

$$\ell_2 = \ell_0\left(1 - \frac{\Delta V}{3V_0}\right) \tag{9.3b}$$

assuming ΔV is small compared to V_0. The force required to produce the stressed state (as shown in Figure 9.6c), assuming that the deformation is small, is

$$F = E\left(\frac{\ell_2 - \ell_1}{\ell_2}\right)A_2 \tag{9.4}$$

where E is Young's Modulus. Therefore, substituting for ℓ_2 from equation (9.3b) and using equations (9.1) and (9.2) to express $\ell_1 = \ell_0(1-^{\Delta V}/_{V_0})$ gives

$$F = \frac{2EA_2\Delta V}{3V_0}\left(\frac{1}{1-\frac{1}{3}\Delta V/V_0}\right)$$

$$\approx \frac{2EA_2\Delta V}{3V_0} \tag{9.5}$$

where powers of ΔV^2 have been neglected. The compression modulus of the bonded block, E_C, is given by

$$E_C = \frac{F(\ell_1 + x)}{A_0 x} \tag{9.6}$$

where x is the contraction from the unstressed to stressed states in the crystalline bonded block. E_C is related to E by a parameter which depends on the shape factor of the

sample. Thus $E_C = cE$ where c is a parameter involving the shape factor. Substitution of equation (9.5) into (9.6) and rearranging gives

$$x = \frac{\frac{2}{3}A_2(\Delta V/V_0)\ell_1}{cA_0 - \frac{2}{3}A_2(\Delta V/V_0)} \qquad (9.7)$$

$$= \frac{2\ell_1 \Delta V}{3c\, V_0} \text{ to a first order in } \Delta V/V_0.$$

The contraction on crystallizing, $y = \ell_0 - \ell_1 - x$. Therefore, to a first order in $\Delta V/V_0$,

$$y = \frac{\Delta V}{V_0}\ell_0\left(1 - \frac{2}{3c}\right) \qquad (9.8)$$

If the shape factor is small, implying that the contraction of the sample is equal in all directions, E_c=E, thus c=1 and equation (9.8) reduces to $y/\ell_0 = \frac{1}{3}\Delta V/V$ as required.

9.5.3 *Experimental method*

A quadruple shear testpiece (Figure 9.2) was fitted in a strain-gauged jig (see Section 9.3.1). The dimensions of each rubber block in the testpiece were 21.3mm in the direction of loading, 12.7mm in the other bonded direction and 3.8mm in thickness. The shape factor, S, was thus calculated from equation (1.61) as 1.05. A small clamp was constructed to enable a second LVDT to be clamped to one of the steel side plates of the quadruple shear testpiece so that it impinged against the other side, thereby measuring the change in thickness (Figure 9.7). The apparatus was placed in a freezer cabinet at the required temperature and measurements of the modulus (see Section (9.3.1)) and change in thickness were made periodically.

Experiments were done at 0°C, -10°C and -25°C on a single testpiece of formulation A. In order to assess whether there was a significant influence of crosslink density, experiments were also done on testpieces containing 2 parts of dicumyl peroxide, (formulations B and C) at -25°C. All testpieces were preconditioned before each experiment by heating at 70°C for 45 minutes.

9.5.4 *Results*

The volume change was calculated from the linear contraction of the testpiece using equation (9.8) with $c = 1+2S^2$ (see equation 1.60). The volume change and modulus were plotted against the logarithm of time in Figures 9.8 and 9.9 respectively. The

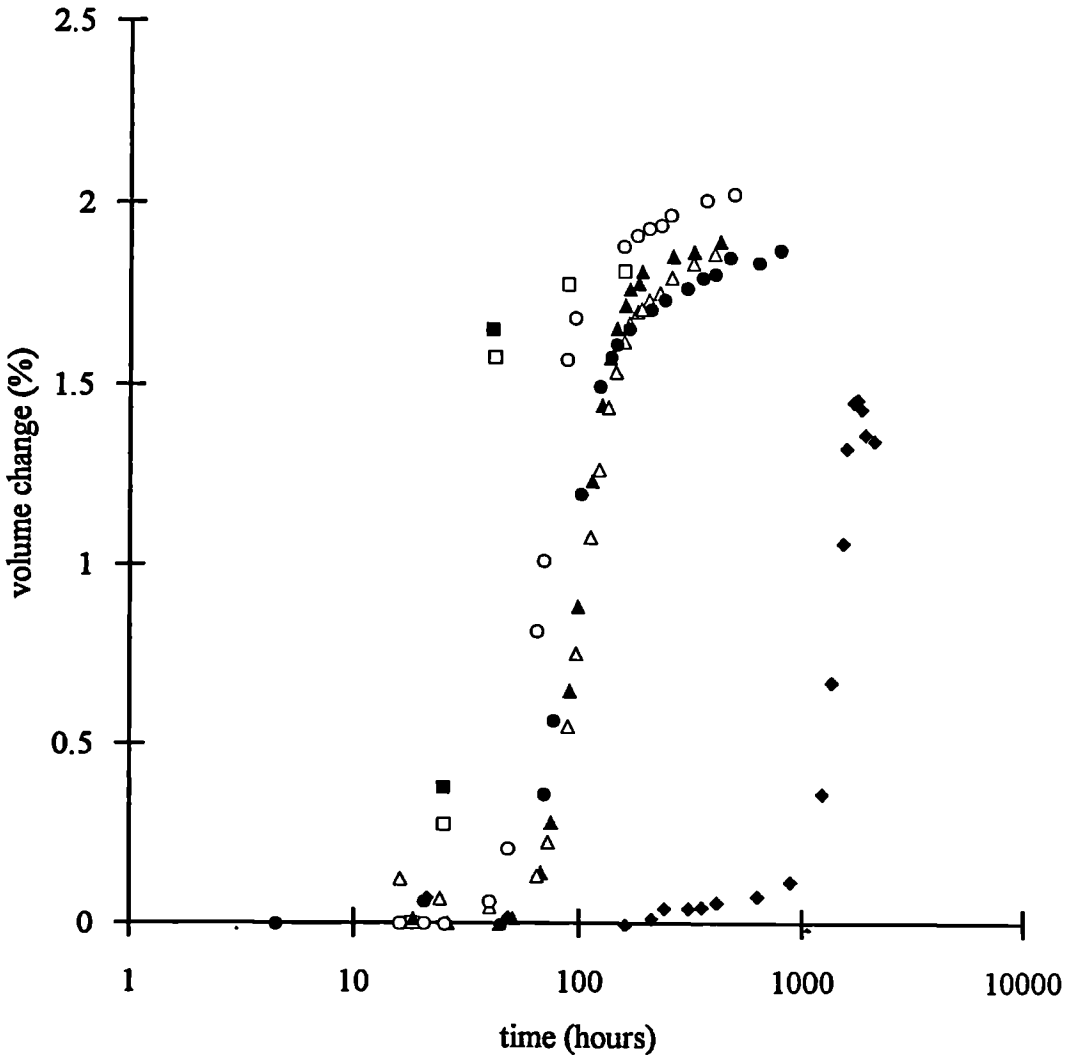

Figure 9.8 Crystallization rates of natural rubbers of different crosslink densities at various temperatures measured by volume change. ●○ 2 pphr dicumyl peroxide at -25°C, ■□ 1 pphr dicumyl peroxide at -25°C, ▲△ 1 pphr dicumyl peroxide at -10°C, ◆ 1 pphr dicumyl peroxide at 0°C.

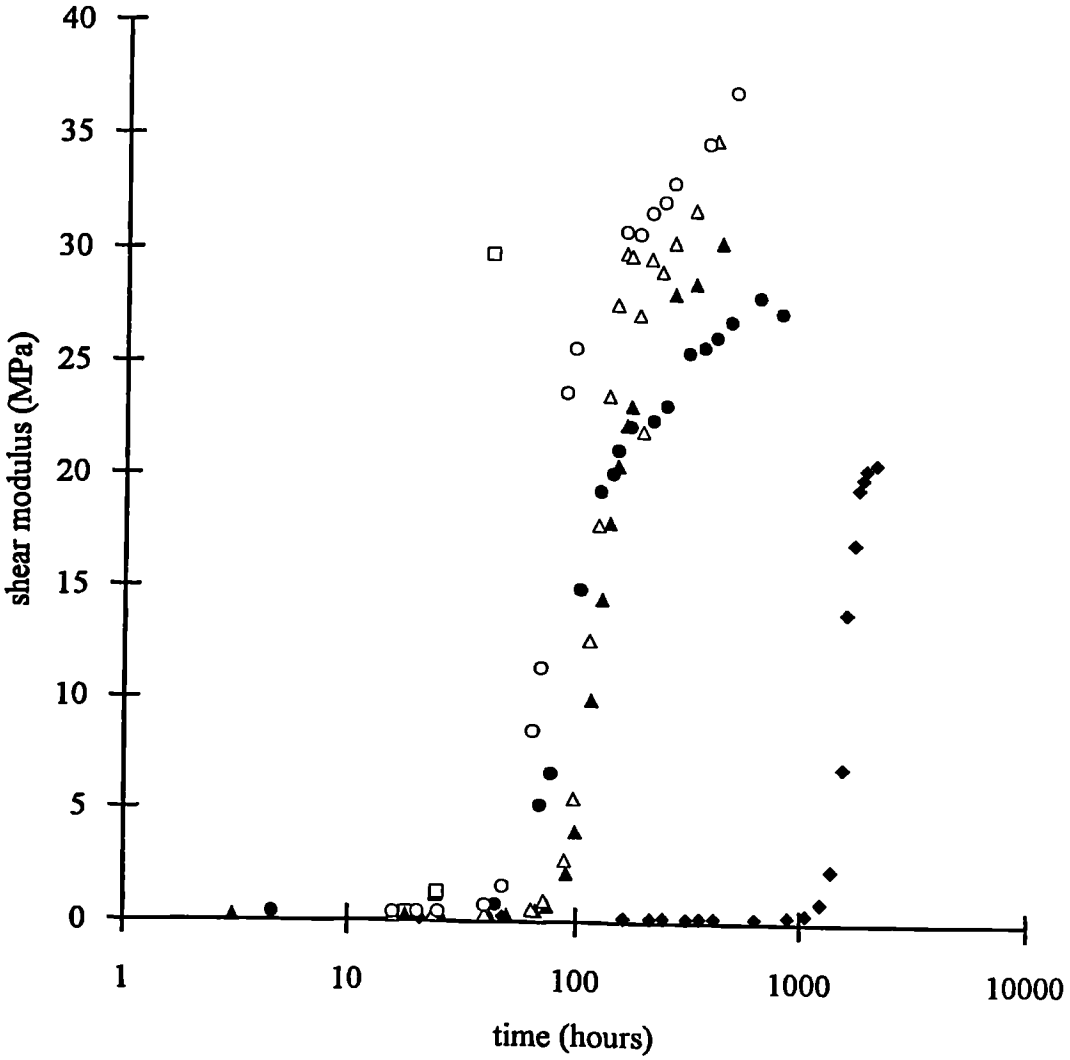

Figure 9.9 Change in shear modulus with crystallization time of natural rubbers of different crosslink densities at various temperatures. ●○ 2 pphr dicumyl peroxide at -25°C, ■□ 1 pphr dicumyl peroxide at -25°C, ▲△ 1 pphr dicumyl peroxide at -10°C, ◆ 1 pphr dicumyl peroxide at 0°C.

direct relationship between the level of crystallinity and the modulus is shown in Figure 9.10, where the modulus has been plotted against the volume change.

9.5.5 *Discussion*

Figures 9.8 and 9.9 show typical sigmoidal crystallization curves with faster rates nearer to the temperature of most rapid crystallization, -25°C. The final volume change of about 2% is consistent with the literature for unvulcanized rubber. (Wood and Bekkedahl, 1946). In Figure 9.10 the volume change-modulus relationship has been compared to Leitner's (1955) results for unvulcanized rubber. In converting Leitner's (1955) plot of Young's modulus, E, to the shear modulus, G, it has been assumed that the partially crystalline rubber obeys small strain elasticity theory and is incompressible so that $E = 3G$.

Although the scatter is large, general agreement between all of the data is seen, indicating that the relationship between crystallinity and modulus is not strongly dependent on either the crystallization temperature or the crosslink density. The absence of a dependency on crosslink density suggests that the modulus of the partially crystalline material is overwhelmingly determined by the modulus of the crystalline regions, rather than the amorphous regions, and that the modulus of the crystalline regions is not dependent on the crosslink density. The absence of a temperature dependence is interesting since it is known that the morphology of the crystals depends on the temperature of crystallization with thicker crystal lamallae being formed at higher temperatures (Andrews et al, 1971). These results suggest that the modulus depends primarily on the volume fraction and overall arrangement of the crystals, not on exact details of their morphology.

The increasing slope of the curve shown on Figure 9.10, especially at low levels of crystallization, indicates that an increase in crystallinity has a greater stiffening effect at higher crystallinities. This is so almost until the final level of crystallinity is reached.

Assuming that a 1% decrease in volume is equivalent to 11% crystallinity (Nyburg, 1954), the maximum amount of crystallinity in these experiments is about 25%. This level of crystallinity resulted in about an 100 fold increase in modulus. As Leitner

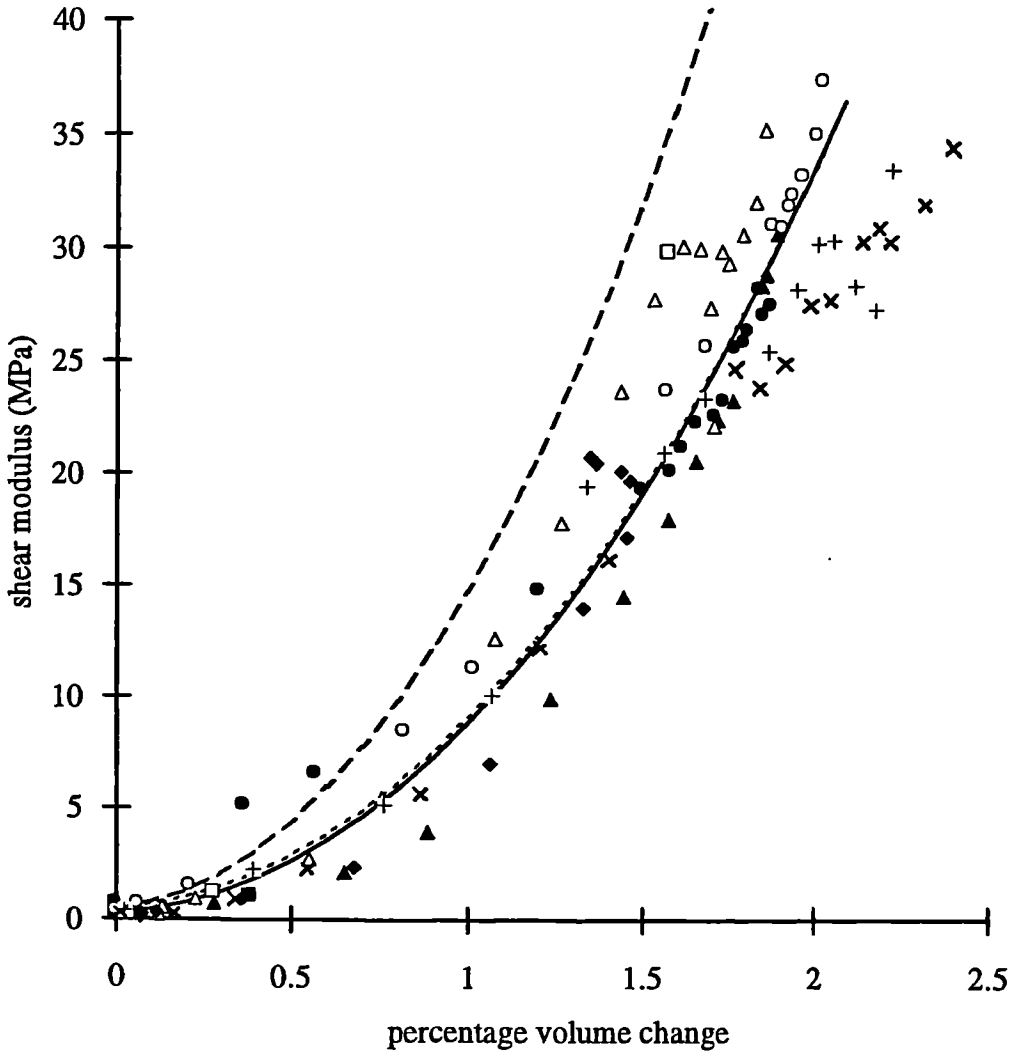

Figure 9.10 Relationship between the amount of crystallinity, as measured by the volume change, and the change in modulus for natural rubber of different crosslink densities crystallized at various temperatures.
●○ 2 pphr dicumyl peroxide at -25°C, ■□ 1 pphr dicumyl peroxide at -25°C, ▲△ 1 pphr dicumyl peroxide at -10°C, ◆ 1 pphr dicumyl peroxide at 0°C, +× unvulcanized rubber crystallized at 0°C (Leitner, 1955). ——— fit to equation (1.69) with α=36.4 and G_g=0.3MPa; – – – fit to equation (1.69) with α=36.4 and G_g=0.5MPa; ------- fit to equation (1.69) with α=27.9 and G_g=0.5MPa;

(1955) observed, if this is to be accounted for by assuming that the crystallites behaved as a rigid filler a very large value for the aspect ratio of the filler particles is required. For example, the shear modulus of the amorphous rubber containing 1 part of dicumyl peroxide is about 0.3MPa and the composite modulus at 22% crystallinity is about 33MPa. Substituting these values for G_g, v and G_f respectively in equation (1.69) gives a value for the aspect ratio of the crystallites, α, of 36.4. The solid line in Figure 9.10 was obtained from equation (1.69) with these values and its shape is consistent with the experimental data. A value of 36.4 for the aspect ratio of the crystallites is not necessarily unreasonable. Electron micrographs indicate that the crystal spherulites have a dendritic structure (Davies and Ong, 1977) for which a high aspect ratio would be expected. However, if a value for α of 36.4 is now used in equation (1.69) for the rubber containing 2 parts of dicumyl peroxide, which has an amorphous shear modulus of about 0.5MPa, the dashed curve in Figure 9.10 is obtained. This is clearly a poor fit to the experimental data and shows that the absence of a dependence of the modulus of the partially cyrstalline rubber on the crosslink density of the amorphous rubber suggests that this simple model of filler reinforcement is inadequate. A good fit may only be obtained from equation (1.69) if the aspect ratio of the crystals is dependent on the crosslink density of the amorphous rubber as shown by the dotted line on Figure 9.10, for which α=27.9. However, such a model of crystal reinforcement is implausible. If the spherulites impinge there is the possibility that the crystalline fraction of the material forms a continuous network. If this is so, the simple model of reinforcement of an elastic matrix by a rigid filler is inadequate; the modulus would be determined predominately from the stiffness of the crystals. This is likely to be much greater than the stiffness of the rubber and a large stiffening effect with a small volume fraction of crystals would be expected, as also would the independence of the modulus of the partially crystalline material to the modulus of the amorphous regions, in contradiction to equation (1.69).

9.6 **Final level of crystallinity**

9.6.1 *Introduction*

Many workers (Wood and Bekkedahl, 1946; Roberts and Mandelkern, 1955; Leitner, 1955) have used the volume change or density change on crystallization to obtain a

measure of the absolute amount of crystallization. The calculation uses Bunn's (1942) value for the density of the unit cell of the crystalline material and a value for the density of the amorphous material. From this Nyburg (1954) estimated that a 1% volume reduction corresponded to 11.2% crystallinity. Taking Roberts and Mandelkerns' (1955) values for the specific volumes of the amorphous and crystalline rubber at 0°C gives 1% volume reduction corresponds to 12.9% crystallinity. In either case the results of the previous section, as well as the other published work (Wood and Bekkedahl, 1946; Roberts and Mandelkern, 1955; Leitner, 1955) suggest that the maximum amount of crystallization in natural rubber is about 25%. The maximum amount of crystallinity may also be obtained from a measure of the latent heat of melting (see Section 1.5.2) and some workers (Burfield, 1984; Zemel and Roland, 1992) have obtained maximum amounts of crystallization in natural rubber as high as 39%.

In this section, the maximum level of crystallinity of natural rubber with one of the formulations used in the previous section was calculated from the latent heat of fusion, measured from differential scanning calorimetry (DSC), and compared to that obtained from the volume decrease in the previous section.

9.6.2 *Experimental method and results*

Small discs, with a nominal diameter of 5mm and thickness of 1mm, were cut from a single sheet of natural rubber of formulation A. They were encapsulated in aluminium foil to ensure even heating during the DSC measurement and crystallized at -25°C. After various intervals of time, two or four of the samples were placed in a precooled glass tube and transported quickly in a flask of dry ice to the sample chamber of a Perkin Elmer DSC 2B machine. The dry ice was needed to prevent melting of the crystals which would occur 10 to 15°C above their crystallization temperature (Wood and Bekkedahl, 1946). The samples were heated at a rate of 20°C per minute.

The percentage crystallinity was calculated from the mass of the sample and the area under the DSC exotherm assuming a value of 64.0 J/g for the latent heat of fusion of natural rubber (Roberts and Mandelkern, 1955). The results are shown in Table 9.2.

Table 9.2: DSC measurement of crystallinity of natural rubber after various times at -25°C				
time at -25°C (days)	percentage crystallinity			
1		19.5	18.2	
2		30.9	26.8	
3		31.3	29.9	
4		29.6	29.6	
9		35.1	34.2	
102	36.9	36.9	35.1	38.4

9.6.3 *Discussion*

Most of the crystallization occurred within one day at -25°C. The maximum amount of crystallinity, obtained from the four values after 102 days, was 37±2%. This figure is considerably higher than the value of 25% estimated from the volume change of the same rubber formulation (see Section 9.5.5). Similar discrepancies exist in the literature; a value of about 30% is typically quoted from volume change measurements (Roberts and Mandelkern, 1955) whereas Burfield (1984) and Zemel and Roland (1992) obtained 39% from DSC measurements. On the other hand, Kim and Mandelkern (1972) obtained good agreement between the two techniques. It is difficult to identify a cause for these discrepancies. The fact that Kim and Mandelkerns' (1972) value of 65.3 J/g for the enthalpy change of melting of natural rubber correlates well with 64.0J/g obtained by Roberts and Mandelkern (1955) by a technique independent of knowledge of the degree of crystallinity (see Section 1.5.2 iii) gives credibility to their results. The higher values obtained from D.S.C. measurements by more recent workers also depend on the use of one of these values so cannot be accounted for by assuming that the discrepancies arise from differences in the measurement techniques.

9.7 Yielding behaviour of partially crystalline rubber

9.7.1 *Introduction*

Since it is possible to obtain a wide range of amounts of crystallization in natural rubber by varying the crystallization time, it is a convenient material on which to investigate the effect of the amount of crystallization on the yielding behaviour of crystalline polymers.

9.7.2 *Experimental method*

A double shear testpiece of formulation A was conditioned by heating for one hour at 70°C before the start of each experiment, and then allowing it to stand at room temperature for between 3 and 20 hours. The testpiece was fitted in the slow cycling rig which had been pre-cooled to -25°C. It was maintained at -25°C without cycling for a specified time between 18 and 169 hours to allow it to reach the required level of crystallization. After the required time had elapsed, the testpiece was subjected to two cycles of ±50% shear strain. The cycle period was 50 minutes.

9.7.3 *Results*

The results for the first loading cycle are plotted in Figure 9.11. Typical results for the two cycles are given in Figure 9.12.

9.7.4 *Discussion*

The range of crystallization times resulted in a large range of initial stiffnesses. A few inconsistencies are apparent on Figure 9.11; the last two or three tests appeared softer than expected, suggesting that some irreversible damage was occurring during the tests. This softening was also observed on subsequent tests which have been excluded from Figure 9.11.

It is clear, however, that the rubbers with a high initial crystallinity support a higher stress before yielding occurs. The yield point is more pronounced in the more crystalline rubbers with little or no further increase in force being required for further deformation. The rubbers with low levels of crystallinity show approximately linear behaviour with no obvious yield point, similar to the behaviour of the amorphous material, although the greater stiffnesses of these slightly crystalline rubbers compared to amorphous rubber suggests that the crystallites have a significant reinforcing effect on the amorphous rubber.

Comparison of the first and second cycle behaviour (Figure 9.12) shows a considerable softening on the second cycle in the case of yielded material, but very much smaller differences for the more linear rubbers. The second cycle stiffness is determined by the extent of softening achieved during the first cycle - the maximum stress reached at the

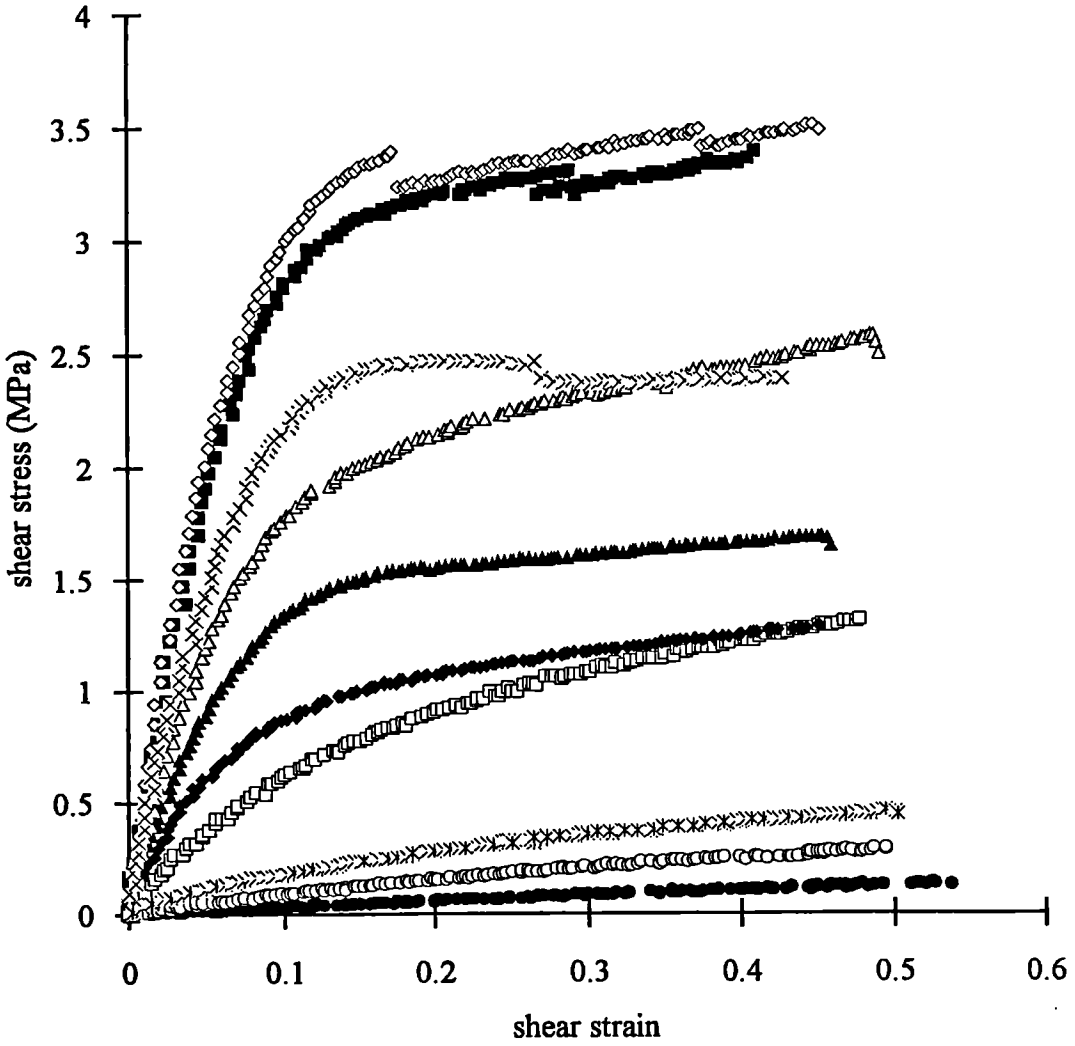

Figure 9.11 Effect of crystallization time, and hence amount of crystallinity, on the subsequent stress-strain behaviour of partially crystalline natural rubber. The testpieces were maintained at -25 °C for the times given, listed in the order that the experiments were done on a single testpiece.
■ 43 hours, 35 minutes, □ 30 hours, 24 minutes, ◆ 40 hours, 5 minutes, ◇ 45 hours, 43 minutes, ▲ 37 hours, 51 minutes, ▵ 41 hours, 37 minutes, ● 18 hours, 21 minutes, ○ 25 hours, 38 minutes, × 169 hours, 6 minutes, ∗ 28 hours, 48 minutes.

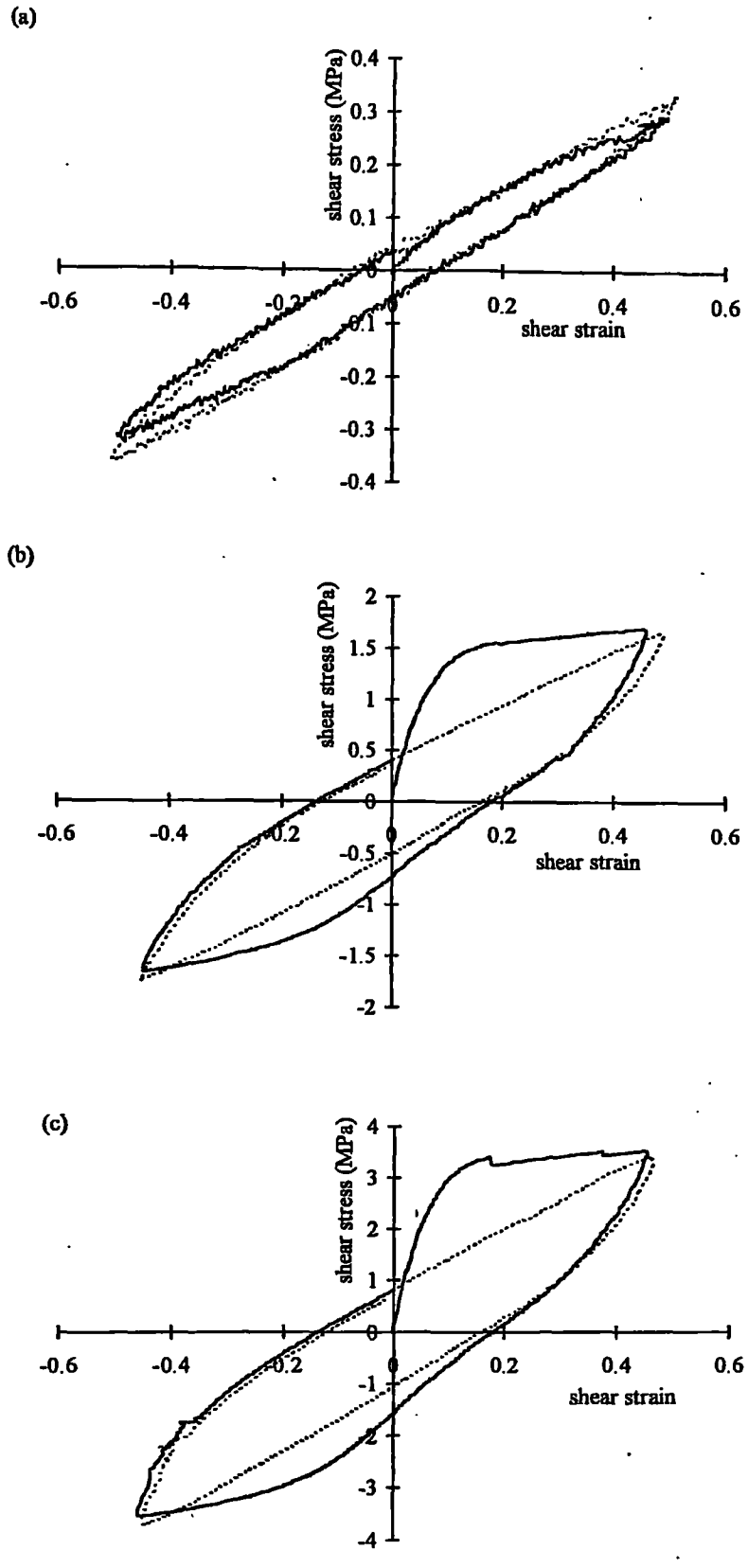

Figure 9.12 Stress-strain behaviour of partially crystalline natural rubber of varying amounts of crystallinity. Crystallization times were (a) 25 hours, 38 minutes, (b) 37 hours, 51 minutes, (c) 45 hours, 43 minutes. Solid lines indicate first cycle and dotted lines second cycle.

maximum strain is the same for both cycles. The first loading cycle in the reverse direction shows a less pronounced yielding effect than in the forward direction, presumably because some damage has already occurred during straining in the forward direction.

The highly crystalline material shows considerable hysteresis - substantially more than the less crystalline specimens. This is expected; crystallization has also been put forward as a possible cause of an increase in hysteresis in unfilled rubbers at high strains. (Harwood and Schallamach, 1967).

The significantly higher stiffness of the yielded material on the second cycle compared to the amorphous material, and the rapid rate of restiffening of yielded rubber if maintained at low temperature (Pettifor and Coveney, 1989) are both indicative of a distinction between yielding and melting behaviour, though yielding could be similar to a partial melting, involving the disordering of some crystals. Further elucidation of the mechanisms involved would require investigation of the behaviour at the microscopic level.

9.8 Conclusions

1. Crystallization kinetics of natural rubber is highly sensitive to minor variability of samples arising from variations in batches of rubber or storage times and temperatures. The most likely reason for this sensitivity is different numbers of nucleation sites.

2. The increase in modulus with amount of crystallization of natural rubber is largely independent of the crosslink density of the amorphous material and the detailed morphology of the crystals. A reasonable fit to experimental data may be obtained using a simple equation for the reinforcement of a rubber with a rigid filler. However, such a model requires the aspect ratio of the crystals to depend on the modulus of the amorphous rubber which is unlikely. Thus a more sophisticated model is required to account properly for the behaviour.

3. The maximum level of crystallization in natural rubber is about 30%, although considerable variations exist between reported values.

4. Partially crystalline natural rubber exhibits yielding behaviour analogous to other partially crystalline polymers. The yield stress increases with the volume fraction of crystals whereas the yield strain is approximately constant.

CHAPTER 10

Final conclusions and suggestions for further work

10.1 Final conclusions

Experimental studies of the stress-strain behaviour of rubber have supported the use of a strain energy function to describe the first cycle quasistatic loading curve. Although not completely general, the use of techniques such as the split pure shear technique are recommended as giving sufficient information for the evaluation of $\partial W/\partial I_1$ and $\partial W/\partial I_2$. Measurement of normal stresses for the conventional simple shear testpiece does not lend itself to interpretation in terms of values of $\partial W/\partial I_1$ and $\partial W/\partial I_2$ because of the influence of the stress free boundaries. These also cause the shear stress to depart from its true value, especially at small strains, affecting the precision of simple shear data by a few percent. The applicability of the pure shear data to combinations of I_1 and I_2 not achievable in pure shear is justified by the good agreement of measurements in pure shear with those in tension and compression using appropriate assumptions about the dependence of $\partial W/\partial I_1$ and $\partial W/\partial I_2$ on I_1 and I_2.

Use of the simplifying assumption that the strain energy function is a function of I_1 only (Gregory, 1979) is recommended because, first, it enables the characterisation of the rubber to be obtained from a simple uniaxial test and, second, its inaccuracies are likely to be smaller than those caused by differences between rubber batches or anisotropy in rubber components. If an explicit functional form of the strain energy function is required,

$$W = \frac{A}{2-n}(I_1-3)^{1-n/2} + \frac{B}{2+m}(I_1-3)^{1+m/2} + \text{constant}$$

(Gregory et al, 1997) has been found to be reasonably accurate and straightforward to use. This equation is to be preferred over the more popular truncated forms of

$$W = \Sigma_{ij} C_{ij} (I_1-3)^i (I_2-3)^j$$

Characterisation of the behaviour in subsequent cycles, or in circumstances where small strains are superimposed upon larger ones such as in dynamic analyses, is more problematic owing to the significant departures from elasticity exhibited by filled natural rubber and many synthetic rubbers. It was shown that the behaviour of filled natural rubber under a small torsion superimposed on a large uniaxial tension cannot be described by a strain energy function. Also, inelastic features, such as stress softening and stress relaxation, are ignored in hyperelastic models. In these circumstances, care must be taken to ensure that experimental characterisations are carried out under conditions appropriate for the application. Further difficulties arise from the fact that the relative amounts of softening due to Mullins' effect or stress relaxation were found, for some rubbers, to depend on the direction in the pure shear experiment. Also, the direction of previous stresses influenced the amount of stress softening. These features limit the applicability of isotropic models based on symmetric functions of the strains, such as those based on modified forms of the strain energy. Nevertheless, isotropic models for Mullins' effect and stress relaxation have been found to give useful, though not perfect, representations of physical behaviour and the additional complexity of anisotropic models is not always justified.

Studies of a rubber containing a compressible filler confirmed the use of straightforward models for describing the behaviour of the materials. In particular, sensible values for the bulk and shear moduli of the compressible material were obtained from measurements of the compression stiffness of bonded pads and the use of a suitable equation, and a plausible estimate of the volume fraction of filler was obtained from modelling the material as an incompressible matrix containing voids.

The stiffening of partially crystalline rubber was found to be independent of the crosslink density of the amorphous rubber and the detailed morphology of the crystals.

10.2 Suggestions for further work

1. The quasistatic stress-strain characterisation focussed mainly on natural rubber, although three synthetic rubbers were investigated in Chapter 5. Further studies of synthetic rubbers of known molecular structure, such as a series of block

copolymers with differing sizes of hard and soft blocks would be worthwhile. The split pure shear technique would enable $\partial W/\partial I_1$ and $\partial W/\partial I_2$ to be evaluated for these materials and the conclusions compared with those for natural rubber.

2. Further development of the split pure shear technique is required if it is to be used with confidence for very sensitive measurements, such as evaluating $\partial W/\partial I_1$ and $\partial W/\partial I_2$ at small strains, and for detailed evaluation of stress relaxation behaviour. One possible improvement would be to enable the width of the slits to be varied, with the aim of reducing transverse stresses introduced during clamping of the testpiece and reducing difficulties associated with rubber protruding into the slit.

3. Although in Chapter 6, measurement of $\partial W/\partial I_2$ from the normal force in simple shear was obscured by the effect of the free edges in the testpiece, reasonably accurate measurements could be obtained from a testpiece with a much higher shape factor; the results of Chapter 6 (Table 6.1) suggest a roughly linear relationship between shape factor and nominal stress. Thus a tenfold increase in shape factor would result in one tenth of the component due to the free edges. Development of such a technique could be reconsidered as an alternative to the split pure shear technique.

4. The existence of the $\partial W/\partial I_2$ term in unfilled rubber is evidence of departures from the assumptions of the statistical theory and has been attributed to molecular features such as chain entanglements. If this is so, $\partial W/\partial I_2$ would be expected to disappear in highly swollen rubber. Measurement of $\partial W/\partial I_2$ for swollen rubbers would help establish the origins of the $\partial W/\partial I_2$ term.

5. Finite element analysis of a rectangular rubber block revealed a significant difference between the apparent shear modulus of a conventional simple shear testpiece with stress free edges and the true shear modulus, especially at small strains. An experimental study, using simple shear testpieces of varying thicknesses, could be carried out, together with measurements in pure shear and further finite element analysis, to confirm quantitatively the effect of testpiece

geometry on measurement of the shear modulus.

6. Work on characterising the quasistatic behaviour of conventional rubbers, both filled and unfilled, is extensive and only minor further progress in this area is likely. However, much difficulty and uncertainty exists in characterising rubbers for dynamic applications and in modelling effects such as stress softening, hysteresis and stress relaxation. There is scope for further development of constitutive models and for experimental evaluation of existing models.

7. The cause of the significant discrepancy between the various values reported for the maximum level of crystallinity in natural rubber requires further investigation, perhaps through more thorough D.S.C. measurements.

REFERENCES

Ahmadi, H.R. and Muhr, A.H. (1992). "Vibration control using rubber components." Int. J. of Materials and Product Technology, **7**, 65.

Ahmadi, H.R. and Muhr, A.H. (1997). "Modelling dynamic properties of filled rubber." Plastics, Rubbers and Composites Processing and Applications, **26**, 451.

Alexander, H. (1968). "A constitutive relation for rubber-like materials" Int. J. of Engineering Science, **6**, 549.

Andrews, E.H. (1962). "Spherulitic morphology in thin films of natural rubber." Proc. Royal Society. **A270**, 232.

Andrews, E.H. (1964). "Crystalline morphology in thin films of natural rubber. II. Crystallization under strain." Proc. Royal Society, **A277**, 562.

Andrews, E.H., Owen, P.J. and Singh, A. (1971). "Microkinetics of lamellar crystallization in a long chain polymer." Proc. Royal Society, **A324**, 79.

Arruda, E.M. and Boyce, M.C. (1993). "A three dimensional constitutive model for the large stretch behaviour of rubber elastic materials." J. Mech. Phys. Solids, **41**, 389.

Avrami, M. (1940). "Kinetics of phase change. II Transformation-time relations for random distribution of nuclei." J. Chemical Physics, **8**, 212.

Becker, G.W. (1967). "On the phenomenological description of the non-linear deformation behaviour of rubberlike high polymers." J. Polymer Science, **C16**, 2893.

Bernstein, B., Kearsley, E.A. and Zapas, L.J. (1963). "A study of stress relaxation with finite strain." Trans. Soc. Rheology, **7**, 391.

Besdo, D. and Ihlemann, J. (1996). "Zur Modellierung des Stoffverhaltens von Elastomeren." Kautschuk Gummi Kunstoffe, **49**, 495.

Blatz, P.J. and Ko, W.L. (1962). "Application of the finite elasticity theory to the deformation of rubbery materials." Trans. Soc. Rheology, **6**, 223.

Blatz, P.J., Sharda, S.C. and Tschoegl, N.W. (1974). "Strain energy function for rubberlike materials based on a generalized measure of strain." Trans. Society Rheology, **18**, 145.

Bonart, R. (1968). "X-ray investigations concerning the physical structure of crosslinking in segmented urethane elastomers." J. Macromolecular Science, **B2(1)**, 115.

Boonstra, B.B.S.T. (1950). "Stress-strain properties of natural rubber under biaxial strain." J. Applied Physics, **21**, 1098.

Boonstra, B.B. and Medalia, A.I. (1963). "Effect of carbon black dispersion on the mechanical properties of rubber vulcanizates." Rubber Chemistry and Technology, **36**, 115.

Bridgman, P.W. (1945). "The compression of sixty-one solid substances to 25000kg/cm^2 determined by a new rapid method." Proc. American Academy of Arts and Sciences. **76**, 9.

Bristow, G.M. and Tiller, R.F. (1970). "Correlation of structure and properties of natural rubber vulcanizates." Kautschuk Gummi Kunstoffe, **23**, 55

Bueche, F. (1960). "Molecular basis for the Mullins' effect." J. Applied Polymer Science, **4**, 107.

Bueche, F. (1961). "Mullins effect and rubber-filler interactions." J. Applied Polymer Science, **5**, 271.

Bunn, C.W. (1942). "Molecular structure and rubber-like elasticity. I The crystal structure of β gutta-percha, rubber and polychloroprene." Proc. Royal Society **A180**, 40.

Burfield, D.R. (1984). "Comparative d.s.c. studies of the crystallization of natural rubber and its synthetic analogues." Polymer, **25**, 1823.

Carmichael, A.J. and Holdaway, H.W. (1961). "Phenomenological elastomechanical behaviour of rubber over wide ranges of strains." J. Applied Physics, **32**, 159.

Chalhoub, M.S. and Kelly, J.M. (1986). "Reduction of the stiffness of rubber bearings due to compressibility." University of California, Berkeley. Report no. UCB/SESM-86/06.

Chow, C.L. and Cundiff, C.H. (1987). "On the characterization of mechanical properties of rubber vulcanizates." Tire Science and Technology, **15**, 73.

Cohen, L.H. (1947). "The mechanism of reinforcement of elastomers by pigments." India Rubber World, **117**, 343.

Cook, J.W. (1994). "Factors affecting the rolling friction of a hard sphere on a viscoelastic substrate." Project submitted in part fulfilment of B. Eng. (Polymer Engineering), University of North London.

Conversey, F. (1967). "Appareils d'appui en caoutchouc fretté pour ouvrages d'art." Annales des Ponts et Chausseés, **6**, 341.

Coveney, V.A., Johnson, D.E. and Turner, D.M. (1995). "A triboelastic model for the cyclic mechanical behaviour of filled vulcanizates." Rubber Chemistry and Technology, **68**, 660.

Davies, C.K.L., De, D.K. and Thomas, A.G. (1994) "Characterization of the behaviour of rubber for engineering design purposes. I Stress-strain relations." Rubber Chemistry and Technology, **67**, 716.

Davies, C.K.L., De, D.K. and Thomas, A.G. (1996) "Characterization of the behaviour of rubber for engineering design purposes. II Stress relaxation under repeated stressing." Progress in Rubber and Plastics Technology, **12**, 208.

Davies, C.K.L. and Ong E.L. (1977). "Morphology of trans-1,4-polyisoprene crystallized in thin films." J. Materials Science, **12**, 2165.

Derham, C.J. (1973). "Creep and stress relaxation of rubbers - the effects of stress history and temperature changes." J. Materials Science, **8**, 1023.

Derham, C.J. and Thomas, A.G. (1977). "Creep of rubber under repeated stressing." Rubber Chemistry and Technology, **50**, 397.

Dillon, J.H., Prettyman, I.B. and Hall, G.L. (1944). "Hysteresis and elastic properties of rubberlike materials under dynamic shear stresses." J. Applied Physics, **15**, 309.

Einstein, A. (1906). "Eine neue Bestimmung der Moleküldimensionen." Annalen der Physik, **19**, 289; with additions in (1911) Annalen der Physik, **34**, 591.

Ferry, J.D. (1970) "Viscoelastic properties of polymers." 2nd edition, Wiley.

Finney, R.H. and Kumar, A. (1988). "Development of material constants for non-linear finite element analysis." Rubber Chemistry and Technology, **61**, 879.

Fletcher, W.P. and Gent, A.N. (1953). "Non linearity in the dynamic properties of vulcanized rubber compounds." Trans. Institution Rubber Industries, **29**, 266.

Flory, P.J. (1947). "Thermodynamics of crystallization in high polymers. I Crystallization induced by stretching." J. Chemical Physics, **15**, 397.

Flory, P.J. (1953). "Principles of polymer chemistry." Cornell, Ithaca, N.Y.

Flory, P.J. and Rehner, J. (1943). "Statistical mechanics of cross-linked polymer networks. I Rubberlike elasticity." J. Chemical Physics, **11**, 512.

Fukahori, Y. and Seki, W. (1992). "Molecular behaviour of elastomeric materials under large deformation. I Re-evaluation of the Mooney-Rivlin plot." Polymer, **33**, 502.

Fuller, K.N.G., Gough, J. and Ahmadi, H.R. (1996). "Predicting the response of high damping rubber bearings using simplified models and finite element analysis." Proceedings of the International atomic energy agency research co-ordination meeting, St. Petersburg, Russia. May 1996.

Fuller, K.N.G., Gough, J., Ahmadi, H.R. and Dusi, A. (1997) "Contribution of the United Kingdom to the activities on intercomparison of analysis methods for seismically isolated nuclear structures." Proceedings of the international Post-SMIRT conference seminar, Taormina, Sicily, Italy. August 1997.

Gee, G., Stern, J. and Treloar, L.R.G. (1950). "Volume changes in the stretching of vulcanized natural rubber." Trans. Faraday Society, **46**, 1101.

Gent, A.N. (1954a). "Crystallization and the relaxation of stretched natural rubber vulcanizates." Trans. Faraday Society, **50**, 521.

Gent, A.N. (1954b). "Crystallization in natural rubber. II The influence of impurities." Trans.Institution Rubber Industries, **30**, 139.

Gent, A.N. (1954c). "Crystallization in natural rubber. III Filled compounds." Trans. Institution Rubber Industries, **30**, 144

Gent, A.N. (1955). "Crystallization in natural rubber. IV Temperature dependence." J. Polymer Science, **18**, 321.

Gent, A.N. (1962a). "Relaxation processes in vulcanized rubber. I. Relation among stress relaxation, creep, recovery and hysteresis." J. Applied Polymer Science, **6**, 433.

Gent, A.N. (1962b). "Relaxation processes in vulcanized rubber. III. Relaxation at large strains and the effect of fillers." Proc. 4th Rubber Technology Conference, London.

*Gent, A.N. and Lindley, P.B. (1959). "The compression of bonded rubber blocks." Proc. Institution Mechanical Engineers, **173**, 111.

Gent, A.N. and Madan, S. (1989). "Plastic yielding of partially crystalline polymers." J. Polymer Science, **B27**, 1529.

Gent, A.N. and Meinecke, E.A. (1970). "Compression, bending and shear of bonded rubber blocks." Polymer Engineering and Science, **10**, 48.

Gent, A.N. and Thomas, A.G. (1959). "The deformation of foamed elastic materials." J. Applied Polymer Science, **1**, 107.

Gough, J. (1805). "A description of a property of caoutchouc or Indian rubber." Mem. Lit. Phil. Soc. Manchester, **1**, 288.

Green, A.E. and Zerna, W. (1954). "Theoretical elasticity." O.U.P.

Gregory, I.H. and Muhr, A.H. (1999). "Stiffness and fracture analysis of bonded rubber blocks in simple shear." Finite Element Analysis of Elastomers. Professional engineering publishing, ed. D. Boast & V.A. Coveney, 265.

*Gent, A.N. (1996). "A new constitutive relation for rubber." Rubber Chemistry and Technology, **69**, 59.

Gregory, I.H., Muhr, A.H. and Stephens, I.J. (1997). "Engineering applications of rubber in simple extension." Plastics, Rubbers and Composites: Processing and Applications, **26**, 118.

Gregory, M.J. (1979). "The stress/strain behaviour of filled rubbers at moderate strains." Plastics and Rubbers: Materials and Applications, **4**, 184.

Gregory, M.J. (1984). "Measurement of rubber properties for design." Polymer Testing, **4**, 211.

Gregory, M.J. (1985). "Dynamic properties of rubber in automotive engineering." Elastomerics, **117, no. 11**, 19.

Gumbrell, S.M., Mullins, L. and Rivlin, R.S. (1953). "Departures of the elastic behaviour of rubbers in simple extension from the kinetic theory" Trans. Faraday Society, **49**, 1495.

Guth, E. (1945). "Theory of filler reinforcement." J. Applied Physics, **16**, 20.

Halpin, J.C. and Kardos, J.L. (1972). "Moduli of crystalline polymers employing composite theory." J. Applied Physics, **43**, 2235.

Hart-Smith, L.J. (1966). "Elasticity parameters for finite deformations of rubber-like materials." Zeitschrift fur Angewandete Mathematik Physik, **17**, 608.

Harwood, J.A.C., Mullins, L. and Payne, A,R. (1965). "Stress softening in natural rubber vulcanizates. II Stress softening effects in pure gum and filler loaded rubbers." J. Applied Polymer Science, **9**, 3011.

Harwood, J.A.C., Mullins, L. and Payne, A.R. (1967). "Stress softening in rubbers - a review." J.Institution Rubber Industries, **1**, 17.

Harwood, J.A.C., Payne, A.R. and Smith, J.F. (1969). "A new approach to rubber reinforcement." Kautschuk Gummi Kunstoffe, **22**, 548.

Harwood, J.A.C. and Schallamach, A. (1967). "Dynamic behaviour of natural rubber during large extensions." J. Applied Polymer Science, **2**, 1835,

Hepburn, C. (1982). "Polyurethane elastomers." Applied Science Publishing.

Hillmer, K-H. and Scheele, W. (1970). "Degradation of highly elastic polymers. VI The intermittent chemo-stress relaxation of crosslinked 1,5-polyenes." Rubber Chemistry and Technology, **43**, 788.

Holownia, B.P. (1975). "Effect of carbon black on Poisson's ratio of elastomers." Rubber Chemistry and Technology, **48**, 246.

Holt, W.L. and McPherson, A.T. (1936). "Change of volume of rubber on stretching: effects of time, elongation and temperature." J. National Bureau of Standards, **17**, 657.

Isihara, A., Hashitsume, N. and Tatibana, M. (1951). "Statistical theory of rubber like elasticity. IV Two dimensional stretching." J. Chemical Physics, **19**, 1508.

James, A.G. and Green, A. (1975). "Strain energy functions of rubber. II The characterisation of filled vulcanizates." J. Applied Polymer Science, **19**, 2319.

James, A.G., Green, A. and Simpson, G.M. (1975). "Strain energy functions of rubber. I characterisation of gum vulcanizates." J. Applied Polymer Science, **19**, 2033.

James, H.M. and Guth, E. (1943) "Theory of the elastic properties of rubber" J. Chemical Physics, **11**, 455.

Johnson, M.A. and Beatty, M.F. (1993). "The Mullins' effect in uniaxial extension and its influence on the transverse vibration of a rubber string." Continuum Mechanics and Thermodynamics, **5**, 83.

Jones, D.F. and Treloar, L.R.G. (1975). "The properties of rubber in pure homogeneous strain." J. Physics, **D8**, 1285.

Kawabata, S. (1973). "Fracture and mechanical behaviour of rubber-like polymers under finite deformation in biaxial stress field." J. Macromolecular Science, **B8**, 605.

Kawabata, S., Matsuda, M., Tei, K. and Kawai, H. (1981). "Experimental survey of the strain energy density function of isoprene rubber vulcanizate." Macromolecules, **14**, 154.

Kawabata, S., Yamashita, Y., Ooyama, H. and Yoshida, S. (1995). "Mechanism of carbon-black reinforcement of rubber vulcanizate." Rubber Chemistry and Technology, **68**, 311.

Keller, A. (1959). "Electron microscope - electron diffraction investigations of the crystalline texture of polyamides." J. Polymer Science, **36**, 361.

Keller, A. and O'Connor, A. (1958). "Study of single crystals and their association in polymers." Disc. Faraday Society, **25**, 114.

Kerner, E.H. (1956). "The elastic and thermo-elastic properties of composite media." Proc. Physical Society, **B69**, 808.

Kim, H-G. and Mandelkern, L. (1968). "Crystallization kinetics of stretched natural rubber." J. Polymer Science, **A2,6**, 181.

Kim, H-G. and Mandelkern, L. (1972). "Multiple melting transitions in natural rubber." J. Polymer Science, **A2,10**, 1125.

Klüppel, M. and Heinrich, G. (1995). "Fractal structures in carbon black reinforced rubbers." Rubber Chemistry and Technology, **68**, 623.

Kugler, H.P., Stacer, R.G. and Steimle, C. (1990). "Direct measurement of Poisson's ratio in elastomers." Rubber Chemistry and Technology, **63**, 473.

Kuhn, W. (1936). "Beziehungen zwischen Molekülgröße, statistischer Molekülgestalt und elastischen Eigenschaften hochpolymerer Stoffe." Kolloid-Zeitschrift, **76**, 258.

Kuhn, W. and Grün, F. (1942). "Beziehungen zwischen elastischen Konstanten und Dehnungsdoppelbrechung hochelastischer Stoffe." Kolloid-Zeitschrift, **101**, 248.

Leitner, M. (1955). "Young's modulus of crystalline, unstretched rubber." Trans. Faraday Society, **51**, 1015.

Lindley, P.B. (1968). "Effect of Poisson's ratio on compression modulus." J. Strain Analysis, **3**, 142.

Lindley, P.B. (1974). "Engineering design with natural rubber." 4th edition, T.A.R.R.C., Brickendonbury, Hertford, U.K.

* Lindley, P.B. and Teo, S.C. (1978). "Some numerical stiffnesses of soft elastic blocks bonded to rigid end plates." Plastics and Rubbers: Materials and Applications, **3**, 113.

Mackenzie, J.K. (1950). "The elastic constants of a solid containing spherical holes." Proc. Physical Society, **B63**, 2.

McKenna, G.B. and Zapas, L.J. (1981). "Response of carbon black filled butyl rubber to cyclic loading." Rubber Chemistry and Technology, **54**, 718.

Medalia, A.I. (1974). "Filler aggregates and their effect on reinforcement." Rubber Chemistry and Technology, **47**, 411.

Medalia, A.I. (1978). "Effect of carbon black on dynamic properties of rubber vulcanizates." Rubber Chemistry and Technology, **51**, 437.

Miehe, C. (1995). "Discontinuous and continuous damage evolution in Ogden-type large-strain elastic materials." Eur. J. Mech A./Solids, **14**, 697.

Moghe, S.R. and Neff, H.F. (1971). "Elastic deformations of constrained cylinders." J. Applied Mechanics, June 1971, 393.

Mooney, M. (1940) "A theory of large elastic deformation." J. Applied Physics, **11**, 582.

Morrell, S.H. and Stern, J. (1952). "Crystallization and tensile strength of vulcanized natural rubber compounds." Trans. Institution Rubber Industries, **28**, 269.

M.R.P.R.A. Natural Rubber Engineering Data Sheets. (1980). T.A.R.R.C., Brickendonbury, Hertford, U.K.

Muhr, A.H. (1991). "Dynamic properties of rubber." Proc. Regional Seminar on Natural Rubber in Engineering, Kuala-Lumpur, Malaysia, September 1991.

Muhr, A.H., Gough, J. and Gregory, I.H. (1999) "Experimental determination of model for liquid silicone rubber: hyperelasticity and Mullins' effect." Constitutive Models for Rubber, Balkema, ed. A. Dorfmann, A.H. Muhr.

* Lindley, P.B. (1979). "Compression moduli for blocks of soft elastic material bonded to rigid endplates. " J. Strain analysis, **14**, 11.

Muhr, A.H., Tan, G.H. and Thomas, A.G. (1988). "A method of allowing for non-linearity of filled rubber in force-deformation calculations." J. Natural Rubber Research, **3**, 261.

Mullins, L. (1947). "Effect of stretching on the properties of rubber." J. Rubber Research, **16**, 275.

Mullins, L. (1950). "Measurement of the dynamic properties of rubber." trans. Institution Rubber Industries, **26**, 27.

Mullins, L. and Tobin, N.R. (1954). "Theoretical model for the elastic behaviour of filler-reinforced vulcanized rubbers." Proc. 3rd Rubber Technology Conference, June 1954, 397.

Mullins, L. and Tobin, N.R. (1965). "Stress softening in rubber vulcanizates. I Use of a strain amplification factor to describe the elastic behaviour of filler-reinforced vulcanized rubber." J. Applied Polymer Science, **9**, 2993.

Murnaghan, F. (1951). "Finite deformation of an elastic solid." Wiley.

Nyburg, S.C. (1954). "X-ray determination of crystallinity in deformed natural rubber." Brit. J. Applied Physics, **5**, 321.

Obata, Y., Kawabata, S. and Kawai, H. (1970). "Mechanical properties of natural rubber vulcanizates in finite deformation." J. Polymer Science, **A2,8**, 903.

Ogden, R.W. (1972). "Large deformation isotropic elasticity - on the correlation of theory and experiment for incompressible rubberlike solids." Proc. Royal Society, **326**, 565.

Ogden, R.W. (1976). "Volume changes associated with the deformation of rubber-like solids." J. Mechanics and Physics of Solids, **24**, 323.

Ogden, R.W. (1982). "Elastic deformations of rubberlike solids." Mechanics of Solids, Pergamon, ed. H.G. Hopkins, M.J. Sewell.

Ogden, R.W. and Roxburgh, D.G. (1999). "A pseudo-elastic model for the Mullins effect in filled rubber." Proc. Royal Society, **A455**, 2861.

Othman, A. bin, Gregory, M.J. (1990). "A stress-strain relationship for filled rubber." J. Natural Rubber Research, **5**, 144.

Payne, A.R. (1962). "The dynamic properties of carbon black loaded natural rubber vulcanizates." J. Applied Polymer Science, **6**, 57.

Payne, A.R. (1965). "Strainwork dependence of filler-loaded vulcanizates." J. Applied Polymer Science, **8**, 2661.

Payne, A.R. and Whittaker, R.E. (1971), "Low strain dynamic properties of filled rubbers." Rubber Chemistry and Technology, **44**, 440.

Payne, A.R. and Smith, J.F. Whittaker, R.E. (1972). "Effect of vulcanization on the low-strain dynamic properties of filled rubbers." J. Applied Polymer Science, **16**, 1191.

Peeters, F.J.H. and Küssner, M. (1999)."Material law selection in the finite element simulation of rubber-like materials and its practical application in the industrial design process." Constitutive Models for Rubber, Balkema, ed. A. Dorfmann, A.H. Muhr.

Peng, S.H., Shimbori, T. and Naderi, A. (1994). "Measurement of elastomer's bulk modulus by means of a confined compression test." Rubber Chemistry and Technology, **67**, 871.

Peng, S.T.J. and Landel, R.F. (1972). "Stored energy function of rubberlike materials derived from simple tensile data." J. Applied Physics, **43**, 3064.

Peng, S.T.J. and Landel, R.F. (1975). "Stored energy function and compressibility of compressible rubberlike materials under large strain." J. Applied Physics, **46**, 2599.

Penn, R.W. (1970). "Volume changes accompanying the extension of rubber." Trans. Society of Rheology, **14**, 509.

Pettifor, J.D. and Coveney, V.A. (1989). "The influence of strain amplitude on low temperature crystallization." Proc. Scandinavian Rubber Conference, Tampere, Finland, January 1989.

Pond, T.J. (1989). "Creep behaviour of rubbers subjected to repeated loadings." J. Natural Rubber Research, **4**, 93.

Pond, T.J. and Thomas, A.G. (1979). "Creep under repeated stressing." Proc. International Rubber Conference, Venice, October 1979.

Puett, D., Smith, K.J. and Ciferri, A. (1965). "Elasticity of semicrystalline polymers." J. Physical Chemistry, **69**, 141.

Rivlin, R.S. (1948a). "Large elastic deformations of isotropic materials. I Fundamental concepts." Philosophical Transactions of the Royal Society, **A240**, 459.

Rivlin, R.S. (1948b). "Large elastic deformations of isotropic materials. IV Further developments of the general theory." Philosophical Transactions of the Royal Society, **A241**, 379.

Rivlin, R.S. (1949). "Large elastic deformations of isotropic materials. VI Further results in the theory of torsion, shear and flexure."Philosophical Transactions of the Royal Society, **A243**, 173.

Rivlin, R.S. and Saunders, D.W. (1949). "Cylindrical shear mountings." Trans. Institution Rubber Industries, **24**, 296.

Rivlin, R.S. and Saunders, D.W. (1951). "Large elastic deformations of isotropic materials. VII Experiments on the deformation of rubber." Philosophical Transactions of the Royal Society, **A243**, 251.

Roberts, D.E. and Mandelkern, L. (1955). "Thermodynamics of crystallization in high polymers: natural rubber." J. American Chemical Society, **77**, 781.

Russell, E.W. (1951) "The crystallization of vulcanized natural rubber at low temperatures." Trans. Faraday Society, **47**, 539.

Shariff, M.H.B.M. (1997). "Single constant strain energy function for rubberlike materials." Plastics, Rubbers and Composites: Processing and Applications, **26**, 285.

Simo, J.C. (1987). "On a fully three-dimensional finite-strain viscoelastic damage model: formulation and computational aspects." Computer meth. Appl. mech. Eng., **60**, 153.

Speckhard, T.A. and Cooper, S.L. (1986). "Ultimate tensile properties of segmented polyurethane elastomers: factors leading to reduced properties for polyurethanes based on non-polar soft segments." Rubber Chemistry and Technology, **59**, 405.

Stevenson, A. (1983). "The influence of low-temperature crystallization on the tensile modulus of natural rubber." J. Polymer Science (Polymer Physics), **21**, 553.

Stevenson, A. (1986). "The effect of shear and compressive strain on the low temperature crystallization of natural rubber." Polymer, **27**, 1211.

Sullivan, J.L, and Mazich, K.A. (1989). "Non separable behaviour in rubber viscoelasticity." Rubber Chemistry and Technology, **62**, 68.

Tang, S.H., Meinecke, E.A., Riffle, J.S. and McGrath, J.E. (1980). "Structure-property studies on a series of polycarbonate-polydimethylsiloxane block copolymers." Rubber Chemistry and Technology, **53**, 1160.

Thomas, A.G. (1955). "The departures from the statistical theory of rubber elasticity." Trans. Faraday Society, **51**, 569.

Timoshenko, S. (1934). "Theory of elasticity." McGraw Hill.

Treloar, L.R.G. (1941). "Crystallization phenomena in raw rubber." Trans. Faraday Society, **37**, 84.

Treloar, L.R.G. (1943a). "The elasticity of a network of long chain molecules. I." Trans. Faraday Society, **39**, 36; Rubber Chemistry and Technology, **16**, 746.

Treloar, L.R.G. (1943b). "The elasticity of a network of long chain molecules. II." Trans. Faraday Society, **39**, 241; Rubber Chemistry and Technology, **17**, 296.

Treloar, L.R.G. (1944). "Stress-strain data for vulcanised rubber under various types of deformation." Trans. Faraday Society, **40**, 59.

Treloar, L.R.G. (1948). "Stresses and birefringence in rubber subjected to general homogeneous strain." Proc. Physical Society, **60**, 135.

Treloar, L.R.G. (1969). "Volume changes and mechanical anisotropy of strained rubbers." Polymer, **10**, 279.

Treloar, L.R.G. (1975). "The physics of rubber elasticity." 3rd edition, Claredon Press, Oxford.

Treloar, L.R.G. and Riding, G. (1979). "A non-Gaussian theory for rubber in biaxial strain. I Mechanical properties." Proc. Royal Society, **A369**, 261.

Trick, G.S. (1960). "The softening of Adiprene L gum stocks during extension." J. Applied Polymer Science, **3**, 252.

Tschoegl, N.W. (1971). "Constitutive equations for elastomers." J. Polymer Science, **A1 9**, 1959.

Tschoegl, N.W. (1989). "The phenomenological theory of linear viscoelastic behaviour." Springer-Verlag, Berlin, Heildelberg.

Twizell, E.H. and Ogden, R.W. (1983). "Non-linear optimization of the material constants in Ogden's stress-deformation function for incompressible isotropic elastic materials." J. Australian Mathematical Society, **B24**, 424.

Valanis, K.C. and Landel, R.F. (1967). "The strain-energy function of a hyperelastic material in terms of the extension ratios." J. Applied Physics, **38**, 2997.

Vangerko, H. and Treloar, L.R.G. (1978). "The inflation and extension of rubber tube for biaxial strain studies." J. Physics, **D11**, 1969.

Varga, O.H. (1966). "Stress strain behaviour of elastic materials." Wiley, New York.

Wall, F.T. (1942). "Statistical thermodynamics of rubber. II." J. Chemical Physics, **10,** 485; Rubber Chemistry and Technology, **15**, 806.

Wang, M.C. and Guth, E. (1952). "Statistical theory of networks of non-Gaussian flexible chains." J. Chemical Physics, **20**, 1144.

Warnaka, G.E. (1963). "Dynamic strain effects in elastomers." Rubber Chemistry and Technology, **36**, 407.

Williams, M.L., Landel, R.F. and Ferry, J.D. (1955). "The temperature dependence of relaxation mechanisms in amorphous polymers and other glass-forming liquids." J. American Chemical Society, **77**, 3701.

Wood. L.A. and Bekkedahl, N. (1946). "Crystallization of unvulcanized rubber at different temperatures." J. Applied Physics, **17**, 362.

Wood, L.A. and Martin, G.M. (1964). "Compressibility of natural rubber at pressures below 500kg/cm^2" J. National Bureau of Standards, **68A**, 259.

Yeoh, O.H. (1990) "Characterization of the elastic properties of carbon-black filled rubber vulcanizates." Rubber Chemistry and Technology, **63**, 792.

Yeoh, O.H. (1997). "On the Ogden strain energy function." Rubber Chemistry and Technology, **70**, 175.

Yeoh, O.H. and Fleming, P.D. (1997). "A new attempt to reconcile the statistical and phenomenological theories of rubber elasticity." J. Polymer Science, **B35**, 1919.

Zemel, S. and Roland, C.M. (1992). "Anomalies in the crystallization of cis-1,4-polyisoprene in blends with poly(vinylethylene)." Polymer, **33**, 3427.

Zubakov, B.I. and Reznikovskii, M.M. (1969). "Experimental study of the influence of crystallization on the strength of unfilled NR vulcanizates." Soviet Rubber Technology, **28-7**, 18.